Surface Chlorophyll Distributions in the Upper Gulf of Thailand Investigated Using Satellite Imagery and Ecosystem Model

by

Anukul Buranapratheprat
B.Sc., Burapha University, 1993
M.Sc., Chulalongkorn University, 1997

A Dissertation Submitted in Partial Fulfillment of the
Requirements for the Degree of

DOCTOR OF PHILOSOPHY

in the Department of Geography

Surface Chlorophyll Distributions in the Upper Gulf of Thailand
Investigated Using Satellite Imagery and Ecosystem Model

by

Anukul Buranaprattheprat
B.Sc., Burapha University, 1993
M.Sc., Chulalongkorn University, 1997

Supervisory Committee

Dr. K. Olaf Niemann, Supervisor
(Department of Geography)

Dr. Mark S. Flaherty, Department Member
(Department of Geography)

Dr. Rosaline R. Canessa, Department Member
(Department of Geography)

Dr. Asit Mazumder, Outside Member
(Department of Biology)

Dr. Max L. Bothwell, External Examiner
(Environment Canada, Pacific Biological Station)

Supervisory Committee

Dr. K. Olaf Niemann, Supervisor
(Department of Geography)

Dr. Mark S. Flaherty, Department Member
(Department of Geography)

Dr. Rosaline R. Canessa, Department Member
(Department of Geography)

Dr. Asit Mazumder, Outside Member
(Department of Biology)

Dr. Max L. Bothwell, External Examiner
(Environment Canada, Pacific Biological Station)

ABSTRACT

MERIS data and Nutrient-Phytoplankton-Zooplankton-Detritus (NPZD) ecosystem model coupled with the Princeton Ocean Model (POM), were used to investigate seasonal variations in surface chlorophyll distributions and their controlling factors to clarify phytoplankton dynamics in the upper Gulf of Thailand. Chlorophyll maps were produced by application on MERIS Level 2 data an empirical algorithm derived from the regression analysis of the relationship between chlorophyll-a concentration and remote sensing reflectance ratio. The results indicated that the patterns of seasonal chlorophyll distributions corresponded to local wind and water circulations. The model simulation highlighted the importance of river water as a significant nutrient source, and its movement after discharge into the sea is controlled by seasonal circulations. High chlorophyll concentration located along the western

coast following the direction of counter-clockwise circulation, forced by the northeast winds, while chlorophyll accumulation was observed in the northeastern corner of the gulf due to clockwise circulation, driven by the southwest winds. These key simulated results are consistent with those of field observations and satellite images captured in the same periods of time, and also described seasonal shifting of blooming areas previously reported. Sensitivity analysis of simulated chlorophyll distributions suggested that not only nutrients but also wind-induced vertical movement plays a significant role in controlling phytoplankton growth. Plankton blooms occur in zones of upwelling or where vertical diffusivities are low. Increasing nutrients in the water column due to river loads leads to increasing potential for severe plankton blooms when other photosynthetic factors, such as water stability and light, are optimized. The knowledge of seasonal patterns of blooming can be used to construct environmental risk maps which are very useful for planning to mitigate the eutrophic problems. Effective measures need to be applied to control amount of nutrients released into natural water in order to minimize severity of red tides.

TABLE OF CONTENTS

Page

Page

Page

LIST OF TABLES

Page

LIST OF FIGURES

Page

Page

Page

Page

Page

Page

ACKNOWLEDGEMENT

The dissertation would not be successful if there were no collaboration and support from many people and organizations as acknowledged here. First of all, I would like to present my profound gratefulness to my professor Dr. Olaf Nieman for his support, generosity and encouragement throughout my study at UVIC. His extra help by correcting my English writing, making the dissertation more readable, is really appreciated. My thanks are also presented to Dr. Mark Flaherty for his support in many ways especially travel grants for data collection and collaboration in Thailand through the CIDA project, and dissertation committees, Dr. Rosaline Canessa, Dr. Asit Mazumder and Dr. Max Bothwell for their valuable comments and suggestions.

Most invaluable oceanographic data are kindly provided by Dr. Satsuki Matsumura, a senior professor at Chulalongkorn University, who also taught me many things in ocean optics. My gratitude is also expressed to Dr. Tetsuo Yanagi from Kyushu University for his prompt suggestions in modeling technique, my senior colleague Dr. Pramot Sojisuporn from Chulalongkorn University for circulation data and all his help, Dr. Pichan Sawangwong and Dr. Kashane Chalermwat from Burapha University, and Dr. Thithaworn Lirdwittyaprasit from Chulalongkorn University for their supports and comments. I would like to give my big thanks to researchers and students of the Chulalongkorn research team for their hard work in the field for data collection.

Thanks are also forwarded to Royal Irrigation Department, Pollution Control Department and Meteorological Department of Thailand for providing ancillary data used in numerical models; the European Space Agency Envisat Project for providing MERIS data (Project ID 3426) and BEAM image processing software; Dr. Reiner Schlitzer for distributing Ocean Data View software; Dr. Alan Blumberg and Dr. George L. Mellor for developing POM.

Living and studying in Canada are impossible without financial support from Thai government that should be strongly acknowledged. I would like to thank all my friends in Thailand, Japan, Canada and Korea for their fruitful suggestions, encouragement and technical helping. To my parents, my wife, my son, other family members, and Joanne and Gordon Campbell, thanks for having all of you in my life.

CHAPTER 1

INTRODUCTION

1.1 Nature of the Problem

Marine phytoplankton is small, but plays a surprisingly vital role in marine ecosystems. It has long been providing food for living creatures on earth for billion years (Attenborough, 1980). Phytoplankton blooms in the open oceans are used as an important index of high productivity of marine life in surrounding areas. The same evidence becomes disastrous due to waste accumulation and in some cases toxin when plankton is overpopulated in coastal sea. Human activities accelerate those adverse problems by adding extra nutrients to natural water. It is, therefore, necessary to understand the mechanism of this eutrophic situation and find ways to mitigate its adverse consequences.

Phytoplankton plays an important role as a primary producer of marine life. The order of magnitude of primary productivity in the world oceans is as high as that of terrestrial plants although its standing stock is very much smaller (Falkowski et al., 1998). Moreover, photosynthetic process throughout the world ocean might help to reduce atmospheric CO_2 which is the cause of global warming due to anthropogenic activities. In the open ocean, high chlorophyll concentrations are closely linked to high productivity which is beneficial to marine ecosystems and human food supply. On the contrary, blooming of phytoplankton in coastal seas might lead to adverse effects of oxygen depletion and water quality deterioration resulting in massive mortality of

marine life in surrounding areas. More devastation might happen if the blooming species produce toxin. Environmental factors contributing to growth, patchiness and dispersion of phytoplankton in an area are related to water parameters such as nutrients, current, light, salinity and temperature. Understanding these relations will help to minimize environmental problems associated with eutrophication in coastal seas. Chlorophyll concentration and phytoplankton populations, therefore, become significant parameters widely used to assess water quality in most monitoring programs.

Both remote sensing and computational modeling are considered to be very powerful tools for marine environmental studies. The former concerns electromagnetic detection and analyses to extract information about the earth's surface, while the latter involves computer simulation based on mathematical equations representing natural phenomena. They provide synoptic data for a wide geographical area, something that is difficult if not impossible to collect with traditional field-based methods. Modern satellite remote sensors such as Sea-viewing Wide Field-of-view Sensor (SeaWiFS), Moderate Resolution Imaging Spectroradiometer (MODIS), Ocean Color and Temperature Scanner (OCTS) and Medium Resolution Imaging Spectrometer (MERIS) have been designed to extract electromagnetic signals appropriate for chlorophyll-a estimation. Satellite-based remote sensing techniques have two fundamental limitations; cloud cover and a limited ability to penetrate into the water column. To reduce the limitations imposed by remote sensing data alone, a variety of numerical models have been alternatively chosen for oceanographic studies (e.g., Xu and Hood, 2006; Cugier and Hir, 2002). Well designed models that can reproduce

chlorophyll distribution of either field-measurement, or satellite data, will eventually reveal ecological factors parameterized in computation. Moreover, predictable models can be applied to investigate chlorophyll distributions in response to changes in phytoplankton growth conditions. Using both numerical model and remote sensing techniques will undoubtedly improve our understanding of chlorophyll dynamics in the sea.

The study presented in this dissertation focuses on the upper Gulf of Thailand (UGoT), a shallow coastal sea located just in the south of central Thailand. Receiving discharges from four main rivers including the Chaopraya River which is Thailand's largest river, the upper gulf is considered to be an estuary due to interaction of salt and fresh water. Primary productivity by phytoplankton is quite high because of large nutrient loads introduced by the river water. Consequently, this small area is very productive and suitable for coastal aquaculture, especially shellfish farming. Green mussel, oyster and blood clam are intensely farmed throughout the area, but with a higher concentration close to the river mouths. Not only aquaculture but also fisheries and tourism are important to both local and national economies. Deterioration of the marine environment from increasing pollutants that might occur will unavoidably affect the standard and quality of life of local inhabitants.

One of serious environmental concerns of the upper gulf is eutrophication (Chongprasith and Srinetr, 1998). By-products released directly into natural water from municipalities, aquaculture, and agriculture activities are major sources of high nutrient concentrations in the water column, stimulating blooms of phytoplankton. The Pollution Control Department (PCD) of Thailand reported increases of averaged

phytoplankton blooms in the upper Gulf from 6 to 19 times a year during 1981-1989 and 1991-1993, respectively (http://www.marinepcd.org/coastalwater/wq10year.html). The dominant algae species are non-toxic, with just one recorded occurrence of Paralytic Shellfish Poisoning (PSP) being reported in May 1983 (Tamiyavanich, 1984). General non-toxic blooming, nevertheless, also has a potential to result in massive mortality of marine organisms owing to dissolved oxygen depletion and metabolite waste accumulation affecting not only aquaculture but also coastal farming.

Although the environmental quality of the upper Gulf region is of great importance to the coastal ecosystems and country's economy, measurement of circulation has rarely been reported due to cost and field work logistics. However, SEAWATCH Thailand deployed two oceanographic buoys to collect meteorological and oceanographic data in the west and the east of the area (Booncherm, 1999). The project provided time series data, which are still very useful for the oceanographic community these days, but in terms of regional circulation, two single points are insufficient to represent circulation patterns. A computer modeling approach has therefore been chosen to derive circulation patterns instead of direct measurement. Results from a two – dimensional model (Buranaprattheprat et al., 2002a) indicate that seasonal circulation responds to local wind field. Clockwise and counter – clockwise flows in the whole area are generated during the southwest and the northeast monsoon, respectively. Nevertheless, there is a limitation that the two – dimensional model cannot account for some forcing, such as influences of pile-up effect and density-driven force. Moreover, such a model does not allow us to see circulation profiles that might be important during the wet season when water layers are formed. It is,

therefore, necessary to re-analyze the circulation by applying a three-dimensional model that can take all significant forcing into consideration for more realistic results.

The current study is composed of three main experiments that focus on investigating chlorophyll-a dynamics in the upper Gulf of Thailand. First, satellite images of MERIS sensor will be applied for analysis of seasonal patterns in chlorophyll-a distribution. The results from this analysis will be used as a reference to verify the results of numerical ecosystem models in experiment three. Second, a three-dimensional circulation model, the Princeton Ocean Model (POM) (Blumberg and Mellor, 1987), will be used to address the issue of seasonal circulation. This modeling exercise will reveal the response of water movement to forcings such as wind, tide, bottom topography, and density gradient. Finally, ecosystem modules will be added into POM to calculate chlorophyll-a distribution. This physical-biological coupling model needs boundary inputs such as nutrients, phytoplankton, and detritus data in addition to standard physical parameters. Measurement data sets used for algorithm development, satellite image verification and model inputs are derived from the collaboration field campaigns between Thai and Japanese scientists with the support of Chulalongkorn University (Thailand), the National Research Council of Thailand (NRCT), the Japan International Cooperation Agency (JICA) and the Japanese Society for the Promotion of Science (JSPS). All the experimental results will help us understand the dynamics of geographical and seasonal variations in chlorophyll-a distribution in the whole upper Gulf of Thailand.

1.2 Research Objectives

The overall goal is to investigate the mechanism of chlorophyll-a distribution in the upper Gulf of Thailand with the use of remote sensing techniques, and hydrodynamic and numerical ecosystem models. The specific objectives are as follows:

1. Develop an empirical algorithm to extract chlorophyll-a distributions from satellite imagery and investigate variations in the distributions;
2. Clarify 3-dimensional circulation within the upper Gulf of Thailand and its influencing forces using a 3-dimensional hydrodynamic model;
3. Apply a lower tropic-level ecosystem model to investigate the controlling mechanisms of the chlorophyll-a distribution;
4. Investigate the response of phytoplankton distributions to environmental conditions that may change in the future; and
5. Suggest possible ways of how to minimize adverse anthropogenic effects such as enhanced eutrophication

1.3 Significance of the Research

The study will contribute to the advancement of knowledge in coastal environmental areas by improving our understanding of seasonal cycles of chlorophyll-a distribution and its controlling factors in a coastal sea. It will assess the potential contribution of satellite technology for marine environmental studies and addresses the need for further development of sophisticated remote sensing techniques

for environmental monitoring in shallow tropical marine environments. The three – dimensional hydrodynamic and ecosystem models can be further applied to issues addressing the distribution and prediction of not only chlorophyll-a, but also any others substances such as sediments and pollutants.

1.4 Organization of the Dissertation

This dissertation contains eight chapters. Chapter 2 provides background information on the importance and dynamics of phytoplankton in both open ocean and coastal sea. Relation of rising and falling of phytoplankton and environmental condition is also thoroughly discussed. Chapter 3 explains concepts, advancements and limitation of remote sensing and modeling techniques for investigation of chlorophyll distribution. Chapter 4 focuses on the general characteristics and oceanographic conditions of the study area by presenting the outcomes of previous researches with additional results from this study. Chapter 5 reports on the remote sensing experiment investigating the most appropriate empirical algorithm for chlorophyll estimation to produce chlorophyll maps from MERIS data. Then, seasonal variations in chlorophyll distribution of the upper gulf are discussed. Results of numerical experiment for investigation of residual circulation in both two and three dimensions in the same months of field observations are presented in Chapter 6. Chapter 7 illustrates the results of the ecosystem model. Simulated chlorophyll distributions under general and modified environmental conditions are discussed to determine their relationship to phytoplankton blooms. Finally, Chapter 8 provides an overall summary of the

research, discusses its implications and outlines directions for further studies. Specifications of MERIS Level 2 full resolution and governing equations of POM are also included in Appendix A and Appendix B, respectively.

CHAPTER 2

MARINE PHYTOPLANKTON: ITS ROLES AND DYNAMICS

The first section of this chapter reviews the importance of marine phytoplankton on ocean primary productivity and also carbon bio-geochemical cycle. Its dynamics which are profoundly related to environmental conditions are also explored. A crucial controlling factor of phytoplankton distributions in all spatial and temporal scales is circulation. Mechanisms are reviewed in order to support the explanation of processes controlling population cycles of marine phytoplankton in ocean provinces. Finally, the last section will focus on eutrophication which is related to massive blooming of plankton. Deterioration in a wide range of marine ecosystems due to this phenomenon is also discussed.

2.1 Roles of marine phytoplankton

Phytoplankton in the sea not only provides the basis of the marine food chain, but also plays an important role in biogeochemical cycles (Berner and Berner, 1996; Smectacek, 1999) such as that of carbon (McGowan and Field, 2002), nitrogen, phosphorus, and silicate. Chlorophyll is a proxy measure of phytoplankton biomass, and its concentration is highly correlated with marine production (Ware and Thomson, 2005), and is used as an index to evaluate potential productivity of fishing grounds (Waluda et al., 2001). Although the plankton cell has a very small size, its great

abundance can lead to significant absorption of atmospheric CO_2 through photosynthesis. It is believed to play a key role in regulating this greenhouse gas which is commonly accepted to be increasing due to anthropogenic emissions.

2.1.1 Primary Producer of the World Ocean

Net primary production (NPP), based on satellite chl-a data, of the world ocean is in the same order of magnitude (48.5 GtC yr^{-1}; GtC is gigaton carbon) as that of terrestrial vegetation (56.4 GtC yr^{-1}) (Field et al., 1998). Productivity of the former is mostly from phytoplankton, with only 1 GtC from macrophytes. Surprisingly, phytoplankton total biomass, or standing crop, is just about 1 GtC or 0.2 % of photosynthetically active C biomass on earth. This suggests that the recycling rate of its biomass in the ocean is very high - on the order of once per week (Falkowski et al., 1998). Consequently phytoplankton is a vital food source to marine as well as terrestrial organisms.

It is possible to estimate the potential of fish production of the world's ocean from primary productivity and ecological efficiency factors in each trophic level. Ryther (1969) has employed this concept to calculate total fish production by assigning long trophic levels-low transfer efficiency for open oceans and short trophic levels-high transfer efficiency for high productive areas (coastal and upwelling regions). He projected annual fish production at 240 million tons, highlighting the importance of upwelling regions that can produce about half of the world's fish production, although the total area is very small in comparable to open ocean. The

estimation also suggests that permanent or temporary disruptions of the upwelling process, which makes productivity abruptly drop, such as that in offshore Peru due to El Nino phenomenon, leads to collapses in the world fishery production and coastal ecosystem (Glantz, 2001).

Total fish production is also estimated using statistical data of fish catches. Data from the UN Food and Agriculture Organization (FAO) indicate that global fish catches remained relatively stable at about 90 million tones a year from 1999 to 2002 suggesting that the maximum marine fishing potential has been reached (FAO, 2004). Available information including FAO estimates indicate that the global maximum potential for marine capture fisheries is about 100 million tones, of which probably 80 million tones can realistically be achieved (http://www.greenfacts.org/fisheries). The information leads to environmental concern of over exploitation, and suggests the necessity of having appropriate measures for sustainable utilization of marine resources. However, this reflects the potential limitation of marine fish production originating from marine primary producers such as phytoplankton.

2.1.2 Primary Productivity and Climate Change

Oxygenic photosynthesis by marine unicellular algae plays a crucial role in absorbing atmospheric CO_2 and releasing O_2 back into the atmosphere. Geochemical evidence indicates that O_2 on earth reached levels comparable to the contemporary atmosphere over 2 billion years ago (Holland, 1984) as a consequence of phytoplankton photosynthesis (Riding, 1992). Presently, primary productivity of

phytoplankton in the world's oceans, which is in the order of magnitude of up to 10^{10} tons of carbon per year (McCarthy, 2000), is related to climate control (Mann and Lazier, 1996; Watson and Liss, 1998) by the potential to reduce increasing anthropogenic CO_2. The flow of autotrophic carbon through grazing or microbial food webs determines a rate of carbon export to deep waters, and has major relevance in the possible role of the ocean in regulating the global biogeochemical cycle and the atmospheric carbon dioxide drawdown (Priddle et al., 1992; Smetacek, 1999; Walsh et al., 2001; Garibotti et al., 2003). Therefore, it is believed that stimulation of phytoplankton blooms in the ocean, especially in "high nutrient, low chlorophyll" (HNLC) regions, will help reduce a large amount of atmospheric CO_2 (Falkowski, 1998).

Structures of the pre-industrial carbon cycle (Siegenthaler and Sarminto, 1993) indicate that deep ocean water, the largest carbon reservoir, stores about 38,000 GtC and 1,000 GtC in surface water. Vegetation, soil and detritus on land account for about 2,000 GtC while the atmosphere contains only 600 GtC. Although, the atmospheric CO_2 component is comparatively small, it is critical to temperature regulation of the earth's surface. Its rise and fall could result in increasing and decreasing in surface temperatures, respectively. Moreover, the structure of trapped gases in ice cores suggests that changes in atmospheric greenhouse gases like CO_2 and CH_4 are closely linked to the fate of the earth climate - glacial and inter-glacial eras (Muslin, 2004). According to Schimel et al. (1994), an annual carbon (in terms of CO_2) flux of 74 GtC is equally exchanged between sea and atmosphere while a flux of about 100 GtC per year is estimated for the terrestrial-atmospheric exchange. Human activities, mostly

from burning fossil fuels, producing cement, and changing land uses, contribute 7.0 GtC into the atmosphere every year (Schimel et al., 1994) and have contributed a cumulating total atmospheric CO_2 of 750 GtC from 1980 to 1989 (Siegenthaler and Sarminto, 1993). This corresponds to a rapid increase in concentration of this greenhouse gas from 280 parts per million by volume (ppmv) in 1750 to 367 ppmv in 1999 (Prentice et al., 2001). Serious concern has been raised that sudden increases in atmospheric CO_2 will accelerate global warming, resulting in adverse consequences such as extreme climate change, sea level rise, and deterioration of global ecosystems (Muslin, 2004).

At a steady state, about 10 GtC per year has been captured by marine biota through photosynthesis, which then sinks to deep water as detritus and dissolved organic carbon (DOC) (Siegenthaler and Sarminto, 1993); this process is called the *biological pump*. The standing stock of marine phytoplankton is just 3 GtC, or less, but the biological pump can transport over 3 times that of its biomass to deep water because of rapid reproduction rate. Following from the above is a key idea to reduce atmospheric CO_2 by stimulating the biological process to move atmospheric CO_2 to the deep ocean and prevent its prompt return backward to the atmosphere (Kauppi and Sedjo, 2001).

The Southern Ocean surrounding Antarctica has been considered as an interesting HNLC area that has a great potential to affect atmospheric CO_2 levels (Sarmiento and Orr, 1991). Upwelling transports nutrients from deep water but these lack micronutrients such as soluble Fe (ferrous). These areas are, therefore, quite unproductive. Other potential terrestrial sources of Fe are distant and are transported to

the deep sea only through aeolian processes (Duce and Tindale, 1991). Falkowski et al. (1998) approximated that if just 50 % of macronutrients from the surface water in the southern ocean were utilized for photosynthesis by Fe stimulation, it would lead to a further drawdown of atmospheric CO_2 to about 190 ppmv. One option to mitigate future climate change might be to stimulate phytoplankton blooms through Fe fertilization of Antarctic Waters (Kauppi and Sedjo, 2001). Limited experimental successes have been reported (Buesseler and Boyd, 2003) in this area.

Increases in atmospheric and oceanic temperatures will in turn alter the marine ecosystems. An experiment in the northeast Atlantic illustrates that warmer sea surface temperature (SST) increases and decreases phytoplankton abundance in previous cold and warm regions, respectively (Richardson and Schoeman, 2004). Warming generates stratification leading to phytoplankton increase in cold water in the same way as a spring bloom. On the contrary, further heating in warm water strengthens existing stratification reducing available nutrients, and primary productivity. Decline in primary productivity will consequently reduce the viability of higher trophic levels. Devastation of coastal ecosystems and fisheries in Peru's offshore is an excellent example of adverse environmental changes resulting from El Niño phenomenon when warm surface water is introduced into the previously cold water (Glantz, 2001).

This section has provided an overview of the role of phytoplankton in a wide range of time and spatial scales. Understanding the population dynamics of phytoplankton in relation to physical oceanographic processes, is crucial in understanding the broader ecological context. The two next sections present some

basic theories of ocean and coastal circulations which are important to support the explanation of phytoplankton dynamics.

2.2 Ocean Circulation

Varying from the equator to the poles, the sun's radiation received by the atmosphere and the earth's surface is the most significant driving force of wind and ocean current generation (Tomczak and Godfrey, 2005). Although there are seasonal and annual variations, the equator on average obtains higher heat energy than the poles. Theoretically, surface air moves equatorward following an atmospheric pressure gradient that is high at the poles and low at the equator while in the upper atmosphere, by replenishment, a poleward air flow exists.

Water also compensates the global heat energy imbalance by generating a cycle of global water circulation. Following wind, surface currents tend to move poleward from the equator while cold deep water flows in the opposite direction from the poles to the equator. Both fluid movements are modified by the *Coriolis Effect*, influenced by the earth's rotation that bends any free motion from their initial direction – to right and left in northern and southern hemisphere, respectively (McKormick and Thiruvathukal, 1981).

2.2.1 Wind-Induced Circulation

Surface currents are generated through shear stress at the air-sea boundary initiated by surface wind flowing over water. Momentum is transferred from wind to

surface water at the boundary and at depth through eddy viscosity. By this process, some energy losses due to friction occur, reducing the current speed with depth. The current at the air-sea boundary turns 45^{O} to the right (in the northern hemisphere) of wind direction as a consequence of the Coriolis Effect. Deeper currents within the depth of wind influence also bend to the right of the upper currents. The deeper the water layers, the smaller the current speeds, and the larger the bending angles. This phenomenon is called the *Ekman spiral* (Duxbury and Duxbury, 1993). The influence of wind extends to the depth at which the current direction is opposite to the current at the sea surface (the *Ekman depth*). This depth varies from a few ten meters to as much as 100 – 200 m, depending on water stratification and wind speed (Open University Course Team, 2001).

Another significant Ekman theory used to describe surface current patterns in the world ocean is *Ekman transport*. By integration of partial currents starting from the sea surface to the Ekman depth, the surface volume is transported at 90^{O} to wind direction (Duxbury and Duxbury, 1993). Based on the Ekman transport, oceanic surface currents such as subtropical gyres, or subpolar gyres, can be explained by the global wind patterns. It is important to note that the Ekman spiral is completely developed under the condition of infinite water depth, or in the deep ocean, where the influence of bottom friction is nil. A partial spiral may develop in shallow water resulting in the distortion of the transport angle to be less than 90^{O} of wind direction (Kershaw, 2000).

Upwelling in the ocean occurs when divergence of water at the sea surface develops, leading to replenishment of water from deeper layers as a consequence

(Gross, 1987). Wind is a significant upwelling generator by inducing surface water to move away from land (coastal upwelling), or from other currents (e.g., equatorial upwelling). In the northern hemisphere, a counter-clockwise eddy makes surface water move away from its center, another form of divergence, causing upwelling of deeper water. Dissolved nutrients, which are enriched in deep water, are transported to the surface where they become an important food source for phytoplankton and other plants. Therefore, upwelling areas are categorized as highly productive. If the processes reverse, surface convergent and downwelling will result (Gross, 1987).

Changes in regional, or global, wind patterns may have more severe impacts on other meteorological conditions such as those associated with El Niño events. These originate through the inversion of atmospheric pressure gradients in the eastern and the western regions of the southern Pacific Ocean. El Niño events occur when warm water masses in the western Pacific Ocean move rapidly east. When atmospheric pressure over southwest Pacific becomes abnormally high, the southeast wind slacks or, in a severe case, reverses its direction entirely. In normal situations, this strong southeast wind functions as a powerful force to drive warm water from east to west in the central Pacific. This movement of water induces a strong upwelling off the Peruvian coast. An El Niño event emerges when there is no strong wind to maintain the warm water bulk in the western Pacific (Kershaw, 2000). Resulting low primary productivity in the southwest Pacific is caused by warm water intrusion and a weaker upwelling. During those events, there are massive die-offs of marine organisms due to lack of food sources (Glantz, 2001).

2.2.2 Density-Driven Circulation

Under the influence of earth's gravity, water adjusts to be physically stable; the deeper the water, the greater its density. Instability happens when water stratification inverts so that the density at the surface is higher than at depth. A water body will attempt to regulate itself back to a stable condition, and, by this process, vertical circulation is established (Gross, 1987). Generally, water density is controlled by temperature and salinity. High temperature results in water being less dense while high salinity makes water denser. Instability occurs through one or both of these surface conditions – low temperature and high salinity. There are two regions on earth where such instability is generated. The first regions are around polar seas where major influence is low temperature due to low solar radiation, and the other is in the Mediterranean Sea where the density is mainly controlled by high salinity due to high evaporation and low precipitation (McKormick and Thiruvathukal, 1981).

Seawater temperature at or below zero degrees centigrade is responsible for water sinking around the Arctic Ocean and Antarctica. Salinity also has a minor effect on density increasing in those regions because of freezing process of sea ice, where salt molecules are driven out of ice crystals making high saline water called *brine* (Gross, 1987). It is important to note that salt contained in natural seawater changes pure-water properties; the freezing point is lowered and the maximum density commonly attained at 4 ^{o}C disappears (Gross, 1987). When the density of surface water is higher than at depth, it will sink to the layer having the same density. Sinking water might form upper, intermediate, deep, or bottom water masses depending on the

density (Davis, 1987). Important regions of deep water mass formations are in the south of Greenland, around the Arctic, in the Weddell Sea and the Ross Sea of Antarctica (Open University Course Team, 2001).

Deep water masses do not form in the Pacific Ocean because salinity is too low to trigger instability of the water column. Interestingly, surface salinity in the Pacific is lower than in the Atlantic although there are many large rivers such as the Amazon and the Congo Rivers emptying huge fresh water into the Atlantic Ocean. The apparent reason for this is the Mediterranean Sea (Open University Course Team, 2001). Located in the earth arid zone where evaporation is much higher than precipitation and limited by a narrow strait to the Atlantic Ocean, the Mediterranean Sea is characterized by highly saline water approximately 37 and 38 ppt (part per thousand) and temperature of about 11 ^{o}C. Water entering the Atlantic from the Mediterranean forms a highly saline layer at about 1,000 m depth (Open University Course Team, 2001). This line of saline water can be detected in most parts of the Atlantic Ocean.

Temperature and salinity can be used as a water mass tracer because of their conservative behavior. It is assumed that after a water body sinks to a great depth, its original temperature and salinity are preserved. By constructing the temperature-salinity (T-S) diagram, the origin of a water mass can be identified by comparing the properties of that water body with those that represent each water mass at its origin (Pickard and Emery, 1990). Radioisotopes such as ^{14}C and H^{3}, or artificial chemical substances such as chlorofluorocarbons (CFCs) can be used for the determination of age and movement of deep water masses after sinking (McGowan and Field, 2002). When the isotopic composition of seawater, before sinking, is known, the age of a

water mass can be estimated from its remaining half-life. CFCs represent a different problem, since many types have been produced at different times. The key to their usefulness as tracers comes from their compositional time stamp. Scientists, in applying these methods, have found that deep water masses in the ocean have a long residency. For instance, water found at the depths of 1,500 m in the Pacific Ocean has been found to have residency times of 500 years (McGowan and Field, 2002). The evidence suggests that deep or bottom water masses could remain in the ocean for much longer periods.

Dissolved and suspended in the sinking water mass are atmospheric gases, and non-biogenic and biogenic substances. While some chemical, biological and physical reactions might occur during transport, the remaining substances will reside in the ocean-bottom reservoir for a long time. Combining with the biological pump, the oceans have a potential to minimize severe global warming due to increases in greenhouse gases.

Sinking process can reduce a significant amount of atmospheric CO_2 dissolved in surface water and extend its returning to the atmosphere (McGrown and Field, 2002). However, deep water mass formation is a fragile process. There is a concern that if the ocean temperature considerably increases and triggers strong stratification, this important process might be shut down resulting in additive effects to global warming in the future (North and Duce, 2002).

2.3 Coastal and Estuarine Circulations

Environmental conditions in coastal seas and estuaries are different than the open ocean because of some key factors. These factors include the boundary effect of coastlines, shallow depth, river runoff and precipitation, and the effects of continental air masses flowing out over the sea (Pickard and Emery, 1990). Temporal and seasonal variations in temperature and salinity are quite large in coastal environments. Salinity might change for example from 0 to 30 ppt within 15 – 20 km (Buranapratheprat et al., 2002b). Variations of this magnitude do not occur in open ocean condition. Therefore, monitoring networks located in coastal environments must be designed appropriately so as to capture these variations, especially when some small-scale patterns like eddies and current menders are dominant. Some phenomena might need sampling on a daily, or diurnal, cycle in order to filter tidal influence from residual signals.

2.3.1 Coastal Circulation

We have seen from previous sections that the Ekman spiral and surface transport are generated by surface winds flowing over very deep water. However, not only surface, but also bottom friction can generate the Ekman spiral due to the balance of frictional force of water flowing over sea floor and the Coriolis Effect. The frictional force is always generated in a direction opposite to the prevailing current, and under the influence of the Coriolis Effect. When water depth is shallower than the Ekman depth, transport due to surface and bottom Ekman will compensate each other. This leads to a reduction in the angles of surface current and net volume transport

approximating the direction of surface wind (Pickard and Emery, 1990). The shallower the water depth, the smaller the bending angle of surface circulation from wind. That means as water depth decreases, the net flow will approximate the wind direction.

Unlike the open ocean situation, strong convergence in coastal sea results from the presence of landmasses that abruptly alter horizontal water flow. Since coastal zones are shallow, approaching water masses cannot move downward but unavoidably pile up against the coast forming sea level set-up or surge. The height of sea level is proportional to wind stress, but inversely proportional to water depth (Tomczak, 1998). Generally, the pile-up effect is the cause of high and low sea levels over downwind and upwind regions, respectively. However, sea level rise in extreme cases like storm surges can pose a severe threat to coastal areas, leading to large-scale flooding and loss of life in low lying coastal regions (Tomczak, 1998).

Tides, and tidal currents, are also important because their magnitudes are greatest in the vicinity of the coast resulting in high energies compared to the open ocean. Tides approach a bay in two long wave forms: standing and propagating. Standing wave results when water elevations and tidal currents are 90^{o} out of phase, while in the case of propagating wave, they are in phase (Yanagi, 1999). Generally, tidal phase propagates counterclockwise in a gulf or shelf sea in the Northern Hemisphere while in the Southern Hemisphere it is in the opposite direction (Yanagi, 1998). This is explained by the superposition of incoming and reflecting Kelvin waves under the influence of the earth's rotation (Taylor, 1920). The water level might be extremely high in the case of a *co-oscillation tide* when the natural resonance frequency of the bay, which is dependent on its dimension, is close to the frequency of

one of tidal harmonic components (Pickard and Emery, 1990). This explains why tidal ranges in the Bay of Fundy, Canada reaches up to 15 m (Yanagi, 1999).

Tidal currents flowing over the sea bottom play a significant role generating turbulence and intensifying vertical mixing by breaking down the stratification of the water column. However, the mixing strength in a coastal zone is influenced by not only tidal influences, in terms of bottom stress, but also by wind stress, fresh water run-off, and surface heating (Yanagi et al., 2001b). Mixing occurs when tidal and wind stresses are larger than the buoyancy forces of fresh water and surface heating that would normally stabilize the water column.

Background circulation pattern also known as residual flow, is important in understanding the trajectory and distribution of pollutants, phytoplankton and sediment. It is extracted from overall water movement patterns through the removal instantaneous tidal currents. Theoretically, if circulation in a coastal zone having a flat bathymetry is influenced only by tidal action, the net flow will be zero because water moves back and forth in equal distances in a complete tidal cycle – 12 hrs 25 min. and 24 hrs 50 min. for diurnal and semi-diurnal tides, respectively (Yanagi, 1999). Such situations, however, are rare due to the nature of the tide and the complexity of the bathymetry. Currents in shelf seas are also modified by many factors such as the shape of the coastlines, bottom topography, local weather conditions, and fronts (Open University Course Team, 1999). Interaction of tidal constituents of different wave periods sometimes support or diminish each other resulting in an imbalance of levels between ebb and flood tides.

2.3.2 Estuarine Circulation

The classical definition of an estuary by Cameron and Pritchard (1963) is *"...a semi-enclosed coastal body of water which has a free connection with the open sea and within which sea water is measurably diluted with fresh water derived from land drainage"*. Common estuarine environments are river mouths, bays, inlets, gulfs, and sounds, where fresh water from land empties into the sea (Thurman and Trujillo, 1999). This definition does not include environments where the salinity inside the estuaries is higher than exterior seawater known as *negative estuary* (Tomczak, 1998).

Estuaries might be categorized by water stratification and vertical mixing of the water column as a result of interaction between fresh water outflow and tidal currents. Water is stratified where the fresh water flow is large and the tidal current is not so strong. Conversely, mixing is triggered by tidal stress when the tidal influence is significantly greater than fresh water flow. Based on this concept, estuaries can be separated into three categories (Pinet, 1998): salt-wedge, partially mixed, and well-mixed. Their order follows from high to low influences of fresh water, respectively, or in other words, from weak to strong influences of tidal current. Halocline, due to stratification could be observed in both salt wedge and partially mixed estuaries, while it is not observable in the well-mixed ones. A negative estuary, where salinity decreases while traveling from the head of the estuary to the sea, occurs when seawater is restricted in a semi-enclosed bay under the conditions of high evaporation and low fresh water input (Tomczak, 1998).

When river water discharges into the sea, due to comparatively low density, it will float and flow over seawater. At the same time, denser seawater will penetrate under fresh water generating riverward flow over the sea bed. This reverse system of circulation, known as *estuarine circulation*, occurs in salt-wedge and partially stratified estuaries. It does not happen in a well-mixed estuary where water flows in the same direction throughout the water column. The direction of instantaneous circulations might change during ebb and flood tides, but residual flows still have seaward-surface flow and riverward-bottom flow components. Generally, the magnitude of the residual current is approximately 10 % of the instantaneous current (Open University Course Team, 1999).

There is a depth where the flows change direction and the net flow is zero. Where this depth coincides with the bed of the channel, divergence will result. This point, known as the *null point*, is important to the dynamics of sediment transport in the estuary. It occurs near the head of the salt intrusion where salinities are as low as 0.1 to 5 ppt, depending on tidal ranges from low to high respectively (Open University Course Team, 1999). Lateral flows might develop and become more important where the areas of the estuaries are very large. In the northern hemisphere, the Coriolis Effect will deflect water flowing into and out of the estuary to be close to the right and left banks, respectively. This phenomenon could be seen in the large estuary like the Chesapeake Bay (Pinet, 1998).

Variations in sediment distribution rely on the dynamics of estuarine circulation, fronts of fresh water and sea water, river discharge, tidal current, and the movement of the null point. Interestingly, sediment re-suspended from the sea bottom

by tidal stirring might be larger than that delivered by river waters in many estuaries (Tomczak, 1998). The largest concentration of suspended sediment can be found close to the null point, and that region is defined as the *turbidity maximum* (Dyer, 1979). Turbid water near seabed generated by tidal stirring will be transported riverward by the tidal current and then trapped at the null point due to divergent condition. Concentrations of suspended sediment in this area can be as high as 100 – 200 mg l^{-1} in an estuary with small tidal range. It might reach up to 10^3 – 10^4 mg l^{-1} where mixing is very strong in the case of a large tidal range (Open University Course Team, 1999).

The null point and the turbidity maximum can move up- and downstream in response to the interaction between river flow and tidal force. Suspended sediments might settle during the ebb tide when the tidal current is weak, and re-suspend during flood tide. Some might deposit permanently in the estuarine channel. Strong river flow, occurring during the wet season or during a storm, plays a crucial role in flooding the deposited sediment out to the open sea. Any changes in the flow regime, such as the lessening of the seasonal flood due to dam construction or creation of artificial lakes located upstream, will allow sediment to accumulate near the mouth downstream and fill in the estuarine channels. This can cause navigation problems, and regular dredging needs to be applied to maintain the shipping channel (Tomczak, 1998).

2.4 Phytoplankton Dynamics

Phytoplankton abundance varies depending on the environmental characteristics of open oceans and coastal environments. Vertical water movement and stratification become important to phytoplankton dynamics in the open ocean. Generally, productivity in such water is very low because phytoplankton and nutrients are separated by depth – plankton lives near the sea surface while nutrients accumulate near the sea bottom. Mixing or upwelling that might happen temporarily, or permanently, will induce deep enriched-nutrient water to the surface; therefore, if there is enough light and optimal temperature for photosynthesis, productivity will be high. Unlike open ocean, the coastal sea is influenced by terrestrial environments through river discharge and run-off, both sources of nutrient supply. Moreover, because of shallow depth and influences of tide and wind, the water column is very well mixed. Productivity in such an area, therefore, tends to be high.

2.4.1 Open Ocean

Phytoplankton growth in the ocean is affected by light intensity, the optical characteristics of water, temperature, salinity, micronutrients and trace metals, and organic factors (Riley and Chester, 1971). Increases in the phytoplankton population in an area are stimulated by an optimal level of these factors in combination with appropriate oceanographic conditions. Occurrence of spring blooms in temperate and polar seas is an excellent case to explain seasonal variations of factors affecting phytoplankton density (Miller, 2004). According to Sverdrup (1953), seasonal

thermocline develops as a consequence of strong light intensity and high air temperature in springtime. This stabilizes the water column, decreases the thickness of the mixed layer and deepens the euphotic zone. The spring bloom is triggered when phytoplankton is confined in the surface layer which now has sufficient light intensity for photosynthesis, and, as a result of winter mixing, is rich with nutrients (Riley and Chester, 1971; Polovina et al., 1995; Arrigo and Weiss, 1998). The bloom will last until the onset of summer and declines when nutrients in surface water diminish due to strong water stratification. Surface water stability is produced, not only by high surface temperature, but also by low salinity water from sea-ice melting; consequently, high phytoplankton biomass can be found in marginal ice zone in the polar sea (Kang et al., 2001). Phytoplankton will not, however, increase significantly if temperature is too low though other factors are optimal (Mei et al., 2002).

Spring blooms differ from area-to-area as a result of the difference in controlling factors. They are timing and magnitude of water stratification, the depletion of a micronutrient (e.g., Fe), grazing pressure by zooplankton (Mochizuki et al., 2002), and variations in species structure of the phytoplankton (Shiomoto et al., 1998; Shiomoto and Asami, 1999). For instance, in the sub-Arctic North Pacific, spring blooms do not occur, although there is seasonal mixing of the water column and an adequate supply of the standard nutrients. Phytoplankton populations do not increase in this case due to high grazing pressures by zooplankton (McGowan and Field, 2002).

Strong stratification as a consequence of a permanent thermocline in tropical zones prevents replenishment of nutrients from the deeper layers (Shaples, 1999), Although phytoplankton cells are always maintained in well-lit regions, the

productivity is low. Vertical chlorophyll maxima are found in some tropical and temperate seas in summer. The photosynthesis of the algae decreases and may even be seriously disturbed at high light intensities near the sea surface. Many phytoplanktonic organisms, particularly diatoms, cannot move independently and tend to sink. Those with a high density will, therefore, remain below the level of high production (Bougis, 1976). Another theory suggests that the chlorophyll maxima occurs because the cycle of phytoplankton growth and decay is faster in the upper mixed layer than in, and below, the pycnocline under the condition that the mixed layer is shallower than the pycnocline (Mann and Lazier, 1996).

Biological productivity is very high in upwelling regions (Fournier et al., 1984; Murty et al., 2000) where nutrients from deep water are vertically convected by wind and current into the euphotic zone. Unlike mixing, this process always limits phytoplankton cells to within the well-lit layer thereby increasing photosynthesis. Upwelling occurs in an area of divergence in surface circulation, possibly induced by wind (equatorial upwelling), wind and continent (coastal upwelling), and circulation (cyclonic gyre and anti-cyclonic gyre in the northern and southern hemisphere, respectively). For example, Murty et al. (2000) found the magnitude of chlorophyll maximum is considerably higher when the deep chlorophyll maximum is shallower due to the occurrence of cyclonic gyre inducing upward flow, showing that the meso-scale circulation patterns affect the spatial distribution of chlorophyll.

2.4.2 Coastal Waters

Coastal waters are subjected to the same seasonal cycles as the open ocean and, in temperate climates, the mixed layer may alternate between being shallow and deep in the same way as in open water (Mann and Lazier, 1996). However, what makes the coastal environment so different from the open ocean is its shallowness and the influence of freshwater run-off, resulting in complexities in water mixing, circulation, and primary productivity. A high level of mixing may occur throughout the water column as a consequence of the extension of the mixed layer to the bottom. Tidal currents, which create turbulence at the bottom boundary, are also significant, and where the depth is not too great in relation to the magnitude of the current, the mixing may extend to the surface. Therefore, nutrients accumulated at the sea bottom due to decomposition of detritus and dead biological materials can be recycled rapidly to the surface water for photosynthesis (Mann and Lazier, 1996).

Frontal zones between stratified and mixed waters can dramatically increase the primary productivity in a coastal environment. Such cases are located at the boundaries induced by strong tidal stirring over the shallow area (Fournier et al., 1984), and the stratified side that could be offshore water (Open University Course team, 1999), and the area influenced by freshwater run-off. Primary productivity is fuelled by recycled nutrients in the well-mixed region that are transported to the stratified side where phytoplankton cells in the upper layer are always exposed to sun light. A frontal system composed of surface water convergence from both sides toward the frontal boundary can induce phytoplankton patchiness along the boundary line

(Dustan and Pinckney, 1989). The tidal mixing front between coastal water and the open sea may last for several months, or seasons, whenever the thermocline in the open sea exists. It tends to disappear in winter, when winds are strong (Open University Course team, 1999) increasing the mixed layer depth. On the other hand, on a smaller scale the front between stratified estuarine water and coastal sea fluctuates in a tidal cycle. It emerges during flood tide when river and tidal flow are in opposition (Dustan and Pinckney, 1989), and disappears during ebb tide when tidal current moves in the same direction as the river flow. The distribution of phytoplankton will change in the same cycle as the formation of the front. It should be added here that small-scale patchiness of plankton in the coastal waters may occur because of wind-generated current called Langmuir circulations (Ledbetter, 1979). The patchiness in such a case occurs as bands parallel to local wind directions.

Freshwater run-off transports not only mineral, organic substances and nutrients from land to sea that support primary productivity (Chen et al., 2000; Yin et al., 2004) but also stabilizes the water column and induces estuarine circulation. Strong opposite flows between surface low saline and bottom high saline water generate turbulence. The resultant strong internal wave plays a significant role in estuarine ecosystems – inducing nutrients to be mixed into the surface water and increasing the phytoplankton residence time in the estuary (Mann and Lazier, 1996). Phytoplankton cells that are transported to the sea will sink but may return back toward land because of landward bottom currents. The plankton cells may be mixed up into surface water again due to strong turbulence, and have more opportunity to bloom in the estuary (Brandt et al., 1986). However, balance stratification in some areas is so delicate,

based on the freshwater-runoff and the mixing effects of tidal current, that it may develop and vanish during neap and spring tides, respectively. This situation, alternating between upwelling of nutrients and stratification, also provides conditions for very high primary production (Webb and D'Elia, 1980). Besides stratification and mixing, estuarine circulation may induce upwelling at the head of the bay supplying nutrients to the euphotic layer (Li et al., 2000). In some specific cases, such as in Saanich Inlet, tidal stress plays a significant role in triggering upwelling. Strong tide-generated mixing at the mouth of the inlet generates upwelling during the spring tide, resulting in high productive from spring throughout summer and early fall (Gargett et al., 2003).

2.5 Eutrophication

One of the serious environmental concerns is eutrophication in coastal waters. This condition can have significant effects such as massive blooms of phytoplankton, anoxic water, waste accumulation, and, in some cases, toxicity. Attempts have been made to minimize the attendant problems by controlling the discharges of organic and inorganic waters. However, side effects from inappropriate loading management might lead to a range of non-harmful to harmful phytoplankton species.

2.5.1 Definitions and Mechanisms

Eutrophication is defined as "*an increase in the rate of supply of organic matter to an ecosystem"* following Nixon (1995). The source of supply, referred as

organic carbon, may be an input of organic matter from outside the system (allochthonus source) or fixation by primary producers within the system (autochthonus source). Due to uncertainty about the amount of allochthonus inputs, and the fraction that is sufficiently unstable enough to be metabolized, we might consider the status of eutrophication from primary production in the system alone (Nixon, 1995). With this definition, trophic schemes in estuarine and coastal ocean ecosystems may be classified by the rate of organic carbon supply into the system (Nixon, 1995). They are oligotrophic, mesotrophic, eutrophic and hypertrophic conditions with the level of organic carbon supply in gC m^{-2} yr^{-1} of < 100, 100 – 300, 301 – 500, and > 500, respectively.

The most common cause of primary productivity stimulation in coastal environments is nutrient enrichment (primarily N and P) from anthropogenic practices (Andersen et al., 2006). Nitrogen and phosphorus emissions are mainly from fertilizer application (Barlow, 1963), aquaculture activities, livestock waste, domestic sewage, fossil fuel combustion (Smith et al., 1999), and also changing land uses. These excessive nutrients finally find the way to the sea through river discharge, ground water and atmosphere. They will promote the growth of primary producers in coastal ocean ecosystem such as phytoplankton or other algae, and then increase overall biomass of zooplankton and higher grazers. If productivity is much higher than grazing, excess plankton will die resulting in an accumulation of dead cells in the water column and sea bottom. Dissolved oxygen is consumed through bacterial decomposition leading to oxygen deficiency or anoxic conditions (Nagai and Ogawa, 1997). Recycling of nutrients from the decomposition process yields an internal source

of nutrients in the system leasing to a decrease in environmental quality. Highly eutrophic conditions can occur in restricted water such as lagoons (Buttermore, 1977) and estuaries that have very limited exchanges with the sea. Long flushing time of nutrient-enriched water in the area increases the opportunity for plants to grow and bloom. Anoxic condition, metabolic wastes and, in some cases, toxins (from harmful algal) will lower water quality and induce changes in structure and function of ecosystems (Wu, 1999) and mass mortality of marine organisms surrounding the area.

2.5.2 Impacts on Coastal Ecosystems

Occurrence of phytoplankton blooms is a competitive response of organisms when the environmental conditions have been adversely treated. Weak species might not tolerate low DO, high nutrient level and waste accumulation. On the other hand, the same conditions might favor some species and let them grow without other competitors. Eutrophication will decrease the number of species and abundances of various organisms, but increase the abundance of some specific species well adapted to the changed environmental conditions (Nagai and Ogawa, 1997).

Besides nutrient abundance, disturbance of nutrient structure might lead to other serious environmental problems. The coincidence of large fertilizer application and dam construction will rapidly lead to the enhancement of nitrogen in natural waters and decrease of dissolved silica resulting from land erosion and weathering. This compositional change might trigger blooms to have a succession of non-harmful algal to harmful algal phytoplankton species. Evidence points to this having occurred

in the northern Gulf of Mexico which is impacted by the Mississippi River (Parsons et al., 2002) and in the East China Sea close to the Yangtze River mouth (Wang, 2006).

Another case of nutrient structure modification is the reduction of phosphorus in natural water following measures to mitigate the problems of plankton blooms in the Seto Inland Sea, Japan (Yamamoto, 2003). Although this program was successful in decreasing the number of annual blooms from 300 cases in 1976 to 100 cases at present time, it has triggered a change in species composition from non-harmful diatoms to harmful dinoflagellates. In the case of harmful algal blooms, in addition to ecosystem collapse, residual toxic in marine life if consumed can be very harmful to human health. This suggests that it is necessary to understand the target ecosystem well before applying any measures to solve a specific problem relevant to eutrophication.

Benthic organisms may experience the greatest consequences of anoxic condition and waste accumulation at the sea bottom. A number of studies (Gacia et al., 1999; Bachetlet et al., 2000; Kraufvelin et al., 2006) have pointed out the occurrence of benthic community succession. Bivalves (Peterson et al., 1993), macroalgae (Peckol and Rivers, 1995) seagrasses (Greening and Janicki, 2006) and coral reefs, for example, have low survival rates under such an extreme condition. For benthic plants, dense concentration of plankton in the water column decreases light intensity available for photosynthesis. This adverse condition also has the same effect on zooxanthellae, a symbiotic algae living in coral cells, and thus interferes the coral growth (Bell, 1991). Corals are also destroyed by high sedimentation rate of dead phytoplankton. Moreover,

high nutrient concentration in water column favors macroalgae over corals, and the situation leads to succession from coral to macroalgae dominance (Bell, 1991).

2.6 Summary

Phytoplankton plays an important role as a primary producer of the world's oceans comparable to land primary production. Small in size but large in abundance, it is also believed to be a key role in atmospheric CO_2 regulation after physical processes of dissolution and sinking of dense surface water masses. This chapter has reviewed some of the dynamics of phytoplankton that profoundly relates to ocean circulations in all spatial and temporal scales.

Major limiting factors for phytoplankton growth in the open oceans are light and nutrient availability. Chlorophyll concentration in water column is high in spring because moderate stratification concentrates phytoplankton cells in well lit and fertilized layers. The concept of limiting nutrients is used to describe the patterns of phytoplankton distributions. Adding key nutrients by any processes into a marine ecosystem can stimulate massive growth of marine plants, mainly phytoplankton and algae.

The chapter has also reviewed eutrophication, which is the case of overgrowth of marine plants, which has a potential to make a wide range of ecosystem deterioration. It is obvious that increasing nutrient levels in coastal waters is a common cause of eutrophication. The source of the excess nutrients is typically anthropogenic. Several measures to reduce nutrient load into marine systems have been applied in

order to mitigate the problems relevant to this phenomenon. Unfortunately, this might bring more serious problems of harmful algal blooms as a result of changing in nutrient structures. The evidence suggests the importance of fully understanding functions and structures of the ecosystems before applying any regulations on the systems.

CHAPTER 3

SATELLITE REMOTE SENSING AND NUMERICAL MODEL FOR CHLOROPHYLL DISTRIBUTION

This chapter reviews the concept, theory and application of remote sensing technology and numerical models for the investigation of chlorophyll distributions in the ocean. The first section, which focuses on ocean color studies, starts with a discussion of optical properties of important constituents in natural seawater. This knowledge is then applied to algorithm development for chlorophyll estimation. The document also provides the philosophy of ocean color sensor designs, which are based, not only on the optical properties of water constituents, but also on atmospheric windows and atmospheric correction. Application of numerical models, another useful tool for environmental studies, is discussed in the second half of the chapter. This part explains the essential issues that need to be considered when applying ocean models to a study area. Finally concepts and applications regarding ecosystem modeling for investigation of chlorophyll distribution in the sea are presented.

3.1 Satellite Remote Sensing

Satellite remote sensing is beneficial for the studies of marine environment in many ways. It provides a rapid scan over large, or remote areas, that could not feasibly be surveyed from the surface. Further, a synoptic overview and clear demarcation of pertinent phenomena is possible. Once reliable calibration has been achieved,

measurement of marine parameters is possible without in situ sampling (Edwards, 2000). For ocean studies, visible reflectance energy has been applied to investigate chlorophyll-a (Yamada et al., 2004) and suspended sediment (Yates et al., 1993). Potential applications include coastal erosion (Kunte, 1994) and bathymetry (Leu and Chang, 2005). Emitted thermal radiation have been widely used for studying of sea surface temperature (SST) (Tang et al., 2002) while active RADAR, microwave imaging, is a useful tool for the detection of sea surface roughness and sea surface wind field delineation (Mondaldo et al., 2005; Kuo et al., 1999). A further application includes altimetry that can be used to estimate geostrophic currents in the ocean (Morimoto et al., 2002).

This first section emphasises theories and applications of satellite remote sensing for investigation of ocean color, especially chlorophyll-a distribution in the sea. It comprises three parts: optical properties of water and constituents namely phytoplankton, suspended sediment and yellow substance or dissolved organic material (DOM); empirical algorithms for chlorophyll-a estimation; and finally satellite sensors for ocean color studies.

3.1.1 Optical Properties of Water and Constituents

Compared to soils and vegetation, the magnitude of reflected energy from water is very small (Lillesand and Kiefer, 2000). Most of the energy is absorbed and transformed to heat (Robinson, 2004). In the ocean, absorbed energy is responsible for warm surface water and development of thermocline. Pure water reflectance is

determined from absorption and scattering throughout the invisible portion of the electromagnetic spectrum. Strong absorption occurs in all wavelengths except in blue-green (within 450 – 500 nm) (Smith and Baker, 1981; Pope and Fry, 1997). Unlike absorption, scattering is very high in the shorter, blue-green, wavelengths and exponentially decreases toward longer, red-infrared (red-IR), wavelengths (Robinson, 2004). Clear water appears blue because the absorption influence is very small in the blue-green where the scattering effect is moderate. Most light energy is absorbed while penetrating into clear water. Blue-green energy can penetrate deepest into the water column and scatter back to observers at the surface (Jensen, 2000). Reflectance in the ultraviolet range is small due to high absorption, although scattering is very high in this region. Both high absorption and low scattering of near infrared (NIR) energy are responsible for very low reflectance in this region. This fact is a useful basis for separation between land and water in remote sensing studies (Lillesand and Kiefer, 2000).

Spectral distributions are more complex when water has a significant cloud of suspended micro algae or phytoplankton. Pigments and structures of phytoplankton alter the spectral characteristics of pure water. Pigments such as chlorophyll-a, b, and c, carotenoids and biliproteins, are used either to capture light energy for photosynthesis or to provide a photoprotecting rather than photosynthetic role (Robinson, 2004). Individual extracted pigments have their own spectral absorption/reflectance features, but together, when with packing effects of pigments within phytoplankton cells (Kirk, 1975), tend to widen the absorption peaks. Algae-laden water will, however, still show a strong absorption feature at around 440 – 450

nm and a smaller one at around 650 - 670 nm, while over the rest of the spectrum, the absorption decreases with wavelength (Suzuki et al., 1998; Robinson, 2004). This suggests the role of chlorophylls, which are found in most phytoplankton species, in absorbing energy in the blue and green regions (*chlorophyll absorption bands* (Lillesand and Kiefer, 2000)).

Reflectance is highest in the 550 – 600 nm spectral range, and does not change due to chlorophyll variation. This is a region suited for calibrating empirical algorithms based on spectral ratios for chlorophyll estimation (Robinson, 2004). Pigments themselves do not scatter light, but the physical structure of the cells which are optically equivalent to particulate material does. Therefore, a reflectance peak around 690 – 700 nm appears due to an interaction of algal-cell scattering and a minimum combined effect of pigment and water absorption (Rundquist et al., 1996). It is important to add here that those spectral characteristics of algae-laden water vary with time and space due to phytoplankton populations and their physiological state (Sathyendranath et al., 2000) such as packing effect (Morel and Bricaud, 1981) and pigment composition (Bricaud and Stramski, 1990).

Some natural water might be mixed with non-biological suspended sediment (SS) resulting from re-suspension at the bottom due to strong mixing, river-borne particles, coastal erosion, dumping and dredging activities. Unlike phytoplankton, these particles do not absorb light strongly, but scatter quite intensely (Kirk, 1994). Complications are dependent upon particle shape, particle size distribution, and refractive index of each type of materials (Sathyendranath et al., 2000). Nevertheless, general patterns of the spectral distribution in several levels of suspended sediment

concentrations have been reported by a number of researchers (e.g., Chen et al., 1992; Mertes et al., 1993; Doxaran et al., 2002). Reflectance increases across the spectrum for increased sediment load. Maximum reflectance is located near 550 nm in moderate concentration, but it will move toward longer wavelengths, up to 720 nm, in very high concentrations (Robinson, 2004). In some cases, there is also another peak of reflectance near 830 – 850 nm (Arst, 2003).

The other significant constituent especially in coastal water is colored dissolved organic matter (CDOM), also known as yellow substance, Gilvin, or DOM. It is a group of complex organic compounds referred to as humic substances, and originates from the decomposition of plant tissues. They originate from leaching of soils and are transported to the sea by river water, or released from the decay products of dead phytoplankton cells, with a fraction derived from zooplankton grazing and excretion (Hu et al., 2006). Although the molecular weights vary from a few hundred up to the millions, the chemical structures are consistent (Kirk, 1994). They are categorized into humin, humic acid and fulvic acid following their molecular weights from large to small, respectively. Solubilities are also dependant on molecular weights: the smaller the molecular weights, the higher their solubility (Kirk, 1994). Optically, CDOM exhibits strong absorption in short-wave spectrum (blue), decreasing exponentially toward longer wavelengths (Robinson, 2004). Therefore, the reflectance characteristic of water with CDOM is low in the 400 – 500 nm region, increasing with longer wavelengths up to a maximum between 560 – 580 nm, then decreasing again toward longer wavelengths (red-IR) (Kutser et al., 1998). Decreases in reflectance in blue region are proportional to CDOM concentrations, and resulting in a yellow water.

If its source is terrestrial, there is a potential to use it as an indicator of freshwater influence in the sea, and hence an inverse measure of salinity (Ferrari, 1998).

Variations in abundance and proportion of each constituent discussed above result in complex spectral patterns. It is consequently difficult to specify which factors contribute to apparent color and subsequently to recover quantitative estimates of water content (Robinson, 2004). According to Morel and Prieur (1977), this leads to the definition of optical water types: *Case 1* and *Case 2*. Case 1 is applied to waters whose optical properties are dominated by only phytoplankton and their associated degradation products, more commonly deep ocean water, while Case 2 is defined for all situations other than this – e.g., the influence of land-derived SS and CDOM, most commonly associated with coastal environments. Therefore, remotely sensed data applied to chlorophyll distribution for Case 2 water must take such disturbances into consideration.

3.1.2 Empirical Algorithms for Chlorophyll Estimation

Two approaches used for chlorophyll-a estimation are empirical algorithms derived from spectral band ratios and semi-analytical techniques based on radiative transfer theory. Empirical algorithms are based on the relationship between chlorophyll-a concentrations and reflectance ratios measured synoptically. The method is straightforward, using regression-based analysis to convert reflectance to chlorophyll-a concentration. Although it is recommended just for Case 1 water, this method might be applicable for Case 2 in a particular place and time, but should not be

extrapolated to other locations or seasons without relevant in-situ observations (Robinson, 2004). The other approach, the semi-analytical technique, is a simulation of electromagnetic reflectance based on optical properties of several constituents found in the water column. The main idea is to balance the reflectance of simulation and measurement. When convergence of both values is achieved, the concentration of constituents comprising the model parameters will supposedly be identified. Theoretically it is more appropriate for Case 2 applications; however, computational methods based on the radiative transfer model are complex and also rely on in-situ sampling and measurement of specific absorption and scattering of water and each constituent. This issue will not be further discussed since it is beyond the scope of the study; however, more details can be found in IOCCG (2000).

Blue-green ratios are mostly used for constructing empirical algorithms for chlorophyll-a estimation because the blue region is very sensitive to chlorophyll absorption while the green-reflecting area is quite stable to chlorophyll variations. However, it should be noted here that phytoplankton absorption at every single wavelength in the visible domain can be parameterized as a function of the chlorophyll-a concentration (Bricaud et al., 1995; Cleveland, 1995). The reflectance ratios of 443/560, 490/560 and 520/560 nm are widely used for algorithm development. Some algorithms employ a fixed ratio, but some consider selection of these ratios based on chlorophyll-a concentration. Spectral sensitivity at the blue end is high in low chlorophyll concentrations, but when the concentration is high, the signal saturates. However, the reflectance in longer wavelengths is still sufficiently sensitive to distinguish variations in high concentrations (Kirk, 1994). The MERIS algorithm,

for instance, applies 443, 490, and 520 nm for ratios at chlorophyll concentrations of less than 1, 1 – 10 and more than 10 mg m^{-1}, respectively (Morel and Antoine, 2000). OC4 (SeaWiFS), OC3M (MODIS) and OC4-GLI are also based on ratio selection, but the criteria is different by picking up the highest reflectance instead of chlorophyll-a levels. This can be used because the changing of chlorophyll-a concentration is strongly related to absorption in blue region which has been previously discussed.

The relationship between reflected blue-green ratios and chlorophyll-a is non-linear. As a result the equations derived from regression analysis are, for example, exponential and polynomial. An algorithm might be as simple as a negative exponential function as shown in the equation below:

$$C = a R^{-b}, \qquad (3-1)$$

where C is chlorophyll-a, R is reflectance, and a and b are constants. This function has been applied for CZCS (Gordon et al., 1983). The following generation of algorithms such as OC2 and OC4 (SeaWiFS), OC3M (MODIS), MERIS-C and OC4-GLI used polynomial functions to fit the correlation (Pinkerton et al., 2005), where the general forms are as the follows:

$$\log_{10} C = A_0 + A_1 R + A_2 R^2 + A_3 R^3, \qquad (3-2)$$

or

$$C = 10^{(A_0 + A_1 R + A_2 R^2 + A_3 R^3)} + A_4, \qquad (3-3)$$

where A(s) are constants. The highest power of the equations might be 3, or 4. The equations are derived by fitting a function to the correlation of the dataset from many parts of the world gathered during the SeaWiFS Bio-Optical Algorithm Mini-Workshop (SeaBAM) in 1997 (O'Riley et al., 1998). Some algorithms such as those

reported in Michell and Kahru (1998) considered *ln* instead of log_{10}. The functions vary due to the data used.

3.1.3 Satellite Sensors for Ocean Color Studies

Satellite sensors with a capability of detecting electromagnetic energy in visible and near infrared spectrum are usually suitable for chlorophyll estimation. Their suitability depends on the spectral resolution of the sensors being fine enough and located in spectrum regions suitable to detect chlorophyll response. CZCS, OCTS, SeaWiFS, MODIS, MERIS and GLI are major sensors that have been widely used for ocean color studies (e.g., Kasai et al., 1998; Sathyendranath et al., 2001; Darecki and Stramski, 2004), and some of their specifications are summarized in Table 3 – 1. The following is a review of the characteristics of sensors designed particularly for ocean color studies.

CZCS is the first sensor for ocean color study developed by NASA operated between 1978 and 1986. Its data were used to produce the first global map of ocean surface of phytoplankton pigment index (illustrated in e.g., Mann and Lazier, 1996). Bandwidths in visible spectrum were between 10 and 20 nm, and those in NIR were from 20 up to 200 nm (Figure 3 – 1). NIR bands were added to address issues related to atmospheric correction (Gordon, 1997). Because CZCS was designed for chlorophyll mapping in the world's oceans, the spatial resolution and swath width designed to be large enough to achieve this. Although there were some issues such as

Table 3 – 1 Characteristics of selected ocean color sensors

Sensor	CZCS	OCTS	SeaWiFS	MODIS	MERIS	GLI
Platform	Nimbus-7	ADEOS-1	OrbView-2	EOS	Envisat	ADEOS-2
Agency	NASA	NASDA	OSC/NASA	NASA	ESA	NASDA
Country	USA	Japan	USA	USA	Europe	Japan
Altitude (km)	955	804.6	705	705	800	803
Resolution at Nadir (km)	0.825	0.7	1.1	1	1.2/0.3	1/0.25
Swath (km)	1566	1400	2800	2330	1150	1600
Recurrent period	6 days	41 days	16 days	16 days	35 days	4 days
Global coverage	No	3 days	2 days	1-2 days	3 days	3 days

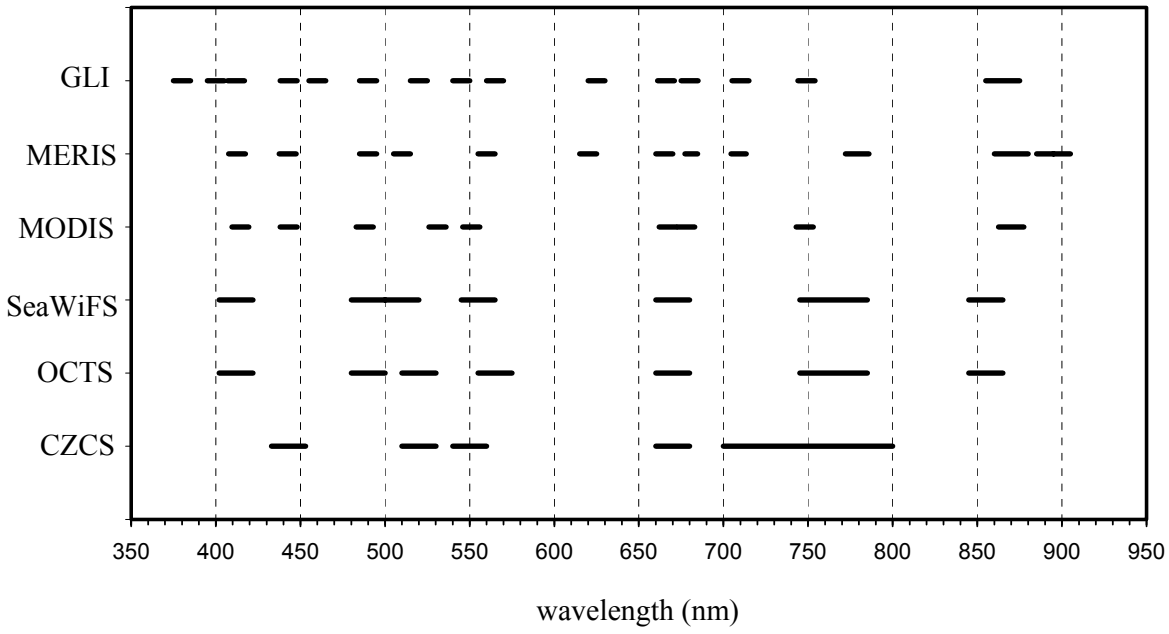

Figure 3 – 1 Channel positions of various ocean color sensors

unreliable radiometric calibration (IOCCG, 1998), experience from CZCS experiments has provided valuable knowledge for the improvement of following sensor designs.

The position of bands is considered from the sensitivity of reflected energy on water constituents and atmospheric windows. Figure 3 – 1 indicates that many sensors have a band center at 443 nm which corresponds to a phytoplankton absorption feature. The bands at 490 and 520 nm were assigned as options to detect chlorophyll variations when the signal at 443 is saturated (Werdell and Bailey, 2005). A channel at 555 or 560 nm is used for normalization purposes in most algorithms intended for chlorophyll estimation. Longer wavelengths in green are not suitable due to strong atmospheric absorption of water vapor between 567 and 637 nm (IOCCG, 1998).

The centers of NIR bands (700 – 900 nm) for atmospheric correction are intended for subtraction dark pixel. Well-designed sensors include at least two channels for initializing the values for extrapolation to estimate aerosol optical thickness from NIR to visible spectrums (Gordon, 1997). Some sensors have added a violet channel at around 412 nm for CDOM detection. Commonly, chlorophyll and CDOM both absorb blue energy, and it is impossible to separate them from each other in this spectral region. Fortunately, for shorter wavelengths in the violet region, chlorophyll absorption tends to decrease while CDOM still exhibits very strong absorption (Bricaud et al., 1981). It might be beneficial to use this fact to distinguish between these two components.

In terms of spectral resolution, the specification discussed above is sufficient for chlorophyll estimation using empirical algorithms. Nevertheless, extra channels are required for greater accuracy by methods employing semi-analytical approaches based

on radiative transfer theory. Modern sensors such as MERIS (Doerffer et al., 1999) and GLI are also designed for this purpose.

Modern sensor design has improved the signal to noise ratio (S/N), with the reduction of noise equivalence radiance to values of 0.05 or less (IOCCG, 1998). Internal radiometric calibration is also very effective. The spatial resolution of a sensor might be varied for multi-purposes – coarse mode for open ocean and fine mode for coastal areas (e.g., MERIS). Global coverage of the orbiting platforms is from 1 to 3 days (Table 3 – 1) which is suitable for observing many ocean phenomena. Since spectral and radiometric resolutions of most sensors are appropriate for chlorophyll estimation and atmospheric correction, temporal and spatial resolutions become more important in consideration of a suitable sensor for each study area.

3.2 Numerical Models

Computer modeling of circulation for diagnostic and prognostic purposes has been used for oceanographic studies. The diagnostic model operates under the condition that some parameters such as salinity and temperature are fixed. However, both parameters are freely adjusted, while running, to external and internal forcing in the case of the prognostic model. A modeling approach is beneficial for testing the concept of complicated systems when relevant factors have been assigned. Once calibrated results have been achieved, the system might be applied to the analysis of phenomena of interest and applied for prediction purposes.

3.2.1 Modeling Considerations

All ocean circulation models are based on the conservation of mass (continuity) and Newton's laws of motion. Unlike for atmospheric modeling, the continuity equation applied to ocean circulation is based on the property that water is incompressible. Equations may have many forms, but here they are presented in Eulerian aspects of differential equations in Cartesian coordinates. The general form of the equation of motion is illustrated as Eq. (3 – 4) while the continuity equation as Eq. (3 – 5). (adapted from Neumann and Pierson (1966)).

$$\frac{\partial \vec{V}}{\partial t} + (\vec{V} \cdot \nabla)\, \vec{V} + 2\vec{\Omega} \times \vec{V} = -\frac{1}{\rho} \nabla P + \vec{F} + \vec{D}, \qquad (3-4)$$

$$\nabla \cdot \vec{V} = 0, \qquad (3-5)$$

where $\vec{V}$ is velocity and the first term on the left hand is the local change of velocity with time (t). The following term is the nonlinear field acceleration, and ∇ is defined as $\frac{\partial}{\partial x} + \frac{\partial}{\partial y} + \frac{\partial}{\partial z}$. x, y and z are Cartesian coordinate components: x is positive toward the east, y the north and z upward. The third term is the Coriolis acceleration where Ω is the angular velocity of the earth rotation (7.29×10^5 $\sec^{-1}$). The first term on the right-hand side is the pressure gradient where ρ and P are water density and pressure, respectively. The minus sign takes care of the fact that the force is directed towards the region of lower pressure. $\vec{F}$ and $\vec{D}$ represent external forces and diffusion, respectively. The external forces might be tidal and wind stresses, for example.

Finally, the continuity equation (Eq. (3-5)) suggests that the net flows in all directions are zero to conserve mass in a defined static volume.

Other governing equations might be included when the density driven force is important. The advective-diffusive equations (Eq. (3-6) and (3-7)) of potential temperature and salinity, which are the most significant controls of water density, are included in the circulation model. However, it also needs an equation of hydrostatic approximation (Eq. (3-8)) to convert salinity and temperature into density which is then substituted into the momentum equation (Eq. (3-4)).

$$\frac{\partial T}{\partial t} + (\vec{V} \cdot \nabla)\, T = \vec{F}_T + \vec{D}_T, \qquad (3-6)$$

$$\frac{\partial S}{\partial t} + (\vec{V} \cdot \nabla)\, S = \vec{F}_S + \vec{D}_S \qquad (3-7)$$

$$\frac{\partial p}{\partial z} = -\rho g\,. \qquad (3-8)$$

Here T and S are temperature and salinity, respectively. $\vec{F}$ and $\vec{D}$ are also referred to external forcing and diffusive terms. The external forces of the temperature equation might be solar radiation and sensible heat flux of air-sea interaction while those of salinity are evaporation and precipitation.

Model forcing can be categorized into two types: barotropic and baroclinic. In barotropic model, high-speed waves such as tidal sea surface elevation and storm surges are the main driving forces. Circulation due to slow changing parameters such as density adjustment is neglected, and the current profile becomes independent of the depth of the water column (Kantha and Clayson, 2000). Therefore, a two-dimensional model based on vertically integrated equations of motion is adequate to reproduce the

barotropic phenomena in such a case. On the other hand, a three-dimensional baroclinic model is necessary when the large, quasi-permanent ocean currents due to slow speed adjustment of internal gravity are dominant. Simulation timescales of both model types have to be different due to their wave speeds. Low speed baroclinic movement requires a longer time period to exhibit noticeable change. This is not the case of fast barotropic waves where changes can be observed over a short time period. In addition, the time-step of model operation in the latter case must be small to maintain stability while a large time-step is permitted for long timescale running of baroclinic model simulation. Historically, to save computational time and limitation of computer resource, it was necessary to compromise between the barotropic and baroclinic models most suitable for each study area.

Two other issues relevant for model forcing are rigid rid (fixed surface) and free surface model conditions. The rigid rid is for baroclinic forcing dominance. Fast-moving barotropic external waves are suppressed to maintain model stability due to long timescale and long time-step operation. The very first rigid rid model (also the first ocean circulation model) was presented by Bryan (1969) in the study of the circulation of the world's oceans. On the other hand, if fast-moving waves such as storm surges and tides are dominant, a two-dimensional free surface model will be a better choice for such simulation. However, limitations arise when both barotropic and baroclinic conditions prevail. Selection of just a rigid rid or a free surface model is not an effective way to address such a situation. Although different speed waves could be included, it is computationally intensive. Small time-steps are required to keep models stable due to barotropic forces, and also long timescale of operation is always needed

to see the change of baroclinic influences. Therefore, a model splitting technique was developed to circumvent this severe limitation. The technique splits computation of fast-barotropic mode with short time-step from slow-baroclinic mode. The success of applying this technique with more detail could be found in several studies (e.g., Blumberg and Mellor, 1987; Higdon, 1999).

Significant driving forces are unique in each study area. The strong variability of synoptic winds has to be included in computations for modeling coastal sea. In some areas close to the river mouths, forcing from buoyancy differences generated by salinity gradient of freshwater and seawater becomes significant in controlling density-driven circulation. Tidal stress exerts a strong effect on mixing processes in a shallow sea, while it can be ignored in an ocean model having a great depth. Wind stress might play insignificant roles in the case of large-scale ocean modeling when the horizontal density gradient is a strong dominant factor. Therefore, some ocean models (Bryan, 1969; Semtner and Chervin, 1992; Semtner, 1995) do not include the surface mixed-layer in computation. Surface heat fluxes, in terms of shot-wave radiation and air-sea exchange, are very crucial to global ocean circulation. However, they might be disregarded in the case of a shallow, coastal sea modeling especially when the study area is located in tropical zones.

Another important issue is geographical projection which is related to horizontal grid design. Coordinate systems generally used in ocean models are based on rectangular Cartesian, spherical coordinate, cylindrical coordinate, and orthogonal curvilinear coordinate (Kantha and Clayson, 2000). The rectangular Cartesian system is applicable for working on small areas or those close to the equator to reduce error

from grid spacing distortion. On a global scale, this problem is minimized by employing a spherical coordinate system. By using this system, the computational grid size along the latitude is adjusted to be smaller while moving from the equator to the poles. The cylindrical coordinate system might be more suitable for polar ocean model. To date, the orthogonal curvilinear coordinate in horizontal has become more popular due to its flexibility to be modified to fit the shape of computational area. Several studies have applied this coordinate system (e.g., Murray and Reason (2001); Lutjeharms et al. (2003)).

The last issue for model consideration is the vertical coordinate and vertical grid application for three – dimensional models. Normally, the vertical axis is initiated at the sea surface – positive upward and negative downward – but vertical grid spacing might be specified in different ways. There are three choices to be considered – z – layer, sigma (σ) layer, and isopycnal layer. Vertical layers are divided equally in the case of a z – grid which has been applied among pioneer ocean models. Bottom-following, sigma coordinate vertical grid is very useful for simulation of circulation in coastal areas because the computational layer can be adjusted to fit the bottom topography, which is necessary to accommodate bottom boundary conditions. The Princeton Ocean Model (POM) (Blumberg and Miller, 1987) is an example where this vertical coordinate system has been applied successfully. Lastly, the isopycnal layer model is developed in order to depict interior mixing which primarily occurs along isodensity surfaces in the deep ocean, where preservation of water mass characteristics are essential. Some such applications can be found in Bleck and Smith (1990).

3.2.2 Lower Trophic-Level Ecosystem Model

Investigation of chlorophyll distribution using lower trophic-level ecosystem models is an alternative synoptic approach for marine ecosystem study. The mechanism of chlorophyll distributions and significant controlling factors might be clarified by model functions and components if the model is validated. This section addresses the concept of lower trophic-level ecosystem modeling, the design of model systems, and provides examples of some works using ecosystem model for the study of phytoplankton distribution.

Lower trophic-level ecosystem modeling is an attempt to simulate phytoplankton, or chlorophyll, dynamics by using computer techniques. It might be better to start with the dynamics of conservative substances in order to use this concept to explain the dynamics of chlorophyll, which is a non-conservative material. After release, a conservative substance will be transported by currents generated by tide, wind, density different and etc., a process called *advection*. It will be dispersed by *diffusion* processes initiated by eddies and turbulence from surface and bottom frictions while being transported. The speed of diffusion rate is expressed by eddy diffusivity (Yanagi, 1999). Based on the conservation of mass, only physical processes such as dilution, advection and diffusion that influence the concentration of a conservative substance, and original form, is not transformed into others. Conversely, in addition to physical processes, chlorophyll or phytoplankton will be modified by biological and/or chemical processes. Phytoplankton might increase into the water

column due to growth and reproduction and decrease due to mortality and being grazed by zooplankton while displacement is occurring. The processes are also dependent on environmental conditions and other living species in the ecosystem.

Simulation designs can vary from simple, with a few components, to highly complex, with many interdependent compartments. Each component can be expressed mathematically to explain and control variability and their relation to both environmental and other components. For example, variation in phytoplankton, zooplankton and nutrients might be written into conceptual equations as follows (adapted from Onitsuka and Yanagi, 2005):

$$\text{Phytoplankton} = \text{Advection} + \text{Diffusion} + \text{Photosynthesis} - \text{Grazing} - \text{Mortality (P)} \quad (3-9)$$

$$\text{Zooplankton} = \text{Advection} + \text{Diffusion} + \text{Grazing} - \text{Mortality (Z)} - \text{Urine} - \text{Faece} \quad (3-10)$$

$$\text{Nutrient} = \text{Advection} + \text{Diffusion} + \text{Mortality (P)} + \text{Mortality (N)} + \text{Urine} + \text{Faece} - \text{Photosynthesis} \quad (3-11)$$

These simple equations provide the whole concept of how the ecosystem model works. All components are related, and changing any of them will influence others. They are also relevant to environmental factors such as the case of photosynthesis which is a function of light, nutrients, salinity and temperature. The grazing rate of

phytoplankton is dependant on grazing ability and amount of food (phytoplankton) in that water column. Other components are also interrelated and controlled by environmental factors via unique functions (Yanagi et al., 1997). Mathematical expressions applied in this study might be a good example of an ecosystem model, which will be detailed in Chapter 7. What we should keep in mind is that the best model is not necessarily the most complex one, because such a model also needs a large number of inputs, some of which are unavailable. Moreover, complicated mathematical functions require high computer performance that can be very problematic especially in the case of the coupling operation of circulation and ecosystem models.

The simulation can be approached in three ways – box model analysis, computational grid methods by taking circulation field into consideration in stand-alone ecosystem model, and circulation-ecosystem coupling models. For box model analysis, the whole system might be designed in only one box, or several boxes, due to water density layer, salinity gradient and characteristic of topography. It is usually used in time series analysis of the changing in designed system (Nurdjaman and Yanagi, 2002). In the case of stand-alone ecosystem models, computational domains are divided into several spatial grids over the study area, and circulations including other physical parameters are included in the computation as separated inputs. This is unlike the coupling model where the ecosystem and the circulation modules are run simultaneously (Kawamiya and Oschlies, 2003). The coupling model has allowed exploration of a range of physical-biological interactions in the ocean (Franks, 2002); however, it requires compatibility and also needs greater computer performance. The

latter two techniques will provide not only temporal, but also spatial changes in the parameters and the processes of interest.

Examples of ecosystem application are presented as follows. One of the most basic models, termed nutrient – phytoplankton – zooplankton (NPZ) provided by Frank et al. (1986) can reproduce the occurrence of spring bloom but in the case that there is no light limitation and no variations in mixed layer depth. It is too simple to describe the real mechanism of lower grazing ecosystem, although it approximates the idea how the model is designed and works. Miller (2004) pointed out the importance of constants and initial parameters of this model that are critical to the results if those values are changed. Evan and Parslow (1985) developed a model that included the effects of light intensity and variations in mixed layer depth but it still has three components like the Frank et al. (1986) model. This model can establish seasonal cycles of bloom, and the magnitude of the bloom cycle is dampened when the variations in mixed layer depth are eliminated. The response of high grazing rate is a flattening of magnitude and variations in phytoplankton population without any bloom. This supports the theory explaining the absence of blooms in many oceanic areas (Miller, 2004). Later ecosystem models (e.g., Frost, 1993; Kawamiya et al., 2000; Walsh et al., 2001; Yanagi et al., 2001a) are much more sophisticated and complicated, most of them integrating details of nutrient types (e.g., NH_4^+, NO_2^-, NO_3^-, PO_4^{3-}), plankton species, and hydrodynamical conditions (e.g., temperature, salinity, water mixing, circulation).

3.3 Summary

This chapter has provided concepts, theories and application of satellite remote sensing and modeling in order to investigate chlorophyll distribution in the sea. The optical properties of chlorophyll and other constituents are somewhere unique, and they are used for algorithm development in order to investigate those components in seawater. However, the spectral signals are complex when there are many water constituents mixed in different portions in the water column. This leads to the difficulties of using remote sensing reflectance to distinguish one constituent from others. The spectral design of most ocean color sensors takes this knowledge into consideration together with atmospheric windows and atmospheric correction. While spectral and radiometric resolutions are appropriate for chlorophyll estimation, temporal and spatial resolutions become important in consideration of an appropriate sensor applied for each study area.

Numerical modeling is a very powerful tool used for the studies of ocean circulation and phytoplankton dynamics. Nevertheless, to apply a model, careful considerations in nature of model and relevant parameters must be ensured. Environmental studies using computer modeling nowadays are becoming increasingly sophisticated due to rapid increase in computer performance and improvement of numerical technique. Ecosystem modeling is an example of one useful application for the study of the dynamics of chlorophyll distribution which is a non-conservative material in the sea.

CHAPTER 4

THE UPPER GULF OF THAILAND

The first part of this chapter describes general characteristics of the upper Gulf of Thailand. Previous investigations of oceanographic condition, circulation, eutrophication and phytoplankton bloom are then reviewed and discussed. The second half of the chapter presents some results from field observations as the distributions of temperature, salinity, chlorophyll-a, SS and CDOM in order to provide a general background of oceanographic conditions during the study period.

4.1 General Characteristics and Previous Investigations

The upper Gulf of Thailand is located in tropical region at 13^{o} N and 100^{o} E. It is surrounded by land along the eastern, northern and western boundaries, and opens to the lower gulf in the south (Figure 4 – 1). The approximate square - like area is approximately 10^{4} km^{2}, with an average and maximum depth of 15 m and 40 m, respectively, with larger depth in the east (Silpipat, 1987). Four main rivers – the Maeklong, the Thachin, the Chaopraya and the Bangpakong – discharge freshwater into the head of the gulf from west to east, correspondingly. The entire area is influenced by the two-inverse monsoon system; the northeast (November to January) and the southwest (May to August) monsoons, owing to the imbalance of land mass in the two hemispheres which is the unique characteristic of Asia (Snidvongs, 1998). The northeast wind brings cool and dry air from Siberia while the west to southwest winds

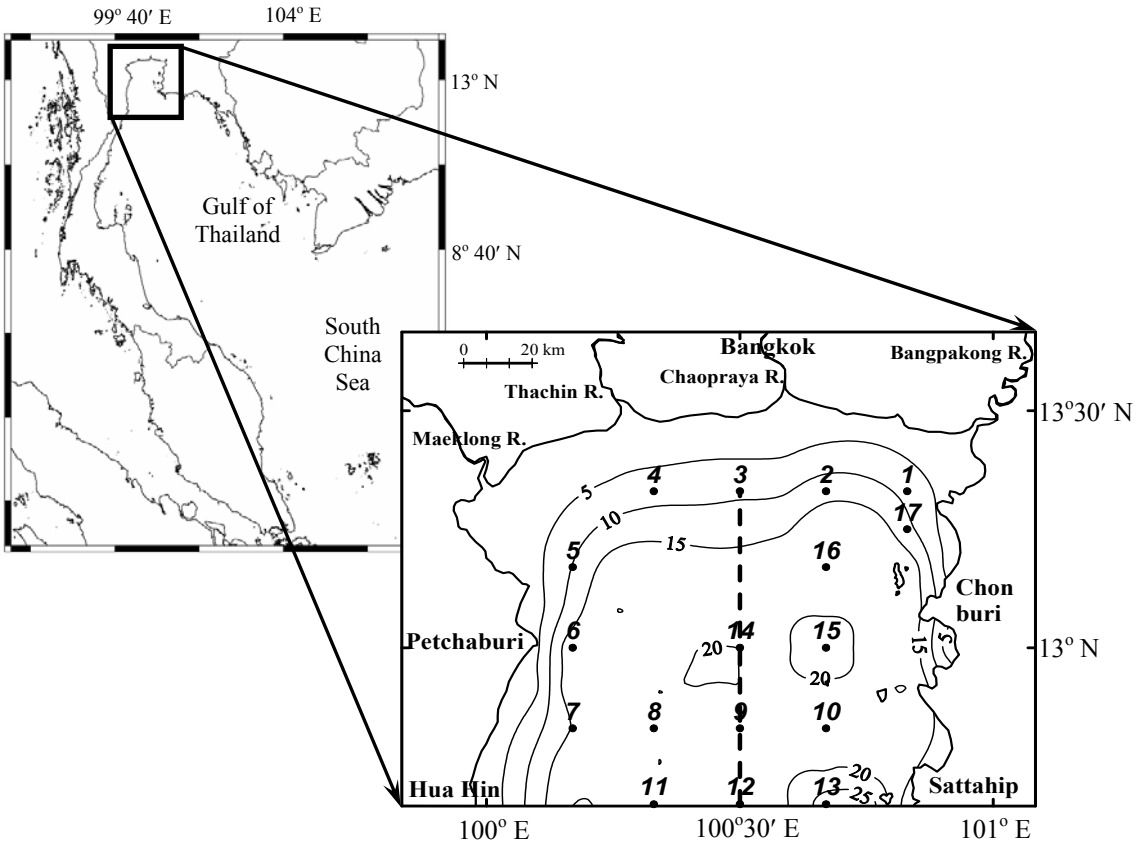

Figure 4 – 1 The upper Gulf of Thailand. Contour lines represent water depth in meters and dots stand for observation points for optical and oceanographic data collections. The broken line is the main axis for vertical distributions of temperature and salinity.

bring moist and warm air from the Indian Ocean into the region (Sojisuporn, 1994). However, heavy rain and tropical storms are predominant when low pressure fronts move northward (May to June) and southward (August to November) over the country. Rainfall measured at Bangkok station in those phases could be as high as 400 – 500 mm a month while little to no precipitation falls in the dry period from December to February (data source: Meteorological Department).

Variations in freshwater discharges are very large following the monsoon. Average discharges of the Chaopraya river can reach the highest peak of over 2,500 m^3s^{-1} in October and drop down to around 300 m^3s^{-1} in March and April (Figure 4 – 2). This variation consequently leads to a wide range of average salinity between wet and dry seasons while water temperature around 27 - 32 C^o is consistent all year round. Stratification in the water column was also observed during wet periods (Bunpapong and Piyakarnchana, 1987). The occurrence of such seasonal changes was found from the river mouth (Buranaprathepprat and Yanagi, 2003) to the middle of the upper gulf (Bunpapong and Piyakarnchana, 1987). With the determination of freshwater and seawater interactions, we may consider the whole area to be an estuarine system especially during the wet season.

Many studies have described the effect of the monsoon winds on the circulation patterns in the upper Gulf of Thailand. NEDECO (1965) first found that seasonal salinity distributions response to local wind patterns and amount of river discharges, and suggested counter–clockwise and clockwise circulation in the northeast and the southwest monsoons, respectively. Neelasri (1981) measured current profiles at 8 stations around the upper gulf in March and April 1979 which is the

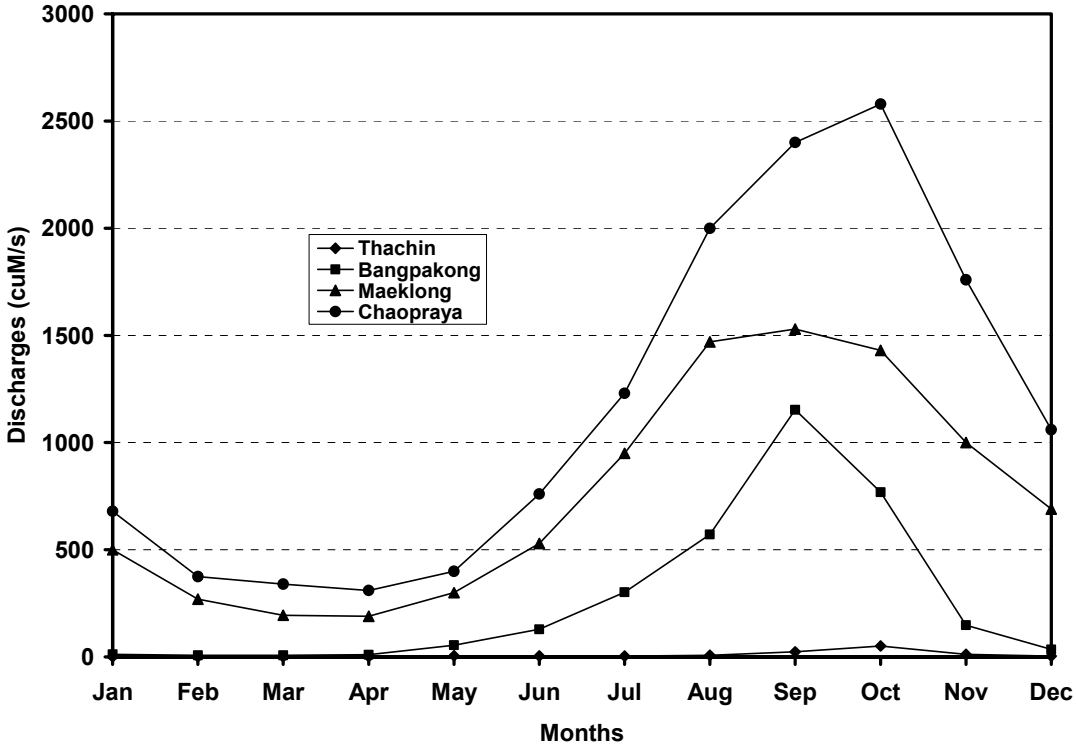

Figure 4 – 2 Monthly averaged discharges of four main rivers in the upper Gulf of Thailand (Data sources: Thailand Irrigation Department; Snidvongs, 1998; Buranapratheprat et al., 2002)

transition period of the northeast and the southwest monsoons. The development of an Ekman spiral could be seen from current profiles. It is responsible for clockwise circulation, related to the wind field from southeast direction. The results also revealed variations in vertical current speeds suggesting the importance of three-dimensional current structures. Subsequently, a two-dimensional model was used to investigate general circulation and found the same seasonal patterns as those of previous studies (Buranapratheprat et al., 2002a). However, a barotropic model such as the one used is limited in that it cannot include some forcing such as buoyancy force and pile up effect. It becomes necessary to apply a three–dimensional model to study current profiles for more realistic results, especially when the water column forms layers during the wet season.

Rapid development in areas bordering the upper gulf and population growth have resulted in pollution and deterioration of the quality of the marine environment. Mostly untreated waste waters from domestic and industrial sources are discharged directly to canals and main rivers (Cheevaporn and Menasveta, 2003), and finally to the upper gulf which is the first area to receive those pollutants before they are transported farther out to the lower Gulf. The most conspicuous and widespread impact on the marine environment is perhaps eutrophication due to very high loading of inorganic nutrients and an increased biological oxygen demand (BOD). Accumulation, resulting in high BOD concentration in the inner gulf was reported (Chongprasith and Srinetr, 1998). Such conditions favor massive blooms of phytoplankton resulting in adverse effects on marine ecosystem, coastal aquaculture,

local and national economies. Continual increase in nutrients and organic supply forces the blooming to be more intense than previous experienced.

Occurrence of red tides in the upper gulf has been investigated. The study during 1991 – 1994 found that the most important causative organism is a green phytoplankton, *Noctiluca scintillans*, and its blooming often occurred during July to October and December to February in the eastern and the western parts of the gulf, respectively (Lirdwitayaprasit et al., 1994). Competitive blooming of *Ceratium furca* was also often observed in the vicinity of the river mouth (Rungsupa, 1997). Recent investigation in the Bangpakong estuary, located in the northeastern coast of the upper gulf, revealed 18 plankton blooms during the study period – June 2003 to November 2004 (Lirdwitayaprasit et al., 2006). Among them, 14 blooms occurred during May and October, which is the period of rainy season or the southwest monsoon. Moreover, a report based on data collected by PCD during 1992 – 1995 illustrated that intense blooming happened more often in the eastern coast than in the western coast (Chongprasith and Srinetr, 1998). The Bangpakong River, which is located there, is the least polluted of the four major rivers flowing into the upper gulf (Hungspreugs et al., 1989; source data: PCD). All the occurrences suggest that there must be other processes (e.g., oceanographic conditions) besides the river load contributing to the blooms.

Excluding phytoplankton species, seasonal distributions of chlorophyll-a, a proxy of phytoplankton abundance, in the whole upper Gulf area have not been synoptically clarified. With advantages of satellite remote sensing and numerical

modeling, this study will investigate the spatial and temporal variations including the factors of concern to the phenomena.

4.2 Field Measurements and Distributions of Water Properties

The distributions of temperature and salinity based on field observations are presented and investigated. The discussion is mostly focused on spatial and temporal changes to properties that are related to variations in environmental factors. The final part illustrates the surface distribution of chlorophyll-a, SS and CDOM which will be used for thorough discussion in subsequent chapters.

4.2.1 Field Observations

All field data have been provided by Department of Marine Science, Chulalongkorn University, Thailand. The properties of water on optics, physics, chemistry and biology were collected at 17 stations covering the entire gulf (Figure 4 – 1). Due to size of the area of interest, it was necessary to take 3 – 4 days to complete a field operation. There were 6 cruises altogether starting from October 2003 to July 2005 (Table 4 – 1).

Salinity and temperature were also probed in-situ employing a CTD while water samples for chemical and biological analyses were collected using a Vandorn water sampler. Some water samples were immediately filtered onboard and then stored in a freezer for further analyses in the laboratory. Different types of filters were

Table 4 – 1 A list of cruises for oceanographic observations

Cruise name	Date
CU – 1	9 – 11 Oct 2003
CU – 2	4 – 6 Dec 2003
CU – 3	13 – 15 Jan 2004
CU – 4	12 – 15 May 2004
CU – 5	7 – 10 Oct 2004
CU – 6	26 – 28 Jul 2005

applied for each purpose – GF/F filters for chlorophyll-a analysis, and Millipore filter for SS and CDOM analyses. Fluorescence method was applied for chlorophyll-a measurement while simple subtraction weight of the filter after and before filtration was utilized for SS analysis (Strickland and Parson, 1972). Chlorophyll-a was extracted from the filter remnant after adding 90 % acetone, stirring vigorously, and centrifuging at 3,700 rpms for 5 minutes. The mixed solution was extracted and measured for chlorophyll-a by using a fluorometer. For SS, the filtered papers were dried at 70 ^{o}C in an oven for a several hours and then placed in a desiccator overnight. This process was repeated until a stable weight of the filters was achieved. Subtraction of the filter after and before filtration was reported as SS weight per water volume. CDOM was measured from filtrated water as light absorption coefficient (A(λ)) per length (cm) (k) from 300 to 700 nm using 10 cm cell on spectrophotometer, but its amount is reported as k (412). Part of the water samples are kept in plastic bottles and then placed in the freezer for further analysis of nutrients (ammonia, nitrate, nitrite,

silicate and phosphate) in the laboratory with the use of Skalar automated nutrient analyzer.

4.2.2 Local Wind Fields

Monthly mean winds of QScatt data (http://www.ssmi.com) in the same time of field observations are illustrated in Figure 4 – 3. Wind fields in October 2003 and 2004 are almost identical, coming from the east with little tendency to the northeast. The dominant direction changes to northeast-north in December 2003. The speed slacks with changing direction to southeast in the following month (January 2004). It is obvious that wind directions have a tendency to change clockwise with time. This shifting could be sensed in May 2004 and June 2005 which is during the southwest monsoon as well. Winds in both months have almost the same magnitude and come from southwest, but the direction in May has a trend of a more southern angle.

4.2.3 Temperature and Salinity Distributions

Horizontal distributions of sea surface temperature and salinity of all cruises are exhibited in Figures 4 – 4 and 4 – 5, respectively. Seasonal changes in surface temperature limit ranges for 26 ^{o}C in January and 31 ^{o}C in May 2004, following the seasonal temperature in wintertime and summertime, correspondingly. Low salinity of 22 psu appears close to western shoreline in October 2004 while the maximum value of about 33 – 34 psu is observed near the mouth of the Gulf in July 2005. These phenomena are clearly controlled by seasonal variability in the amount of freshwater

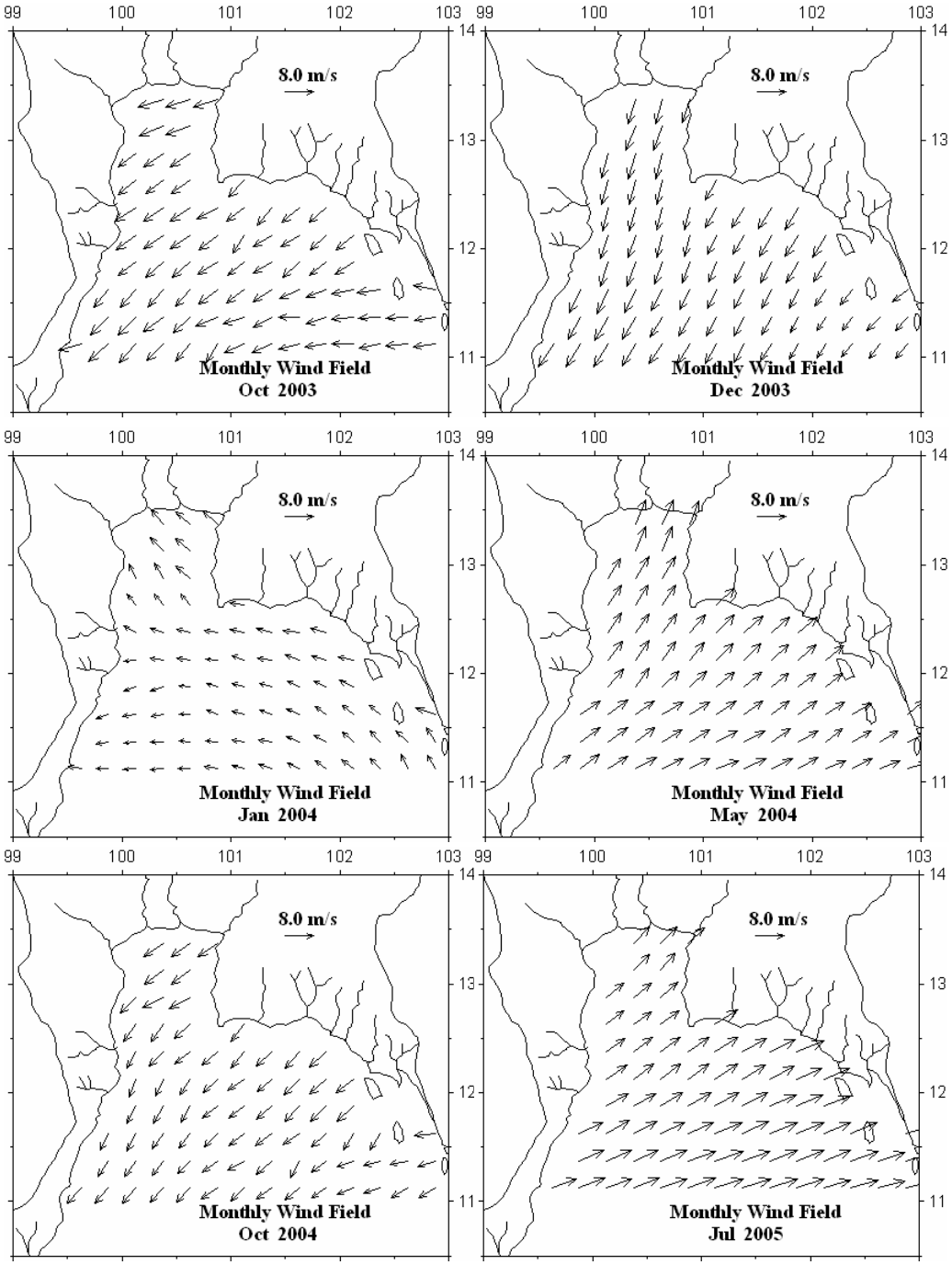

Figure 4 – 3 Monthly mean wind fields of QScat data (http://www.ssmi.com) in October 2003, December 2003, January 2004, May 2004, October 2004 and July 2005

discharges and also water stratification (more discussion in the following T-S diagram). In terms of spatial variation, the salinity gradient (7 – 9 psu) of horizontal distributions from the northern coast toward the sea boundary is largest in October. Temperature does not show such distinction and its spatial difference greater than 1 ^{o}C is hardly seen in any observations across the Gulf.

Horizontal distributions of both temperature and salinity also reveal seasonal changes in contour patterns that might be related to local circulation and interaction with water from the lower Gulf. Temperature contours in the northern area trend to the west or counter-clockwise in October 2003 and 2004, January 2004 and July 2005 (Figure 4 – 4). The trends of temperature distribution in other months are unclear; a northward warm water intrusion around southeastern area in December 2003 and northeastward penetration in the west of the sea boundary in May 2004 are observed. However, movement of salinity distributions could be found in every cruise. Contours in the central and northern areas bend to the west in October 2003 and 2004, January 2004 and October 2004 in the same way as temperature contours, while those in May 2004 and July 2005 clearly move eastward or northeastward (Figure 4 – 5). Higher salinity water penetration similar to that of from the west of the sea boundary could be observed in May 2004. Nevertheless, instead of intrusion along the east coast similar to the temperature distribution, there is evidence of saline water flowing northward through the middle sea boundary in July 2005.

Seasonal circulation might be assumed from consideration of the patterns of wind fields (Figure 4 – 3), surface temperature (Figure 4 – 4) and surface salinity

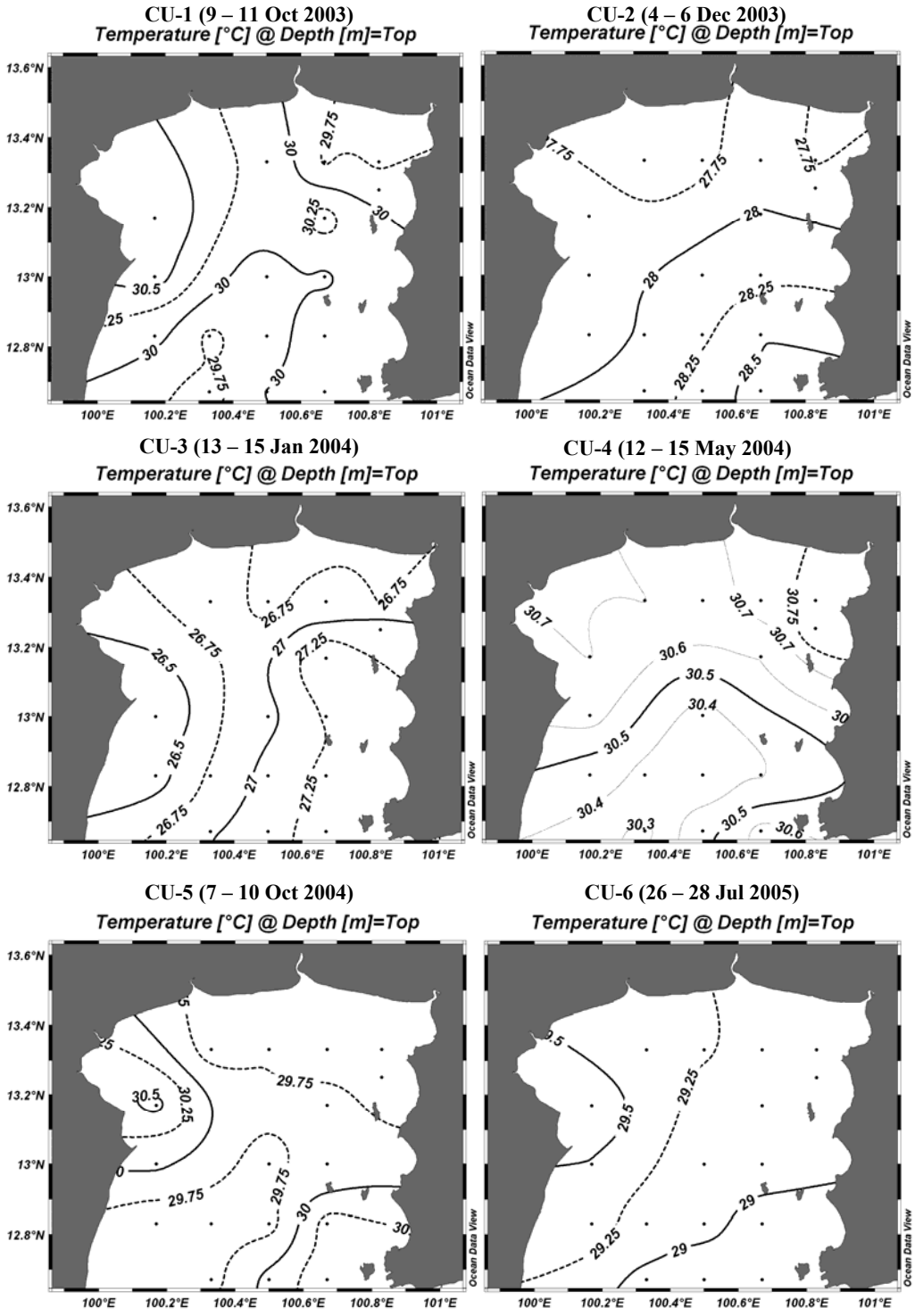

Figure 4 – 4 Horizontal distributions of sea surface temperature of all cruises

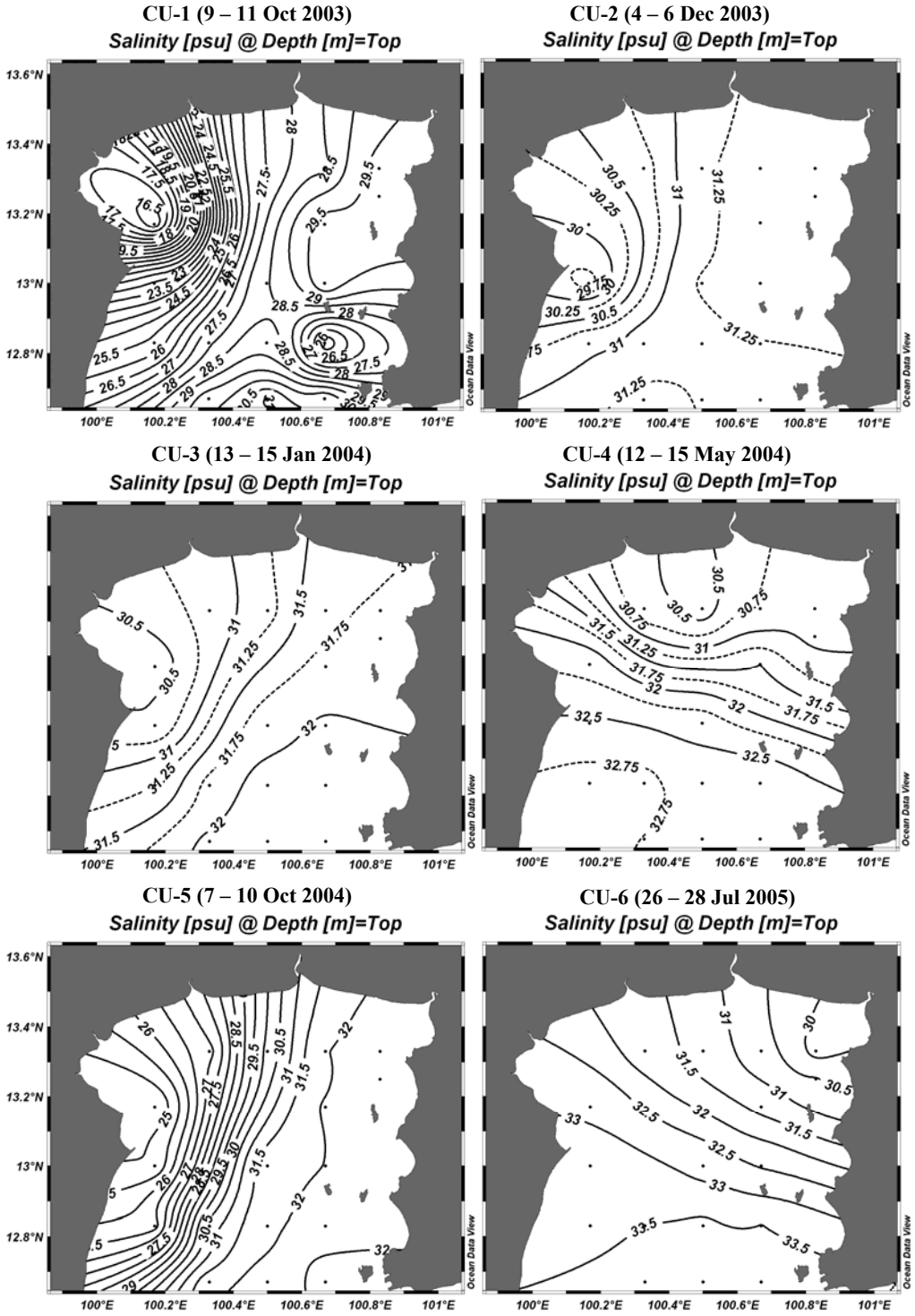

Figure 4 – 5 Horizontal distributions of sea surface salinity of all cruises

distributions (Figure 4 – 5). Counter-clockwise circulation has developed in October 2003 and 2004, Dec 2004 and January 2004 while clockwise circulation was characteristic of May 2004 because of the tendency of water to move downwind, corresponding to the temperature and salinity contour. However, an interesting phenomenon occurred in July 2005 when temperature and salinity contours show opposing directions of movement – clockwise and counter-clockwise for salinity and temperature, respectively. In terms of circulation, they might follow the salinity patterns that correspond to local wind directions. Moreover, salinity has been demonstrated to be the most influential control of water density in this estuarine area (Buranapratheprat et al., 2002b), and water density patterns are usable for water mass tracking. Therefore, it could be assumed that clockwise circulation might develop during this time. The reason why surface temperature contours show the opposite trend of movement is still unclear but possibly come from the interaction with offshore water from the lower gulf.

Temperature and salinity data along the main axis shown in Figure 4 – 1 are also plotted in the form of vertical distribution contours to investigate seasonal variations in water stratifications (Figure 4 – 6 and 4 – 7). Stratification develops during the wet season - October 2003 and 2004, and July 2005. Well – mixed conditions happen in December 2003 and January 2004 due to low freshwater discharge and low surface temperature leading to comparatively large influences of wind and tidal stresses. These mixing factors occur all year round, but in the wet season they do not have enough energy to disrupt water stratification which is very stable at this time (Yanagi et al., 2001). Transitional change between stratified and

well-mixed conditions was detected during cruise CU – 4 (May 2004), at the onset of the rainy season. At this time, the water column in the area close to the river mouths is stratified while it is well-mixed in the southern area around the mouth of the gulf. Vertical distributions of salinity suggest that the upper gulf be categorized as stratified estuary in wet season (October 2003 and 2004, and July 2005), well-mixed estuary in dry season (December 2003 and January 2004) and partially mixed estuary in transition period between the seasons (May 2004).

Seasonal changes of water masses in the gulf could be investigated through the use of T-S diagram (Figure 4 – 8). Large range and low temperature (26 – 28 ^{o}C) water masses appears in December 2003 (CU – 2) and January 2004 (CU – 3) corresponding to spatial differences in temperature of water mass near the northern coast which is influenced by land temperature and that near the sea boundary in the south (Figure 4 – 4). Temperature ranges are quite large in those months due to the difference in heat carrying capacity between land and water. The land is cooler and warmer than water in winter and summer, respectively. This also explains the case of the large summertime temperature gradient in May 2005 (CU – 4). The salinity gradient is very large in October 2003 and 2004 (CU – 1 and 5) and small in December 2003 (CU – 2) and January 2004 (CU – 3). These phenomena are easily explained by seasonal variations in river discharges emptying into the head of the upper gulf – larger discharges always create higher salinity gradients.

Vertical distributions of salinity and T – S diagram disclose the influence of high salinity (32 – 34 psu) intrusion from the lower gulf in all seasons even in October

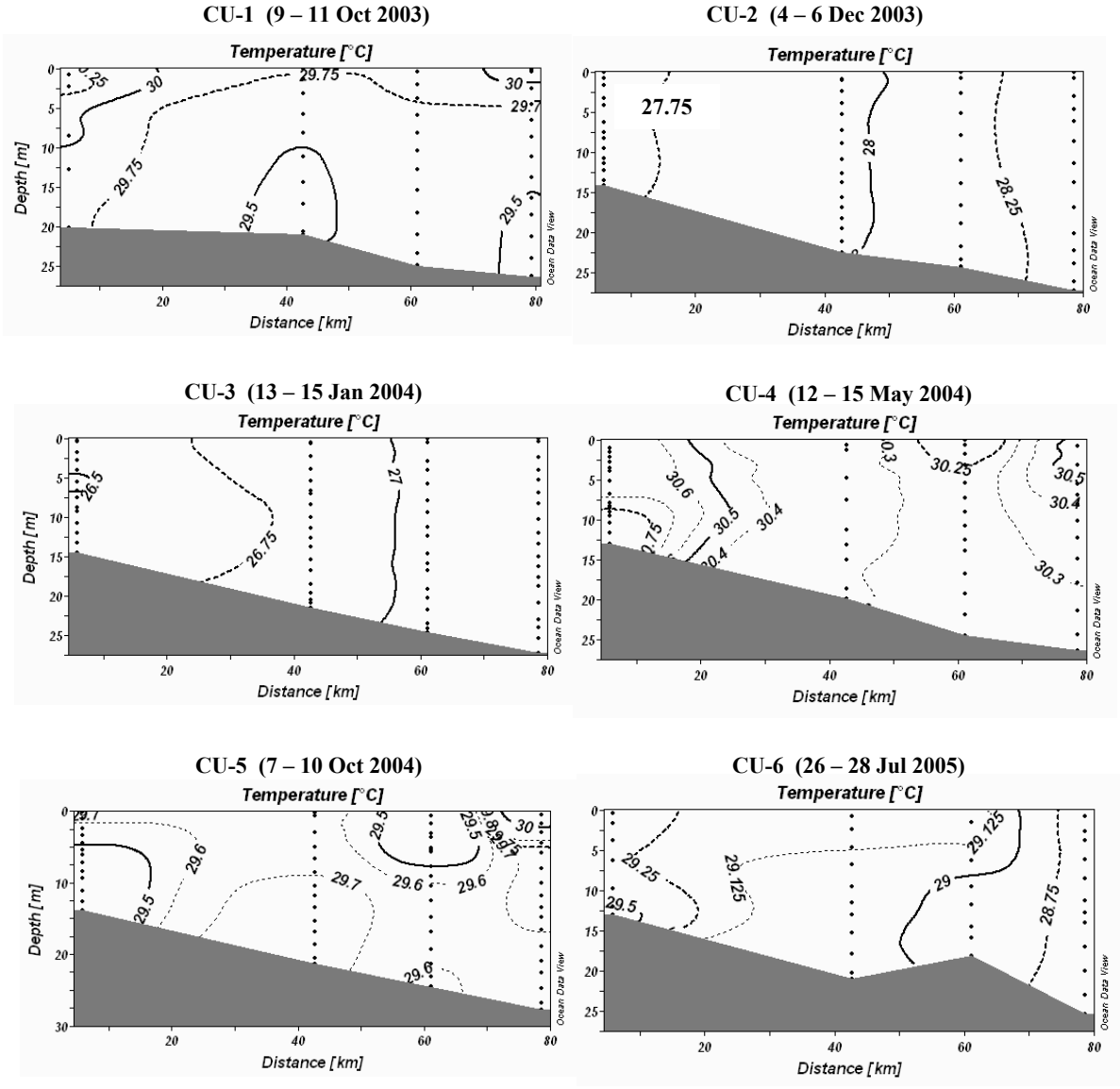

Figure 4 – 6 Vertical distributions of temperature along the main axis of all cruises

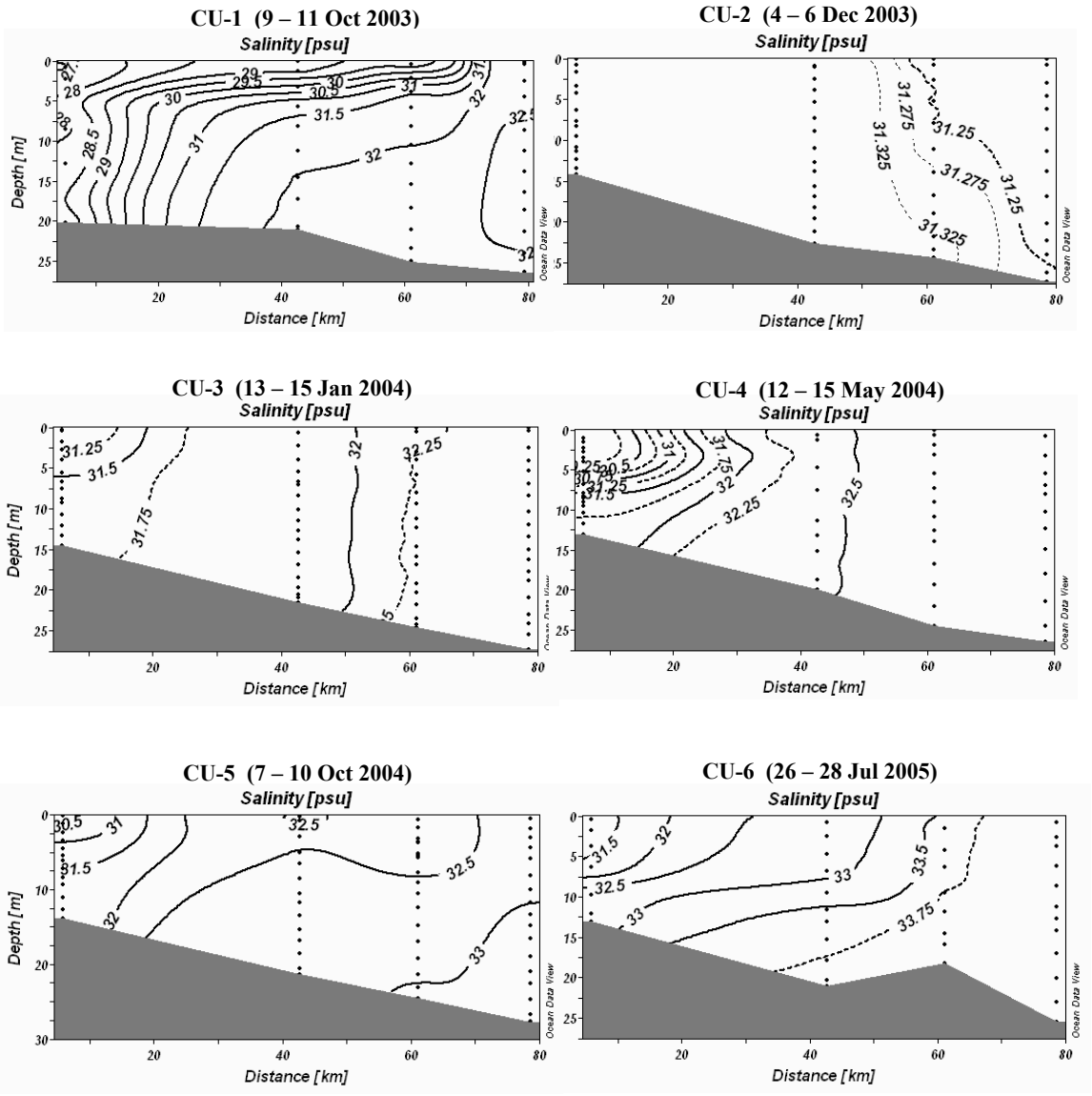

Figure 4 – 7 Vertical distributions of salinity along the main axis of all cruises

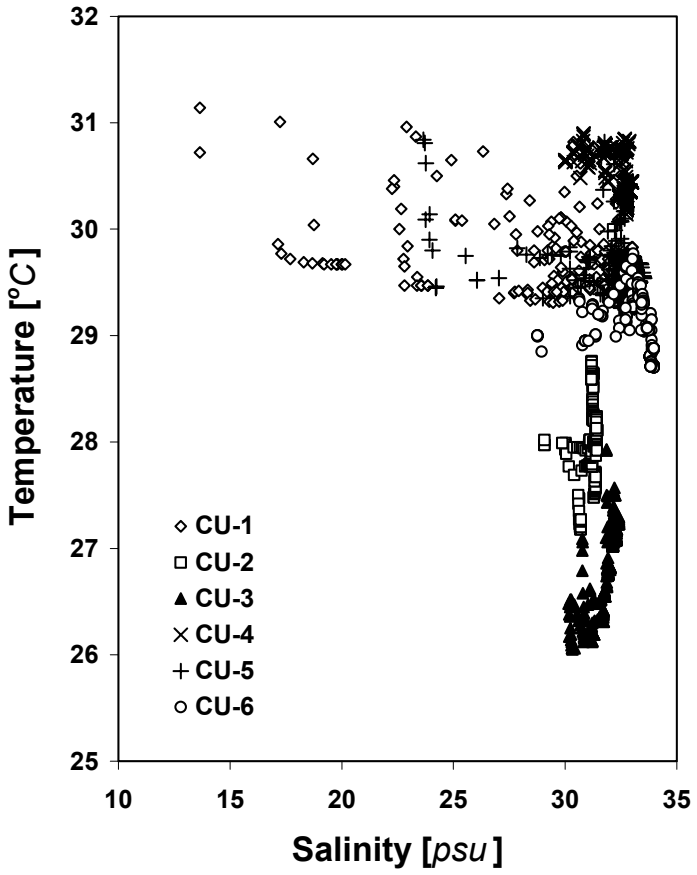

Figure 4 – 8 T-S diagram from the data of all cruises

when river discharges are very large. However, stratification also plays a significant role in controlling salinity in the water column. This was observed by comparing the results of January 2004 and July 2005. Maximum salinity emerges in July instead of January although discharges in January are smaller than those in July. A well-mixed condition in January is responsible for seawater dilution despite small freshwater inputs. Conversely, salt water intruding northward from the lower gulf is well preserved near the sea bottom due to strong stratification. The salinity is still high because there is no chance of dilution by low salinity water floating on the sea surface in July.

4.2.4 Surface Distributions of Water Constituents

The distribution of chlorophyll-a, SS and CDOM at the sea surface are presented in Figure 4 – 9, 4 – 10 and 4 – 11, respectively. Seasonal movement of their distributions corresponds to salinity contours (Figure 4 – 5) resulting from the influences of river discharges and local wind fields. It is noticeable that high concentrations are located downwind in all cruises. However, processes controlling the distribution of these components are more complicated than those of salinity and temperature as a consequence of non-conservative behavior. Although, the trend of movement is the same in October of both years, the concentration of chlorophyll-a in 2003 is considerably larger than that experienced in 2004. This suggests that the year-to-year variability of high concentrations due to phytoplankton blooms happened in 2003 but not in 2004. It is quite complicated and difficult to explain this phenomenon

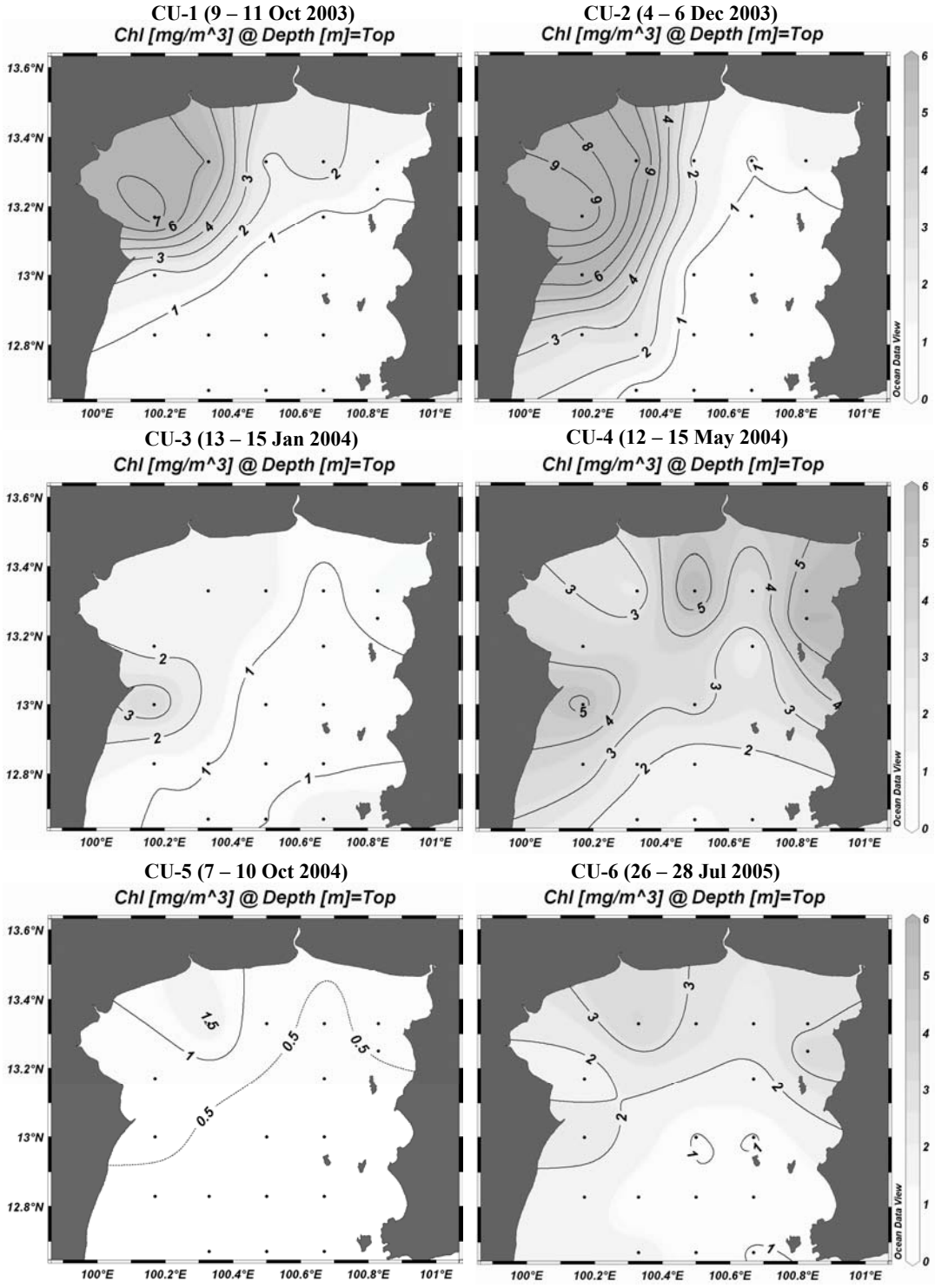

Figure 4 – 9 Horizontal distributions of chlorophyll-a at the sea surface of all cruises

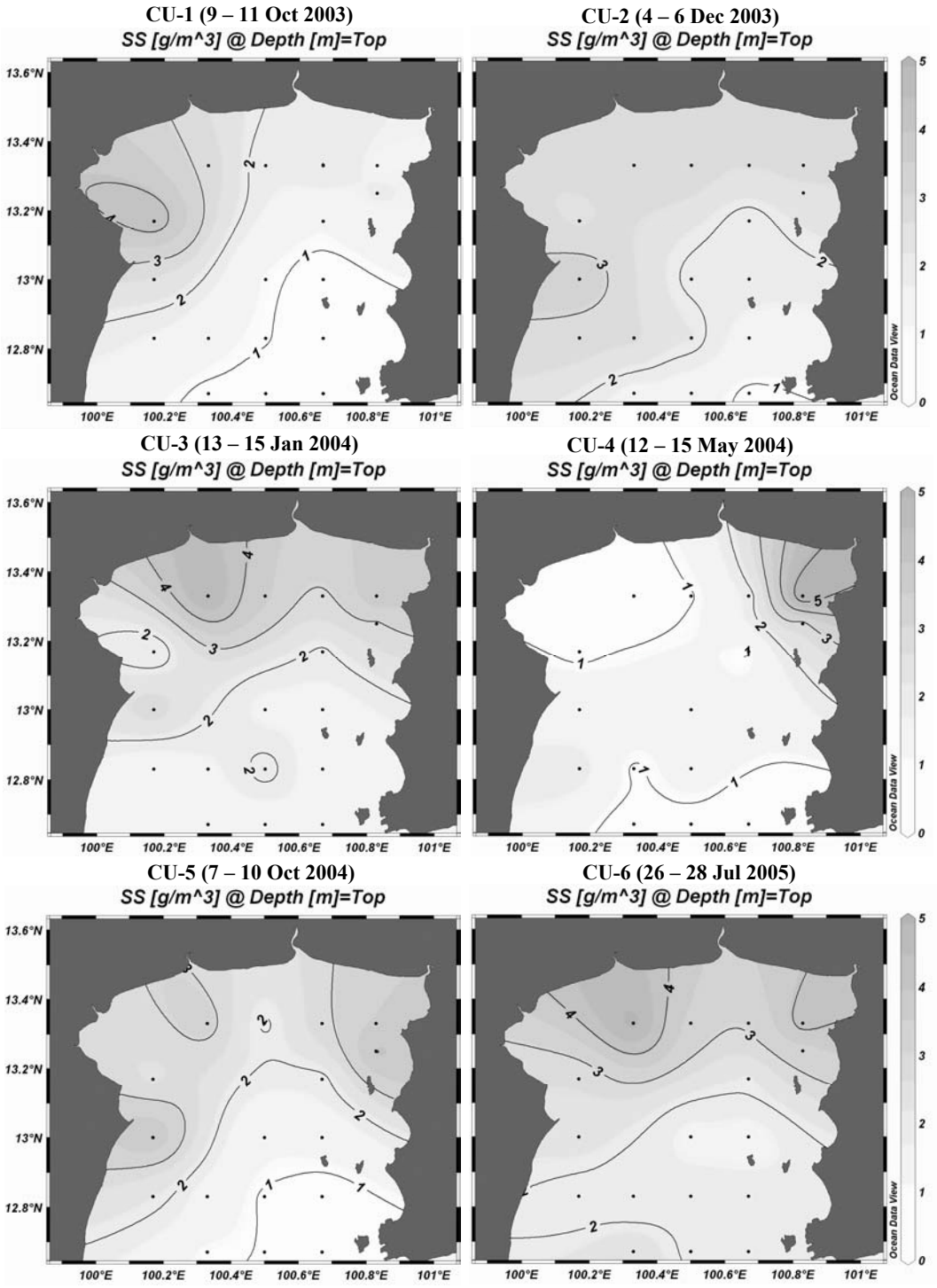

Figure 4 – 10 Horizontal distributions of suspended sediment at the sea surface of all cruises

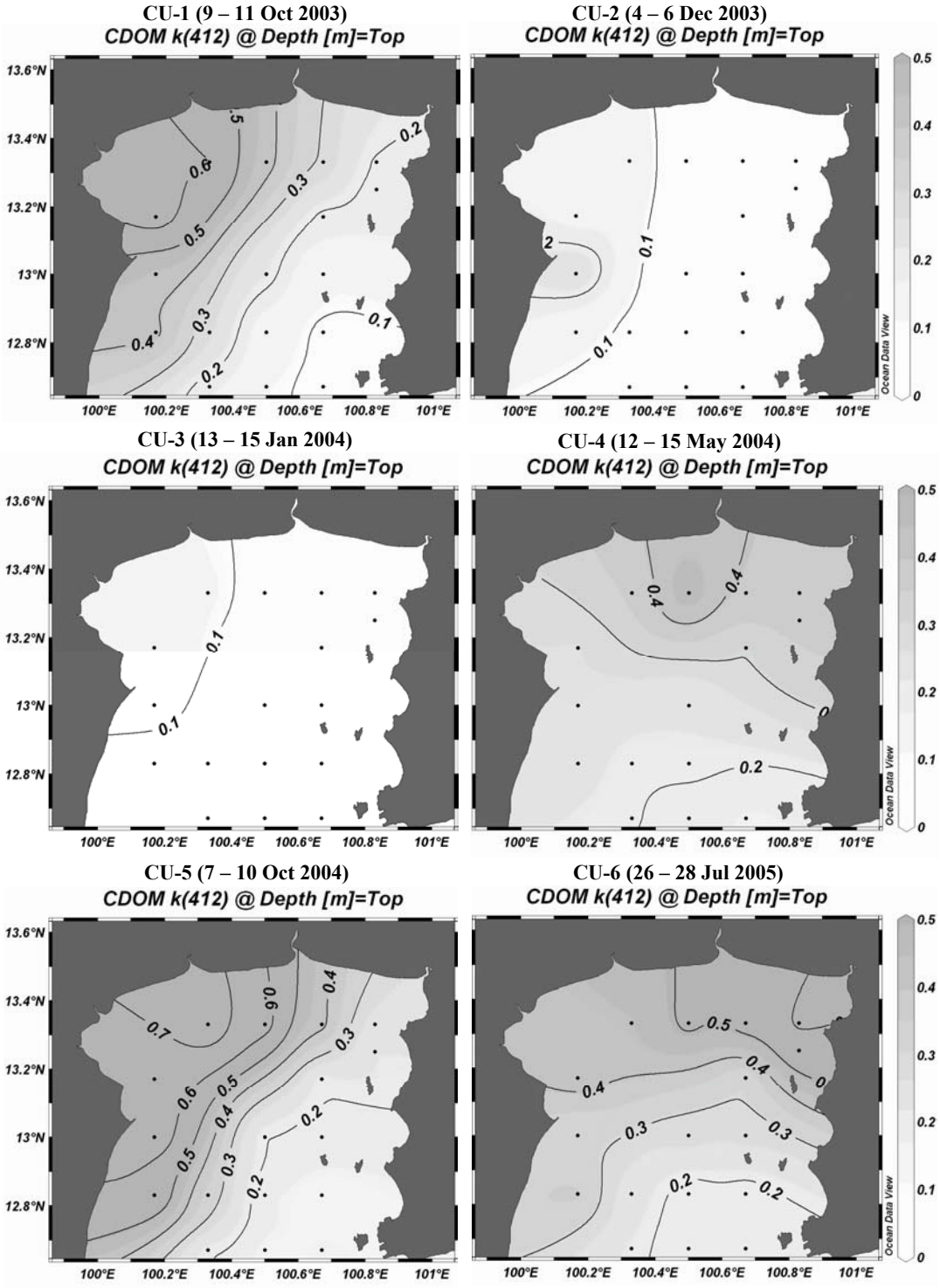

Figure 4 – 11 Horizontal distributions of CDOM at the sea surface of all cruises

because there are many relevant factors involved. More discussion about seasonal variations in chlorophyll-a distribution is included in Chapter 5 and 7. It should be noted that SS and CDOM distributions will not be discussed further due to the scope of the study, but they are used for discussion about chlorophyll-a retrieving by using MERIS data in Chapter 5.

4.3 Summary

This chapter reviewed the general characteristics of the upper Gulf of Thailand which is a small coastal sea located in tropical zone. In spite of its shallowness, water stratification could be observed when river discharges are very large. Due to intense interaction of sea water and freshwater, the upper gulf might be categorized as an estuarine system. Seasonal variation in wind fields and river discharges are large because the area is located under the influence of the two inverse-monsoon system. These factors undoubtedly influence variations in oceanographic conditions, circulation and eutrophication in the entire area. Horizontal distributions of surface salinity disclose seasonal circulation patterns corresponding to variations in local wind fields. Stratification of the water column could be studied from vertical distributions, and the results suggest strong stratified and well – mixed water column during wet and dry seasons, respectively.

Surface distributions of chlorophyll-a, SS and CDOM also reveal their seasonal movement as a consequence of wind fields likewise salinity distributions. However, while the study is focused on chlorophyll-a distribution, its controlling factors are

more complicated than salinity and temperature due to its non-conservative behavior. Variations in surface chlorophyll-a distribution will be investigated and further discussed in Chapter 7 which is relevant to lower-trophic level ecosystem model.

CHAPTER 5

MERIS IMAGERY FOR CHLOROPHYLL DISTRIBUTIONS

This chapter, which is the first of three main results, is concerned with the application of MERIS data for chlorophyll-a estimation. The MERIS sensor was selected because of its spatial resolution (300 m in full mode), which is a suitable for a smaller study area, while spectral resolutions were appropriately designed for chlorophyll detection. The chapter highlights the necessity for algorithm development for chlorophyll-a estimation, especially for the study area. Work is based on the relationship between chlorophyll-a data and reflectance ratios, a local algorithm is developed, tested and applied to the MERIS data.

5.1 Material and Methods

Optical and chlorophyll-a data from 17 stations (Figure 4-1) from cruises CU-1 (October 2003) to CU-6 (July 2005) are applied for algorithm development. Downward irradiance (E_d) and upward radiance (L_u) were measured in situ by using a Profiling Reflectance Radiometer model 600 (PRR-600). The instrument is capable of measuring profiles with 7 channels, each of which has 10 nm bandwidth (Table 5-1). Due to surface roughness, values just below sea surface (*Ed* (0-) and *Lu* (0-)) were consequently obtained by extrapolating data from 1-5 m depth (Matsumura et al., 2006). Then, remote sensing reflectance (R_{rs}) just above the sea surface is defined as Eq. (5-1).

Table 5 – 1 Summary of the capabilities for electromagnetic detection of PRR – 600 and MERIS in visible region

PRR - 600		MERIS in visible region	
Band center (nm)	**Bandwidth (nm)**	**Band center (nm)**	**Bandwidth (nm)**
412	10	412.5	10
443	10	442.5	10
490	10	490	10
520	10	510	10
565	10	560	10
-	-	620	10
670	10	665	10
683	10	681.25	7.5

$$R_{rs} = 0.519 \frac{L_d(0-)}{E_d(0-)} \qquad (5-1)$$

Chlorophyll-a measurements, described in Chapter 4, are used in both regression analysis for algorithm development and validation. SS and CDOM data are not included in computation but are taken into consideration in the process of algorithm improvement.

The developed algorithm is applied to chlorophyll-a estimation of MERIS Level 2 (L2) products. These data have been atmospherically, radiometrically and geometrically corrected (Antoine and Morel, 1999). Although band centers in visible regions of MERIS are not exactly the same as those of PRR-600, the bandwidth of 10 nm of most channels provides sufficient overlap (Table 5-1). They are, therefore, assumed to be equivalent, and algorithms developed by using in situ reflectance data measured by PRR-600 could be directly applied to MERIS data without any modification. This assumption is tested in section 5.5.

There are two chlorophyll-a products included in MERIS L2 namely algal_1 and algal_2. Algal_1 is estimated using empirical algorithm (MERIS-C) applied to normalized water reflectance after atmospheric correction (Morel and Antoine, 2000), while algal_2 is based on a radiative transfer model derived by using a neural network algorithm (Buckton et al., 1999). SS and CDOM are other outcomes of the latter method and also included in the L2 product. Both chlorophyll-a products will be evaluated and then compared with estimated results of new algorithm developed from this study. All satellite images are processed with Basic ERS & Envisat (A)ATSR and MERIS (BEAM) software provided by European Space Agency (ESA).

The coefficient of determination (R^2) from the regression analysis is used to assess the most suitable function representing the relationship between chlorophyll-a and reflectance ratios. The standard error of estimate (S_{est}), as defined by Eq. (5 - 2), is used for evaluation of chlorophyll-a estimated by the new algorithms and also MERIS chlorophyll products.

$$S_{est} = \sqrt{\frac{\sum (X_{cal} - X_{obs})^2}{n-2}}, \qquad (5-2)$$

where X_{cal} and X_{obs} are calculated and observed values respectively; and n is the number of observations. The sample correlation coefficient (R) is sometimes used for investigation of the relation between two parameters. All statistical analyses are carried out using SPSS and Microsoft Excel software.

5.2 Evaluation of MERIS Algorithms

The empirical algorithm of the MERIS algal_1 product, based on an exponential – polynomial function of R_{rs} ratios (Eq. (5 – 3)), is tested for its reliability for the study area. R_{rs} and constants in calculation process are switched following the level of chlorophyll-a concentrations.

$$C_a = 10\,\hat{}\,(a_0 + a_1 R + a_2 R^2 + a_3 R^3 + a_4 R^4 + a_5 R^5)\,, \qquad (5-3)$$

$$R = \log_{10}\left[\frac{R_{rs}(\lambda_0)}{R_{rs}(560)}\right],$$

$C_a < 1$; $\lambda_0 = 443$ nm; $a = [0.2115, -1.844, 1.282, -2.747, 2.865, -1.204]$,

$1 < C_a < 10$; $\lambda_0 = 490$ nm; $a = [0.3866, -2.626, 2.572, -7.156, 10.15, -6.895]$,

$C_a > 10$; $\lambda_0 = 510$ nm; $a = [0.3900, -3.864, 3.168, -20.33, 63.21, -113.9]$.

Here C_a is chlorophyll-a concentration (mg m^{-3}); λ is wavelengths; and a_x are arbitraries. Observed R_{rs} ratios are processed to get chlorophyll-a concentrations which are then verified with the data from field observations.

Results indicate an extreme over estimation (Figure 5 – 1) of some of the data (8 out of 101) which are greater than 100 mg m^{-3}. Those errors increase the predicted average up to 6,979.05 mg m^{-3} while that of the field measurement is as low as 1.71 mg m^{-3}. Correlation coefficient of 0.05 reinforces the poor relationship between both datasets. S_{est} is as large as 6.88×10^4.

Overestimation is initiated from the functions applied to transform R_{rs} ratios to chlorophyll-a. Simulated chlorophyll-a values are large when the R_{rs} ratios approach

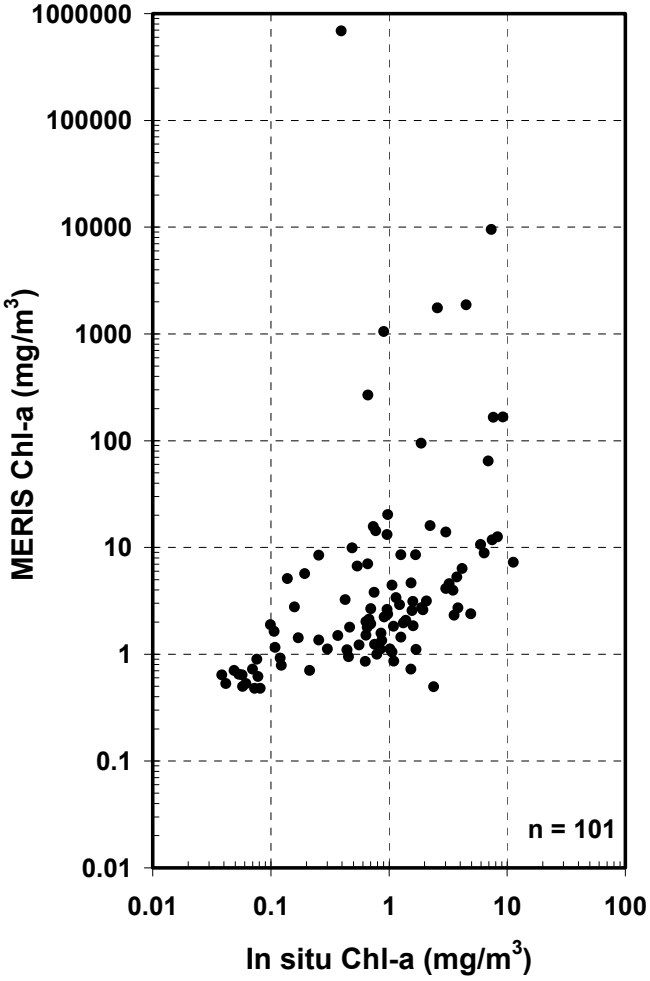

Figure 5 – 1 Validation of MERIS-C algorithm for algal_1 product by application of in situ R_{rs} ratios

zero and exponentially decreases when the ratios increase (Figure 5 – 2). The MERIS algorithm is composed of three functions, here defined as MERIS1, MERIS2 and MERIS3, for three chlorophyll levels – less than 1 mg m^{-3}, 1 – 10 mg m^{-3} and higher than 10 mg m^{-3}, respectively. Horizontal broken lines in Figure 5 – 2 indicate boundaries where the functions are switched. Changing to MERIS3 when concentrations are higher than 10 mg m^{-3}, however, leads to an increased error of estimation because slope of this function is the greatest and the intercept on y-axis (chlorophyll-a concentration) is also exceedingly large. This range lies cut side of naturally occurring concentrations and helps explain the abnormally large chlorophyll-a in results.

The outcome of this work suggests that the MERIS algorithm is inappropriate for chlorophyll-a estimation in the study area. Therefore, it is necessary to develop an alternative algorithm for use in the upper Gulf of Thailand.

5.3 Spectral Distribution of R_{rs}

The spectral distribution of R_{rs} at the sea surface is investigated in this section. Generally, each level of chlorophyll generates a specific pattern of R_{rs} signatures that have been described in Chapter 3. The accuracy of the empirical algorithms in predicting chlorophyll-a from R_{rs} ratios for Case 1 water is quite high because of their strong correlation. However, this is not the case of water column in the study area which is categorized as Case 2 due to terrestrial influences and water-sediment interactions. SS and CDOM can alter spectral signatures decreasing the accuracy of

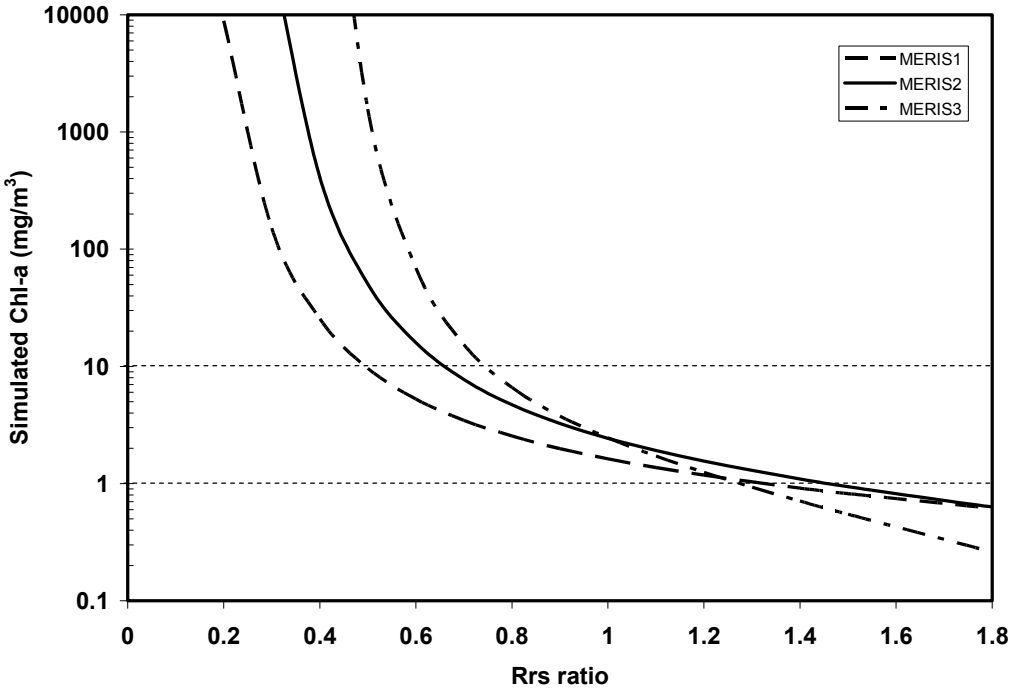

Figure 5 – 2 Simulated curves of MERIS standard algorithm for chlorophyll-a prediction

chlorophyll-a estimation. This section will present characteristics of R_{rs} for 3 chlorophyll-a ranges – less than 1 mg m^{-3} (low; group 1), 1 – 3 mg m^{-3} (medium; group 2), and greater than 3 mg m^{-3} (high; group 3). Influences of SS and CDOM on the spectral signatures in each group are also analyzed and discussed.

R_{rs} distributions when chlorophyll-a concentrations are less than 1 mg m^{-3} can be visually separated into three groups namely group 1 – 1, group 1 – 2, and group 1 – 3 in upper, middle and lower panels of Figure 5 - 3, respectively. High peak of group 1 – 1 are at 490 nm while those of group 1 – 3 shift to 565 nm. Transition of the reflectance peak can be seen in group 1 – 2 when R_{rs} (520) and R_{rs} (565) become dominant. There are also three unique patterns of spectral distribution, similar to the group 1 spectra when chlorophyll-a concentrations are in the range of 1 – 3 mg m^{-3} in group 2 (Figure 5 – 4). The main difference between group 1 and 2 is the number of samplings that belong to each sub-group. Most data in group 1 are located in group 1 – 1 and 1 – 2, while in group 2 most of them are in category 2 - 3. Lastly, group 3 represents the characteristic of R_{rs} distributions when chlorophyll-a is larger than 3 mg m^{-3} (Figure 5 – 5). The pattern like group 1 – 1 and 2 – 1 has disappeared. A few data display the plateau feature from 490 – 565 nm while most of them belong to group 3 – 2 where the pattern is similar to group 1 – 3 and 2 – 3. The largest and average chlorophyll-a concentrations in group 3 – 1 are 4.93 and 4.10 ± 0.72 mg m^{-3} ($n = 3$) and those of group 3 – 2 are 11.26 and 6.29 ± 2.46 mg m^{-3} ($n = 13$), respectively. Averaged R_{rs} distributions of all groups are summarized and presented in Figure 5 – 6.

Understanding of the contribution of chlorophyll-a, SS, and CDOM on variability of R_{rs} signatures is based on knowledge of their optical properties.

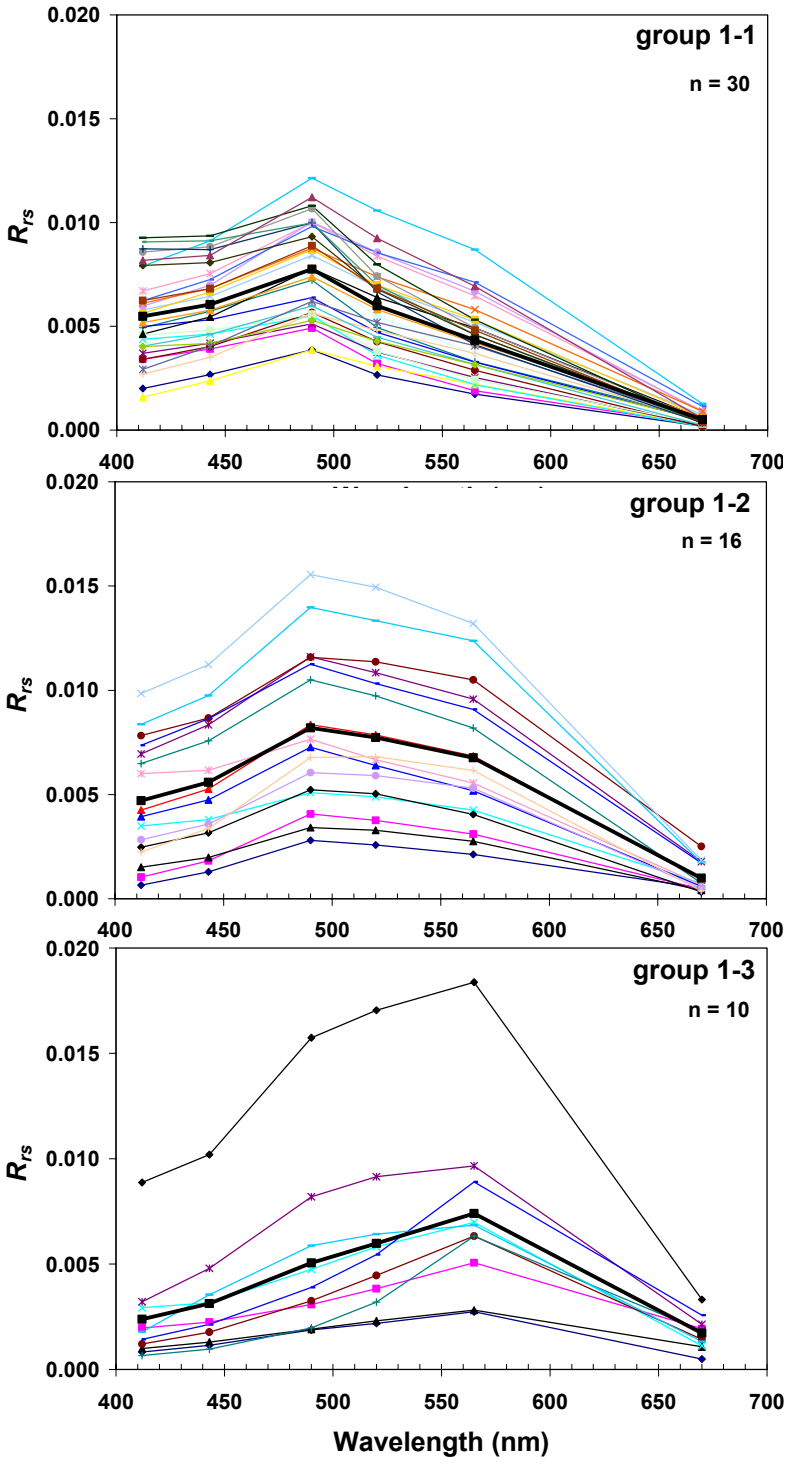

Figure 5 – 3 Spectral distributions of surface R_{rs} when chlorophyll-a concentrations are lower than 1 mg m^{-3}. Thick line in each figure represents mean values of each group.

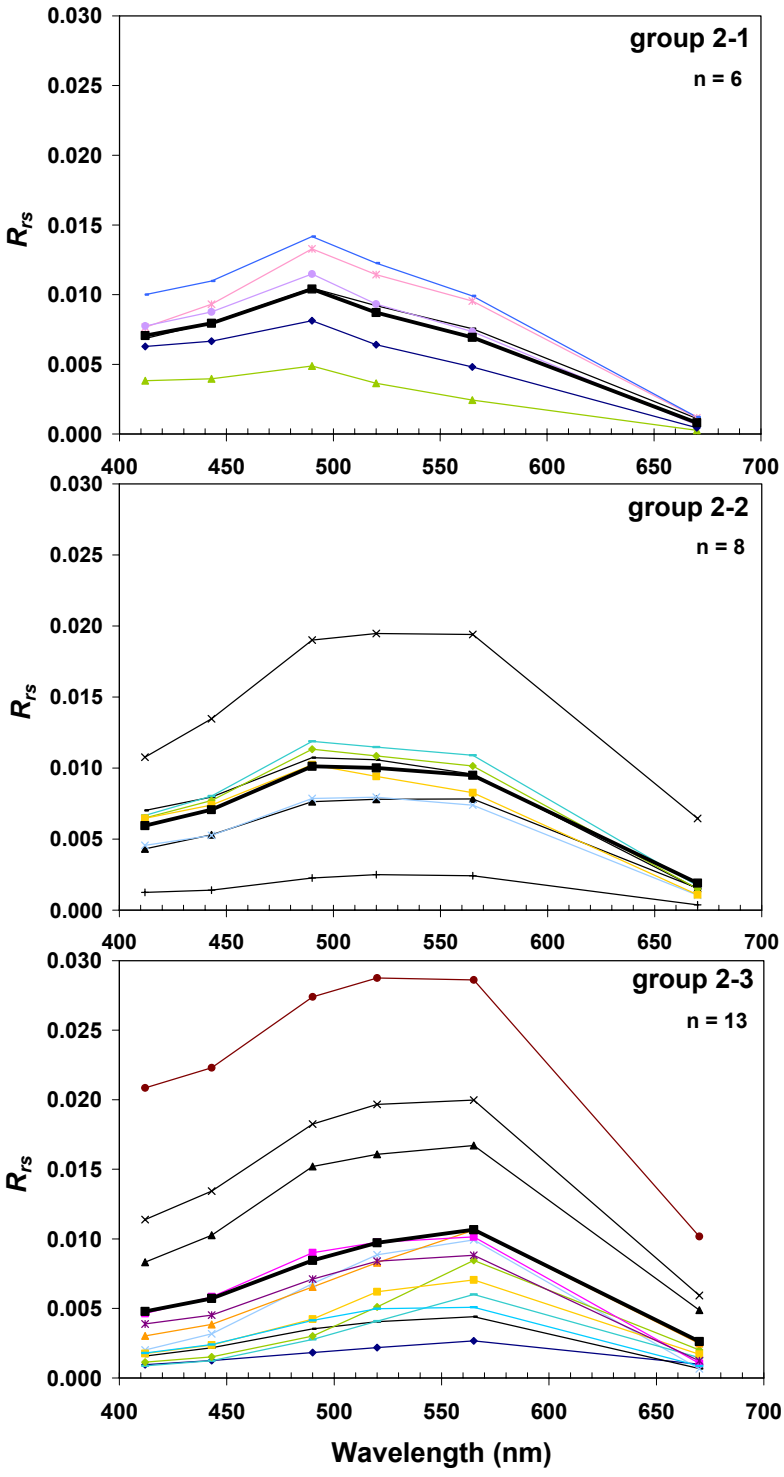

Figure 5 – 4 Spectral distributions of surface R_{rs} when chlorophyll-a concentrations are between 1 and 3 mg m^{-3}. Thick line in each figure represents mean values of each group.

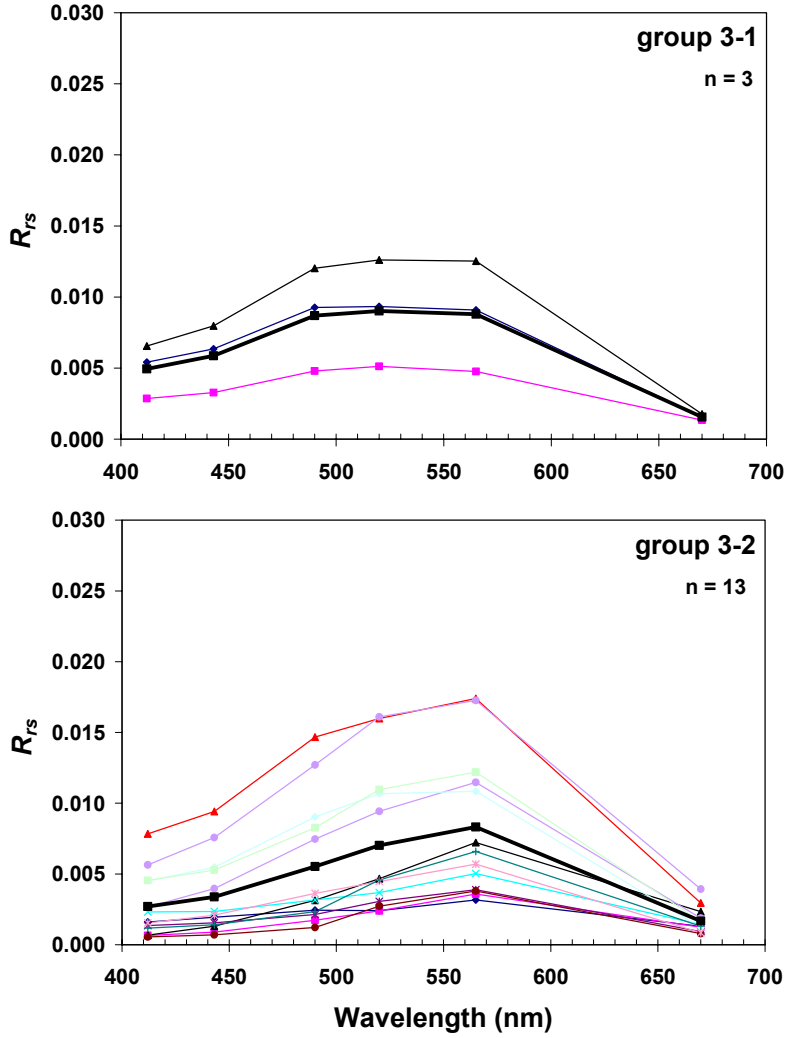

Figure 5 – 5 Spectral distributions of surface R_{rs} when chlorophyll-a concentrations are larger than 3 mg m^{-3}. Thick line in each figure represents mean values of each group.

Chlorophyll-a absorbs blue and red, and reflects green, while SS increases intensity of reflectance in almost all wavelengths. The peak of R_{rs} in low SS is near green (550 nm) while it shifts toward red and NIR (up to 720 nm) when concentrations increase. CDOM, or yellow substances, absorb energy in ultraviolet and blue wavelengths. Combining all those constituents in various fractions in water column undoubtedly complicates R_{rs} signatures. More detail about spectral response due to water constituents is found in Chapter 3.

The influence of CDOM is clearly observed especially in low chlorophyll-a concentrations by reducing R_{rs} signals in shorter wavelengths (412 and 443 nm). By considering averaged concentrations of constituents in each group (Figure 5 – 7) and averaged R_{rs} signatures of group 1 (Figure 5 – 3), it can be assumed that low signal in shorter wavelengths around the blue region of group 1 – 3 occurs because of high CDOM. Continual peak displacement from 490 to 565 nm comes from increasing in SS concentrations from group 1 – 1 to 1 – 3.

The influence of SS, however, is clear due to the different concentrations between groups 2 – 1 and 2 – 2, while CDOM in both groups is low, resulting in stronger signals at 520 and 565 nm of the latter group (Figure 5 – 4 middle panel). Influence of CDOM could be distinguished between groups 2 – 2 and 2 – 3 when SS are small and while CDOM of the latter is visibly higher than the former. Signals at wavelengths shorter than 520 nm are treated to be lower than normal resulting in a shift of the peak from 490 to 565 nm. Water constituent compositions of group 3 (Figure 5 – 7) suggest that high chlorophyll-a is usually found when SS is also high. The influence of CDOM is still observed in group 3 – 2 through a decreasing signal in

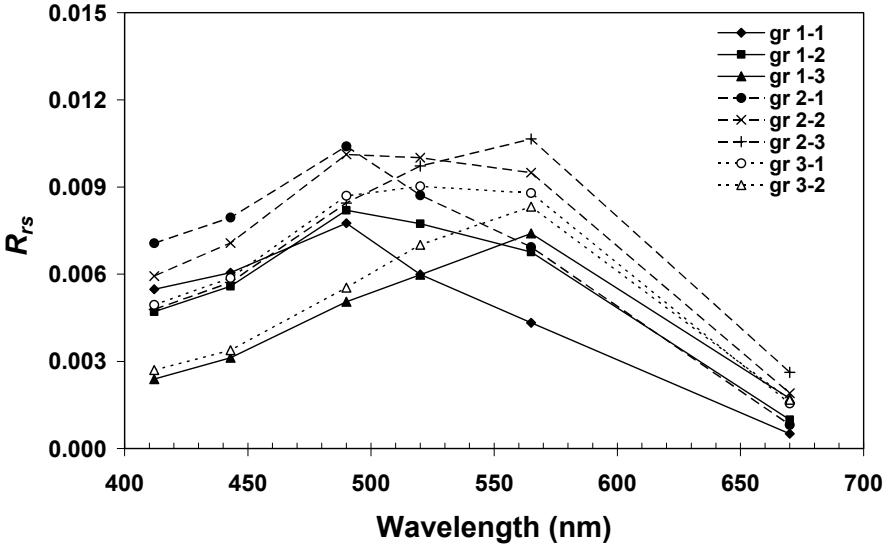

Figure 5 – 6 Summary of averaged surface R_{rs} of all groups

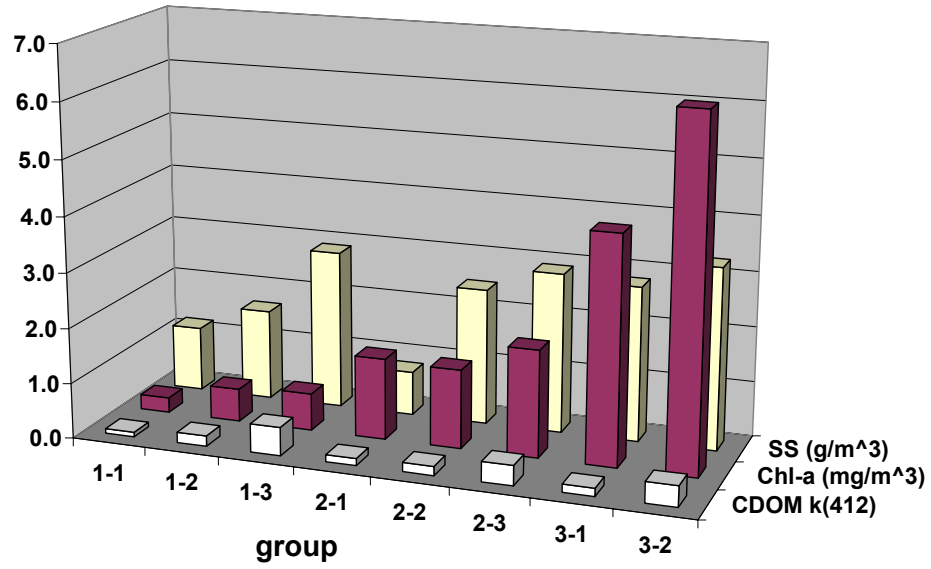

Figure 5 – 7 Summary of water constituents of each group

wavelengths shorter than 520 nm. However, it should be considered with caution since high chlorophyll-a concentrations in this group might significantly contribute to lowering signal in blue spectrum as well.

It can be summarized that the patterns of R_{rs} signatures of water in the study area are modified by not only chlorophyll-a but also SS and CDOM, which are considered to be the disturbing factors in the processes of algorithm development. If a concentration of chlorophyll has several R_{rs} patterns, the accuracy of estimation will be very low. An example of error initiation is obviously seen in the signatures of group 1 – 3 and group 3 – 2 (Figure 5 – 6). Both patterns appear similar while chlorophyll-a levels in those groups are very different – less than 1 mg m^{-3} in group 1 and larger than 3 mg m^{-3} in group 3. When those R_{rs} ratios are used to construct algorithms, such an error will generate poor chlorophyll estimation. These factors will be taken into consideration in the process of algorithm development.

5.4 Algorithm Development

Details of algorithm development based on R_{rs} ratios for chlorophyll-a estimation are performed in this section. The objective is to investigate the best empirical algorithm to convert MERIS reflectance to chlorophyll-a images. Regression analysis is utilized to find suitable mathematical equations representing the relation between those parameters. Basically, using R_{rs} instead of L_u can significantly minimize uncertainty from environmental factors such as differences in solar radiation,

atmospheric and sea surface conditions, but it cannot deduct the disturbances of SS and CDOM.

Three ratios, $R_{rs}(443)/R_{rs}(565)$, $R_{rs}(490)/R_{rs}(565)$, and $R_{rs}(520)/R_{rs}(565)$, are considered in algorithm development because of wide application in most sensors (Robinson, 2004) such as CZCS, SeaWiFS, MODIS, GLI and MERIS. Those ratios are tested by using codes Algor1, Algor2 and Algor3, respectively. However, there is alternative algorithm available by selecting the largest values among those ratios (OC4V4) or by the level of chlorophyll-a concentration (MERIS-C). The algorithm based on OC4V4 criterion will be tested by the name of Algor4. However, MERIS-C criterion is difficult to apply in practice because chlorophyll-a itself is the result of calculation. Such an unclear definition might be problematic; therefore, it is excluded from the process of algorithm development. It should be added that R_{rs} in NIR can also be applied for chlorophyll-a approximation because there is a prominent reflectance peak around 690 – 700 nm in algae-laden water (Jensen, 2000). Anyway, this study will not take it into consideration due to unavailability of the dataset detected by PRR-600.

5.4.1 Algorithms Derived from All Dataset

Scatter plots between R_{rs} ratios and chlorophyll-a indicate a consistent non-linear relationship (Figure 5 – 8). Inverse proportional relations in all cases can be seen as a nearly straight line of scattered points after logarithmic scale is applied to the *y*

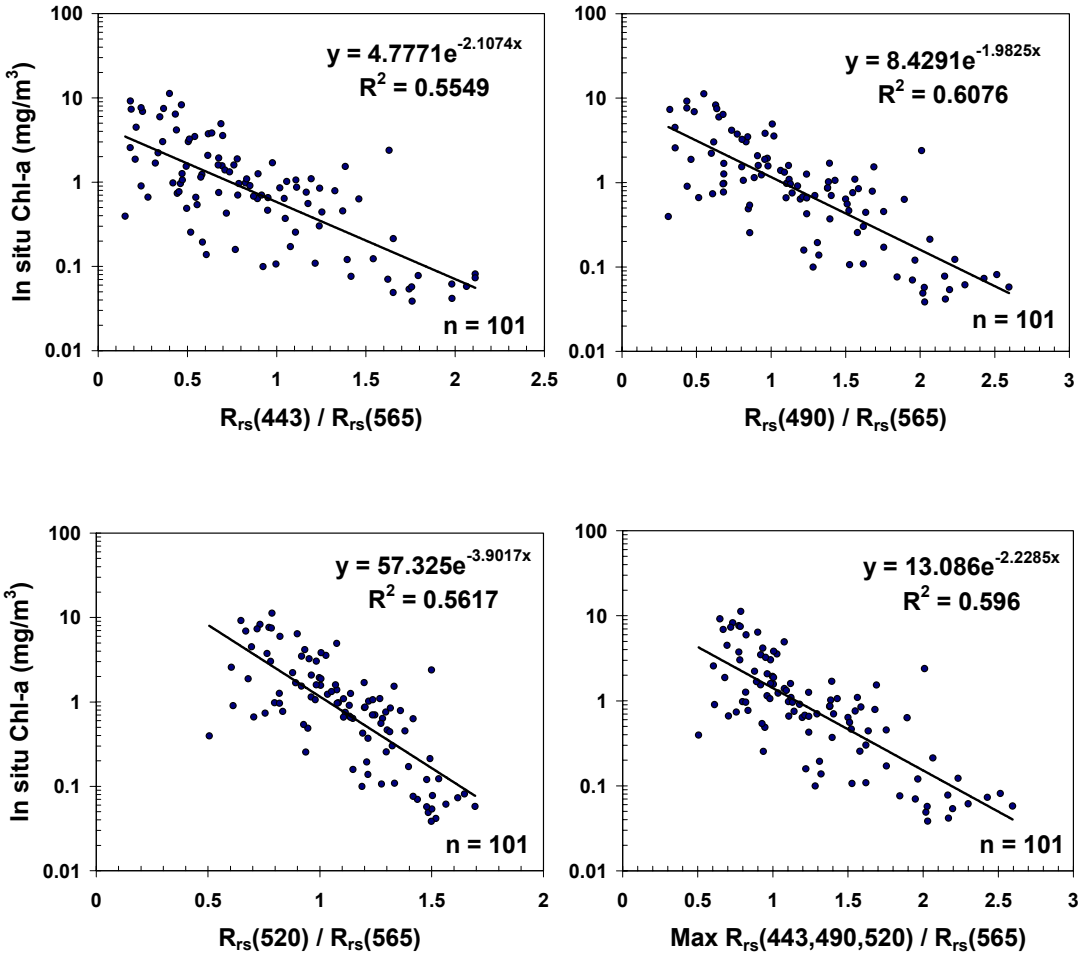

Figure 5 – 8 Regression plots between various R_{rs} ratios and in situ chlorophyll-a of all data from field observations

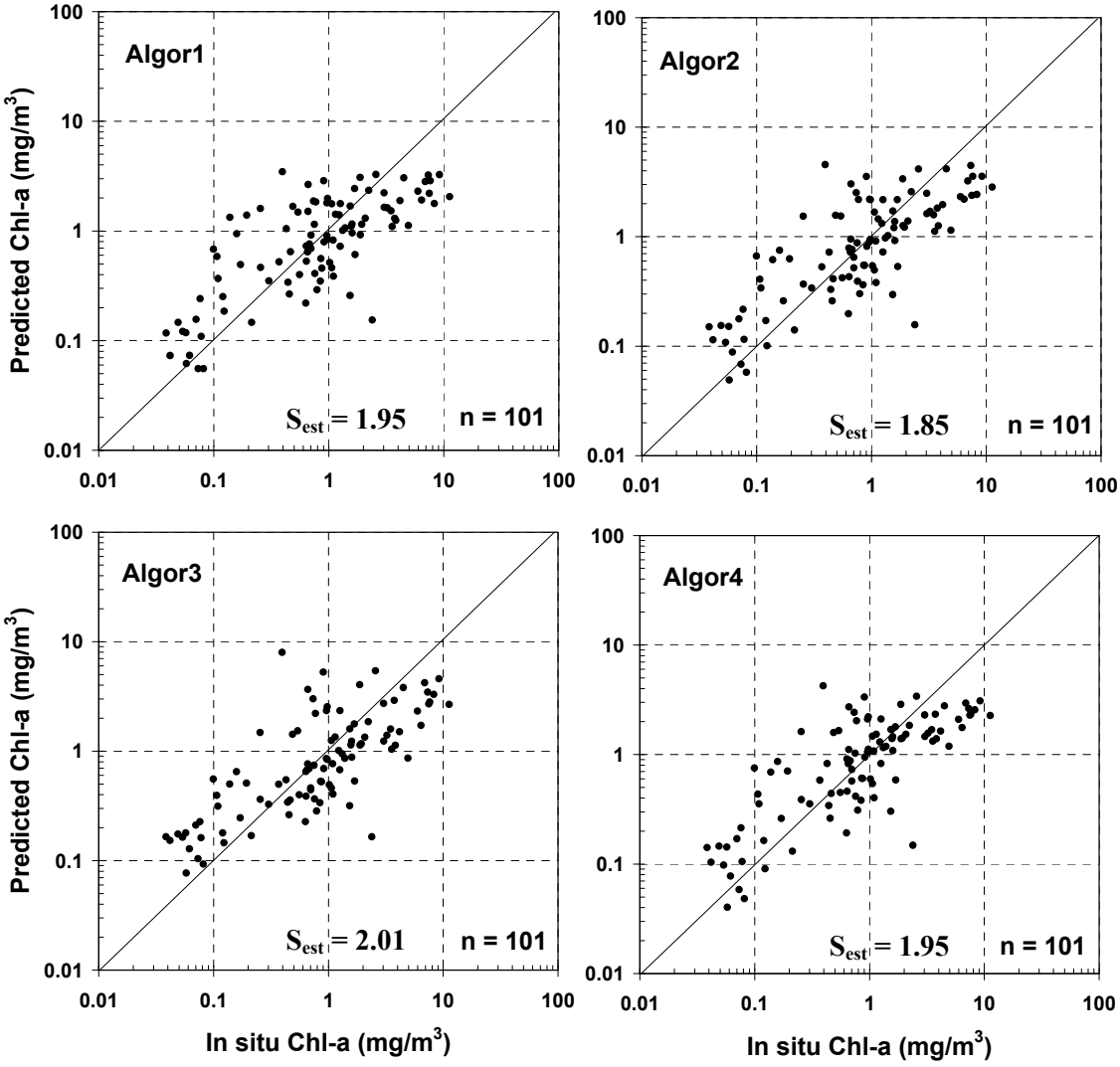

Figure 5 – 9 Validation of various chl-a algorithms derived from regression analysis of all data set

axis. A mathematical equation in the form of $y = a\ exp\ (-bx)$, when a and b are arbitrary constants, is the most suitable function for such relation. Therefore, it is selected to fit on the data plots and then analyzed for the coefficient of determination (Figure 5 – 8). Due to the high degree of scatter, R^2 values are moderate as from 0.56 to 0.61 ($p < 0.01$).

Equations derived from the analyses are validated by using them to estimate chlorophyll-a and then comparing the results with in situ data. Scatter plots suggest positive correlation since the data points are located within orthogonal lines but quite dispersed (Figure 5 – 9). Means of all cases are underestimated (Table 5 – 2) and those of Algor1 and Algor4 are significantly different from that of measured data ($p < 0.05$). Lowest and Highest S_{est} are 1.85 and 2.01 in the cases of Algor2 and Algor3, respectively. Although Algor2 provides largest R^2 (0.61), it is still not sufficient, resulting in poor chlorophyll-a predictions and high S_{est}. The developed algorithms can possibly be applied for chlorophyll-a estimation in the study area but with a low accuracy expected. Results also suggest that Algor4, which is based on OC4V4 criterion, is not better than fixed ratios in chlorophyll-a prediction because spectral sensitivities are modified by not only chlorophyll but also SS and CDOM.

5.4.2 Adjusted Algorithms

A possible way to minimize errors in chlorophyll-a prediction is to exclude some bad data out of the regression analyses in algorithm development processes. R_{rs} distributions (from Figure 5 – 3 to 5 – 6), and concentrations of water constituents in

each group (Figure 5 – 7) including the knowledge of their relationship described in section 3.1.1 and 5.3 are taken into consideration for this process. It is obvious that spectral signatures of low chlorophyll-a water in group 1 – 3 and 2 – 3 are distorted by high CDOM making unusually low reflectance with wavelengths lower than 520 nm. Both datasets have the potential to generate large errors because such phenomenon should happen in high chlorophyll-a water. Therefore, data belonging to those groups are omitted while those of others are included in the analytical process because of two reasons. First, CDOM concentrations in those groups are comparatively small except group 3 – 2 while the disturbance of SS appears throughout, and it is impossible to separate its effects from the dataset. Second, although CDOM is quite high in group 3 – 2, high chlorophyll-a concentrations also contribute to decreases of R_{rs} signals in blue spectrum. Thus, it is impossible to separate their effects, and the data belonging to this group have to be included in algorithm derivations.

Regression analyses after the elimination of the spurious data in group 1 – 3 and 2 – 3 are illustrated in Figure 5 – 10. A lower scattering points is observed in the high chlorophyll-a region of all cases particularly of $R_{rs}(520)/R_{rs}(565)$. R^2 also increases from 0.5 – 0.6 in the case of the entire dataset to be 0.6 – 0.7 ($p < 0.01$) with the maximum value of 0.75 in the new analyses. The modified algorithms were applied to in situ R_{rs} ratios to investigate their performance on chlorophyll-a prediction. The results of this analysis are shown in Figure 5 – 11 and Table 5 – 2. The names adjusted Algor1 (AA1) to adjusted Algor4 (AA4) which are equivalent to Algor1 to Algor4 are assigned to those newly modified algorithms. Compared with the previous analyses

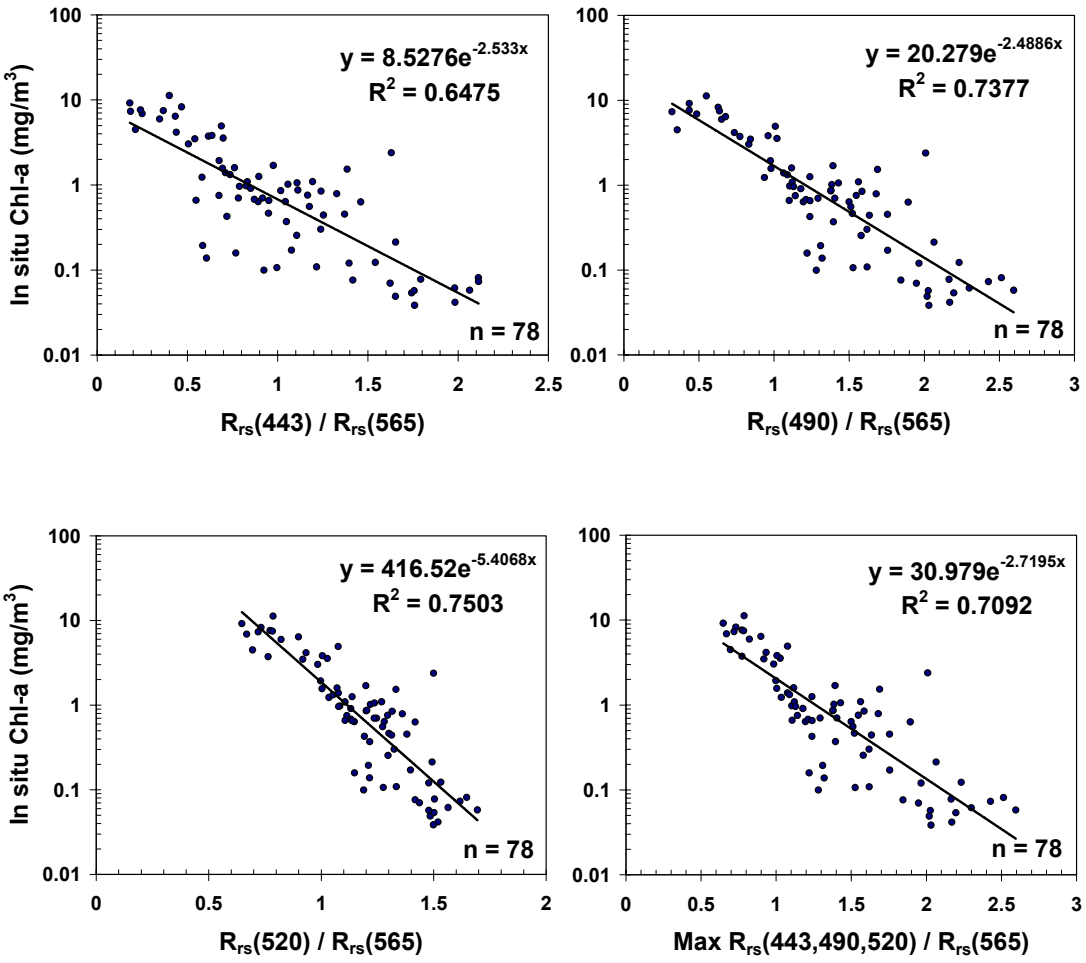

Figure 5 – 10 Regression plots between various R_{rs} ratios and in situ chlorophyll-a after observational data in group 1 – 3 and 2 – 3 were excluded

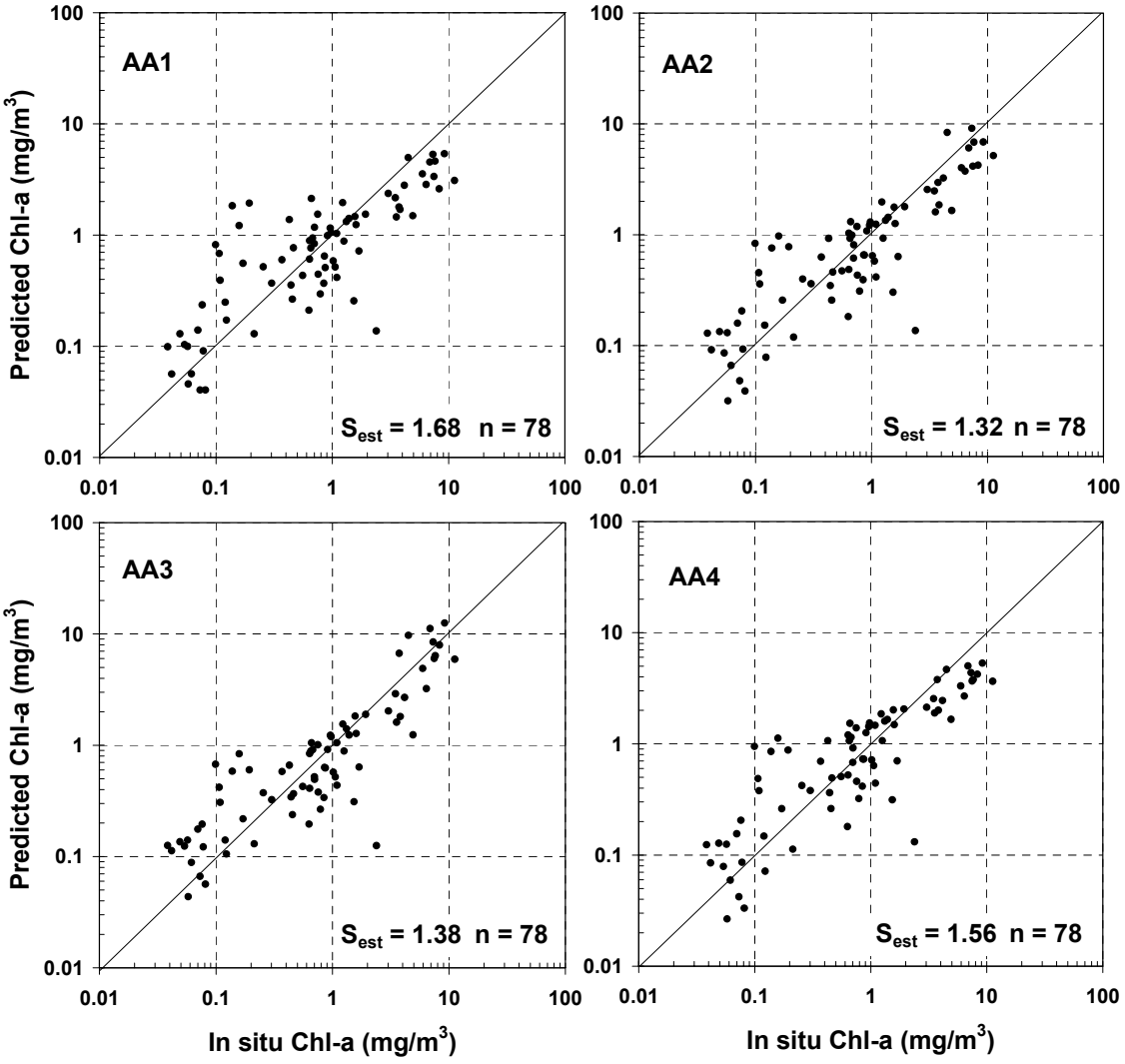

Figure 5 – 11 Validation of various chlorophyll-a algorithms derived from regression analysis after the data set of group 1 – 3 and 2 – 3 were excluded

with all data, S_{est} values decrease in all validation results indicating improvement in chlorophyll-a predictions of all algorithms.

Table 5 – 2 Summary of accuracy assessment of algorithms for chlorophyll-a estimation

Variables	R^2	Mean ± SD	S_{est}	n
All chl-a data		1.70 ± 2.25		101
Algor1	0.56	1.15* ± 0.90	1.95	101
Algor2	0.61	1.23 ± 1.12	1.85	101
Algor3	0.56	1.27 ± 1.39	2.01	101
Algor4	0.60	1.17* ± 0.93	1.95	101
Selected chl-a data		1.80 ± 2.51		78
AA1	0.65	1.23 ± 1.30	1.68	78
AA2	0.74	1.45 ± 1.95	1.32	78
AA3	0.75	1.66 ± 2.67	1.38	78
AA4	0.71	1.28 ± 1.32	1.56	78

*$p < 0.05$

Selection of the best algorithm to be applied to the MERIS data is considered from R^2 in regression analyses and S_{est} together with mean and SD of estimated chlorophyll-a (Table 5 – 2). AA1 and AA4 are first rejected because of low R^2, high S_{est}, and strong underestimation even though their means do not show significant differences ($p < 0.05$) from the measured chlorophyll-a. AA3 gives largest R^2 while AA2 provides lowest S_{est}. The differences in both values, however, are not large enough to judge which one is better; therefore, means and SD have to be taken into consideration. It is apparent from the mean values that AA3 performs better than AA2. Moreover, the larger SD of the former suggests a wide range of estimated chlorophyll-a which corresponds to that of the measurements. Both of them have preliminarily been tested with MERIS data, and AA3 gave better predictions in the chlorophyll

ranges. For these reasons, the AA3, derived from $R_{rs}(520)/R_{rs}(565)$, will be used as the local algorithm with MERIS data to investigate the chlorophyll-a distribution in the study area. The final algorithm is shown as the following equation.

$$C_a = 416.52 \exp(-5.4068 \cdot R), \qquad (5-4)$$

$$R = \frac{R_{rs}(520)}{R_{rs}(565)}.$$

5.5 Application of Local Algorithm to MERIS Data

This section is separated into two parts starting with the validations of chlorophyll-a estimated by application of the local algorithm, which is from now referred as UGoT algorithm, on MERIS data. Standard chlorophyll products namely algal_1 and algal_2 are also evaluated in order to compare their performances with the results of UGoT algorithm. The second part includes the discussion of chlorophyll-a distribution in the study area following chlorophyll-a maps produced from MERIS L2 data.

5.5.1 Validations of Estimated Chlorophyll-a

Due to the dynamic nature of the coastal water, MERIS data collected at the same time as the field observations are used for verification purposes. The study area which is located in a tropical zone has almost continuous cloud cover during the southwest monsoon and transition periods between seasons. Therefore, there was only one cruise (CU – 2; 4 – 6 December 2003) where the data collected were closely

synchronized with the satellite over pass (5 December 2003) and when the sky was clear. Other high quality scenes were detected in the same months of cruise CU – 1 (October 2003) and CU – 6 (July 2006) but observational dates are separated by 10 – 20 days, which is too large to be used for validation. BEAM software was utilized for all satellite image processing and data extraction. Data from three-by-three pixels centered on each observational station were averaged and used for the analyses in order to minimize error of rapid changes due to fast moving phenomena such as tidal current and turbulence.

Although the scope of the study was not concerned with atmospheric correction, it is worth knowing the reliability of MERIS R_{rs} data before they are applied with UGoT algorithm. The corrected reflectance centered on 520 and 565 nm of MERIS will be verified with in situ data at closest wavelengths of 510 and 560 nm, respectively. These two bands and their ratios are selected to test because of their contribution to UGoT algorithm. All validation results of MERIS R_{rs} and ratios are illustrated in Figure 5 – 12. Here the normalized standard error of estimation (*Nor.* S_{est}), which is calculated by dividing the S_{est} by the means of measured values, is introduced for comparing the level of error between plain R_{rs} and the ratio because of the differences in their units and ranges. Both MERIS R_{rs} are overestimated, observed from scattered points over the orthogonal lines in upper and middle panels of Figure 5 – 12. This corresponds to relatively high *Nor.* S_{est} of 6.1 in both cases. Great improvement appears in the case of R_{rs} ratios (Figure 5 – 12 lower panel) that *Nor.* S_{est} reduces to 0.1, and the scattered points seem to follow with the orthogonal line.

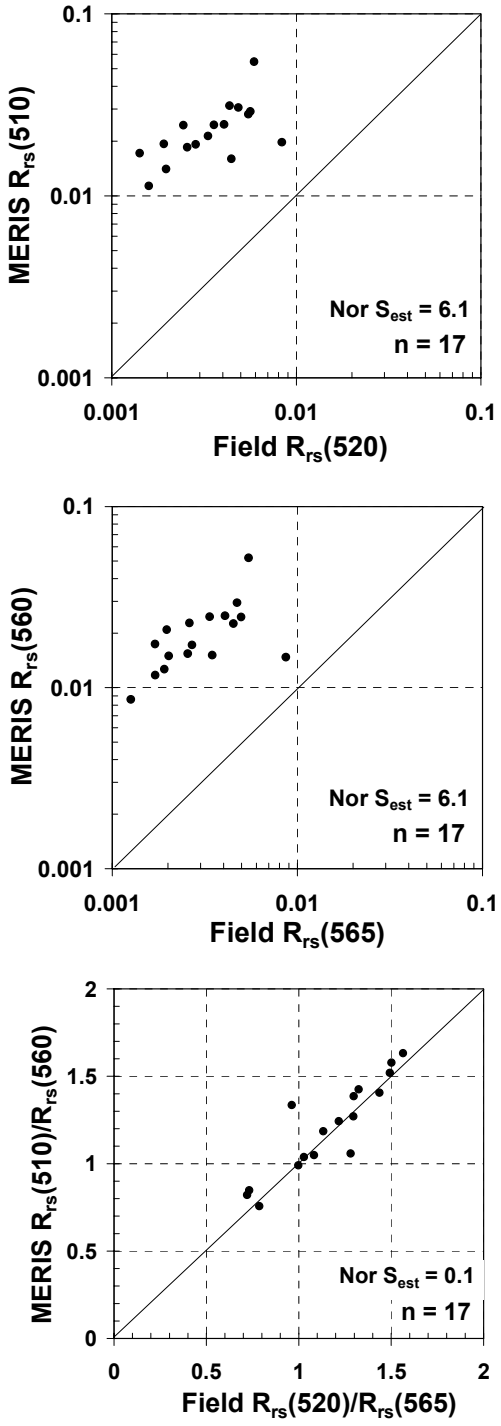

Figure 5 – 12 Validation of R_{rs} in two wavelengths and R_{rs} ratios of MERIS data detected on December 05, 2003

Overestimation of R_{rs} could have originated from atmospheric path radiance effects on the surface reflectance. The disturbances are not so different at 520 and 565 nm, and they can be reduced by conducting R_{rs} ratios. This fact indicates the advantage of using ratios instead of plain R_{rs} in chlorophyll-a algorithms. The experiment also suggests that MERIS R_{rs} ratio of $R_{rs}(510)/R_{rs}(560)$ could be applied with UGoT algorithm without any modification although band centers of the algorithm ($R_{rs}(520)/R_{rs}(565)$) are a bit different. However, this examination is based on the dataset from just one cruise due to data unavailability. More verification might be needed in the future to confirm the reliability in other seasons.

Calculated chlorophyll-a from application of UGoT algorithm on MERIS data together with MERIS chlorophyll-a products are validated. Datasets from cruise CU – 2 are used in the analyses. Scatter plots of predicted and in situ chlorophyll-a (Figure 5 – 13) indicate that UGoT algorithm gives better performance than both MERIS products. More details of the comparisons can be seen by considering plots of all estimated and measured chlorophyll-a in station-by-station of each cruise (Figure 5 – 14). Strong overestimation of algal_1 and/or algal_2 is clearly seen in most stations. The reason has been explained in section 5.2 that error of algal_1 is generated by assigning inappropriate functions on the data range of the study area. However, sources of errors on algal_2 are difficult to clarify due to the complexity of the neural network algorithm based on a radiative transfer model. It is obvious that estimated chlorophyll-a of UGoT algorithm is well correlated with measured data, and shows the same peak with close magnitude around stations 2 – 4 to 2 – 6. Algal_2 seems to present better results than algal_1 which is highly overestimated in these stations.

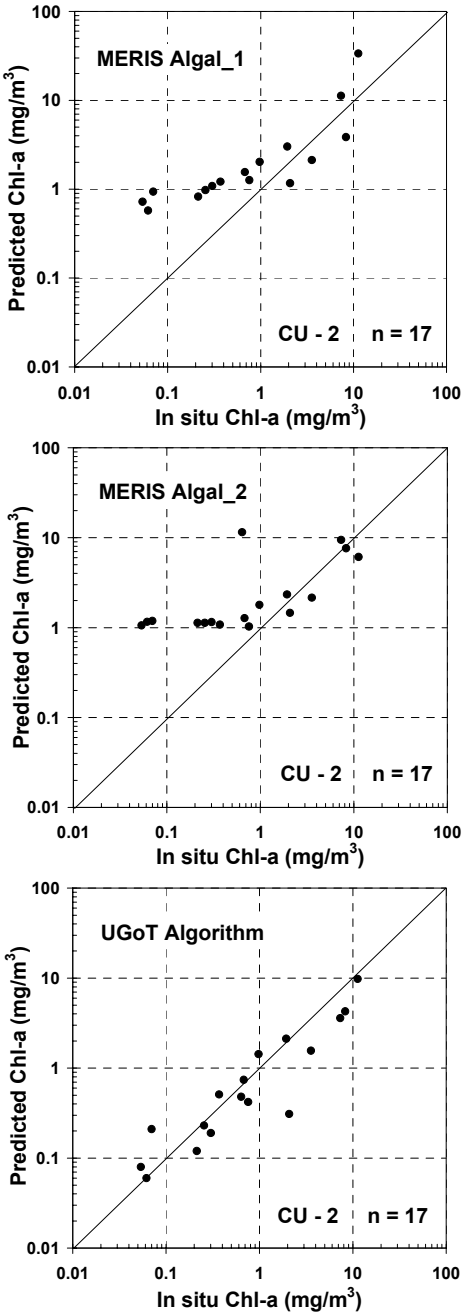

Figure 5 – 13 Validation of estimated chlorophyll-a of MERIS algal_1 and algal_2 products and UGoT algorithm during cruise CU – 2

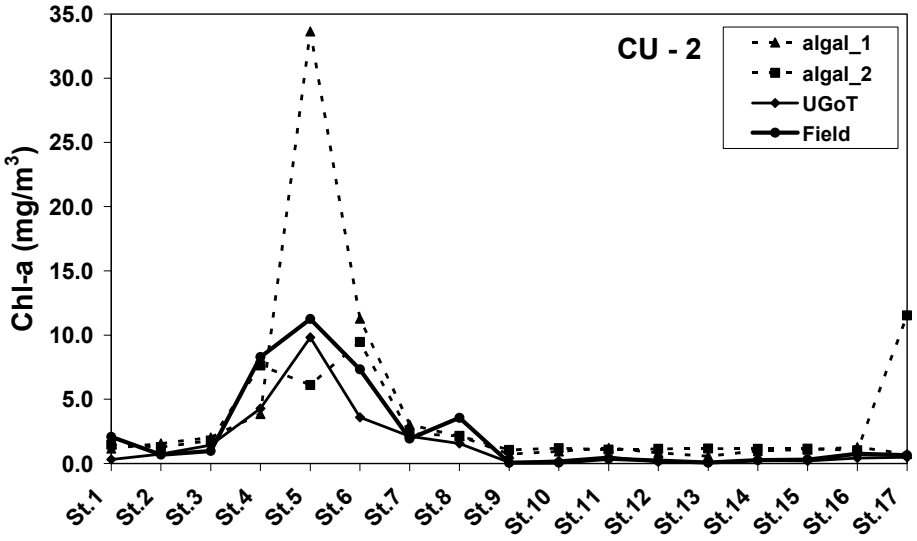

Figure 5 – 14 Comparison of chlorophyll-a concentrations estimated by MERIS and local algorithms with those of field measurement during cruise CU - 2

Table 5 – 3 Summary of accuracy assessment of several chlorophyll-a products derived from MERIS data

Cruise	Cruise Date	MERIS Date	Variables	Mean ± SD	S_{est}	% Accuracy ± C.I.*
CU - 2	4-6 Dec 2003	5 Dec 2003	Field	2.28 ± 3.39		
			algal_1	3.94 ± 8.06	6.0	- 7.6 ± 118.6
			algal_2	3.09 ± 3.37	3.3	23.9 ± 58.7
			UGoT	1.53 ± 2.47	1.6	78.1 ± 16.9

* 95 % Confidence interval

Statistical analyses of validation results are summarized in Table 5 – 3. Results of cruise CU-2 are analyzed for S_{est} and % accuracy by using Eq. (5 – 5) as the following:

$$\%\, Accuracy = 100 \times (1 - \frac{|X_{cal} - X_{obs}|}{\overline{X}_{obs}}) . \qquad (5-5)$$

The equation is based on the deviation of calculated (X_{cal}) from observed (X_{obs}) values normalized by means of the observed value ($\overline{X}_{obs}$). The averaged percent accuracy with 95 % confidence interval is presented in the table. The analysis confirms the improvement of UGoT algorithm on chlorophyll-a prediction by significantly reducing S_{est} and increasing the predictive power in comparisons to algal_1 and algal_2. Examination suggests that UGoT algorithm provides accuracy from about 60 to 95 % in chlorophyll-a prediction with 95 % confidence interval. Anyway, due to data limitation, more testing should be conducted in the future to verify the reliability of the algorithm in other seasons.

5.5.2 Chlorophyll-a Distributions

Chlorophyll-a maps of MERIS L2 data with application of UGoT algorithm have been produced to study chlorophyll-a distributions in the study area. Variations in river discharges (Figure 4 – 2) and wind fields (Figure 4 – 3) are also considered when explaining seasonal changes in the patterns of chlorophyll-a distribution. Only five high quality scenes were retrieved during October 2003 (CU – 1) and July 2005 (CU – 6) because of cloudiness. Data were processed and images were produced by using the

BEAM software. Land and clouds were masked in dark gray and white colors, respectively. All chlorophyll-a final maps are presented from Figure 5 – 15 to 5 – 19.

Satellite images present the same trend of movement but with clearer details of chlorophyll distributions than images of interpolated in situ data (Figure 4 – 9). Chlorophyll-a is quite high in the areas close to main river mouths in all seasons while their movement corresponds to wind directions. High chlorophyll-a bands move to western coast when east, or northeast, winds prevail over the area in October and December (Figure 5 – 15, 5 – 16 and 5 – 18). Wind patterns and distributions of low concentration near the sea boundary and eastern coast suggest that there was a penetration of surface water from the lower gulf to the east of the upper gulf. Southward outflow of high chlorophyll-a water along the west coast during these times was also observed. Plankton blooms occurred in December 2003 not in December 2004 although the distribution patterns appear similar. Surface distributions of in situ chlorophyll-a in Figure 4 – 9 also demonstrate the same phenomena between cruises CU – 1 and CU – 5 in October 2003 and October 2004, respectively. This indicates variations in some controlling factors of phytoplankton population that might vary from year to year. This issue is dealt with in greater detail in Chapter 7.

Chlorophyll-a accumulated near the northern coast (Figure 5 – 17) when the prevailing wind came from the south in February 2004 (Figure 4 – 3). Clearer water is still located in the east while high chlorophyll-a patches near river mouths move westward. These clues suggest a counter-clockwise flow system in the same way as those generated during the northeast monsoon. The image from July 16, 2005 represents the patterns of chlorophyll distributions during the southwest monsoon.

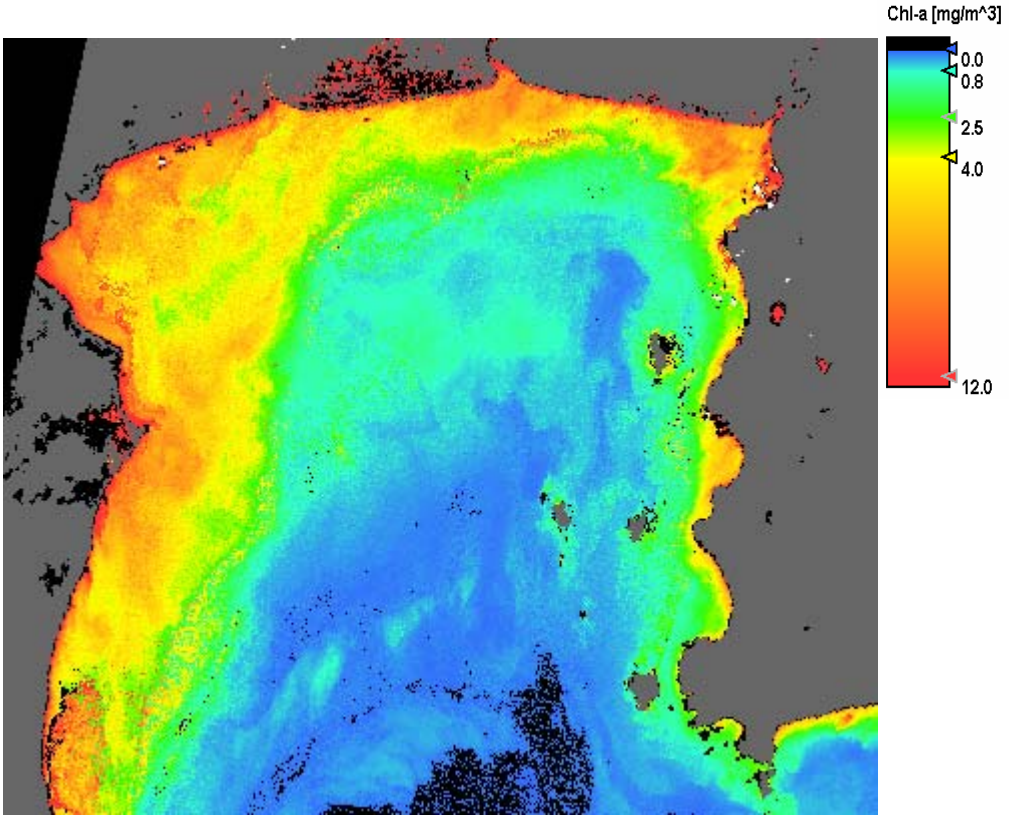

Figure 5 – 15 Chlorophyll-a distributions estimated by application of UGoT algorithm on MERIS data detected on October 28, 2003

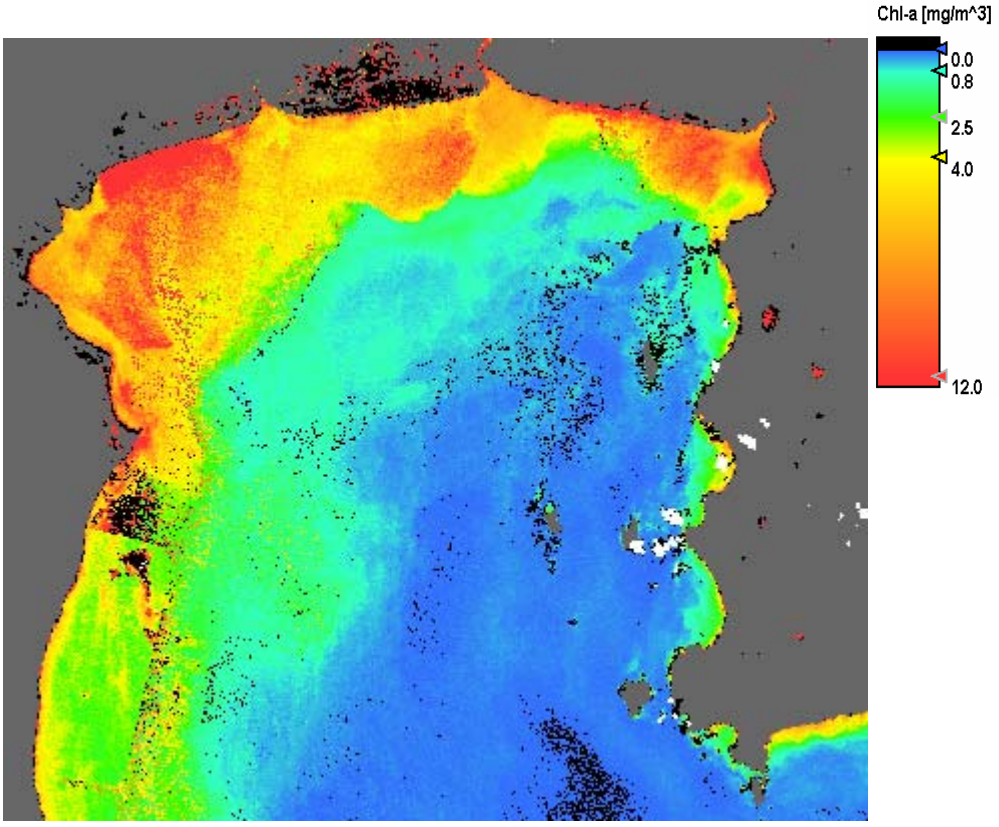

Figure 5 – 16 Chlorophyll-a distributions estimated by application of UGoT algorithm on MERIS data detected on December 05, 2003

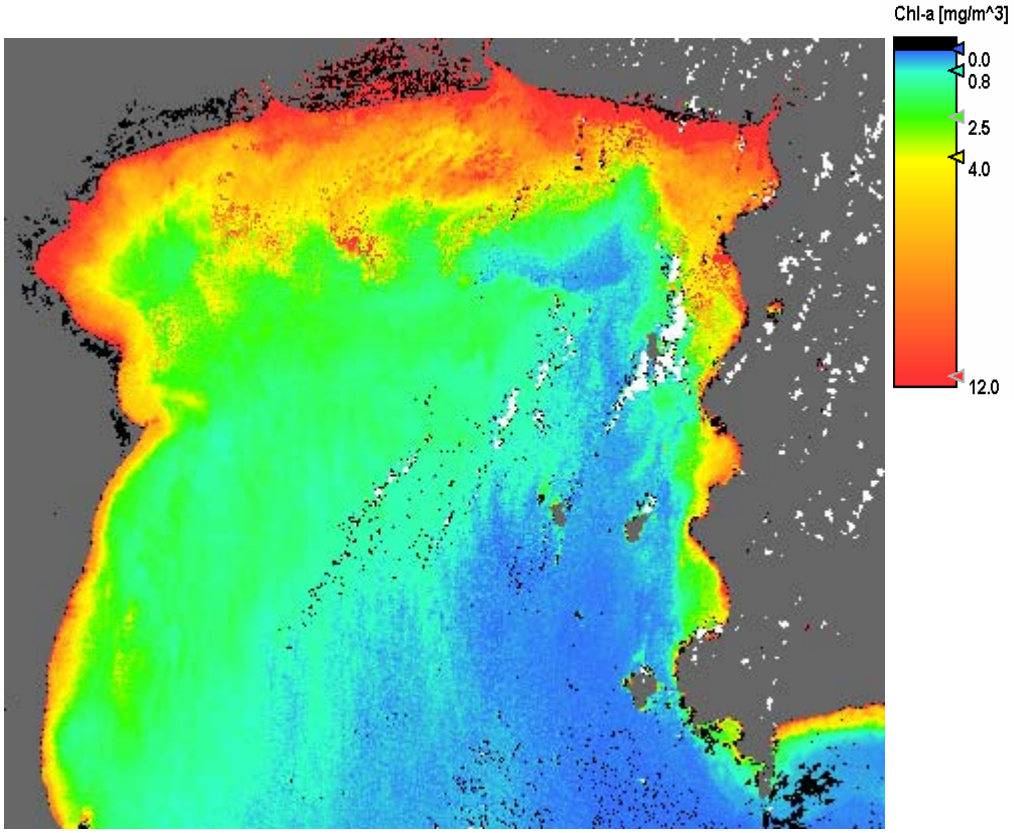

Figure 5 – 17 Chlorophyll-a distributions estimated by application of UGoT algorithm on MERIS data detected on February 29, 2004

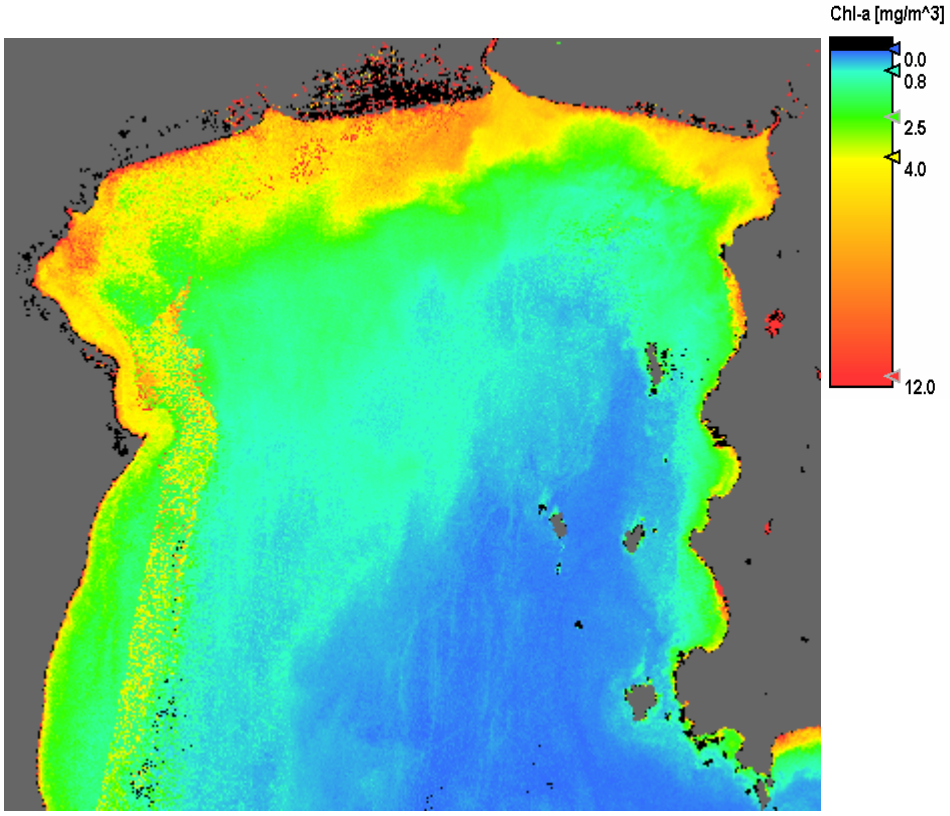

Figure 5 – 18 Chlorophyll-a distributions estimated by application of UGoT algorithm on MERIS data detected on December 02, 2004

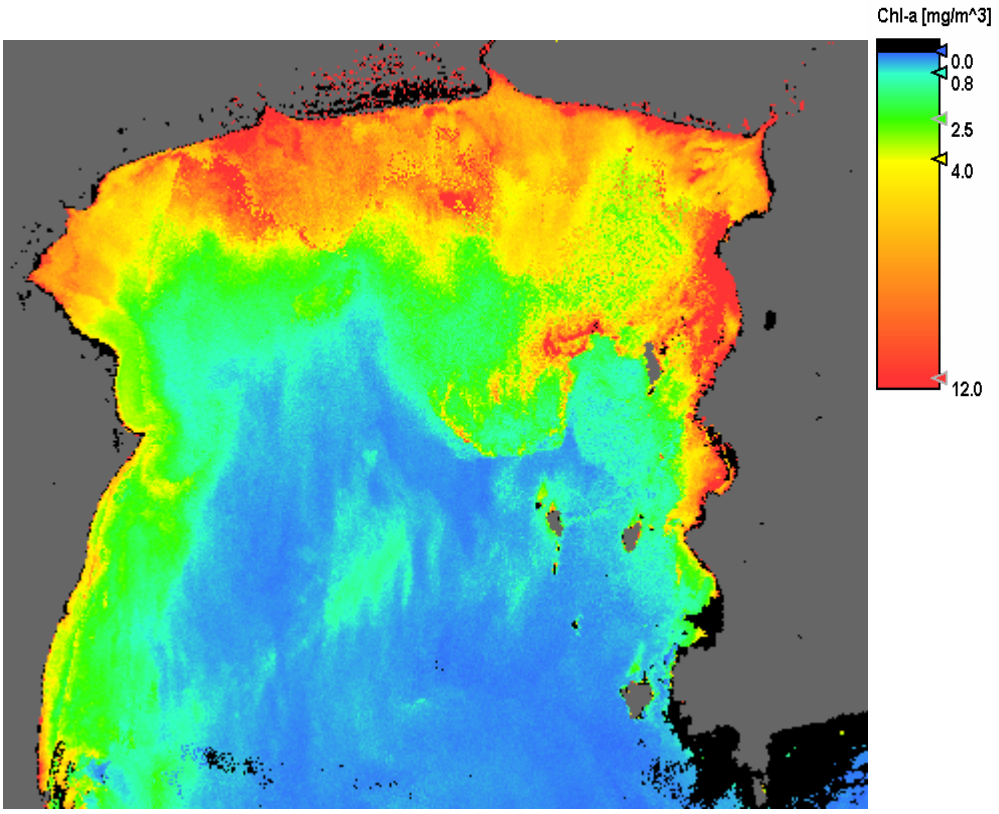

Figure 5 – 19 Chlorophyll-a distributions estimated by application of UGoT algorithm on MERIS data detected on July16, 2005

A high chlorophyll band appears along the northern coast, including an accumulation in northeastern corner of the gulf near the Bangpakong river mouth. Seasonal movement of high chlorophyll concentrations during the northeast and the southwest monsoons agrees well with seasonal plankton blooms that have been reported by Lirdwitayaprasit et al. (1994).

5.6 Summary

MERIS L2 data were used in the study of chlorophyll distribution in the upper Gulf of Thailand. Empirical algorithms for chlorophyll-a estimation were developed by using regression analysis of the relation between R_{rs} ratios and chlorophyll-a data from field measurements collected during October 2003 and July 2005. SS and CDOM found in the analyses of R_{rs} distributions were considered to be sources of errors in algorithm development process. Accuracy in chlorophyll-a prediction is much improved when data strongly influenced by CDOM are excluded from the analyses. The effects of SS could not be removed because they appear in all datasets. The final algorithm from the analyses is a natural logarithmic function of $R_{rs}(520)/R_{rs}(565)$ which is then referred as UGoT algorithm.

MERIS R_{rs} data at 510 and 560 nm, and $R_{rs}(510)/R_{rs}(560)$ ratio were validated with an in-situ dataset before being applied to the UGoT algorithm for chlorophyll-a estimation. R_{rs} in both bands overestimated results, but the ratio provided an excellent validation. The examination confirms reliability of MERIS R_{rs} when they are used in terms of R_{rs} ratios. Estimated chlorophyll-a was then validated, with the results

suggesting that the performance of UGoT algorithm is better than MERIS products of algal_1 and algal_2. Averaged percent accuracy in chlorophyll-a estimation by UGoT algorithm ranges from 60 % to 90 % with 95 % confidence interval.

Chlorophyll maps derived from MERIS data reveal the dynamic characteristics of frontal zones of high and low chlorophyll-a corresponding to wind direction. High chlorophyll bands always appear downwind; therefore, during the northeast monsoon, they move to the west while during the southwest monsoon, they accumulate in the northeast corner of the gulf. The results agree well with the occurrences of seasonal plankton blooms around western and eastern coasts during the northeast and the southwest monsoon, respectively.

CHAPTER 6

CIRCULATION PATTERNS IN THE UPPER GULF OF THAILAND

This chapter is dedicated to the investigation of circulation patterns in the upper Gulf of Thailand, carried out through the application of a numerical circulation model. Model setting and pre-processing are first described for clear understanding of how each computational domain and input are selected and prepared. Meteorological and oceanographic data including wind, discharge, tide, salinity and temperature during cruises CU – 1 and CU – 6 are used as key computational inputs. Two and three dimension circulation patterns resulting from this numerical model are thoroughly investigated to gain an understanding of the relationship between seasonal variations and major driving forces. For reliability, the simulated results are validated with measured data from the study of Booncherm (1999). Vertically averaged currents are also compared. Although circulation and ecosystem models are coupled and solved simultaneously, only the circulation results are presented and discussed in this chapter.

6.1 POM and Model Setting

The Princeton Ocean Model (POM) (Blumberg and Mellor, 1987) is applied to simulate three-dimensional circulation of the upper Gulf of Thailand. Governing equations of the model include conservation of mass, and momentum, salinity, temperature and turbulence equations under the hydrostatic and Boussinesq

approximations written in a bottom-following, sigma coordinate system when vertical layers are scaled following bottom topography (Figure B – 1 in Appendix B). POM can take both barotropic and baroclinic forces into consideration by using the splitting technique. Time steps are separated into two different modes – two-dimensional mode with a short time step of external wave speed (external mode) and three-dimensional mode with a long time step of internal wave speed (internal mode). To maintain operational stability, both different time steps have to be controlled under the Courant-Friedrichs-Levi (CFL) condition (Mellor, 1998). A vertical mixing coefficient is calculated in an imbedded second moment turbulence closure sub-model instead of being assumed as a constant as in several models. The Smagorinski diffusivity is applied to estimate horizontal mixing coefficients, which are proportional to the divergence and shear conditions of water mass (Eq. (B – 19)). More details of POM, including a mathematical description are continued in Blumberg and Mellor (1987), and Mellor (1998) and are presented in Appendix B.

6.1.1 Pre-Processing

The study area is divided horizontally into 124 × 102 grids in the spherical coordinate with grid spacing 0.5 × 0.5 minutes in latitude and longitude, respectively (Figure 6 – 1). Vertical domain is set to 10 σ-levels without logarithmic portions. Both grid designs are considered from a computational resolution to be suitable for the study area which is around 100 × 100 km^2. The horizontal grid size is designed to maintain the details of small-scale phenomena including eddies and current meanders in the

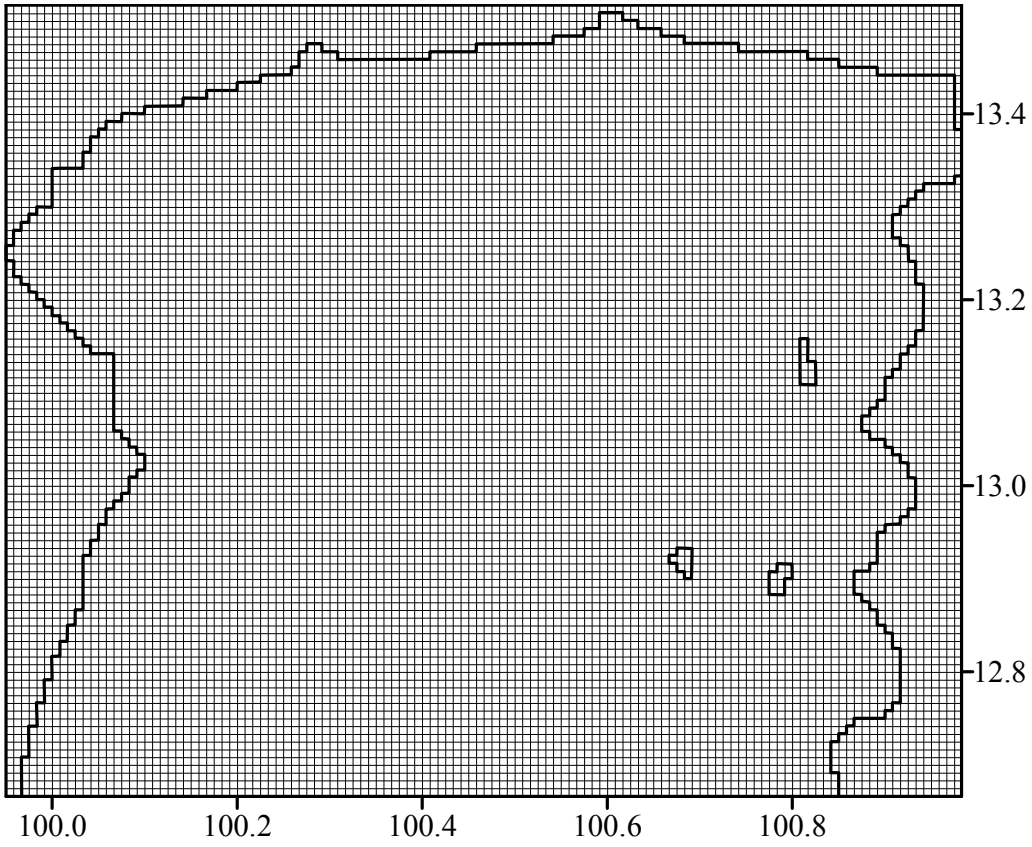

Figure 6 – 1 Horizontal grid design for computational domain

simulation results, keeping in mind computer capability and processing speed. The model used bathymetric data from a 5-Minute Gridded Global Relief Data (ETOPO5) from the World Data Center for Marine Geology & Geophysics (http://www.ngdc.noaa.gov/mgg/global/relief/ETOPO5/). Measured salinity and temperature were interpolated three – dimensionally using a Gaussian method to fit the data to all grid-spacing of computational domain. Details of the interpolation procedures are described below. Discharges of four main rivers (Figure 6 -2), used as a boundary condition at the river mouths, were collected by the Royal Irrigation Department (RID) of Thailand. Monthly averaged winds of QSCAT (Figure 4 – 3) are also interpolated to fit all horizontal grids and used as an important driving force. Tidal currents, as water elevations, were set to drive the water system through sea boundary.

General equations of complete three–dimensional Gauss's function applied for interpolation process are shown as the follows.

$$\zeta = \frac{\sum_{i=1}^{n}(W \cdot \tau)}{\sum_{i=1}^{n} W}, \qquad (6-1)$$

$$W = \exp\{-\frac{(r_i - x)^2}{I^2} - \frac{(r_j - y)^2}{J^2} - \frac{(r_k - z)^2}{K^2}\}, \qquad (6-2)$$

where ζ is an interpolated parameter at any grid point; τ is observed data; n is the number of observed data points; x, y and z are interpolated grid positions – x and y are horizontal, and z is vertical; r_i, r_j and r_k are positions of observed data in x, y, and z

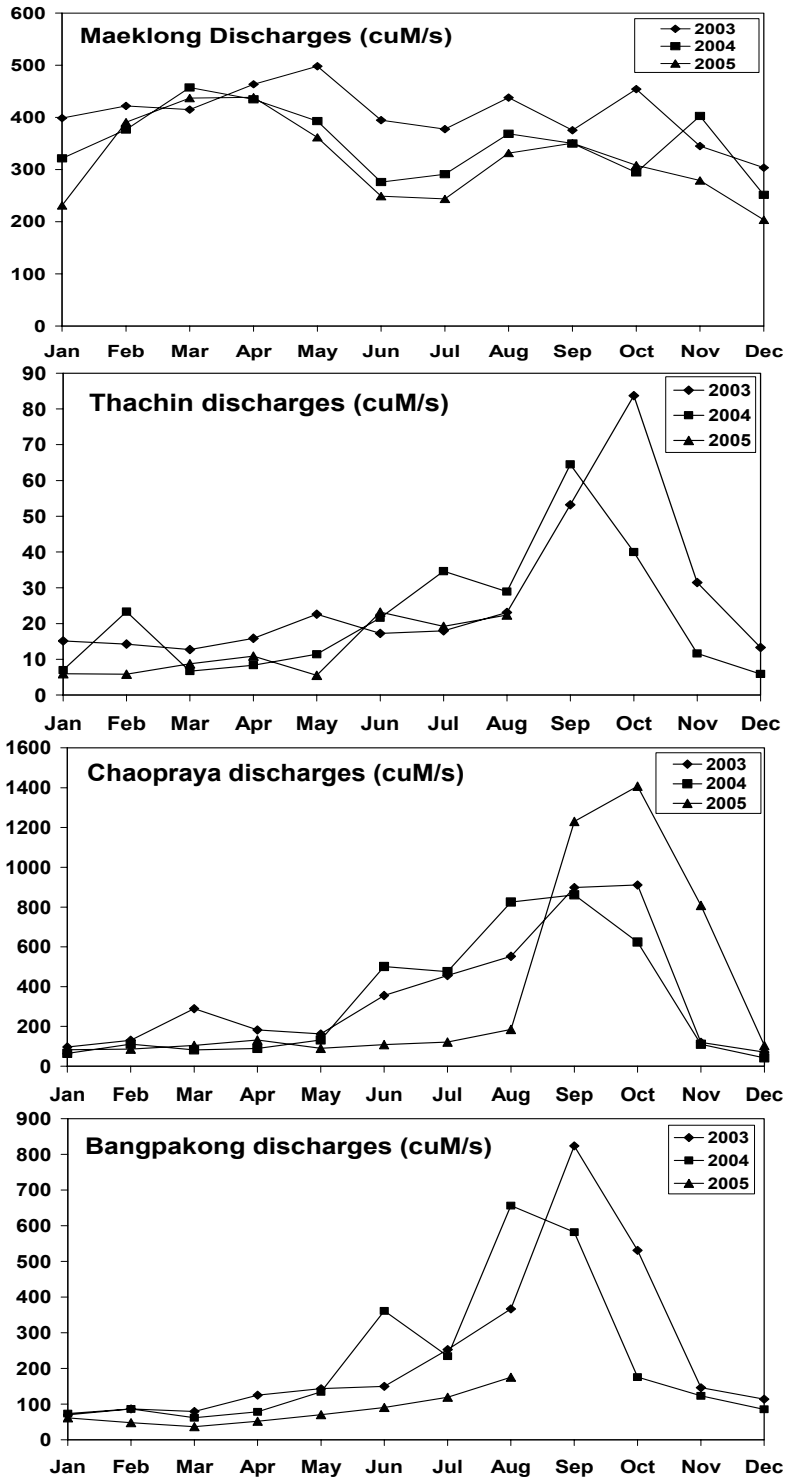

Figure 6 – 2 Monthly mean discharges of four main rivers emptying into the head of the upper Gulf of Thailand

directions, respectively. *I* and *J* are the horizontal decorrelation scales, set to 30 km, while *K* is that of vertical scale, set to 2 m. The function suggests that the closer the observed data points, the more influential the interpolated values received. Temperature and salinity used as inputs for all computational grids are interpolated in three – dimensional space. On the other hand, wind and bathymetry are interpolated in two–dimensional space, so the vertical term on the right hand of Eq. (6 – 2) is excluded in this case. All interpolations are processed using FORTRAN 77 programming.

Discharge data of four main rivers provided by RID were derived from stage-discharge relationships. This application is useable only where the disturbance of tidal force is small, so the stations need to be located a distance upstream where the effects are lessened. Estimated data at stations closest to the river mouths where water curves are still reliable are used in the case of the Maeklong and the Chaopraya Rivers. If data in those stations were incomplete, those of the next upstream stations were chosen instead. Due to strong tidal influence especially in dry season, an alternative method of estimation was necessary in the case of the Bangpakong River discharges. Fortunately, this river has a nearly complete dataset of discharges in most sub-basins located upstream; therefore the summation of known and extrapolated values of unmeasured sub-basins are representative of the total discharge at the river mouth. Water discharge through a water gate located downstream was used instead of real discharge due to strong tidal influences in the case of the Thachin River, the smallest river and a tributary of the Chaopraya. Although such data seem to be underestimated when compared to real discharges, they represent the most reliable data sources available.

Seasonal variations in flow are evident in the Chaopraya, the Bangpakong and the Thachin Rivers where high peak discharges occur in September or October (Figure 6 – 2). This phenomenon does not occur to the Maeklong River when discharges remain constant at around 200 – 300 m^3 s^{-1}. The possible reason is that this river has many huge dams obstructing watercourses; therefore, discharges are dependent on water regulation instead of seasonal precipitations. Monthly averaged discharges in the same months of the 6 observational cruises are used as the river boundary condition in the circulation model.

6.1.2 Lateral Boundary Conditions

Divided by the cross section of the river mouth, river discharge can be converted to velocity and then added to computational grids of the river boundary. This method has been tested, and found to decrease the stability of model operation considerably resulting in overflows near river mouths. The simplest, but not the best, way to minimize such problems is to reduce time-steps until stability is achieved, although the runtime of the model increases significantly (up tp 1 to 3 days). An alternative approach to deal with the river boundary issue is by transforming discharge to water level and adding it to water elevation of computational grids at the river mouths. This method is based on the concept of continuity of incompressible fluid dynamics described in Kourafalou et al. (1996). Elevated water owing to discharges then flows to surrounding grids following surface slope and driving forces such as

wind and tide. This technique not only provides for flexible river flows, but also helps to increase model stability by reducing overflow near the river mouths.

The ocean boundary in the south of the area is forced by tide via water elevations which are transformed to velocities in the model by continuity equation. Water levels in the east (Sattahip) and the west (Huahin) (Figure 4 – 1) were first computed by using a harmonic analysis technique. The intervening data were then derived using linear interpolation. Four tidal harmonic constituents namely K1, O1, M2 and S2 are considered in harmonic analysis where their amplitudes and phases at Sattahip and Huahin (Table 6 – 1) were reported in Sojisuporn and Putikiatikajorn (1998). During model operation, water elevations along the sea boundary are updated in every external time step (two-dimensional mode) under radiation condition (Mellor, 1998), illustrated by the following equation.

$$H\overline{U}_B = H\overline{U}_{B-1} \pm C_e \eta \,, \qquad (6-3)$$

$$C_e = \sqrt{gH} \,,$$

where $\overline{U}$ is the vertically averaged velocity, normal to the boundary; subscript B and $B - 1$ are referred as values at the boundary and at a consecutive grid inside computational domain, respectively; H is water depth, η is water elevation; g is the gravitational acceleration; and C_e is long-wave phase speed. Eq. (6 – 3) supports the idea that water transport at the sea boundary results from the balance of interior and exterior long wave propagations, which are generated inside and outside computational system, respectively.

Table 6 – 1 Tidal harmonic constituents used to calculate water elevation at the sea boundary

Harmonic Constituents	Huahin		Sattahip	
	Amplitude (cm)	Phase (deg.)	Amplitude (cm)	Phase (deg.)
K1	61.2	155.1	58.7	162.0
O1	39.0	119.2	29.3	112.0
M2	29.7	139.9	26.1	121.0
S2	15.3	212.8	12.3	192.0

Components of velocities perpendicular to land boundaries are set to be zero while radiation condition is also assigned at the sea boundary of the internal mode (three-dimensional mode) as shown in the following equation.

$$U_B^n = GAI \cdot U_{B-1}^{n-1} + (1-GAI) \cdot U_B^{n-1} , \qquad (6-4)$$

$$GAI = \sqrt{\frac{H}{H_{\max}}} ,$$

where U is velocity normal to the boundary; n and $n-1$ are referred as present and previous time steps, respectively; and GAI is a weighing factor which is dependant on water depth and the maximum depth (H_{max}). Finally, open boundary for salinity, temperature, and turbulence parameters are set by a condition called "upstream advection" as defined in Eq. (6 – 5).

$$\frac{\partial T}{\partial t} + U \frac{\partial T}{\partial x} = 0 , \qquad (6-5)$$

where T is referred to those parameters; and t and x are time and length, respectively.

6.1.3 Model Operation

The model is operated using a technique called the robust diagnostic, where damping terms are introduced to the temperature and the salinity equations. These additional terms are γ ($T^* - T$) and γ ($S^* - S$), respectively. Here, γ is called the nudging constant (= ΔT_i /(86,400 s ×5)); ΔT_i is internal time step (300 s); and T^* and S^* are the observed water temperature and salinity, respectively. These terms create artificial sources and sinks of heat and salt that push the predicted fields toward the observed values (Sarmiento and Bryan, 1982). A small γ makes the modeling approach prognostic, while a large γ will restricts conditions of calculated T and S to be close to the observed values, which favor diagnostic operation (Yanagi, 1999). In POM operation, the damping terms are added in the process of data updates before going to the next round of calculation.

The model is set to have no momentum fluxes generated by exchanges of heat and salt from the atmosphere, or sea bottom, because they are considered to be insignificant when compared to wind, discharges, and tide. Seawater state is set at rest at the initial time of model operation (t = 0). Time steps are 10 s and 300 s for the external and the internal modes, respectively. The model is driven by all forces from start until reaching a quasi-steady state around days 10 which could be examined by checking averaged kinetic energy. Computed circulations for 30 days after days 20 are averaged to present as residual circulations of the study area.

6.2 Circulation Results

This section presents the results of three- and two-dimensional circulations in the form of vector plots and contour maps by using Ocean Data View (ODV) and Surfer software. The circulation patterns are then visually evaluated with the measured results of residual circulations analyzed by Booncherm (1999). Moreover, vertically averaged currents are also compared to the results from Buranapratheprat et al. (2002a) to investigate the dissimilarity of circulation patterns resulting from two- and three-dimensional model simulations.

6.2.1 Three-Dimensional Circulations

Monthly mean horizontal circulations at the sea surface and 10 m depth of corresponding months to Chula cruises which are October and December 2003, January, May and October 2004, and July 2005 are illustrated from Figures 6 – 3 to 6 – 8. The results of mean vertical circulations at a 5 m depth are presented in Figure 6 – 9 for investigation of upwelling and downwelling. Wind patterns in Figure 4 – 3 are used to explain dominant circulation patterns.

October 2003 and October 2004 (Figures 6 – 3 and 6 – 7)

Current speeds during these times are quite strong, flowing to the west following wind directions from northeast. Most surface water comes into the Gulf from the east and moves out in the west of the sea boundary. Divergence at the sea surface appears in northwestern area close to the Maeklong river in both year but that

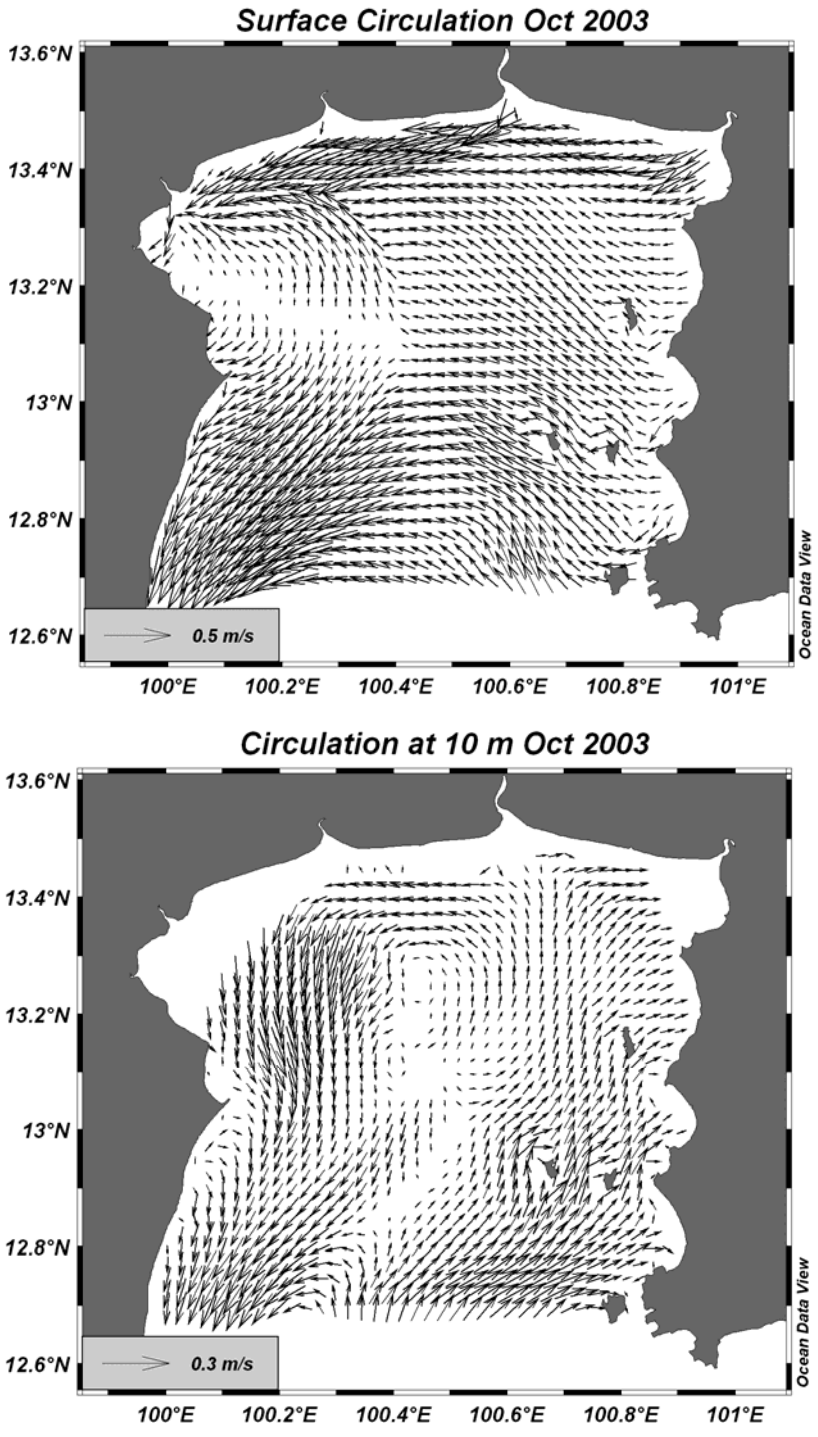

Figure 6 – 3 Simulated circulations at the sea surface and 10 m depth in October 2003

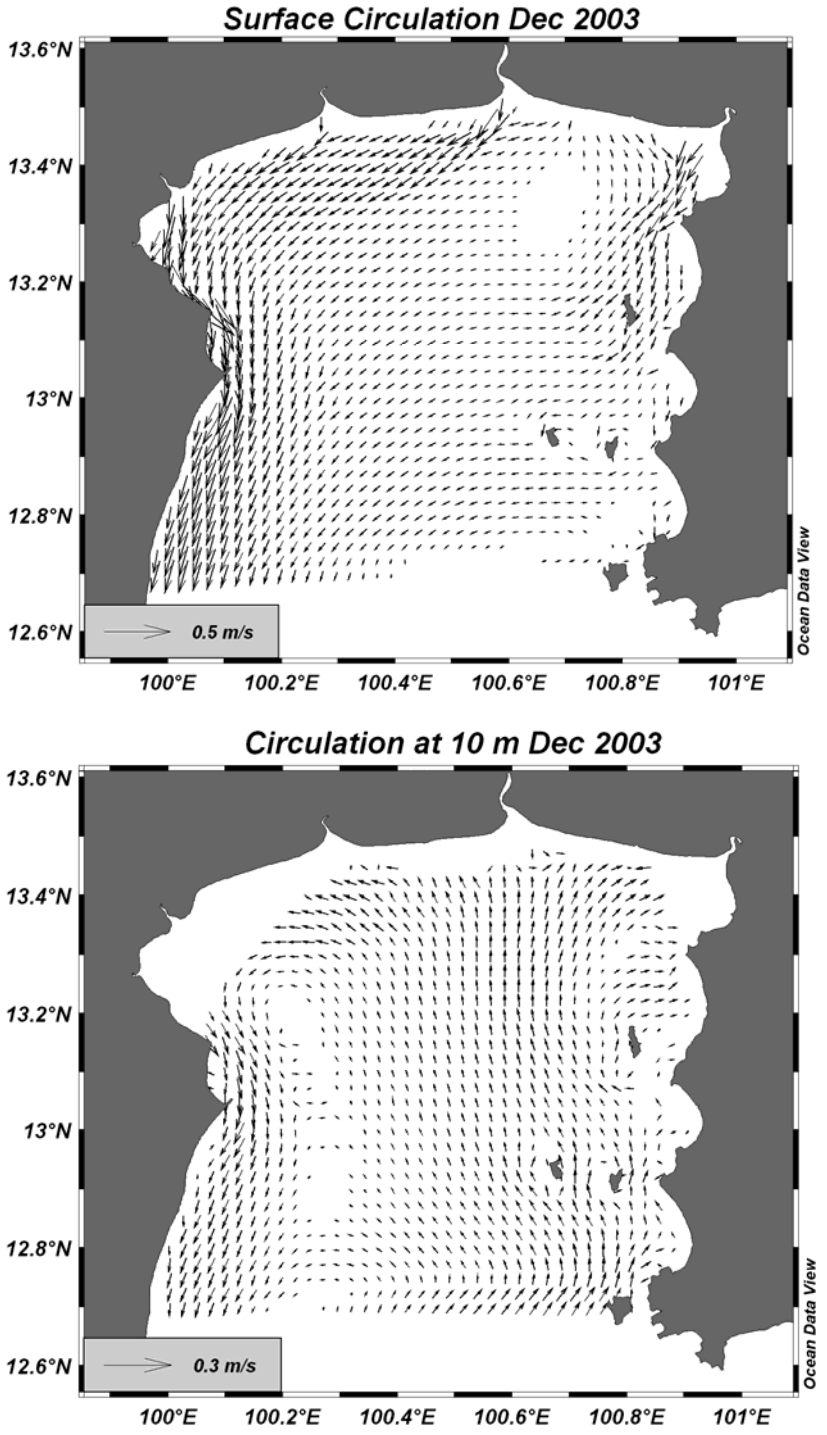

Figure 6 – 4 Simulated circulations at the sea surface and 10 m depth in December 2003

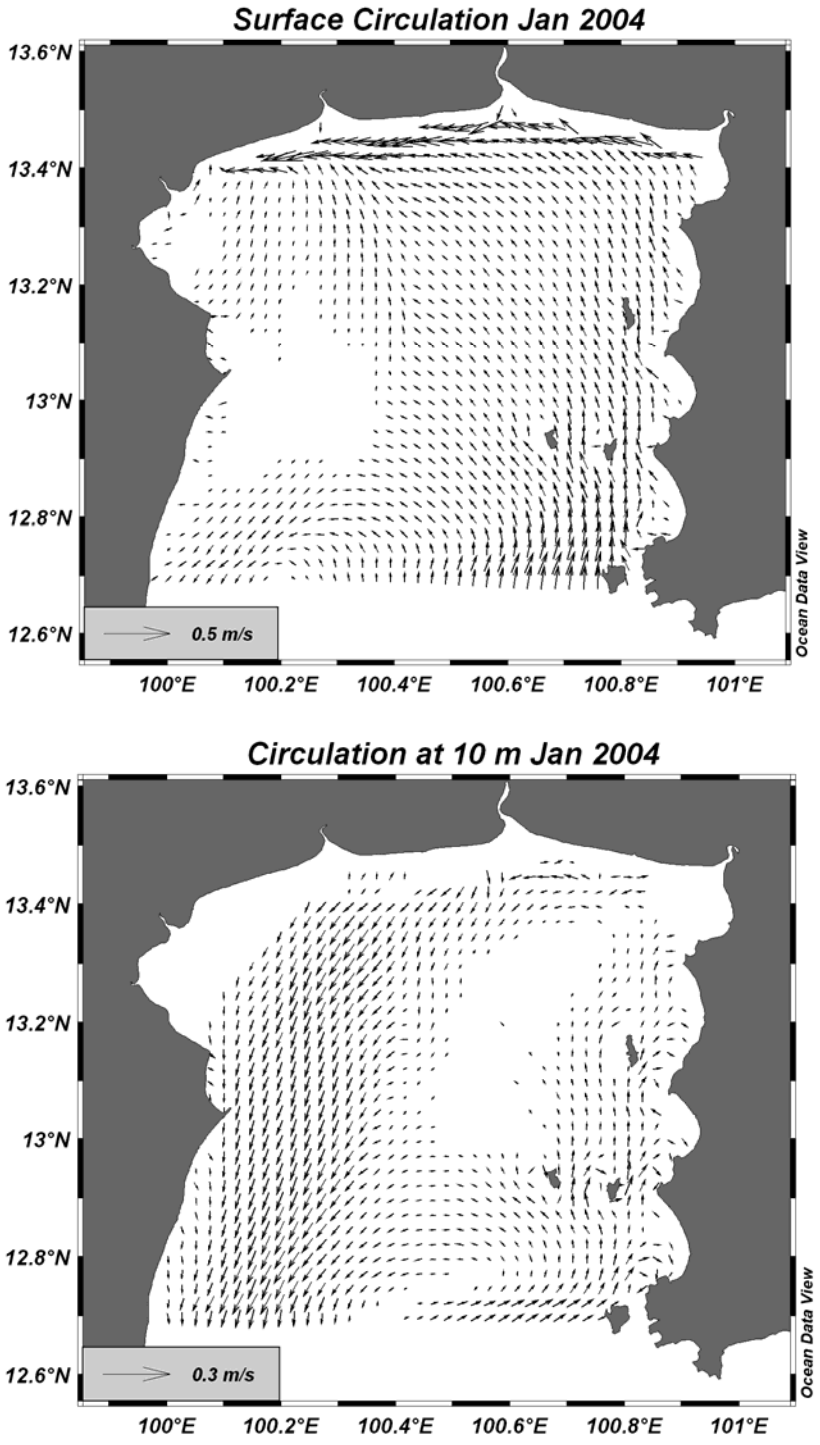

Figure 6 – 5 Simulated circulations at the sea surface and 10 m depth in January 2004

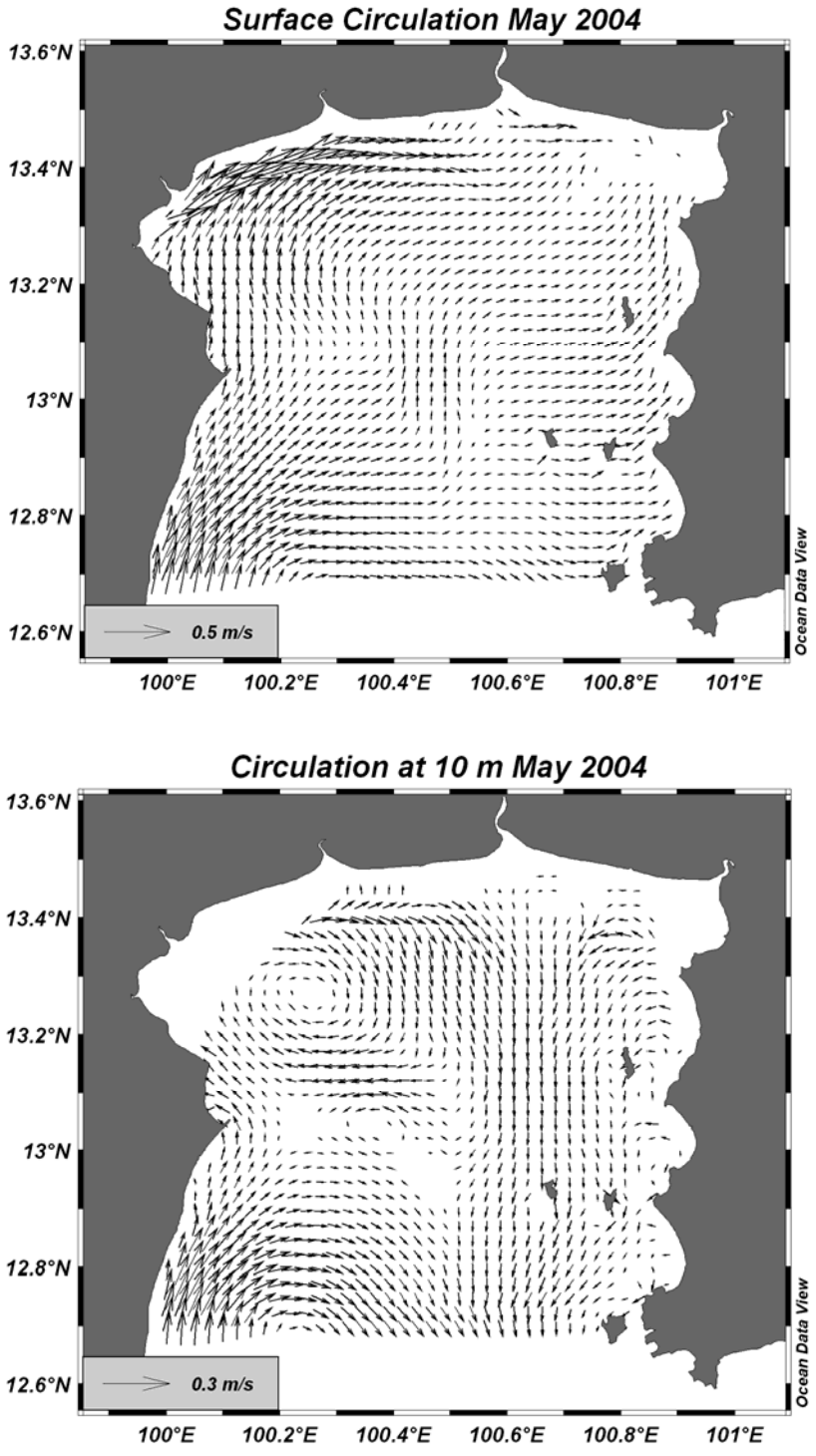

Figure 6 – 6 Simulated circulations at the sea surface and 10 m depth in May 2004

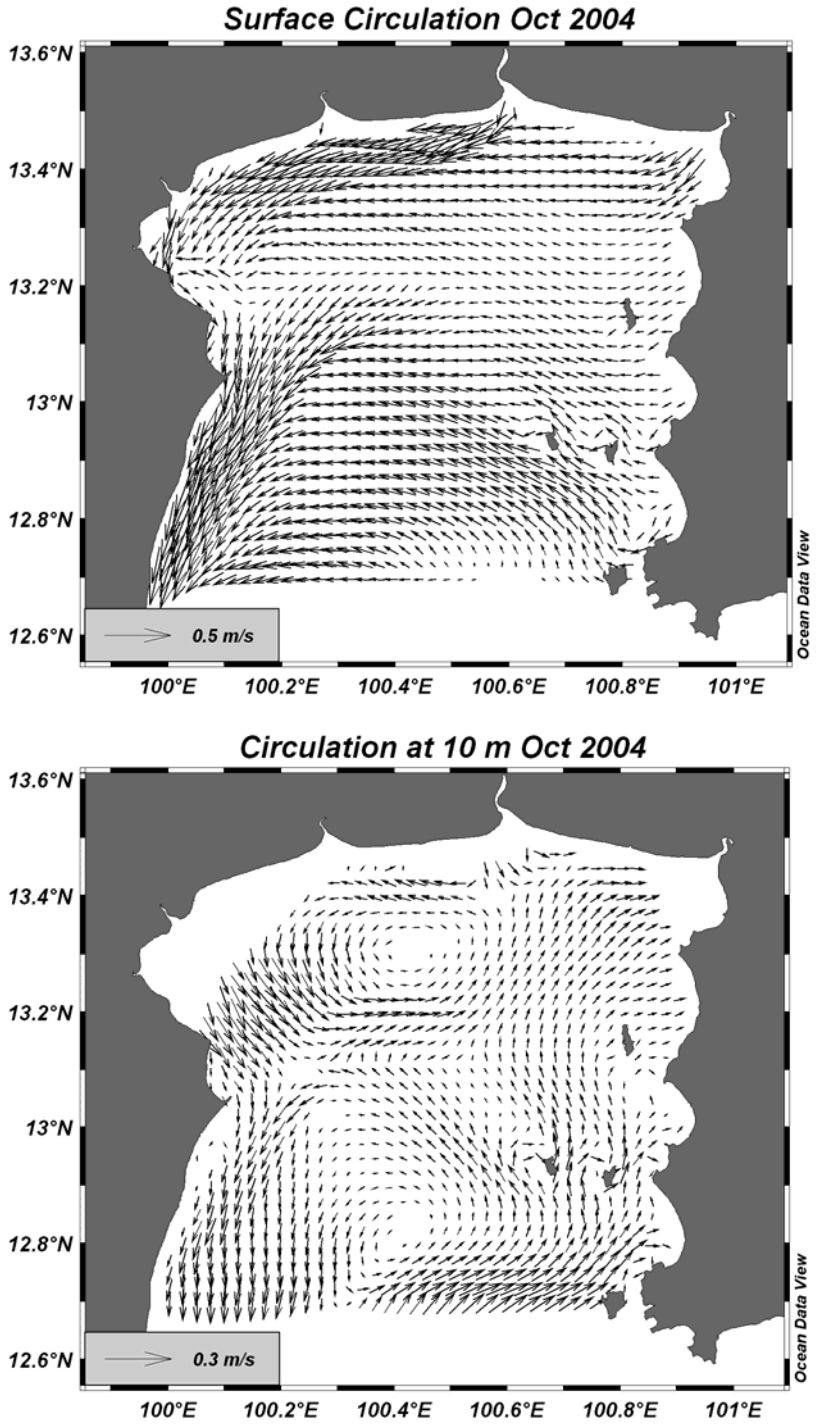

Figure 6 – 7 Simulated circulations at the sea surface and 10 m depth in October 2004

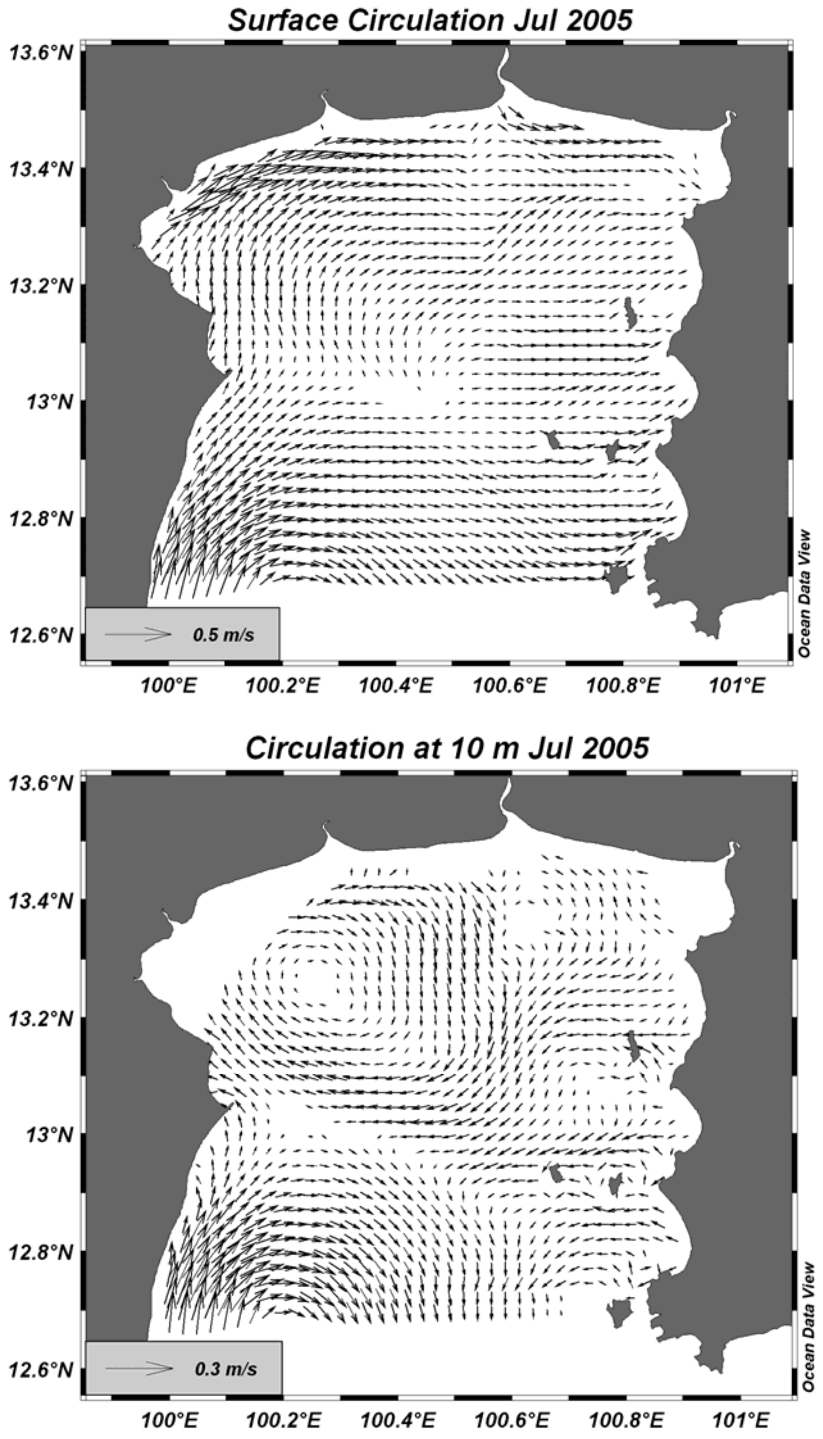

Figure 6 – 8 Simulated circulations at the sea surface and 10 m depth in July 2005

in October 2003 seems to be stronger. A counter – clockwise gyre at 10 m depth in the north is clearly observed in both periods while the second one in the south near open boundary emerges just in October 2004.

December 2003 (Figure 6 – 4)

Surface current has a trend of moving out of the gulf through the west of the sea boundary following wind that directs to southwest direction. Moderate speed currents (0.2 - 0.3 m s^{-1}) flow along western coast starting from the Chaopraya river mouth to the southern boundary. Currents in almost equal speed near the Bangpakong river mouth are observed flowing to the south along eastern coast. Most currents at 10 m depth run into the gulf to compensate outflow surface currents. They also have a tendency of inflow and outflow in the east and the west coasts, respectively.

January 2004 (Figure 6 – 5)

The southeast wind drives surface water northwestward during this time. Only some weak currents remain flowing out through the west of the sea boundary. Weak divergence current flow occurs to the north and the south near the central of western coast. The deeper current trends counter – clockwise starting from eastern, northern and western coasts, respectively, similar to those in October and December.

May 2004 (Figure 6 – 6)

Wind directions, which are mainly from the southwest, are almost opposite to those experienced in December 2003. Therefore, surface water responds by moving

into the gulf from southwest toward northeast directions. Water along the western coast moves northward instead of southward as in previous months. Currents at 10 m depth run into and out of the gulf through the west and the east of sea boundary, respectively, which is the opposite direction to the case of the east winds. A clockwise gyre develops in northwestern area where a counter – clockwise gyre developed over the same area in December 2003.

July 2005 (Figure 6 – 8)

Current patterns at both sea surface and 10 m depth in this month are almost the same as those in May 2004 because of the similarity in wind patterns from the southwest.

Vertical circulations at 5 m depth (Figure 6 – 9) were used to study upwelling and downwelling which are found to correspond to divergence and convergence conditions of surface circulations. Coastal divergence happens when currents near the coastline flow seaward bringing water offshore; upwelling by replenishment of deeper water will be a consequence. On the contrary, if surface currents run shoreward, which is the case of coastal convergence, the downwelling process will happen. Based on these facts, variations in coastal upwelling and downwelling can easily be explained by considering the directions of wind, surface currents and shoreline positions. Upwelling and downwelling along eastern and western coastlines, respectively, are generated when the easterly winds prevail over the area. The situation will reverse when wind directions change to the west.

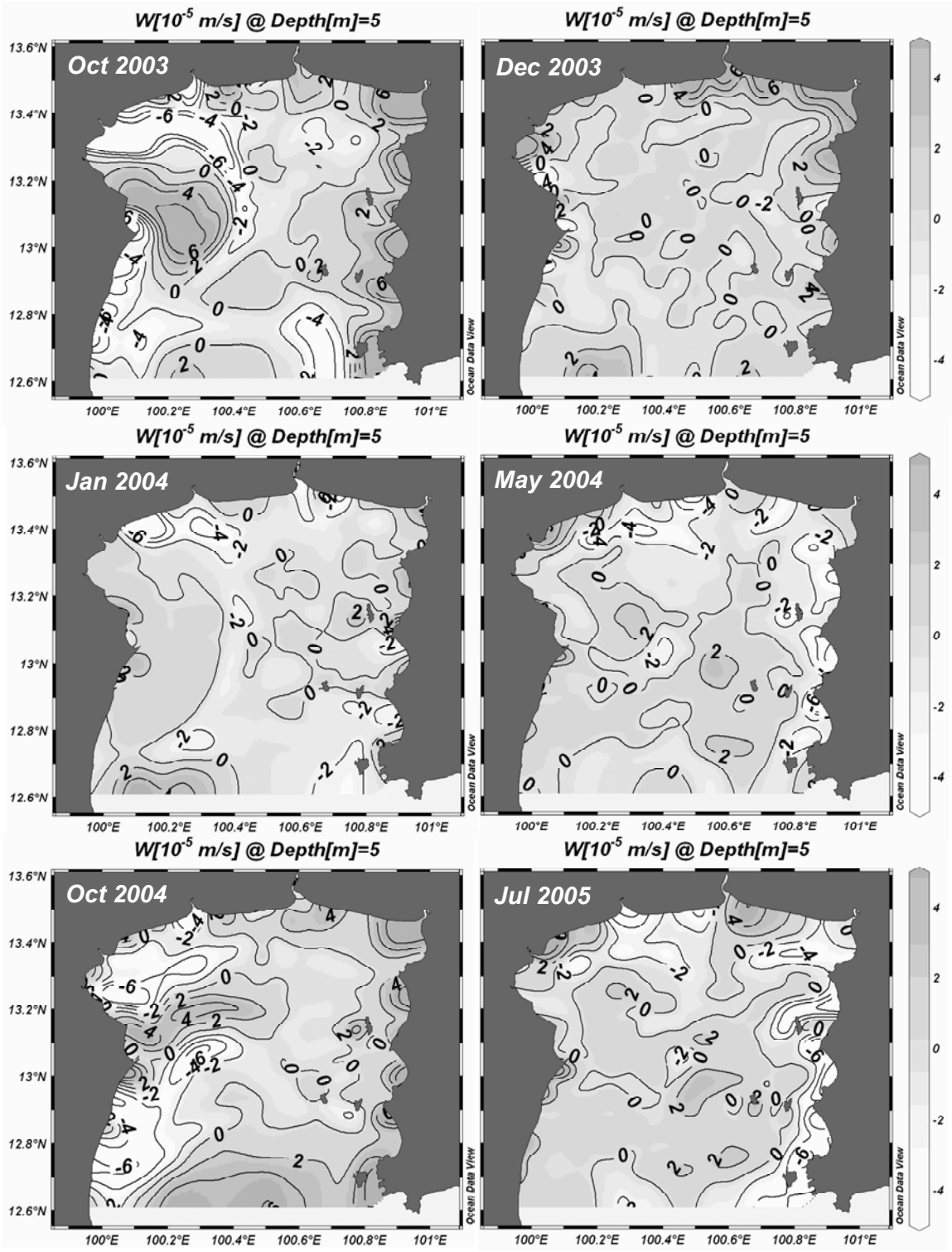

Figure 6 – 9 Computed vertical circulations in the same months of all cruises

In offshore regions, divergence and convergence at the sea surface are generated when currents move apart and move toward each other, respectively. Strong upwelling in the middle of the western coast in October 2003 and 2004 can be explained by the strong divergence of surface current over the area (Figures 6 – 3 and 6 – 7). Convergence in the north of this area, which is responsible for strong downwelling, is also explained by this mechanism. It should be noted that eddies might contribute to vertical movement but it is not the case of the upper gulf where small circular currents at the sea surface are hardly observable.

6.2.2 Two-Dimensional Results

Two important outputs of POM in two – dimensional modes, averaged sea surface elevations and vertically integrated currents, are presented and discussed in this part. Monthly mean sea level (Figure 6 – 10) indicates water pile – up in downwind areas. Sea level rises when winds flow landward in all experimental months except December 2003. Maximum elevation about 4 – 5 cm happens in May 2004 when strong southwest winds push water to rise at the northeastern corner of the gulf. It is just in December 2003 that the elevation is lower than mean sea level because surface water is induced to move out of the gulf following north-northeastern wind.

Circulation patterns are clearly seen in the case of vertically averaged circulations (Figure 6 – 11). Counter – clockwise circulations develop when the east winds (the northeast or the southeast) prevail over the area in October 2003 and 2004, December 2003 and January 2004 while a complete counter – clockwise gyre near

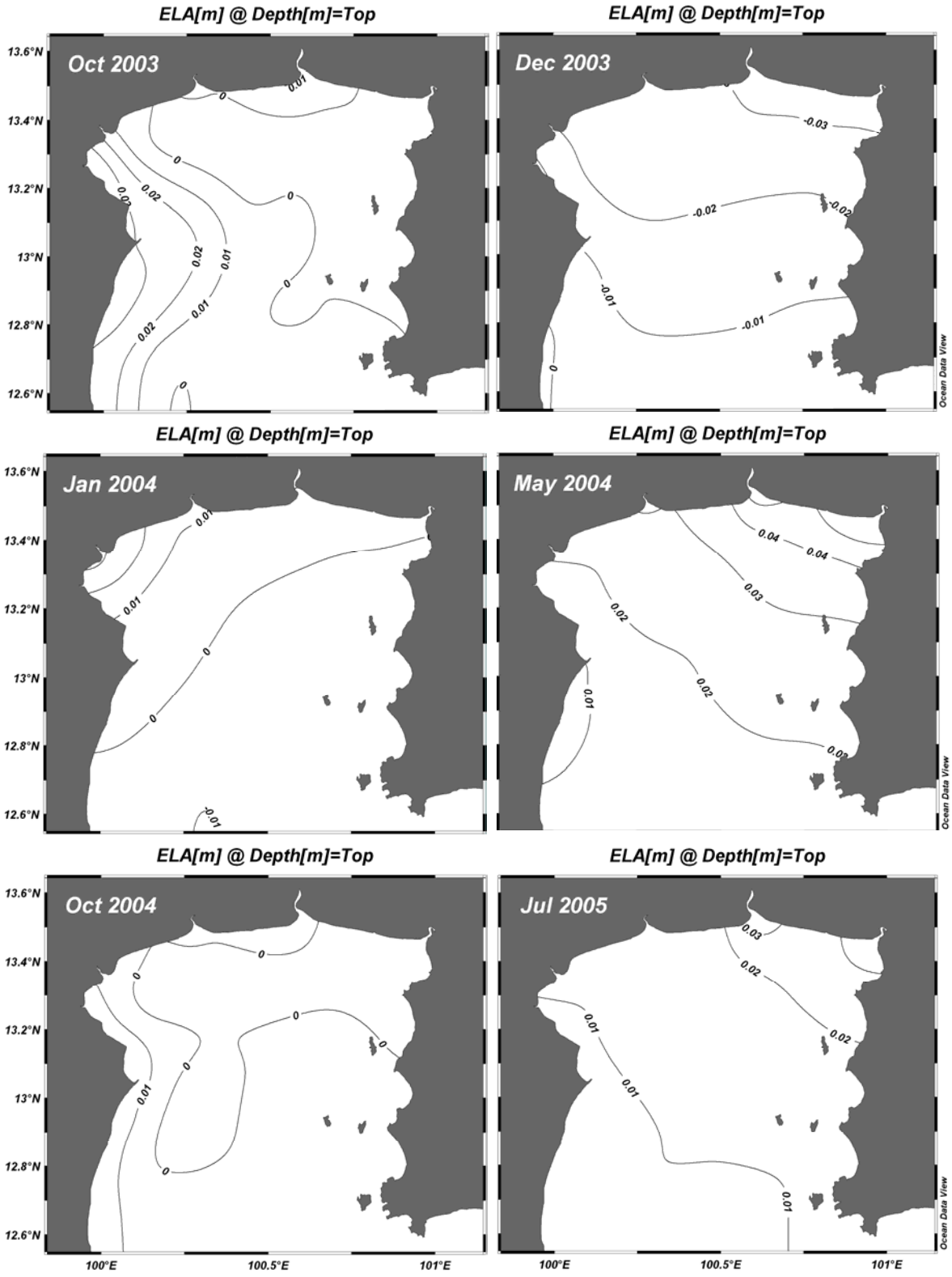

Figure 6 – 10 Monthly-averaged water elevations calculated by POM in the same months of all cruises

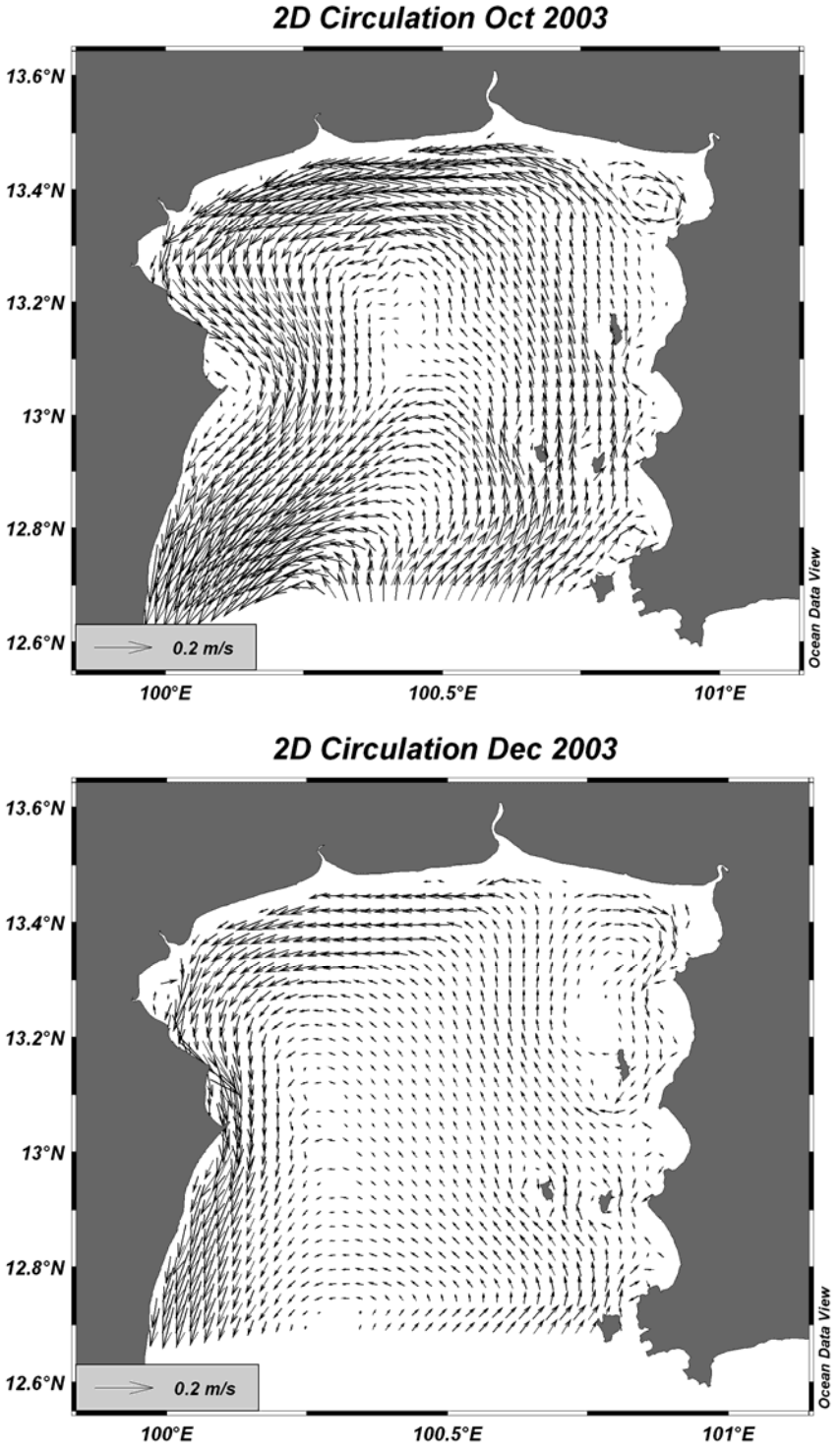

Figure 6 – 11a Vertically averaged currents calculated by POM for October and December 2003

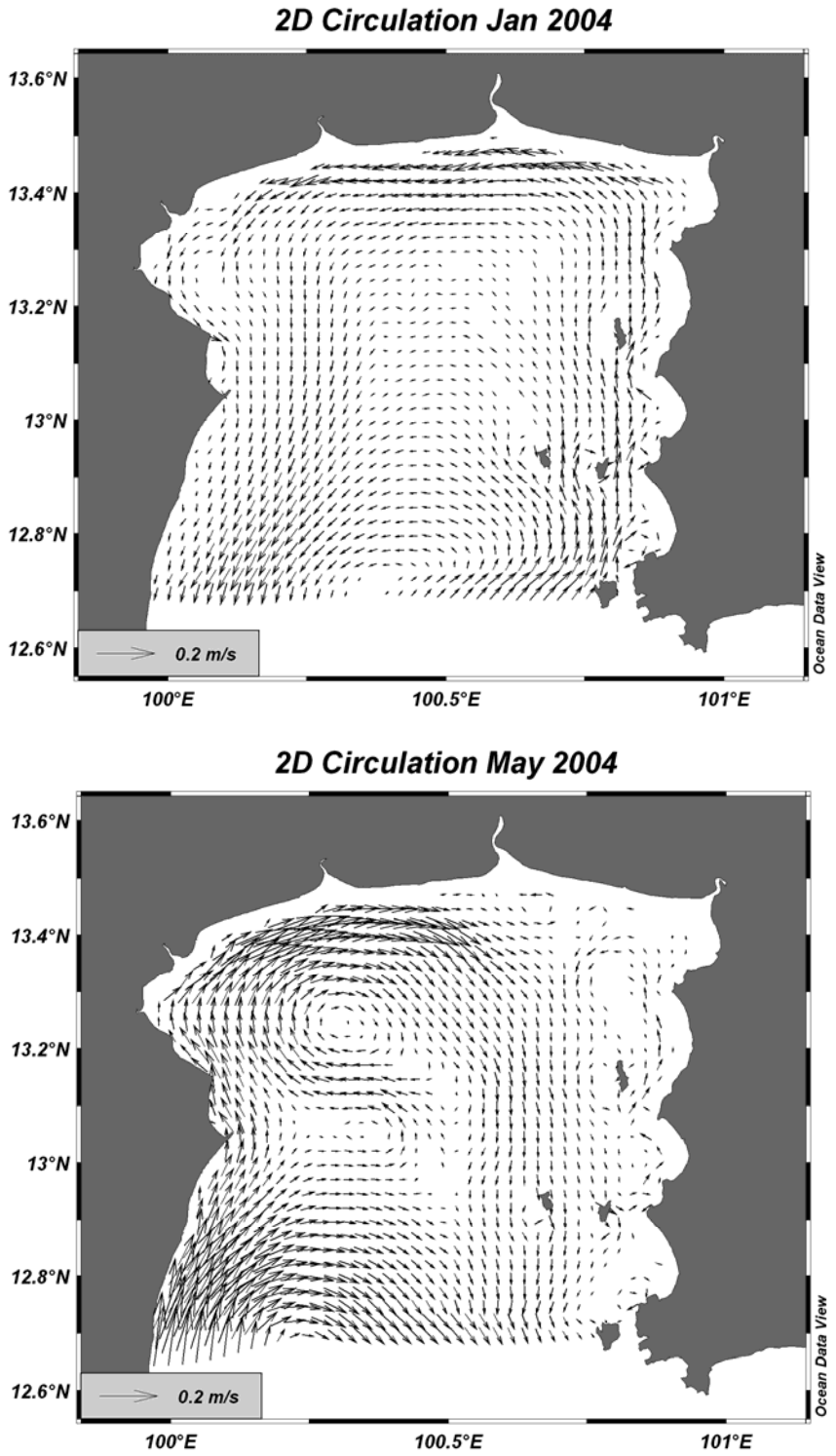

Figure 6 – 11b Vertically averaged currents calculated by POM for January and May 2004

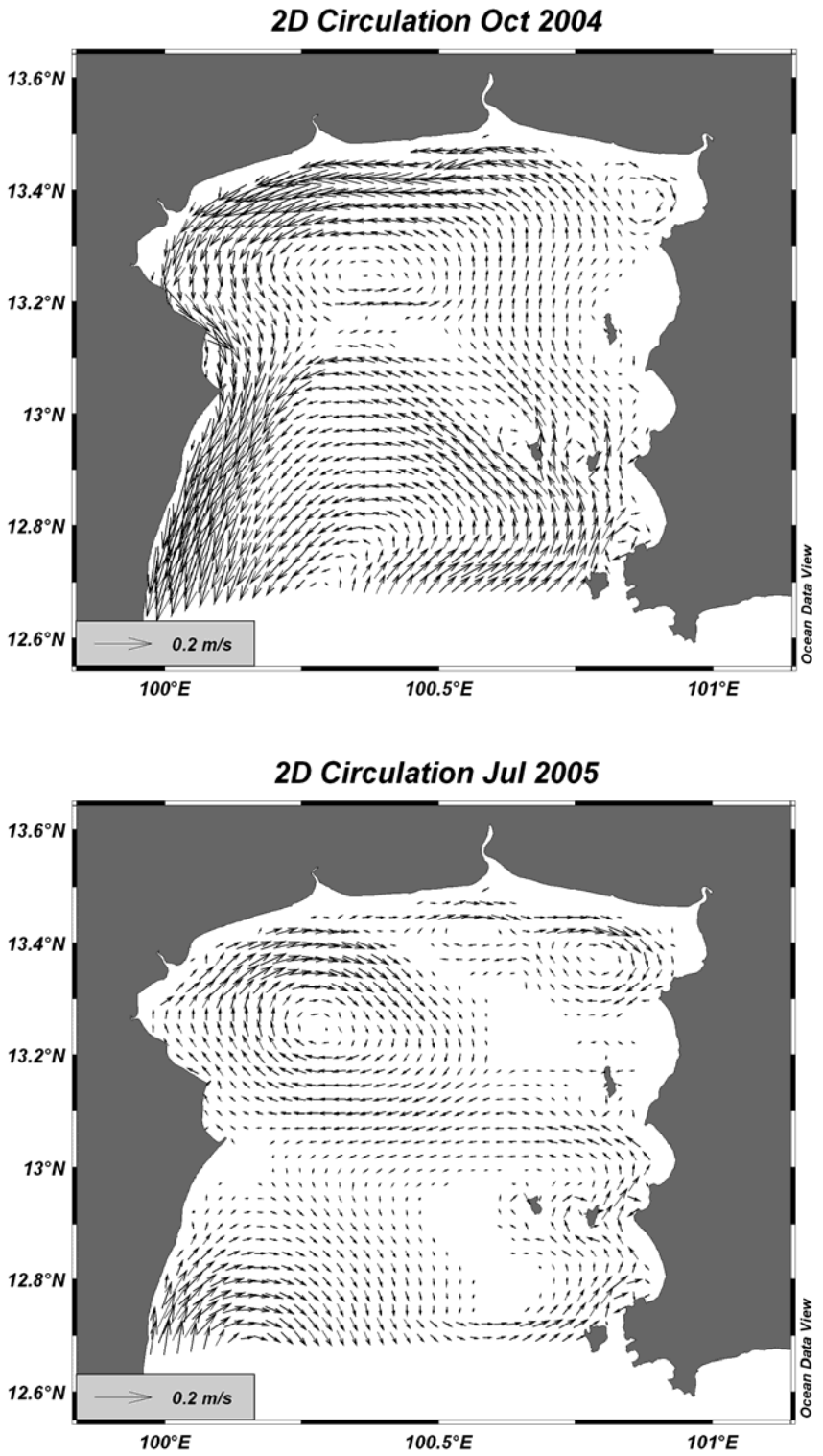

Figure 6 – 11c Vertically averaged currents calculated by POM for October 2004 and July 2005

northern coast is formed in October 2004 during the time of strong northeast wind. Circulations are reversed and more complicated under the influence of the southwest winds in May 2004 and July 2005. A big clockwise gyre develops in the northwest, while numerous eddies or small gyres, are seen dispersing throughout the eastern portion of the area. Water in this season has moved into, and out of, the gulf through the west and the east of the sea boundary, respectively.

6.2.3 Result Verification and Discussion

Simulated current patterns are verified with the results of residual currents reported in Booncherm (1999). Those data were retrieved by filtering high frequency tidal influences out of instantaneous currents measured by two SEAWATCH buoys deployed in the upper gulf during 1996 – 1998. These residual currents are redrawn in a series of current plots of each month of the year (Figure 6 – 12). The figure does not include the results from November due to data unavailability. Because buoy sensors were installed at the depth of about 3 – 5 m, surface current patterns will be mainly used with contributions of the results at 10 m depth (Figure 6 – 3 to 6 – 8) for verification purpose.

Most simulated results agree well with those of measurement in terms of surface inflows and outflows, and clockwise and counter clockwise circulations of the same months. However, discrepancies are observed in the case of July when both results indicate opposite trends of circulations – clockwise and counter – clockwise for simulated and measured results, respectively. There are two possible explanations for

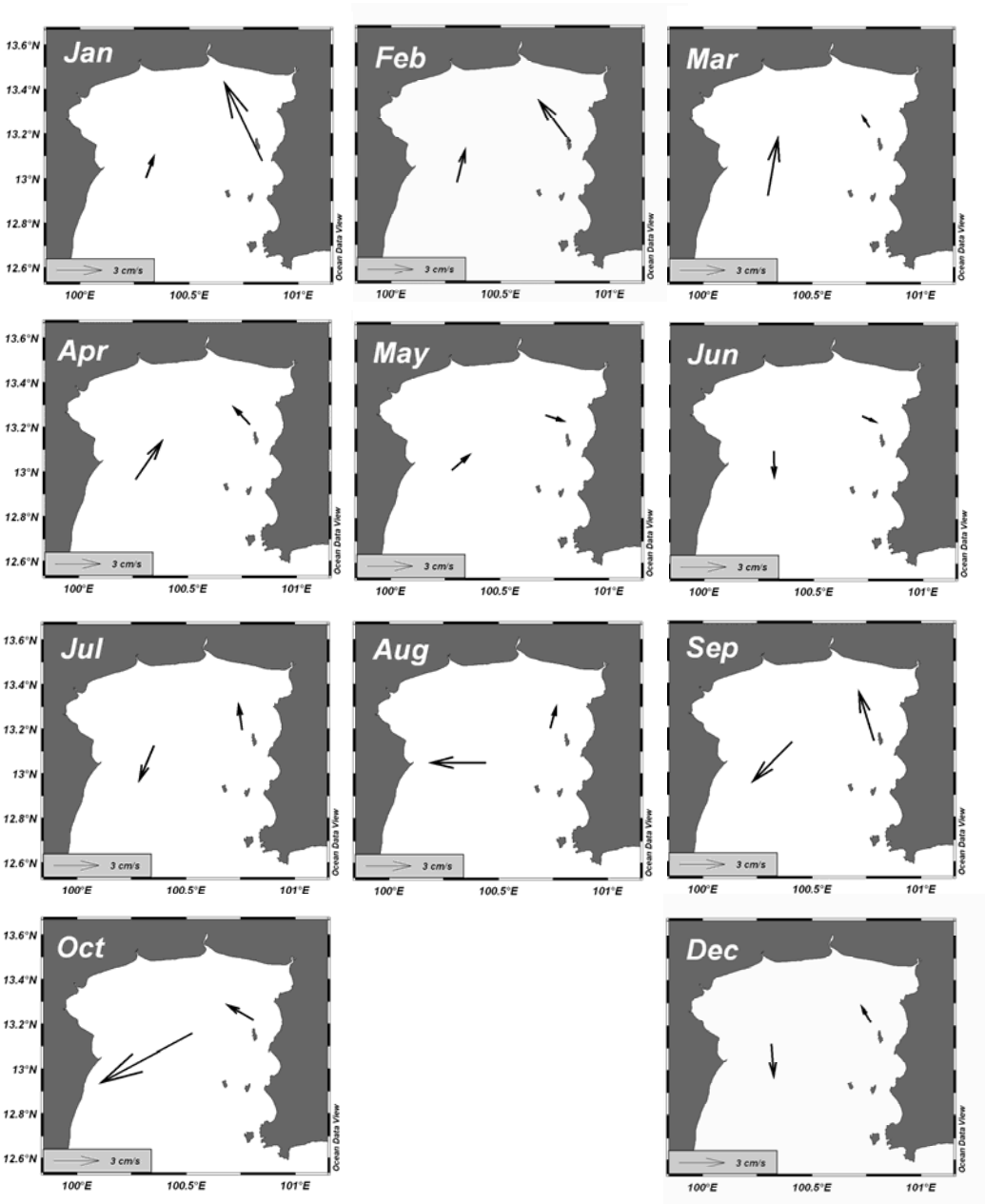

Figure 6 – 12 Residual surface currents analyzed from SEAWATCH data during 1996 – 1998 (data from Booncherm, 1999)

this difference; one is year–to–year variations of wind fields, and the other is due to interactions of water from the lower Gulf (Buranapratheprat et al., 2006). In general, if uniform wind blows from the southwest, clockwise – circulation will be generated. In the case of non-uniform wind fields, if wind curl is positive, counter – clockwise circulation might be a consequence. Such conditions happen when wind speeds in the east or in the south are stronger than those in the west or in the north, respectively. The study also suggested that if there is a strong flow coming through the east of the sea boundary (following the results of Buranapratheprat and Bunpapong, 1998) in the same time, the possibility of counter – clockwise development will increase.

Based on the results reported by Booncherm (1999), it was found that wind speeds in the south were much stronger than those in the north in July of those years. This evidence confirms the role of non-uniform winds on the patterns of residual circulation during the southwest monsoon. The situation is more complicated because the strong southwest wind itself might be a driving force of water intrusion from the lower Gulf. This issue is very interesting and needs to be clarified in the future. This study does not include the lower gulf influence due to data unavailability. The evidence suggesting that the influence of the lower Gulf is not high during this time period is found in the surface salinity distribution of cruise CU – 6 (Figure 4 – 5). A clockwise circulation pattern develops because low salinity and high chlorophyll-a near northern coast to the east. In this case, if the external influence is high, those parameters will move to opposite direction.

Vertically integrated circulation patterns are also compared with the results of Buranapratheprat et al. (2002a) to examine dissimilarities when two different

circulation models are applied to the same study area. Unlike the three-dimensional model applied in this study, the two – dimensional barotropic model of the previous study cannot include the influence of water pile–up effect and density – driven force. Overall patterns are similar especially during the northeast monsoon when counter – clockwise circulation is developed. However, dissimilarity appears during the southwest monsoon. The results of the two – dimensional model show the development of a large clockwise gyre covering the whole northern part of the gulf area. A similar pattern also appears in this study, but at a reduced size (Figure 6 – 11 in May 2004 and July 2005). It can be explained by the occurrence of reflecting force from rising water in the northeastern corner of the gulf (Figure 6 – 10 in May 2004 and July 2005) that limits extension of the gyre. All comparisons indicate that major and minor influences on circulation in the upper gulf are barotropic and baroclinic forcing, respectively.

6.3 Summary

POM was used to investigate seasonal circulations in the upper Gulf of Thailand which were found changing due mainly to influences of seasonal winds. Intrusion of surface water through the sea boundary in the east and the west corresponds to wind fields from the same directions. Water pile – up occurs when wind directs landward or to the north in almost every month of the experiments. It is just in December 2003 that wind flows to the south making the monthly averaged water level lower than mean sea level (MSL). Water in deeper layer tried to adjust

itself to the movement of surface water and characteristics of bottom topography. This phenomenon agrees well with vertical circulation that reveal water upwelling and downwelling owing to divergence and convergence conditions at the sea surface, respectively. Circulation patterns in the gulf are clearly seen in the case of vertically averaged current results. Clockwise and counter–clockwise patterns are developed during the influences of the southwest and the northeast winds, respectively, in the same way as those of previous investigation by using a two – dimensional circulation model. Comparisons between the results of both models show some discrepancy as a consequence of the water pile–up effect. Model validation indicates that general circulation patterns agree well with observations. Reverse circulations between both results in July are, however, due to year–to–year variations in wind patterns and interaction of water from the central Gulf of Thailand.

CHAPTER 7

AN ECOSYSTEM MODEL FOR INVESTIGATION OF SURFACE CHLOROPHYLL DISTRIBUTIONS

This chapter focuses on the investigation of the relationship between surface chlorophyll distributions and environmental factors by using a numerical model for the lower trophic level of marine ecosystem. The concept and structure of the model are thoroughly explained in the first part. Coupled with POM, it is used to simulate chlorophyll distributions under the general environmental conditions of the study area. Calculated results are compared and verified with those of MERIS data and field observations, and then analyzed to explain the occurrence of high and low chlorophyll levels with supporting factors. They are carefully re-investigated in sensitivity analyses when key influencing parameters namely nutrient loads, discharges and wind magnitudes are modified. The main purpose of all experiments is to clarify the mechanism of seasonal variations in surface chlorophyll dynamics in the upper Gulf of Thailand.

7.1 Ecosystem Model

This section describes details of an ecosystem model for the simulation of chlorophyll distributions, starting from basic concepts to practical operation. The first part discusses the model structure, its compartments, and transformation from conceptual to mathematical forms. Such a model is composed of several biochemical

functions, whose parameterization are explained. Data preparation and pre-processing are subsequently articulated, and finally the details of model operation are presented.

7.1.1 Model Structure

NPZD (Nutrient-Phytoplankton-Zooplankton-Detritus), a pelagic ecosystem model (Onitsuka and Yanagi, 2005), is selected for this study due to its simplicity. It has been applied successfully in several studies such as Yanagi et al. (1997) and Guo and Yanagi (1998). Generally, an ecosystem model is composed of a number of biochemical functions that require a range of related parameters and inputs. Ecosystem models cover a range of complexity, but commonly the most successful implementation is with the simpler ones owing to a lack of detailed supporting data. This is the case with the current study where physiological data of phytoplankton and zooplankton required by the model have rarely been reported.

The ecosystem model has five compartments instead of four following its NPZD name, because nutrients are separated into dissolved inorganic nitrogen (DIN) and dissolved inorganic phosphorous (DIP) (Figure 7 – 1). Silicate, another important nutrient for some plankton species such as diatoms, is not considered in the model system because the study is focused on chlorophyll distributions which are independent to plankton species. The diagram in Figure 7 – 1 illustrates that changing one model component will influence others. Phytoplankton growth reduces the amount of nutrients via photosynthesis but increases the number of zooplankton at the same time by grazing. Phytoplankton and zooplankton mortality, together with solid waste

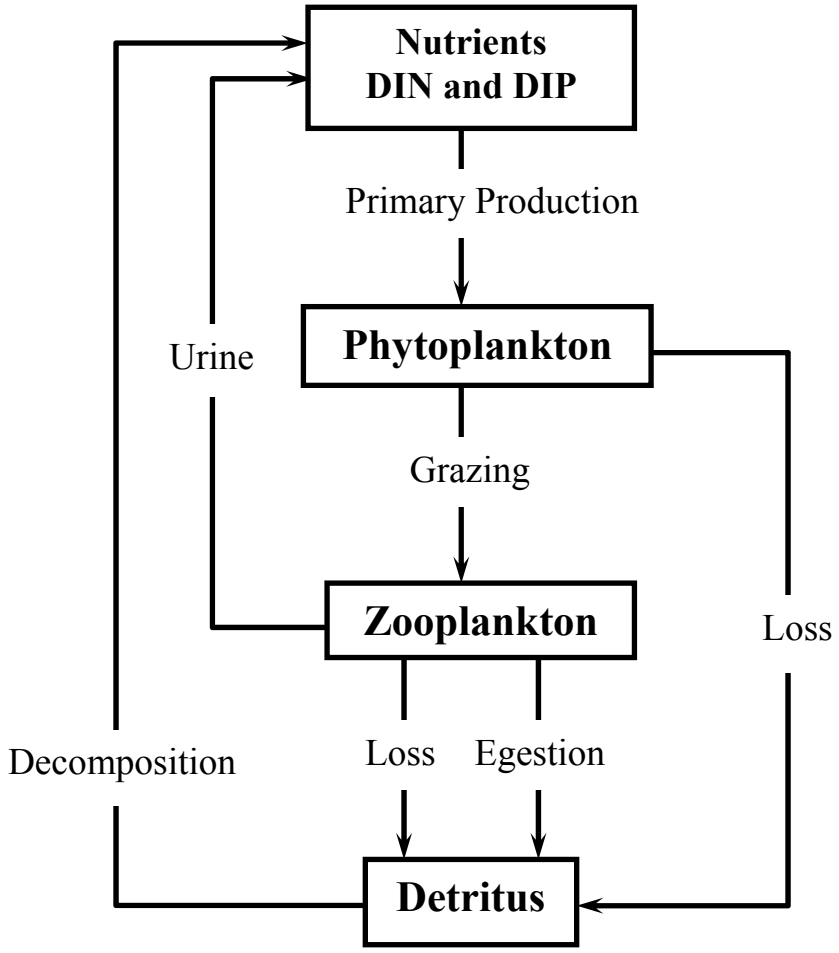

Figure 7 – 1 Schematic diagram of the ecosystem model

(egestion) of zooplankton, contribute to detritus that accumulates in water column. The cycle of the system is complete when detritus and urine of zooplankton are decomposed back to nutrients for phytoplankton use. Besides being controlled by others, each component might be altered by environmental factors such as temperature, salinity, light and water circulation. All of these relations can be transformed into mathematical functions, which are presented below.

7.1.2 Governing Equations and Biochemical Parameters

The five compartments in the diagram of Figure 7 – 1 are incorporated into five governing equations (Guo and Yanagi, 1998), written in the Cartesian coordinate, shown as follows.

Phytoplankton (P):

$$\frac{\partial P}{\partial t} + \vec{V} \cdot \nabla P + S_P \frac{\partial P}{\partial z} = DIF(P) + A_1 P - R_1 P - A_2 P^2 - A_3 Z \qquad (7-1)$$

Zooplankton (Z):

$$\frac{\partial Z}{\partial t} + \vec{V} \cdot \nabla Z = DIF(Z) + A_3 Z - A_4 Z^2 - A_5 Z - A_6 Z \qquad (7-2)$$

Detritus (D):

$$\frac{\partial D}{\partial t} + \vec{V} \cdot \nabla D + S_d \frac{\partial D}{\partial z} = DIF(D) + A_2 P^2 + A_4 Z^2 + A_6 Z - A_7 D \qquad (7-3)$$

DIN (N_N):

$$\frac{\partial N_N}{\partial t} + \vec{V} \cdot \nabla N_N = DIF(N_N) - A_1 P + A_6 Z + A_7 D \qquad (7-4)$$

DIP (N_P):

$$\frac{\partial N_P}{\partial t} + \vec{V} \cdot \nabla N_P = DIF(N_P) - A_1 P + A_6 Z + A_7 D \qquad (7-5)$$

where

$$DIF(\,) = \frac{\partial}{\partial x}\left(K_h \frac{\partial}{\partial x}\right) + \frac{\partial}{\partial y}\left(K_h \frac{\partial}{\partial y}\right) + \frac{\partial}{\partial z}\left(K_v \frac{\partial}{\partial z}\right), \text{ and}$$

$$\vec{V} \cdot \nabla(\,) = u\frac{\partial}{\partial x} + v\frac{\partial}{\partial y} + w\frac{\partial}{\partial z}.$$

$\vec{V}$ is three-dimensional velocity composed of *u, v,* and *w* which are velocity components in *x, y* and *z* directions, respectively; *x* and *y* are axes in horizontal plane, and *z* is that on vertical directions; *t* is time; and K_h and K_v are horizontal and vertical diffusivities, respectively. Velocity and diffusivity data used in the ecosystem model are the results of POM computed in the same time step. The biochemical terms in the governing equations are described as follows.

A_1P: Photosynthesis of phytoplankton in which the growth rate A_1 is decided by:

$$A_1 = V_m \, k_T \min\{V_1(N_N), V_1(N_P)\} \cdot V_2(I), \qquad (7-6)$$

$$V_1(N_N) = \frac{N_N}{K_{SN} + N_N}, \tag{7 – 7}$$

$$V_1(N_P) = \frac{N_P}{K_{SP} + N_P}, \tag{7 – 8}$$

$$V_2(I) = \frac{I}{I_{opt}} \exp\left(1 - \frac{I}{I_{opt}}\right), \tag{7 – 9}$$

where V_m denotes the maximum photosynthetic rate of phytoplankton at 0 ^{o}C; K_{SN} and K_{SP} the half saturation constant for DIN and DIP uptakes, respectively; I_{opt} is the optimum light intensity for the growth of phytoplankton; I is the light intensity at a given depth which is expressed as:

$$I(z) = I_s \exp\left[-\int_0^z k(z)\,dz\right], \tag{7 – 10}$$

$$k(z) = 0.04 + 0.054\, C(z)^{\frac{2}{3}} + 0.0088\, C(z), \tag{7 – 11}$$

$$C(z) = P(z) + \delta(Z(z) + D(z)), \tag{7 – 12}$$

where I_s denotes the light intensity at the sea surface; k is the extinction coefficient; and C is the concentration of chlorophyll-a. The self-shading, a phenomenon contributing to decreased under water light resulting from suspended plankton cells and other organic particles, is represented by Eq. (7 – 11) (Riley, 1956). Not only phytoplankton, but also zooplankton and detritus, are taken into consideration (Eq. (7 – 12)) in the simulation. δ is a constant representing the contribution of zooplankton and detritus on self-shading effect.

Temperature and salinity might be included in the growth function A_1 (Eq. (7-6)) if they have a strong influence on phytoplankton abundance or distribution. In this

study, neither factor is considered in the function because the results of scatter plots demonstrate no significant relationship with chlorophyll-a (Figure 7 – 2). This is consistent with the finding of Rungsupa et al. (2003).

Chlorophyll independence of salinity and temperature can be explained by a number of factors. Euryhaline ability and species succession are explained the occurrence of blooming in a wide salinity range. *Noctiluca scintillans*, *Ceratium furca* and *Tricodemium erythraeum* are three dominant blooming species having been reported (Menasveta, 2000; Lirdwittayaprasit et al., 2006), with the first two belonging to the euryhaline group. *Noctiluca* and *Ciratium* red tides in the Bangpakong estuary were found in the salinity ranges of 22 – 33 and 12 – 27 psu, respectively (Lirdwittayaprasit et al., 2006). This fact suggests that red tide in the upper Gulf could happen all year round since salinity variation in the whole gulf (22 – 34 psu) is close to those ranges. Species succession might also play an important role because optimal salinity of *Noctiluca* bloom is higher than that of *Ciratium* bloom. Thus, rise and fall of salinity will lead to switching from one to another dominant species while total plankton density or chlorophyll concentration is still unchanged.

Water temperature is considered not to be important in changing in phytoplankton population owing to the tropical location. The range of surface temperatures in this study is just about 26 – 31 ^{o}C while those in temperate sea, for example in the Sea of Japan is as large as 1 – 20 ^{o}C (Yanagi et al., 2001). Undoubtedly, a temperature increase in spring is an important factor to stimulate the bloom in temperate water. This phenomenon is not evident in the Thailand gulf, where phytoplankton bloom could be found even in December (see Chapter 4 and 5) which is

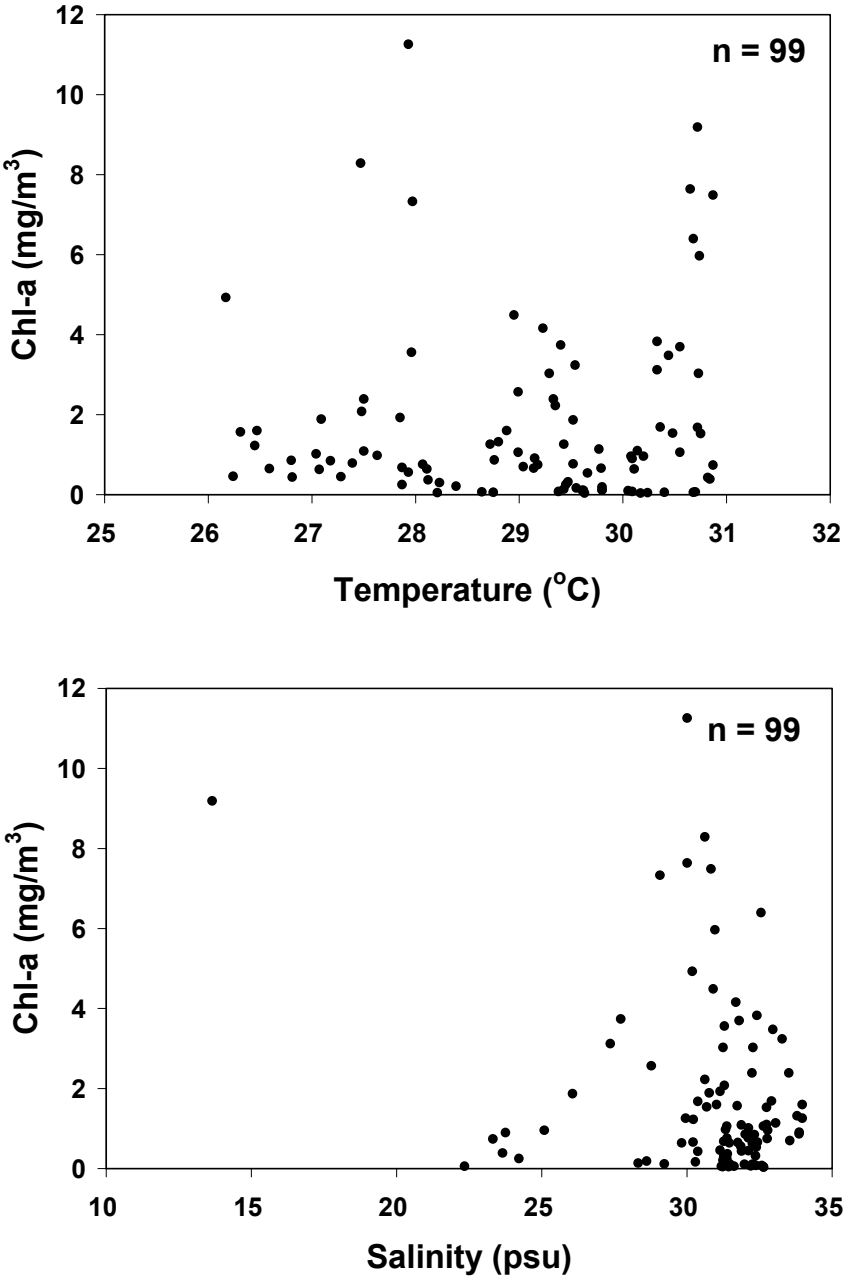

Figure 7 – 2 Scatter plots of chlorophyll-a and temperature (upper panel), and chlorophyll-a and salinity (lower panel) at the sea surface of data from all cruises

the local wintertime, because temperature is always high with small seasonal variation. Therefore, chlorophyll concentration becomes independent of fluctuations of water temperature in this study area.

The temperature coefficient k_T is used in the functions of photosynthetic rates (Eq. (7 – 6)), respiration rate of phytoplankton (Eq. (7 – 13)), mortality rate of phytoplankton (Eq. (7 – 14)) and zooplankton (Eq. (7 – 16)), grazing of zooplankton (Eq. (7 – 15)), and decomposition rate of detritus (Eq. (7 – 19). It is derived from a function of $\exp(k \cdot T)$: where k is a constant 0.0693 (Kawamiya et al., 1995) and T is water temperature in ^{o}C. Here T is assigned as 30 ^{o}C which is approximated from observed data; therefore, k_T is equal to 7.9964. k_T can be set as a function dependent on temperature if seasonal variations of temperature are large, or there is a clear evidence of its relation with chlorophyll and other relevant parameters.

R_1P: Respiration rate of phytoplankton which R_1 is dependent to k_T and the respiration rate at 0 ^{o}C (R_0).

$$R_1 = k_T R_0 \qquad (7 - 13)$$

A_2P^2: Natural mortality of phytoplankton. A_2 is a function of k_T and mortality rate of phytoplankton at 0 ^{o}C (M_p) which is defined as:

$$A_2 = k_T M_p . \qquad (7 - 14)$$

A_3Z: Grazing of zooplankton, A_3 is expressed by:

$$A_3 = k_T \, R_{\max} \left[1 - \exp \lambda \left(- P + P^*\right)\right], \qquad (7 - 15)$$

where R_{max} denotes the maximum grazing rate at 0 ^{o}C; λ is the Ivlev constant; P^* is the threshold of phytoplankton concentration for possible grazing by zooplankton. When P is smaller than P^*, A_3 is set to zero which means phytoplankton will not be eaten if its concentration is smaller than the grazing threshold.

A_4Z^2: Natural mortality of zooplankton. A_4 is set to be equal to:

$$A_4 = k_T M_z, \qquad (7-16)$$

where M_z is mortality rate of zooplankton at 0 ^{o}C.

A_5Z: Egestion of zooplankton. The production rate of fecal pellets of zooplankton (A_5) which is proportional to A_3, is given by:

$$A_5 = (1-\alpha_z)\cdot A_3, \qquad (7-17)$$

where α_z is assimilation efficiency of zooplankton.

A_6Z: Excretion of zooplankton. The generation rate of urine of zooplankton A_6 is expressed by:

$$A_6 = (\alpha_z - \beta_z)\cdot A_3, \qquad (7-18)$$

where β_z is the growth efficiency of zooplankton.

A_7Z: Decomposition of detritus. The decomposition rate of detritus A_7 is defined as:

$$A_7 = k_T V_{PN}, \qquad (7-19)$$

where V_{PN} is the decomposition rate of detritus at 0 ^{o}C.

$S_p \partial P / \partial z$ and $S_d \partial D / \partial z$: Sinking of phytoplankton and detritus, respectively. Here both sinking velocities (S_p and S_d) are set as constants.

Because relevant parameters especially physiological properties of plankton in the Gulf of Thailand have rarely been reported, it is necessary to use the data measured from other regions, or as applied to other ecosystem model experiments instead. Table 7 – 1 summarizes all parameters used in the ecosystem model with their previously reported values and references. Most of them are in ranges of the reported values but some are not due to adjustment to keep the results of chlorophyll concentration within observed ranges.

7.1.3 Pre-Processing and Model Operations

This section provides the details of data preparation for the operation of an ecosystem model which needs as inputs chlorophyll-a, DIN and DIP at the river and the sea boundaries, and solar radiation at the sea surface. Nutrient concentrations at all major river mouths are required to calculate nutrient loads, but no such data were collected during the times of field observations. Therefore, data from the closest stations to each river mouth are applied for this purpose instead. It is realized that they might not be representative of values found at the river mouths because of long distances between the referred and the measured points. Accordingly, sensitivity

Table 7-1 Parameters and their references used in the ecosystem model

Definitions	Symbols	Values	Units	Reported values	References
Maximum photosynthetic rate at 0℃	V_m	1.5	day^{-1}	0.05 – 8.10	Parson et al. (1984)
Half saturation constant for DIN	K_{SN}	1.0	μmol-N l^{-1}	0.04 – 4.21	Parson et al. (1984)
Half saturation constant for DIP	K_{SP}	0.05	μmol-P l^{-1}	0.008 – 0.530	O'Conner et al. (1975)
Optimum light intensity for phytoplankton	I_{opt}	16.0	$MJ/m^2/day$	1.8 – 12.0	Parson et al. (1984)
Temperature coefficient	k_T	7.80			
Respiration rate of phytoplankton at 0℃	R_0	0.02	day^{-1}	0.030 – 0.051	Di Toro et al. (1971)
Natural mortality rate of phytoplankton at 0℃	M_p	0.03	$(\mu mol\text{-}N\ l^{-1}.day)^{-1}$	0.04	Onisuka and Yanagi (2005)
Maximum grazing rate of zooplankton at 0℃	R_{max}	0.3	day^{-1}	0.3	Kawamiya et al. (1995)
Ivlev constant	λ	0.47	$(mgChl\text{-}a/m^3)^{-1}$	0.47	Smayda (1973)
Threshold of phytoplankton in grazing	P^*	0.05	$mgChl\text{-}a/m^3$	0.08 – 0.09	Kawamiya et al. (1995)
Natural mortality rate of zooplankton at 0℃	M_z	0.06	$(\mu mol\text{-}N\ l^{-1}day)^{-1}$	0.06	Kawamiya et al. (1995)
Assimilation efficiency of zooplankton	α_z	0.7		0.7	Onisuka and Yanagi (2005)
Growth efficiency of zooplankton	β_z	0.3		0.3	Onisuka and Yanagi (2005)
Bacterial decomposition rate pf detritus at 0℃	V_{PN}	0.05	day^{-1}	0.05	Fasham et al. (1990)
Sinking velocity of phytoplankton	S_p	10	cm day^{-1}	33	Smayda (1970)
Sinking velocity of detritus	S_d	100	cm day^{-1}	100	Nakata (1993)

analysis of nutrient variation at the river mouths (Section 7.3) was conducted to investigate the response of the system to this potential effect. The results are also interpreted as a scenario when nutrient loads might be changed in the future due to regulations (smaller loads) and increasing pollution (larger loads).

For the sea boundary, chlorophyll-a, DIN and DIP at all cross-sectional grids are derived from extrapolation and interpolation of data of the stations close to the boundary line. The Guass function for two-dimensional approximations (Eq. (6 – 1) and (6 – 2)) is applied for this purpose. The model also needs phytoplankton and detritus data at the open boundary, but neither was available. Based on energy transfer in the trophic level system (Nybakken and Bertness, 2004) which is also applied to the biomass, zooplankton is assumed to be 10 % of phytoplankton biomass while organic detritus is assumed to be equal to phytoplankton biomass. These assumptions are also applied at the river boundaries and the initial conditions of model simulation.

Due to data unavailability, averaged solar radiation measured at the Bangkok meteorological station of years 1993 to 2000 (Figure 7 – 3) were used to characterize the radiation over the study area to calculate underwater light intensity (Eq. (7 – 10) and (7 – 11)) instead of using data simultaneous field measurements. High and low radiation occurs from March to June and October to December, which are summertime and wintertime, respectively, and the annual average is as high as 18.64 MJ m^{-2} d^{-1}.

Computational domain, grid spacing and time steps are the same as those of POM described in Chapter 6. Lateral sea boundary condition of ecosystem parameters namely P, Z, N_N, N_P and D are the same as those of temperature and salinity with fixed values at all grid locating along the boundary plane throughout model operation.

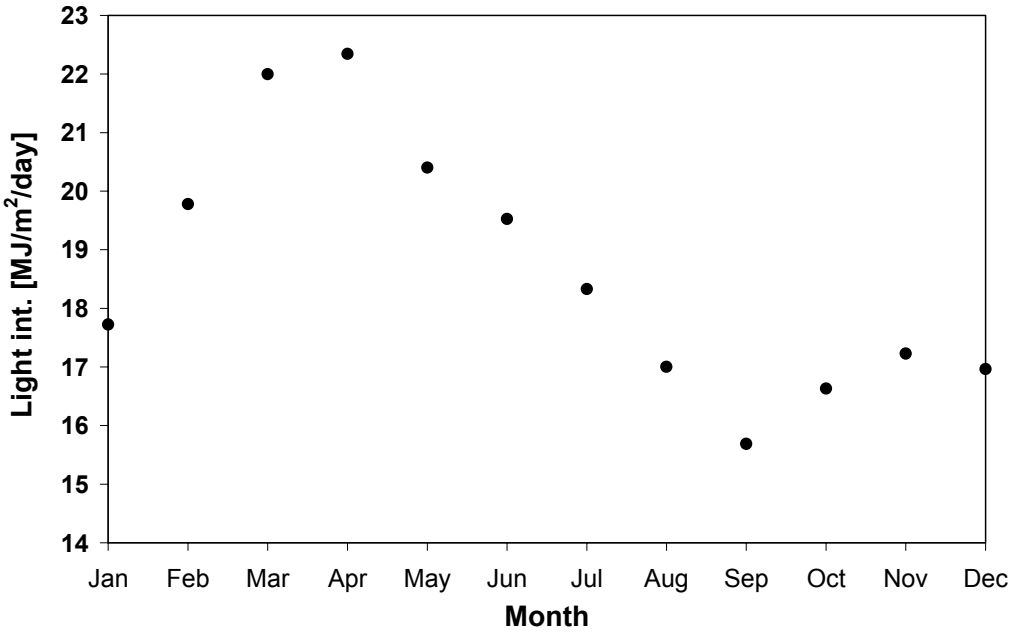

Figure 7 – 3 Monthly-averaged light intensities of the data from 1993 to 2000 measured at the Bangkok meteorological station

Exchange fluxes of those parameters at the sea surface and bottom boundaries are not permitted because they are unknown but assumed to be small when compared to the river loads. However, they are set to be recycled in the system until being transported out through the sea boundary. Just the loads of major rivers are taken into consideration, while non-point source nutrients along coastlines are ignored due to a lack of reliable data. Here DIN and DIP loads presented in figure 7 – 4 are calculated by multiplication of monthly averaged discharges and their concentrations at the river boundaries. This condition is appropriate for the objective of this study that needs to investigate the seasonal dynamics of these nutrient sources and their roles to phytoplankton distributions.

Initial values of ecosystem parameters, derived from the overall average of measured data, are set to be identical in all experiments which are 1.65 mg m^{-3}, 10.70 μM-N l^{-1} and 0.33 μM-P l^{-1} for chlorophyll-a, DIN and DIP, respectively. Zooplankton and detritus are assigned as 10% of chlorophyll-a and equal to chlorophyll-a concentrations, respectively, similar to lateral boundary setting. By application of this computational technique, units of all parameters have to be identical, and μM-N l^{-1} is selected as the standard unit for this experiment. Redfield mole ratio of C:N:P (= 106:16:1) (Redfield et al., 1963) and C:Chl-a mass ratio (= 50) (Parson et al., 1984) are major converters to modify parameter units. Values of the ratios might be different area-by-area due to dominant plankton species and their physiological properties. However, it is appropriate to apply the standard values in order to relatively compare the seasonal variations of chlorophyll distributions when local environmental factors have been changed.

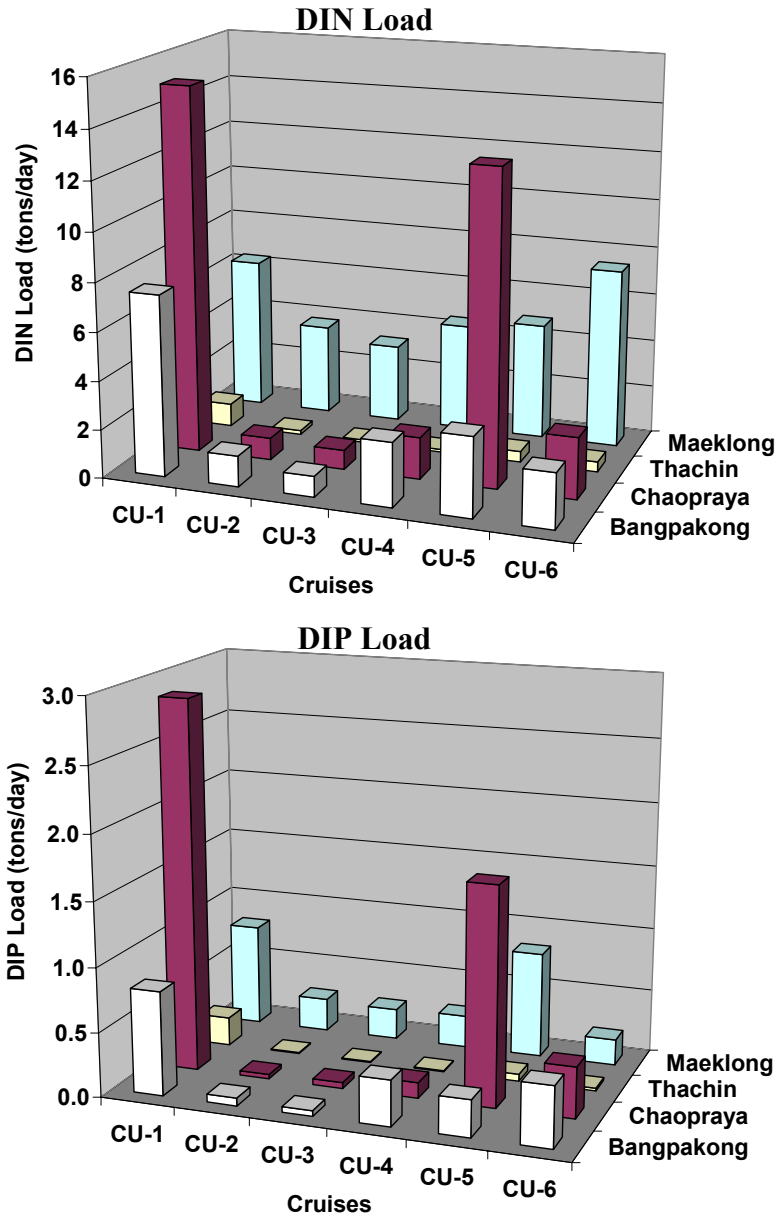

Figure 7 – 4 Averaged DIN and DIP loads of major rivers

The model operation was tested. The steady state of all simulated parameters was attained at days 10 of computation. Calculated results were collected and averaged from days 20 to 50 in the same ways as those of circulation model. Simulated chlorophyll distributions in the same months of observational cruises are presented and discussed in following sections.

7.2 General Simulations

The results of the general simulation under the conditions described in section 7.1 are presented and discussed in this section. Calculated chlorophyll distributions at the sea surface in the same months of observational cruises (Figure 7 – 5) clearly reveal their seasonal variability. However, in order to explain their variability, the patterns of wind fields (Figure 4 – 3), river discharges (Figure 6 – 2), nutrient loads (Figure 7 – 4) and circulation (Chapter 6) have to be taken into consideration.

High chlorophyll bands always appear downwind or aligned with surface currents. Winds and currents moving to the west induce high chlorophyll-a concentrations along the west coast in October 2003 and 2004, December 2003 and January 2004. On the other hand, when circulation changed by moving to the east in May 2004 and July 2005, dense plankton areas followed. Without consideration of bloom sizes, seasonal surface chlorophyll movements agree well with those of MERIS data illustrated in Chapter 5. These phenomena are explained by the movement of nutrient sources from the rivers after being discharged into waters at the head of the gulf. Currents along the northern coast play an important role in moving those

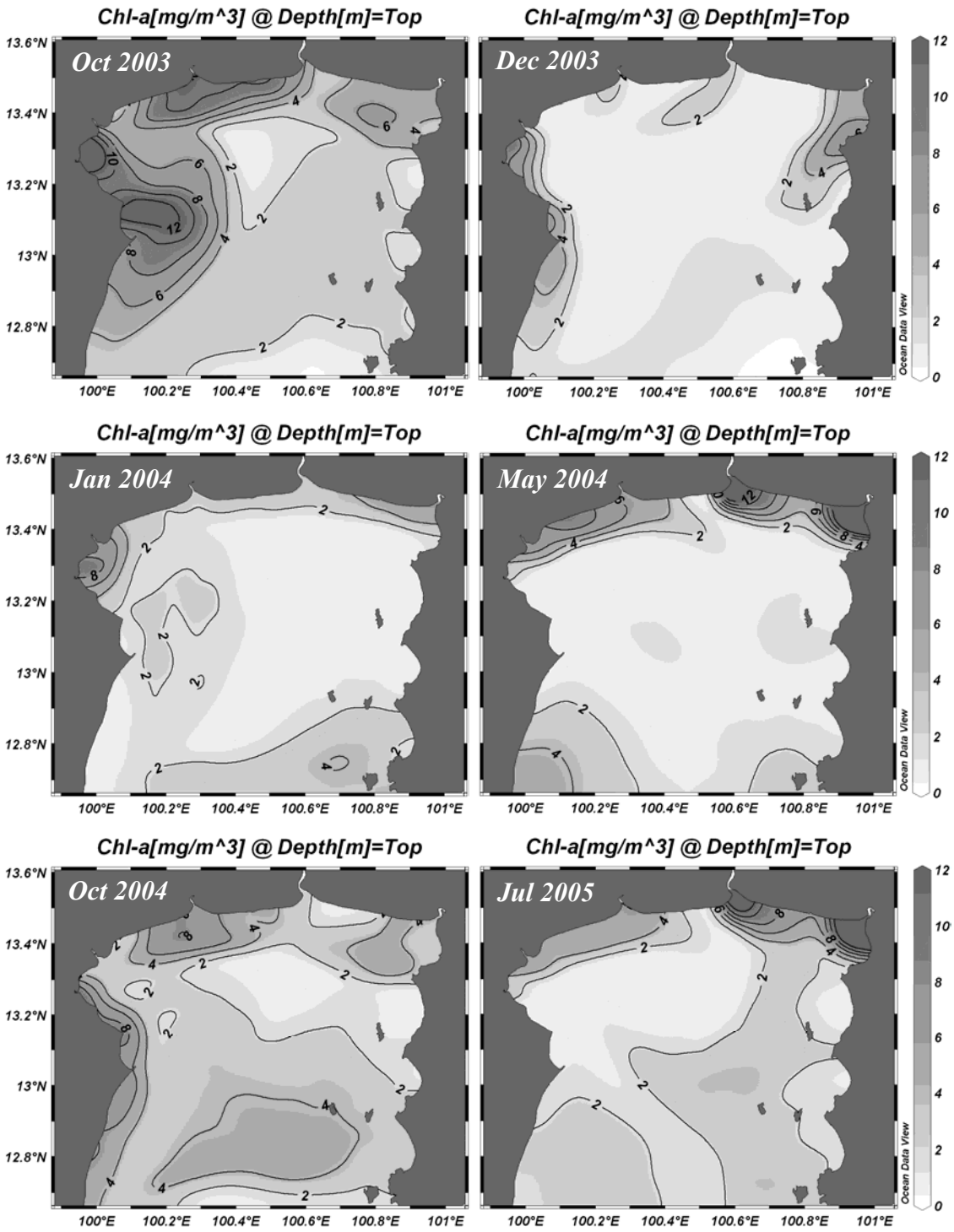

Figure 7 – 5 Simulated chlorophyll-a distributions at the sea surface under general condition

nutrients and other dissolved and suspended materials eastward and westward in relation to seasons (Figure 7 – 6 and 7 – 7). Phytoplankton concentrations found in this part of the Gulf are especially high in areas with high concentration of dissolved fertilizers. It is observed that the centers of high chlorophyll concentrations are not located exactly at the river mouths where the nutrients are originally loaded because phytoplankton needs a period of time for growth. It might be conveyed farther from the river mouths in a distance following ambient currents before they reach their peak concentrations.

Comparisons of simulated chlorophyll distributions with those of field observations (Figure 4 – 9) and MERIS data (Figure 5 – 15) show consistency in spatial and temporal variations of plankton blooming in October 2003. All results indicate areas of large blooms near the western coast, thought to occur from large nutrient loads (Figure 7 – 4) imbedded in large river discharges (Figure 6 – 2). High chlorophyll concentration in the middle of the west coast corresponds to strong upwelling (Figure 6 – 9). This reason is also used to explain non-blooming incidents in October 2004 (the same month in following year) owing to lacking of such strong upwelling. Differences in upwelling development are likely to result from variations in wind patterns between both periods, as has been discussed in Chapter 6.

Upwelling plays an important role in helping to maintain plankton cells to remain near the sea surface thereby increasing photosynthetic rates. The distributions of the vertical diffusivities in October 2003 (Figure 7 – 8) strongly confirm this, due to coincidence of strong upward velocities (Figure 6 – 9) and weak vertical diffusivities over the same area located in the western coast. Upwelling-induced blooms will not

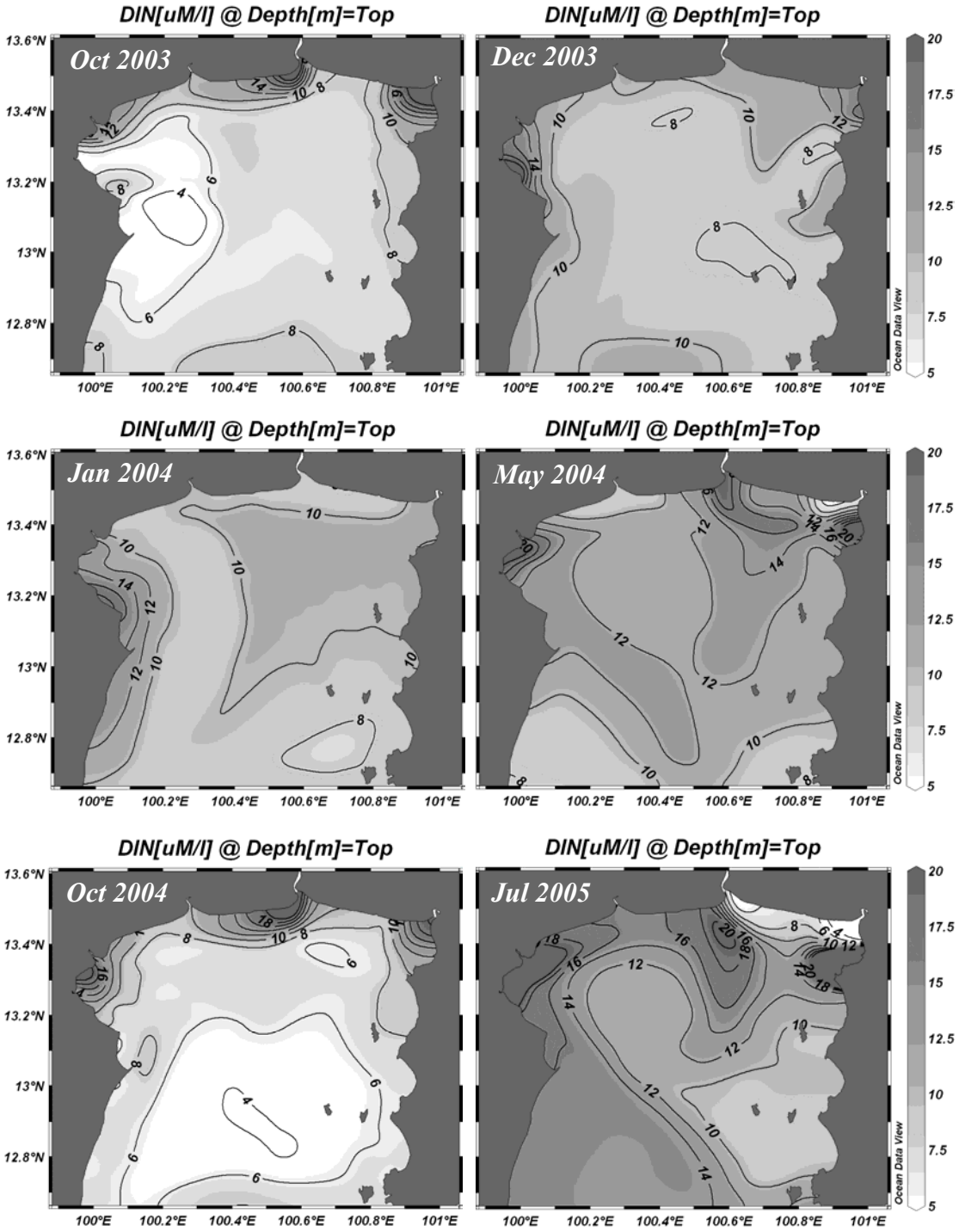

Figure 7 – 6 Simulated DIN distributions at the sea surface under general condition

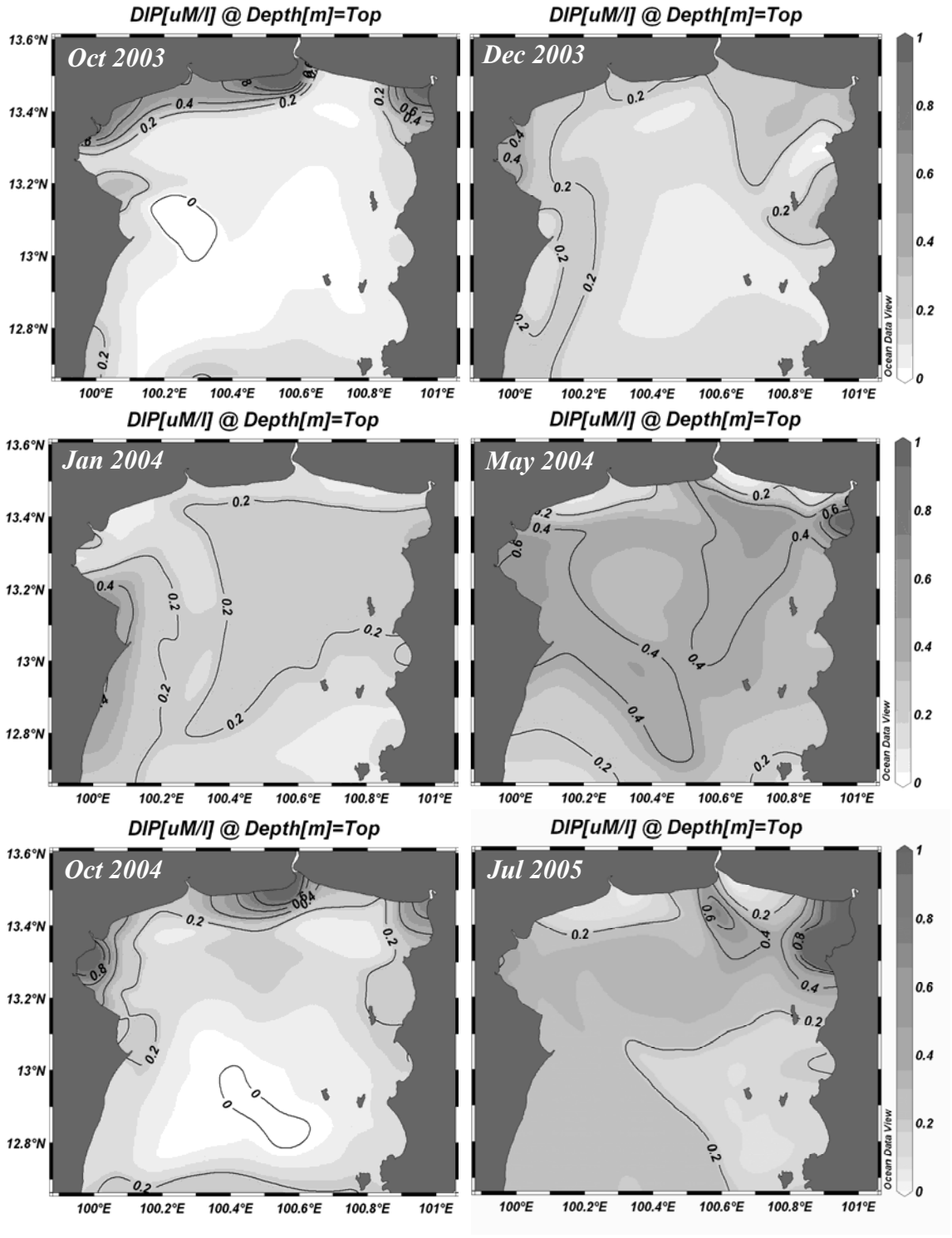

Figure 7 – 7 Simulated DIP distributions at the sea surface under general condition

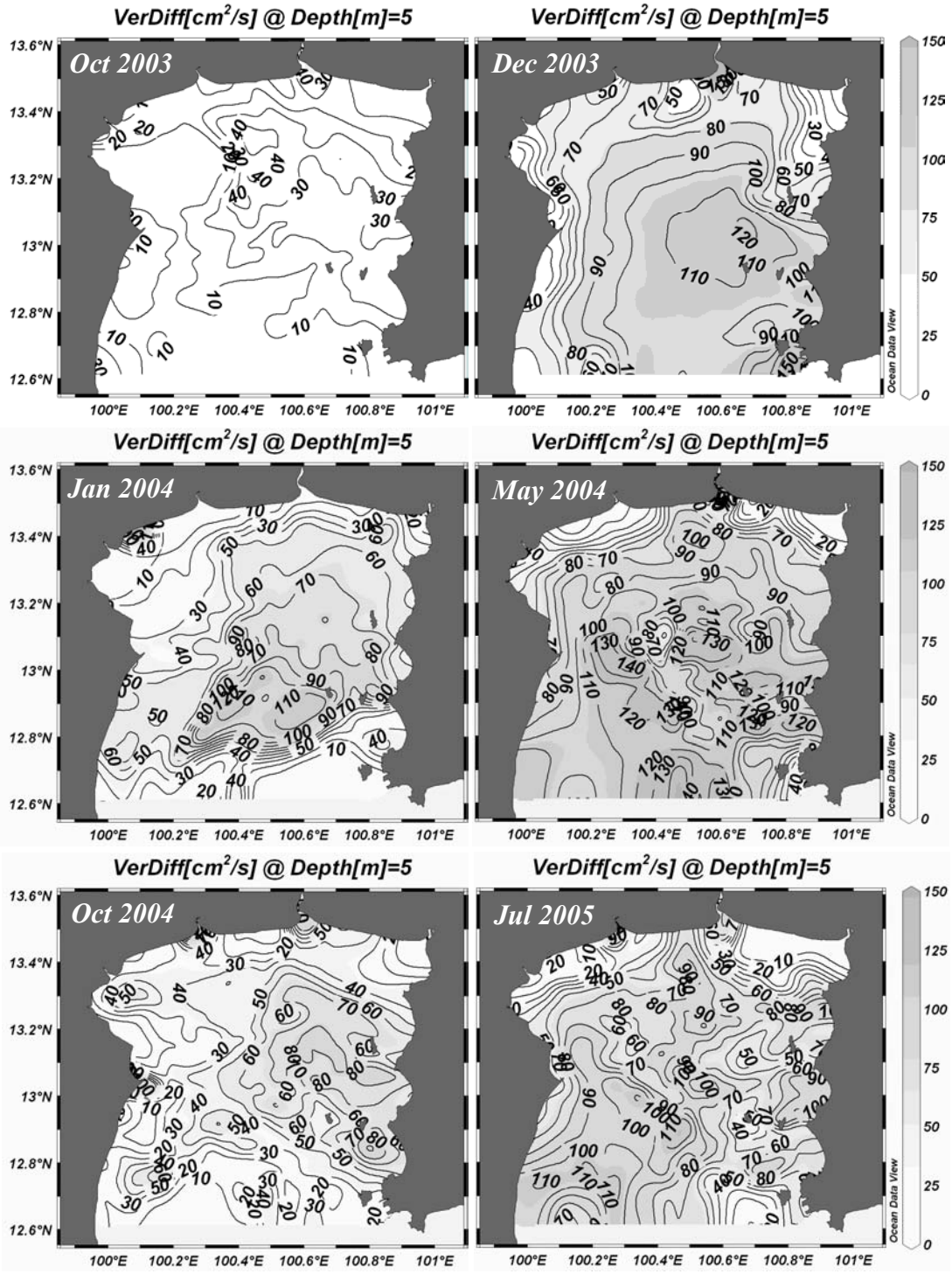

Figure 7 – 8 Simulated vertical diffusivities at 5 meter depth under general condition

happen if there is not enough nutrient support from river loads. This is the case for the east coast in October 2003 and 2004 when strong upwelling arises, but chlorophyll-a is low (Figure 7 – 5) because nutrient loads are transported away to the west.

Disagreement with the results can be seen in December 2003 when ecosystem model cannot reproduce blooming near the northwest coast corresponding with the field and MERIS data. Massive growth of phytoplankton does not happen in the model simulation because river discharges and nutrient loads are very low. There may be other nutrient supplies that are not taken into consideration, such as those from resuspension of bottom sediment due to water shallowness, and organic substances from mangrove forests located around there. This phenomenon does not dominate in every year because chlorophyll distributions analyzed by MERIS data in December 2004 (Figure 5 - 18) do not illustrate a massive bloom. The processes are complex and should be further investigated in future studies.

The coincidental results of chlorophyll distribution modeling for May 2004 and July 2005 (Figure 7 – 5) are discussed with those of MERIS detected on 16 July 2005 (Figure 5 – 19) because those periods of time are under the influence of the southwest wind. They all illustrate the same trend of movement of high chlorophyll-a to the east coast following the southwest winds and east currents along northern shoreline. However, a discrepancy in model simulation is noticed in terms of continuity and expansion of high concentration region. Modeled high chlorophyll-a bands have separated from the main area of concentration, while the MERIS image shows continuity in the region between the Thachin and the Chaopraya rivers. Furthermore, high concentration seems to remain very close to the shoreline in the model results

while those of satellite data illustrate wider seaward expansion, especially in the northeast area. It is possible that the discontinuity results are addressing underestimation of nutrient loads of the Thachin Rivers, which is supposed to fulfill that empty area by following current induction. Expansion of high chlorophyll regions is likely to be controlled by vertical diffusivities (Figure 7 – 8). Strong vertical diffusion reduces photosynthesis by moving phytoplankton cells to a great depth where light intensity is less available than near the sea surface. Therefore, with sufficient nutrient supplies, high chlorophyll-a at the sea surface is then located over the area of low vertical diffusivities. This phenomenon can explain not only the cases in May 2004 and July 2005 but also the distributions in other periods of time.

7.3 Sensitivity Analysis

The sensitivity of simulated chlorophyll-a to three environmental factors namely nutrient concentrations at the river boundaries, river discharges and wind magnitudes are investigated and discussed here. The key objective of testing the response of the system to variability of nutrient concentrations is to study the consequences that might happen due to nutrient decreasing and increasing by possible success and failure of pollution controls. River discharges play another significant role in maintaining water stability though buoyancy fluxes. This distinctive characteristic might alter the distribution of surface chlorophyll from just increasing nutrient concentration alone. Therefore, both factors contributing to nutrient loads are separately analyzed. The last experiment concerns the sensitivity of chlorophyll to

variations in wind magnitude, which is strongly related to vertical diffusivities. This factor is included in the analyses because previous results of general simulation indicate that high concentration of chlorophyll is spatially limited to vicinities of low vertical diffusivities. It follows that patterns of chlorophyll distribution should be considerably modified if wind magnitudes are changed.

Tested factors are set to be 50 % larger and smaller than those in the general cases while model setting and operation are the same as those of general simulations. Since each cruise needs 6 model operations to assess 3 factors (nutrient, discharge and wind speed), 18 cases altogether have to be conducted for 6 cruises. The calculated surface chlorophyll is then plotted as contours by using ODV software and presented from Figure 7 – 9 to 7 – 14. Each figure contains all the results of sensitivity analyses in the same month of each observational cruise.

The results of this analysis suggest that sensitivity of chlorophyll distribution to wind magnitude is greater than that of nutrient loads. Changes in wind magnitude strongly alter both intensity and spreading area of the distributions. Decreases in wind strength not only increase chlorophyll-a, but also expand the blooming areas to be much larger compared to those of normal and increasing wind speed in all seasons. The influence of nutrients and discharge are not as large as wind. They induce increases and decreases in chlorophyll-a in almost the same order of magnitude, but in an unchanged blooming area, when they are added and cut through the river boundaries, respectively.

Increases in nutrients loads can trigger massive growth of phytoplankton in a wide area if upwelling combines with of nutrient transport. This situation occurs along

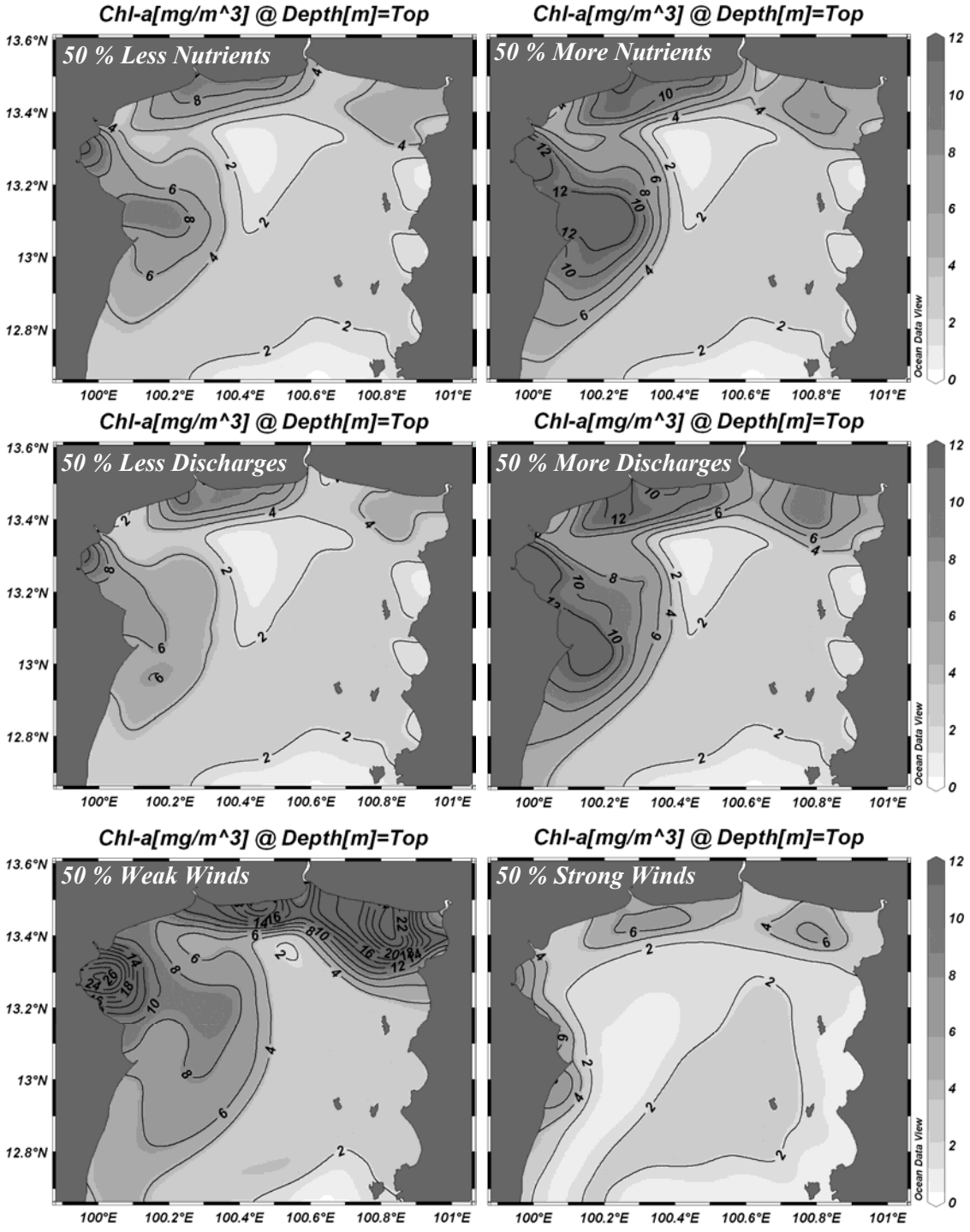

Figure 7 – 9 Responses of simulated surface chlorophyll-a distributions to variations of nutrients at the river mouths, discharges and wind magnitudes in October 2003

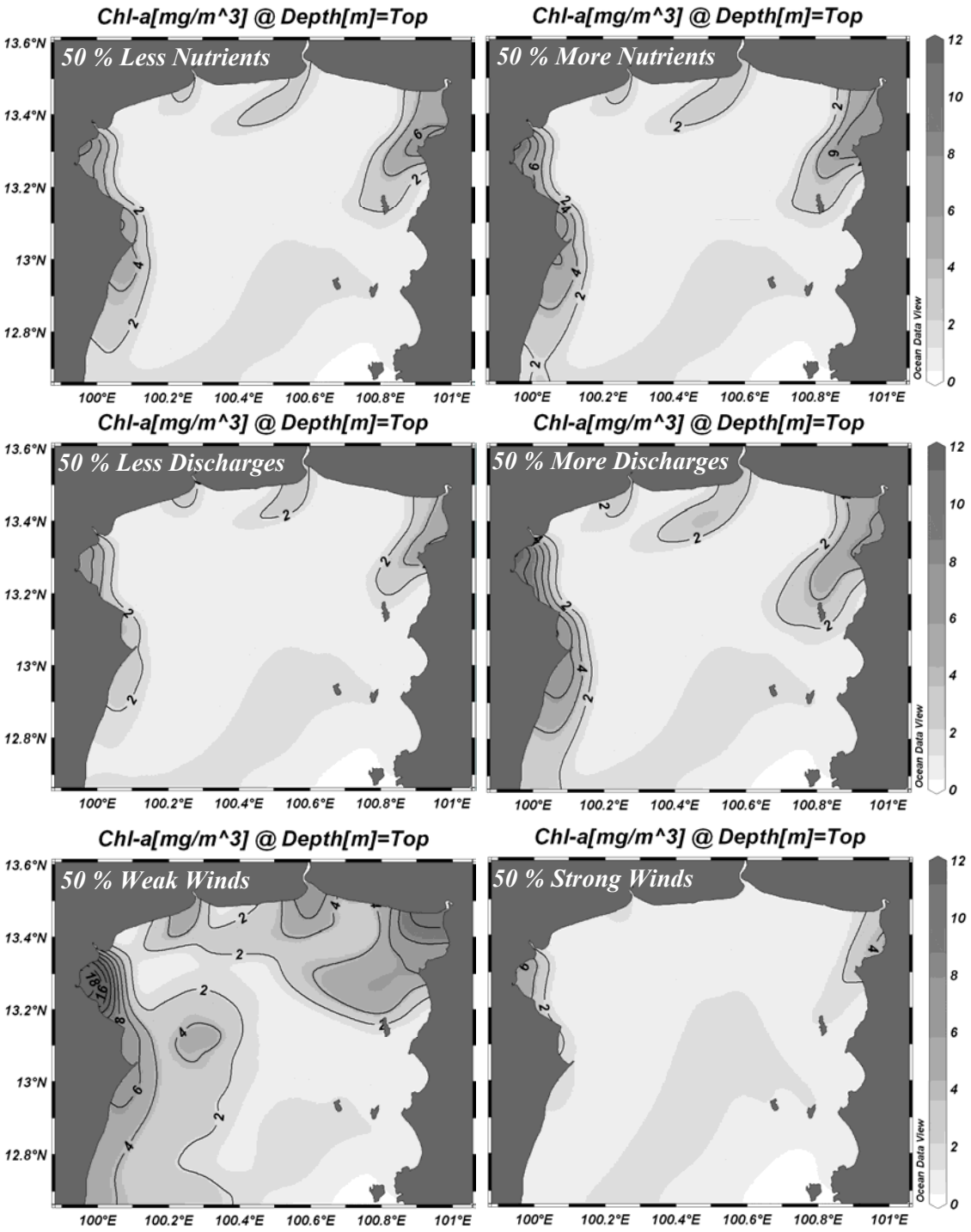

Figure 7 – 10 Responses of simulated surface chlorophyll-a distributions to variations of nutrients at the river mouths, discharges and wind magnitudes in December 2003

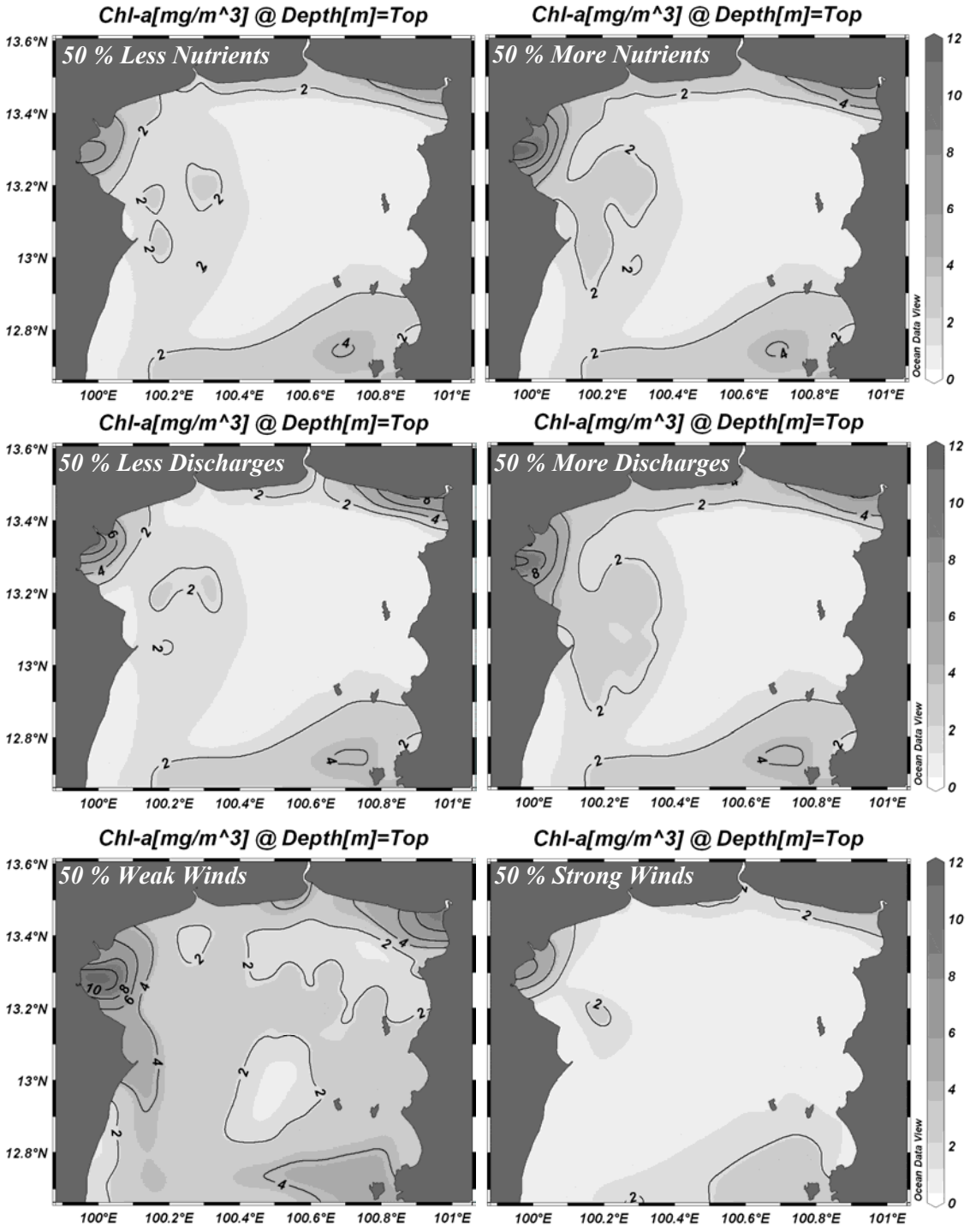

Figure 7 – 11 Responses of simulated surface chlorophyll-a distributions to variations of nutrients at the river mouths, discharges and wind magnitudes in January 2004

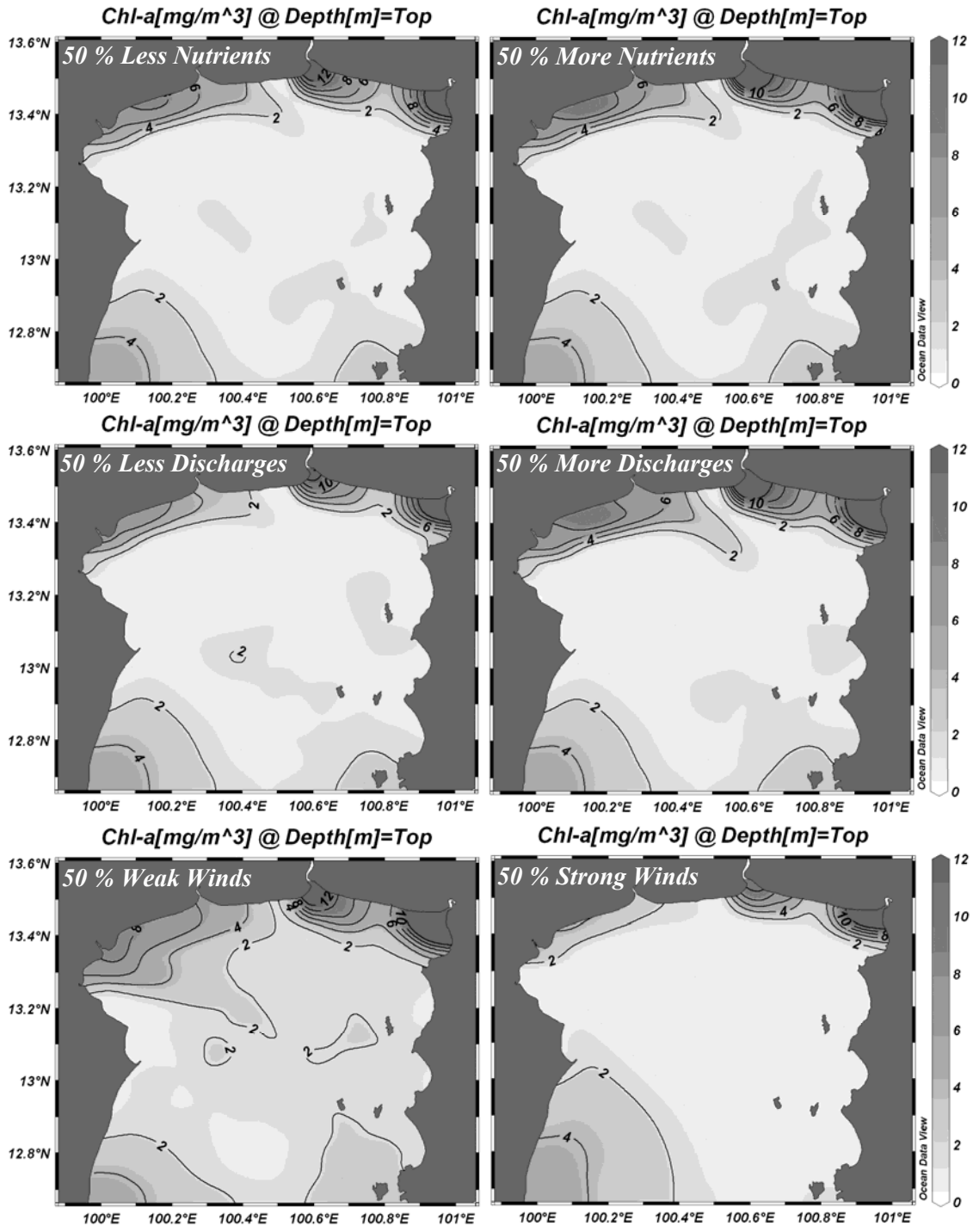

Figure 7 – 12 Responses of simulated surface chlorophyll-a distributions to variations of nutrients at the river mouths, discharges and wind magnitudes in May 2004

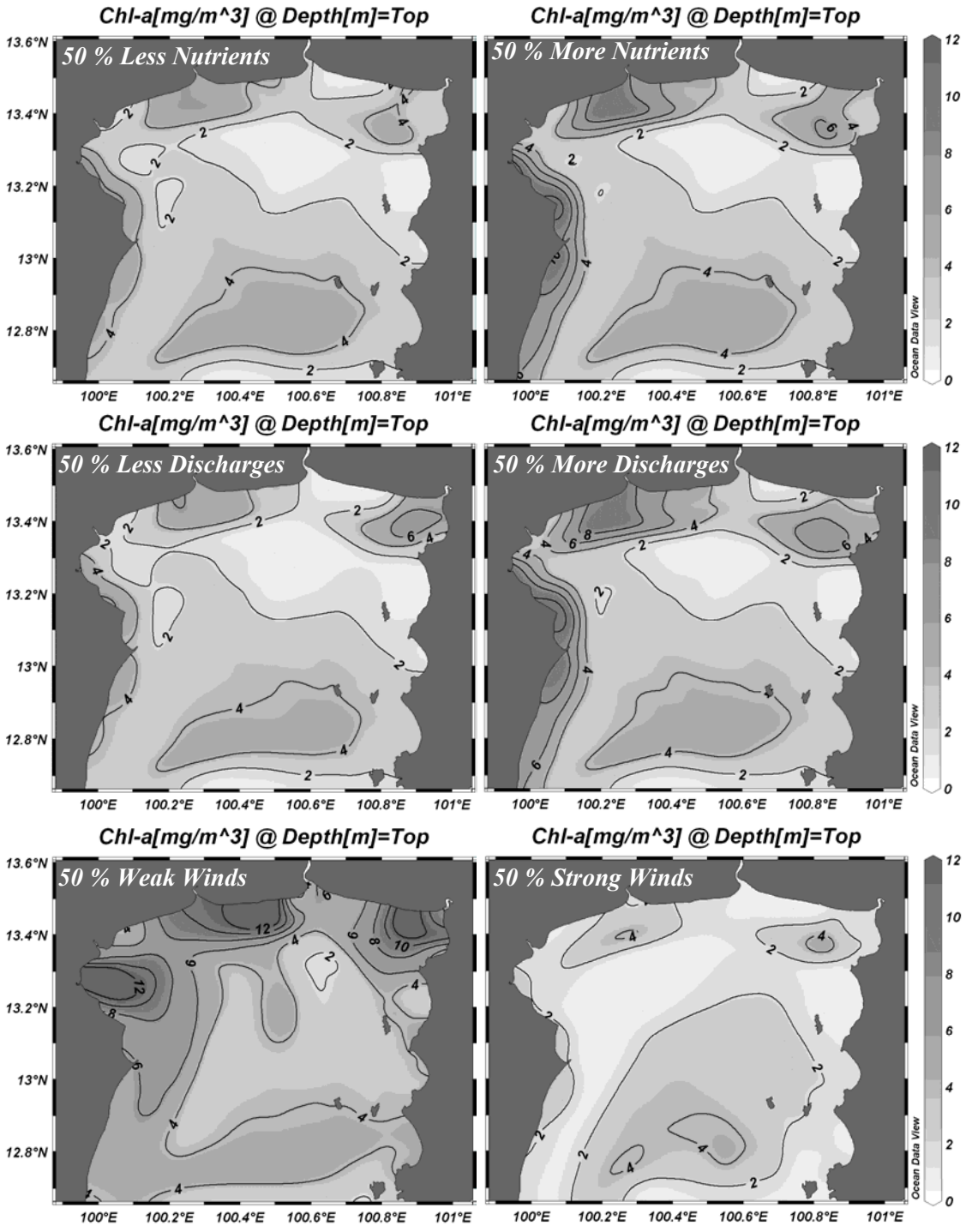

Figure 7 – 13 Responses of simulated surface chlorophyll-a distributions to variations of nutrients at the river mouths, discharges and wind magnitudes in October 2004

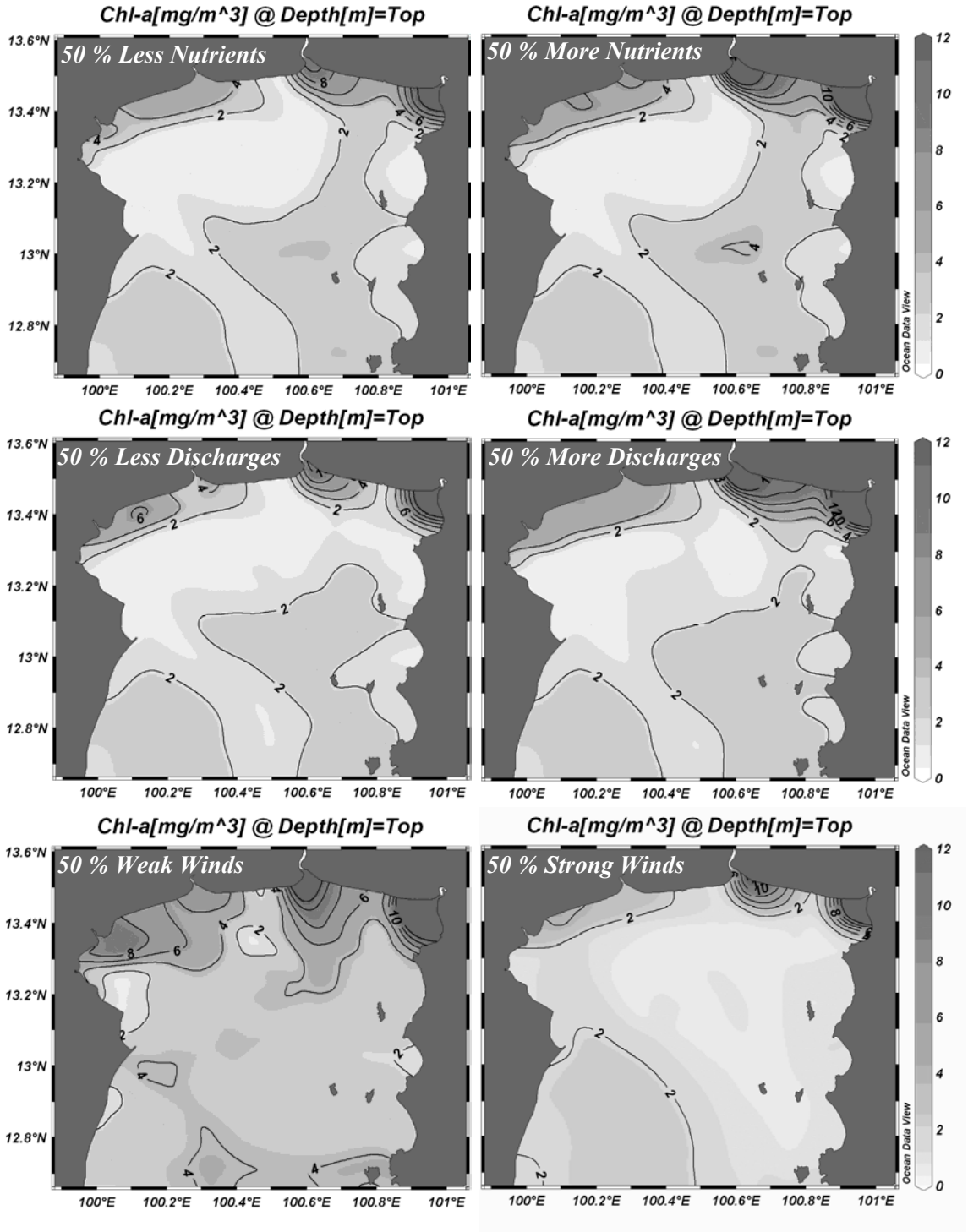

Figure 7 – 14 Responses of simulated surface chlorophyll-a distributions to variations of nutrients at the river mouths, discharges and wind magnitudes in July 2005

the west coast in October 2003 (Figure 7 – 9) and January 2004 (Figure 7 – 11). Upwelling in both periods (Figure 6 – 9) maintains plankton cells near the sea surface increasing the chance of photosynthesis. Without sufficient nutrient supply, such as in the case of nutrient and discharge reduction, blooming, due to upwelling alone, is suppressed. The results of this analysis have shown that the contribution of both factors is necessary in increasing the possibility of plankton bloom.

The analysis reveals that chlorophyll distributions in this area are very sensitive to water stability, which is inversely related to vertical diffusivity. High chlorophyll water is geographically bounded within the area of low vertical diffusivities (Figure 7 – 5). Water stability is increased by buoyancy fluxes from river water; therefore, plankton blooms are usually found near the river mouths and the area under the influences of river water. However, the sensitivity analyses to river discharges do not suggest large chlorophyll variations because strong vertical mixing overwhelms their influence. Wind speed plays a crucial role in controlling vertical diffusivities which are clearly seen in Figure 7 – 15a and 7 – 15b. Decreases in wind velocities, resulting in reduction of vertical diffusivities, increase the chance of plankton photosynthesis and surface diffusion. Alternatively, when wind speed and vertical mixing are strong, the blooming area is shrunk leading to conditions of high nutrients and low chlorophyll. However, increasing water stability can trigger plankton dynamics wherever nutrients in water column are not a limiting factor to plankton growth.

Occurrence of year-to-year variations in plankton blooms between October 2003 and October 2004 is uncovered by sensitivity experiments on wind variability. Nutrient loads are high during this time of the year (Figure 7 – 4), but intense plankton

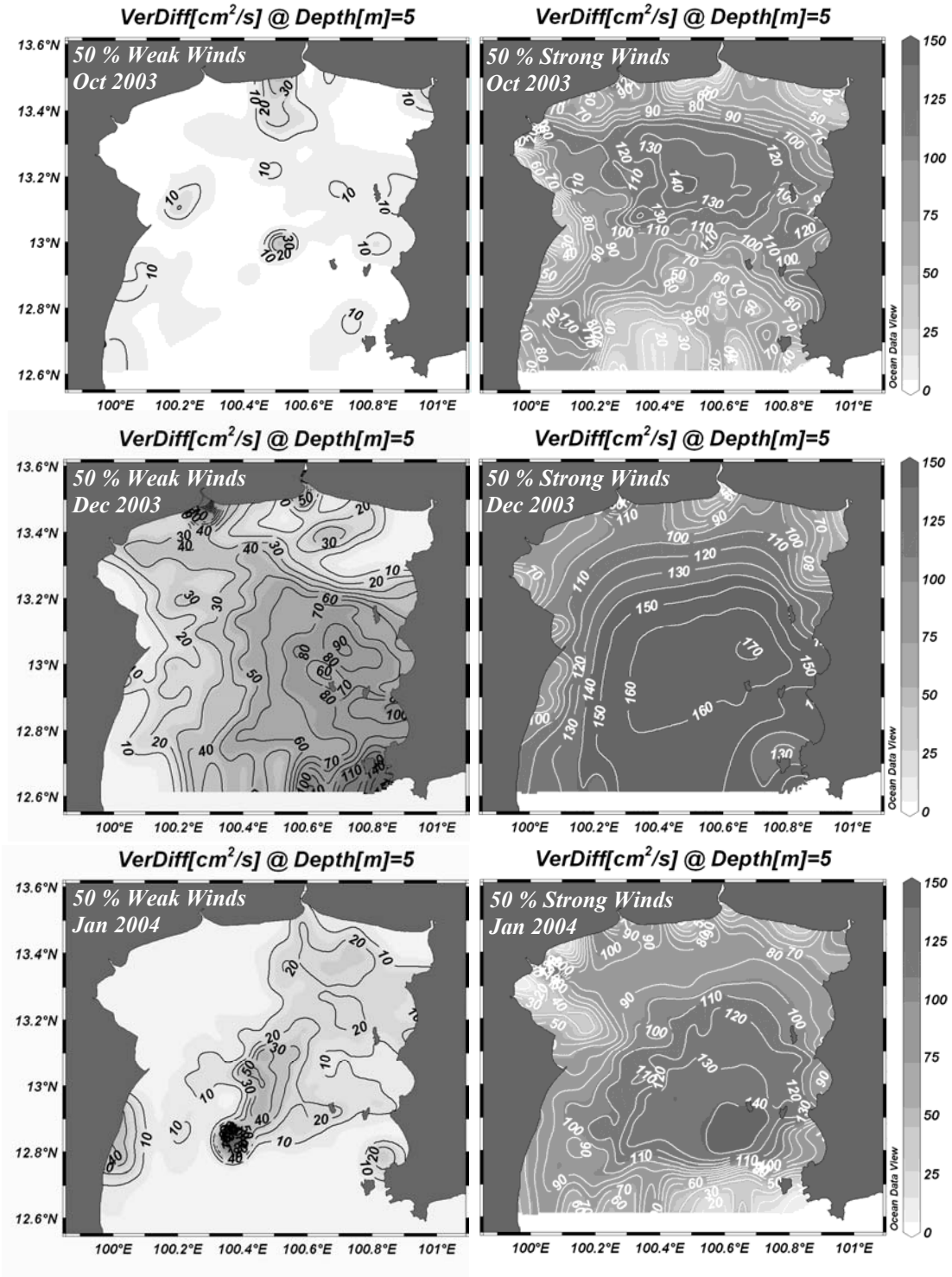

Figure 7 – 15a Vertical diffusivities at 5 m depth under simulated weak and strong winds in October 2003, December 2003 and January 2004

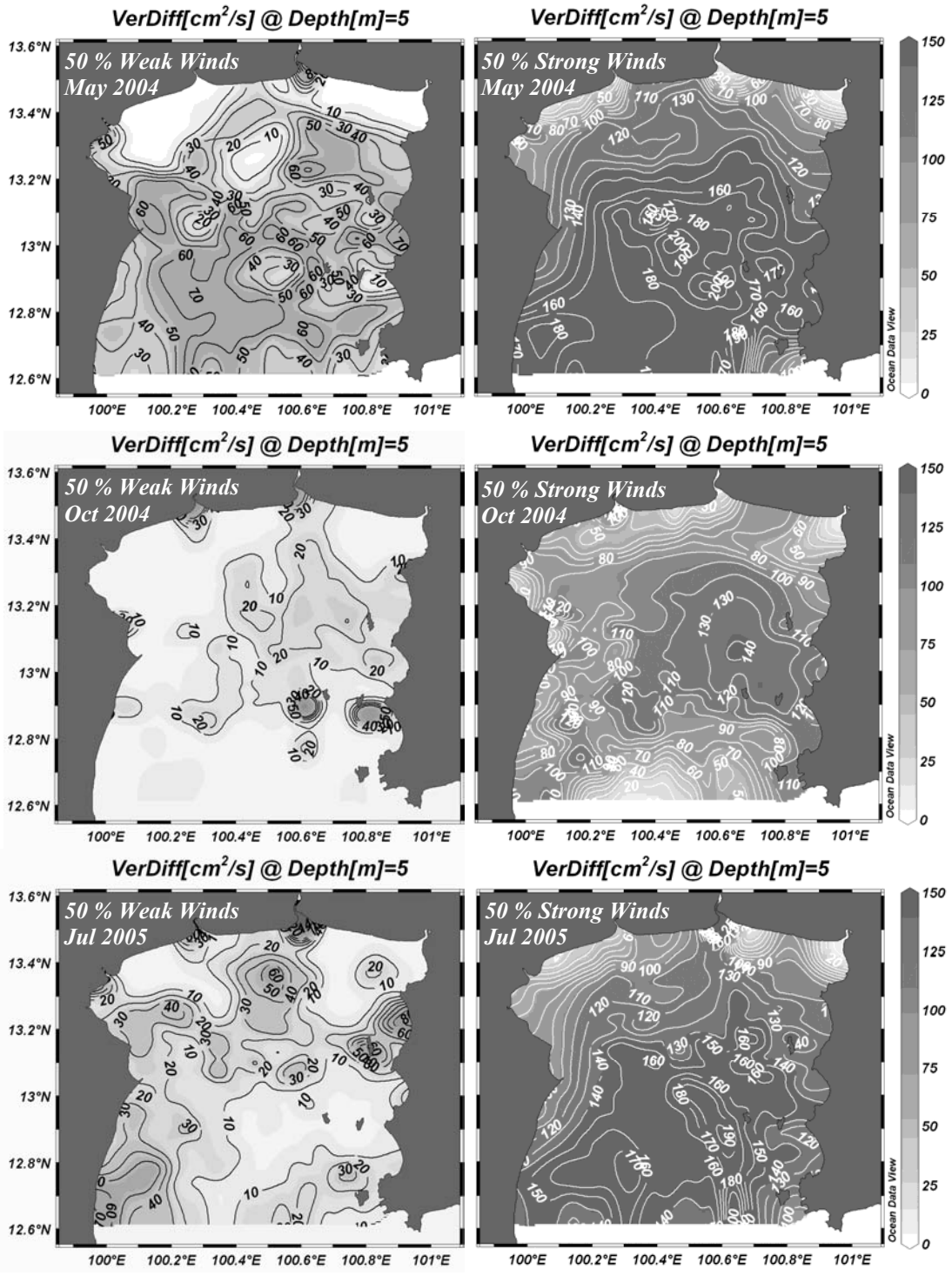

Figure 7 – 15b Vertical diffusivities at 5 m depth under simulated weak and strong winds in May 2004, October 2004 and July 2005

bloom just occurs in October 2003 not in October 2004 (Figure 7 – 5). It is possible that the condition October 2004 is generated by characteristic wind fields that are different from those of October 2003. Upwelling along the western coast, which is a major factor to support blooming, does not develop in the latter period. Interestingly, after the wind magnitude is decreased, the patterns of blooming are almost the same as in October 2003 occur (Figure 7 – 13). Vertical chlorophyll distributions along an east-west transverse in October 2004 (Figure 7 – 16) strongly support this evidence by illustrating high accumulation of chlorophyll near the sea surface when wind speed decreases. The results verify the critical role of stability condition on water column to plankton growth which can be used to explain this annual variation successfully.

Monthly averaged wind applied as major forcing in the ecosystem model might not represent actual conditions of short-term wind variations. Wind speeds are not always stable, and do not fix in the same direction all the time; they are variable in intensity and direction due to local influences of sea breeze or land breeze, depending on times of the day and seasons. Alternating strong and slack winds induce turbulence in the water column to wax and wane that might favor phytoplankton growth. Strong mixing period shortens nutrient recycling time while a calm period gives plankton a chance to develop. Balancing of those lengths of time might play a key role on plankton distributions.

Long-time surveys of the upper Gulf area indicate that red tides usually happen after rainfall coupled with strong sunshine (Lirdwitayaprasit et al., 2006). Sensitivity analysis clarifies the mechanism of phytoplankton bloom. It starts with high turbulence, an important process to bring nutrients from deeper water or sediment to

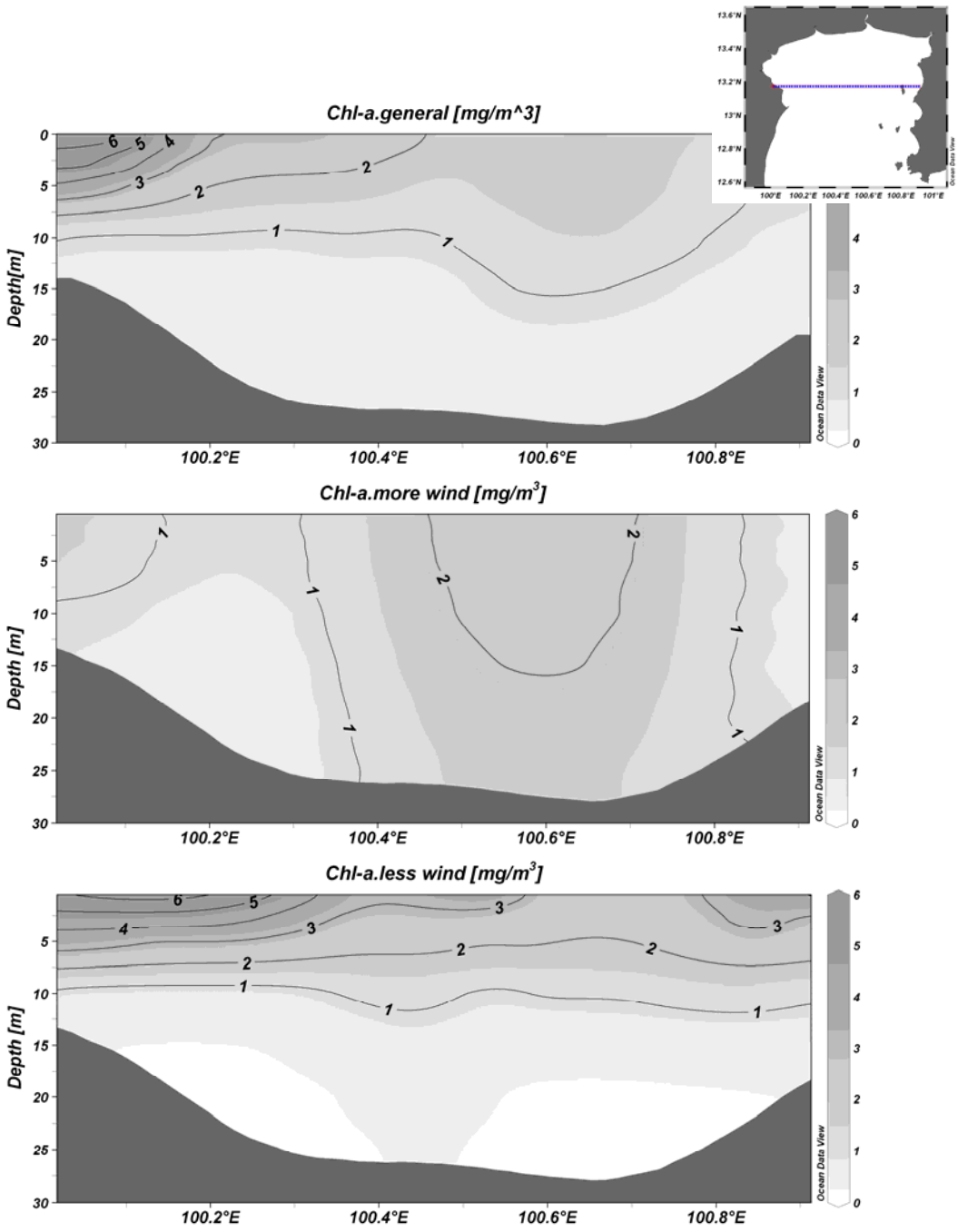

Figure 7 – 16 Comparison of vertical chlorophyll distributions of general condition and simulated results when wind speeds were increased and decreased by 50 % in October 2004

the sea surface, because of strong wind before and during storms or rainfall. Nutrients in the system might also be increased by larger river discharges due to precipitation, contributing to increased fertility of the water column. However, an increase in nutrient load is not enough. Water stability and sun light are still required to initiate plankton blooming. Coincidently, slack wind and calm water, lasting about 2 – 3 days, usually come after the rain. Moreover, falling rain might help to increase water stability by adding buoyancy flux on the sea surface. If there is strong sun light during this quiet time, the bloom will increase especially in the vicinity of the river mouths and where the nutrient loads are transported. This mechanism is very interesting and warrants further attention.

Differences of modeled values of surface chlorophyll-a after nutrients at the river boundaries, discharges, and wind velocities were increased and decreased by 50 % in every month of the experiment (Figure 7 – 17a and 7 – 17b), and are plotted in order to investigate the level of influence of these factors. Chlorophyll distributions in all seasons are most sensitive to wind variations and water stability conditions wherever the nutrients are sufficient. Magnitudes of nutrient concentration and discharge sensitivities are much smaller than those of wind. However, sensitivity to river discharges is a little greater than those of nutrients alone due to buoyancy flux from river water that helps stabilize the water column.

The above analyses suggest that if nutrient loads are changed, the potential for red tide incidence can be modified. Nutrient levels are related directly to intensity of the blooms while water stability is really required to support plankton growth.

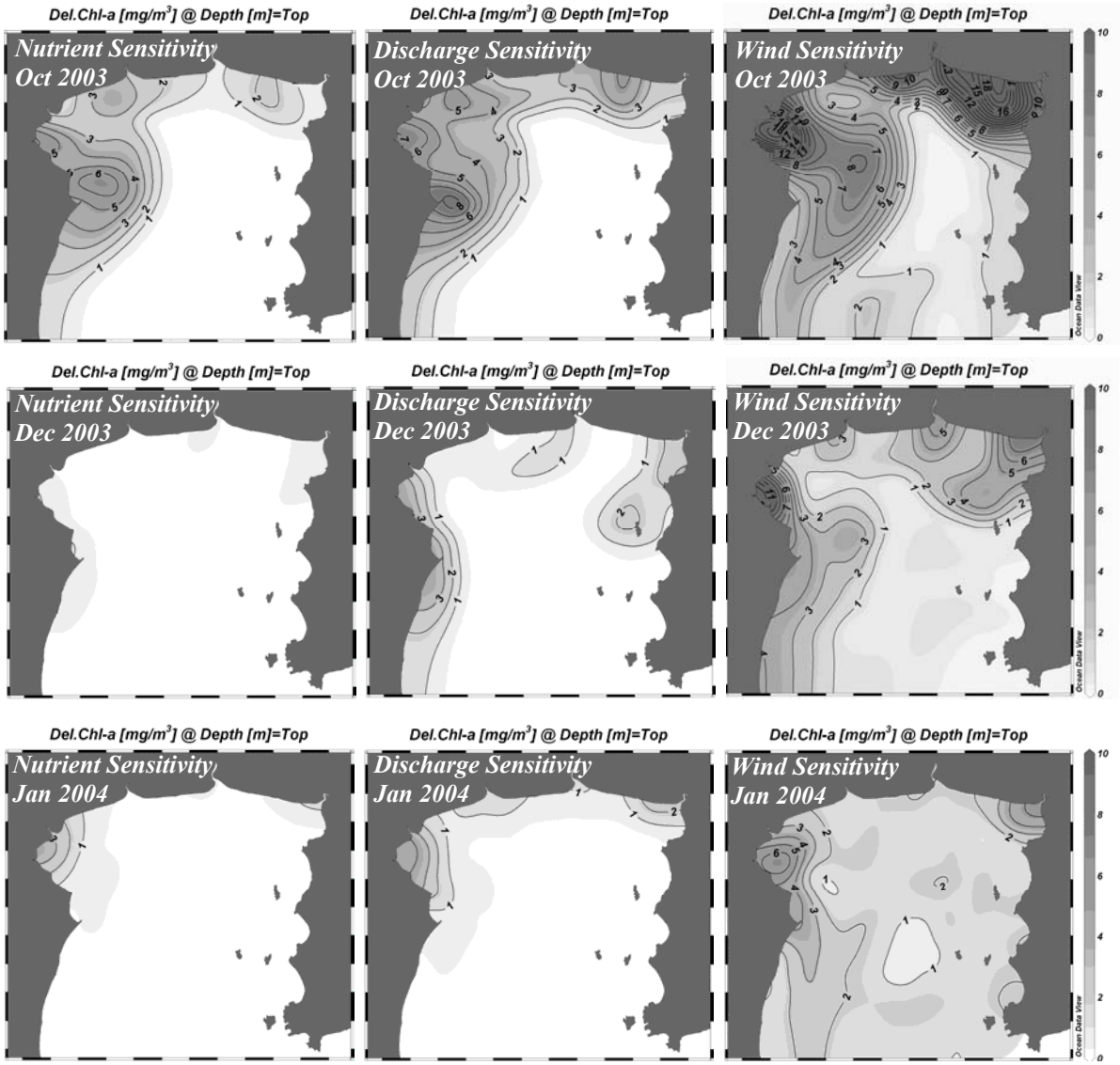

Figure 7 – 17a Differences of simulated surface chlorophyll-a after nutrients at the river mouths, river discharges, and wind velocities were increased and decreased by 70 % in October 2003, December 2003 and January 2004

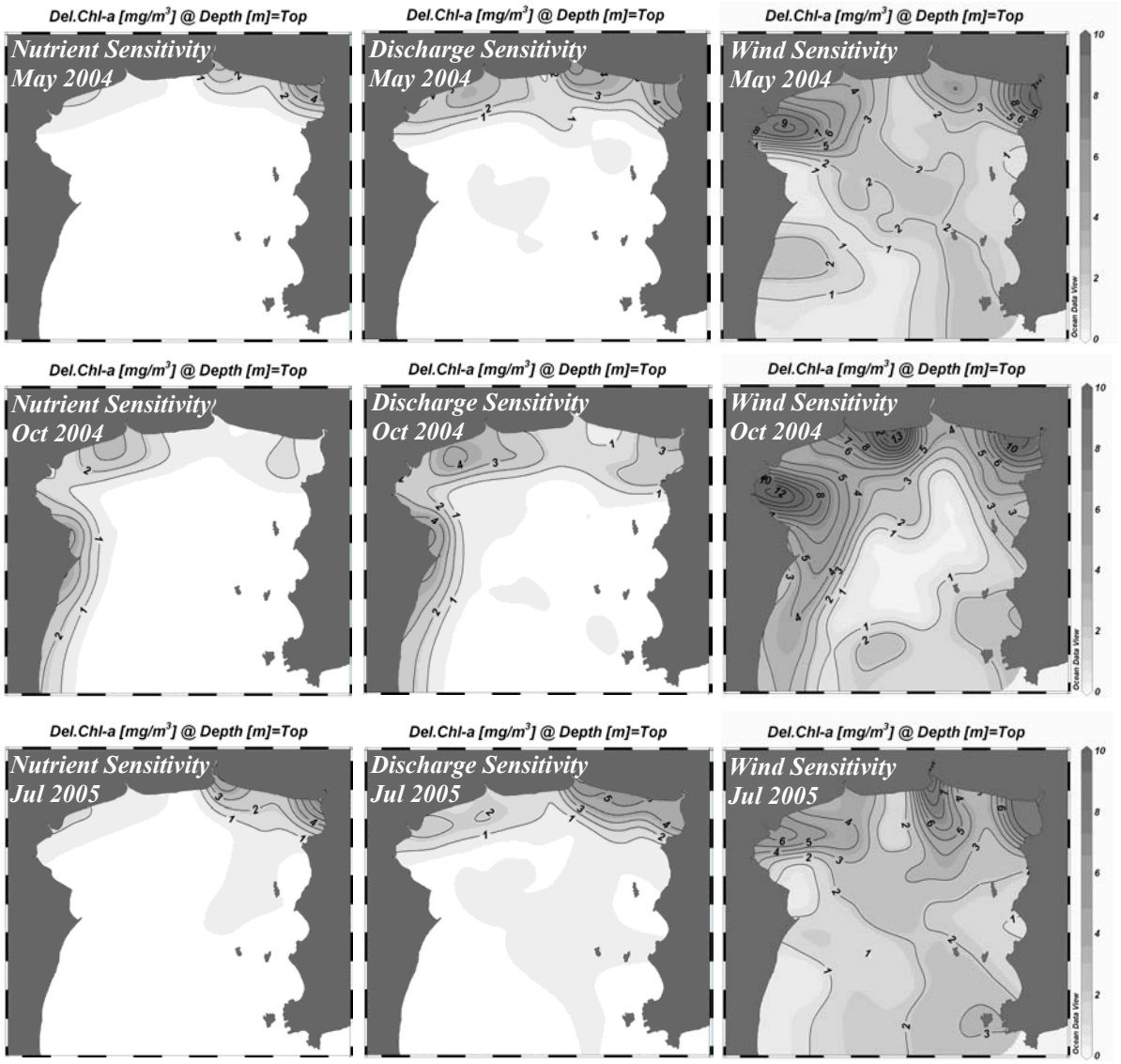

Figure 7 – 17b Differences of simulated surface chlorophyll-a when nutrients at the river mouths, river discharges, and wind velocities were increased and decreased by 50 % in May 2004, October 2004 and July 2005

Accordingly, increasing nutrient loads, which means putting more nutrients into the water column, will enhance the severity of blooming that might not occur instantly unless other optimal conditions arise. Therefore, regulations to reduce nutrient loads are necessary to be implemented in order to minimize the problem of red tide and eutrophication in the upper Gulf of Thailand.

7.4 Summary

NPZD ecosystem model coupled with POM was applied to investigate surface chlorophyll distributions in the upper Gulf of Thailand. The results clearly indicate that seasonal variations in the distributions are related to winds, currents and nutrient loads from the rivers. High chlorophyll patchiness is located near western coast following the direction of westward circulation developed during the northeast monsoon while accumulation of high concentration could be observed around northeastern coast due to eastward flow during the southwest monsoon. Intensity of plankton blooming near the coasts and the river mouths is proportional to nutrient loads, while in offshore areas, vertical movement and stability of water column in addition to nutrients are crucial. If nutrients are not limited, chlorophyll-a will be high wherever vertical diffusivities are low, or upwelling occurs. The experiments also reveal that strong vertical mixing prevents surface phytoplankton dispersion even in fertile water.

Sensitivity analysis has demonstrated that factors with the greatest influence on chlorophyll distribution in the study area are variations in wind speeds. Nutrient loads contribute to the intensity of plankton blooms, but not significant to the spreading.

River discharge plays a minor role in supporting plankton growth by increasing water stability through buoyancy flux, but the area of its influence is still limited to the vicinity of the river mouths. Sensitivity experiments in the case of wind variations have demonstrated the occurrence of year-to-year variations in plankton blooms between October 2003 and October 2004. Nutrient loads in both periods were similarly high, but blooming just occurred in the former case due to strong upwelling and low diffusivity induced by winds. Massive plankton growth, such as in October 2003, could be reproduced by decreasing wind magnitudes in October 2004. The results also suggest the necessity to apply nutrient load regulations in order to decrease potential and risk of red tide incidents in the upper Gulf of Thailand.

CHAPTER 8

CONCLUSIONS

8.1 Research Summary

Eutrophication is one of several serious environmental problems in the upper Gulf of Thailand. It is initiated by increasing nutrient loads from major rivers located along the northern coast of the gulf. Adverse effects such as the triggering of massive phytoplankton blooms lead to temporary collapses of coastal ecosystems, coastal aquaculture (e.g., sea farming of mussels, oysters and fishes), and tourism. The increasing trends of annual blooming incidents are an obvious indicator that the problem is getting worse. Fortunately, the dominant plankton species do not produce toxin; therefore, they are not harmful to human health. Escalation of anthropogenic nutrient loads is typically blamed as the most important cause of the problems. Integrated studies in dynamics of chlorophyll, an indicator of eutrophic conditions, have lead to an understanding of this complex phenomenon which is beneficial to management in order to minimize severity of such environmental problems in this area.

Rapid development of ocean color remote sensors has helped synoptic surface chlorophyll studies. With spatial resolution of 300 m pixel size and appropriate spectral resolution for ocean color studies, MERIS data were selected to apply to an investigation of chlorophyll distribution in this small coastal sea. Due to unrealistic chlorophyll estimation by MERIS standard algorithms over the study area, a local algorithm was developed and applied to MERIS L2 products. By considering patterns

of spectral distributions, if data strongly influenced by CDOM are excluded from algorithm analyses, the accuracy of chlorophyll prediction increases significantly. Furthermore, error is minimized when the algorithm, as a function of reflectance ratios instead of just plain reflectance, is applied to the MERIS data. By doing this, disturbances due to unwanted signal embedded almost equally in each spectral waveband are compensated and eliminated from the calculated results.

Geographical and seasonal variations in chlorophyll distribution revealed by the application of the local algorithm on MERIS images have revealed that high chlorophyll areas tend to remain close to major river mouths where nutrients show distribution patterns that follow prevailing seasonal winds. Westerlies induce high chlorophyll bands to move eastward while easterlies initiate migration in the opposite direction. Areas of high chlorophyll disperse continually from north to south along the western coast during the northeast monsoon, whereas they concentrate mostly in the northeastern corner of the gulf during the southwest monsoon. These observations agree well with the occurrence of seasonal red tides previously discovered by Lirdwittayaprasit et al. (1994).

Circulation, which is an important factor in plankton transport, was investigated by using POM, a three-dimensional circulation model suitable for coastal application. Driving forces for model simulation are wind, tide, river discharge, and water density in terms of salinity and temperature. The results reveal that barotropic forces due to seasonal prevailing winds are the most influential in driving circulation. Most surface currents always move parallel to wind fields while deeper currents result from the balancing of wind, volume compensation, and density. Water piles up when

winds are directed landward generating seasonal water surface elevation within ranges of 3 – 5 cm. In contrast, low mean sea level within these ranges of magnitude was found when winds move seaward inducing water to flow out of the gulf. Upwelling usually emerges when surface currents move away from shoreline following dragging wind. Depth-averaged results indicate that large-scale clockwise and counter-clockwise circulation develops during the southwest and the northeast monsoon, respectively, agreeing well with results of the previous investigation using a two-dimensional circulation model (Buranapratheprat et al., 2002a). Verifications with measured data from SEAWATCH oceanographic buoys also yielded good agreement in trends of general seasonal patterns.

Seasonal variations in surface chlorophyll distributions similar to those of MERIS and field observations could be reproduced by NPZD-POM, an ecosystem-circulation coupling model. The simulations indicate that river discharges are the most important nutrient sources supporting phytoplankton growth in the gulf. Movement of nutrients and plankton along the northern coast has been shown to be controlled by seasonal circulation. The amount of chlorophyll along the shoreline is related to the transport of the river loads while those in offshore areas are governed by not only nutrient abundances but also vertical motions of the water column in terms of vertical velocity and diffusivity which are under the influence of wind speed. Plankton blooms occur in zones of upwelling or where vertical diffusivities are low. Furthermore, dispersion of high chlorophyll patches is limited by wind-induced strong diffusion although nutrients are high. Model-generated blooms are obviously smaller than those

of MERIS images because abnormally high vertical diffusivities generated by stable winds might be unrealistic in natural conditions.

The importance of water stability in contributing to intensity and spreading of high chlorophyll areas has been confirmed by sensitivity experiments. Decreases in vertical diffusivities due to slacking wind increase the chance for phytoplankton to access available light at the sea surface for photosynthesis. Chlorophyll concentrations and spreading areas are significantly amplified by reducing wind speed. By this simulated evidence, “high nutrients, low chlorophyll” condition in October 2004 could be changed to massive blooming in the same way as those in October 2003. However, growth stimulation by increasing water stability is inconsequential if nutrients in the water column are scarce. Buoyancy fluxes of river discharges also play a minor role in supporting plankton blooms by promoting water stratification, but their influence extends only to the waters in the vicinity of the river mouths and immediate near-shore areas. The last case, elevations of nutrient loads without changing amount of discharges can modify only blooming intensity, not dispersion. However, increasing nutrient loads into the water column leads to increasing potential for severe phytoplankton blooms when other photosynthetic factors such as water stability and light are optimized.

The understanding of seasonal dynamics of high chlorophyll areas can be used for coastal management to minimize severity of the problems resulting from plankton blooms. Charting high risk areas to inform of when and where the blooms occur can help mitigate future impacts. This information will be used for planning to protect the affected activities, such as fish and shellfish farming and tourisms, from blooming

consequences. Movement of husbanded marine animals to low risk water and early harvesting are examples of two practices that might be applied. The information also helps local people and business sectors, which depend on tourisms, organize their investments during the incident of unpleasant environmental conditions and temporarily declined tourists. Such public awareness should be done in the provinces along the western coast during the northeast monsoon influence (October – February) and the eastern coast during the southwest monsoon influence (May to September).

Sensitivity experiments suggest that relevant measures be required to control nutrient loads into UGoT water. Nutrient concentrations at the present time might be in critical level to stimulate massive plankton bloom especially in near-shore areas, but it is overwhelmed by strong mixing and turbulence. Adding more nutrients to the water column does not intensify blooming instantly unless other optimal conditions of water stability and light intensity arise coincidently. Lacking of understanding of these processes will increase the potential for severe blooms. Control of nutrients released into natural water is, therefore, necessary in order to minimize such eutrophic problems. The modeling experiments of the present study could not specify the level of nutrients to be removed from the water system due to the lack of fundamental data such as phytoplankton physiology, nutrient loads from non-point sources, and seawater-bottom interaction. Model improvements and intensive verification are required to achieve this goal of coastal environmental management.

8.2 Implications of the Research

This research represents pioneer work in this area of interest by trying to apply several tools namely satellite remote sensing, circulation and ecosystem models to specifically investigate mechanisms driving a coastal phenomena. The satellite data provide a synoptic overview of chlorophyll distributions in fine detail while the model simulations are used to help explain these occurrences.

The appropriate selection of an ocean color sensor and its distributed products plays a key role in the successful investigation of chlorophyll distribution. In terms of spatial resolutions, MERIS products are separated into fine and coarse mode of pixel sizes, 300 m and 1.2 km, respectively (see Appendix A). This specification is very beneficial for users to choose the most suitable product for the study size or the scale of phenomena of interest. Most ocean color sensors (e.g., SeaWiFS and MODIS) are designed for the investigation of primary productivity of the world's oceans; therefore, pixel sizes around 1 km are considered appropriate. Such spatial resolution might be too large for a small coastal area like the upper Gulf of Thailand whose dimensions are about 100 × 100 km. Some small-scale phenomena such as meanders or eddies might not be detected at the coarser resolutions. Fine resolution MERIS data are an excellent choice for estimating chlorophyll distribution in this small coastal sea.

The study illustrates that it is possible to develop a simple empirical algorithm based on satellite data for chlorophyll estimation over Case 2 water. It is obvious that the error of estimation can be partly separated when R_{rs} data abnormally influenced by SS and CDOM are taken into consideration in the algorithm development process.

This might be an alternative approach to estimate chlorophyll-a for Case 2 water rather than the application of more complex techniques based on radiative transfer modeling. Although this model is spatially limited, it is still valuable because local algorithm developed from the experiment provides better results of chlorophyll estimation than those of standard algorithms assigned for MERIS L2 products. However, this depends on the objective of the research and what level of accuracy is needed for analyses. Application of a relatively simple empirical algorithm, with accuracies in the order of 60 – 90 % is sufficient for this study since the major purpose is to investigate the patterns of variation in chlorophyll distributions. If research is focused on the investigation of primary productivity, for example, which needs highly accurate chlorophyll data as inputs, other sophisticated methods that can provide high accuracy of estimation have to be applied to meet this requirement.

That seasonal variations in chlorophyll distributions have been revealed in the research is a significant step in understanding the patterns of plankton blooms in the upper Gulf of Thailand. Variations in river discharges and nutrient loads have been mentioned for massive plankton blooms that frequently occur during wet season or the southwest monsoon (Piemsomboon, 2003). This research highlights not only temporal, but also spatial dynamics of the phenomenon. Severe blooming usually happens during the wet season, but is concentrated in the northeastern area of the gulf following prevailing wind and circulation. Induced by southwest wind and eastward current, large nutrient loads from river water are accumulated in the northeastern corner of the gulf; therefore, plankton blooms during that time become so intense that they commonly induce mass mortality of marine organisms (Lirdwittayaprasit, 1994).

However, this is not necessarily the case during the period of the northeast wind. Blooming incidents are not as intense and are dispersed along the western coast due to large dispersion of nutrients following southward wind and small nutrient loads during this time.

The study results also highlight the advancement of understanding of some oceanographic conditions. Agreement between circulation and chlorophyll distribution has another crucial role in the verification of the circulation model, besides revealing the causes of the distributions induced by both fluid motions. Seasonal movement of high chlorophyll bands in MERIS images and model results could be referred backward to monsoon-influenced circulation patterns in the whole gulf. The research is also significant by unfolding seasonal variations in three-dimension circulation patterns, upwelling and sea level elevations of the study area with application of POM. Besides the studies of chlorophyll distributions by coupled with ecosystem model, POM can be further modified to investigate other material transports in the sea such as sediments, pollutants, and fish larvae.

A great benefit of using POM for ecosystem simulation concerns the turbulence closure sub-model used for calculation of vertical diffusivity. Since chlorophyll in the artificial system is very sensitive to the stability of the water column, this capability of POM becomes a key role of successful simulation. Explanation that plankton bloom is triggered by low turbulence addressed by the research has never been pointed out before for the area of interest. This is an important issue that needs to be verified for greater understanding of the mechanisms of eutrophication in the study area.

8.3 Directions for Further Research

The findings of this study have highlighted the need for further research in several issues which are shown as listed below:

- Development of algorithms based on radiative transfer model is required for greater accuracy in chlorophyll prediction to support further investigations into primary productivity and long-term variations of environmental change due to eutrophication. These experiments need accurate data to minimize the error of estimation and misinterpretation. More field observations are needed for result verification. Measurement of absorption and scattering coefficients of water constituents is also required for parameterizing the radiative transfer model.
- Verification of calculated circulation patterns is necessary to strengthen the reliability of POM simulation. In the circulation experiments, Eulerian current data measured by two oceanographic buoys were used for comparison with model results. Although these datasets are excellent in terms of time series, two isolated points do not provide clear patterns of circulation in the whole upper gulf. Largrangian method of current measurement by deploying drogues might alternatively be applied to tracking residual currents since the objective of investigation is focused especially on trajectory of seasonal currents.
- Influence of wind on current and chlorophyll distribution should be further investigated. Due to the lack of data availability, monthly averaged wind was used as major forcing in the model simulations instead. Because chlorophyll in

the water column is very sensitive to wind-induced vertical mixing, hourly or daily winds become crucial for realistic simulations. However, preliminary research is needed to investigate those fine temporal wind patterns since such data have rarely been reported and distributed.

- That plankton blooms in the study area are triggered by increasing water stability due to slack wind and fresh water flux onto the sea surface after storm or rainfall is very interesting and needs investigation because it is the key to understanding the mechanisms of red tide occurrences in this area. Ecosystem modeling and intensive field surveys are both required for future research emphasizing the relations of chlorophyll or phytoplankton and those triggering situations.
- The role of nutrients from non-point sources on chlorophyll distribution that might be the cause of discrepancy of calculated results in December 2003 should be clarified. Those organic substances and nutrients have possibly originated from mangroves and developed areas distributed around the area, and sediment re-suspension due to shallowness. More research is required to estimate the magnitude of nutrient sources released into water column since no such data are available.

8.4 Conclusions

The upper Gulf of Thailand, a semi-enclosed coastal sea, acts as a receptor of pollutants delivered by discharges of four main rivers into the head of the gulf.

Eutrophication is one of several serious environmental problems in the area resulting in the deterioration of the coastal ecosystem, human health, and local and national economies. The problem is getting acute as indicated by the increasing trend of red tide incidents in every year. Understanding the mechanism of this phenomenon is essential in order to apply suitable practices to minimize the severity of the adverse effects caused by it. Dynamics of surface chlorophyll, a proxy of phytoplankton population, is therefore investigated by using satellite images and circulation-ecosystem coupling model. Chlorophyll maps derived from MERIS data reveal that high chlorophyll concentrations are always observed within the vicinity of the river mouths along the northern coast, while trends of patch movement to the east and the west are also found to be related to seasonal westerlies and easterlies, respectively. Results of ecosystem modeling have uncovered that river water is the most important nutrient source, and its movement after discharged into the sea is controlled by seasonal circulations. The patterns of chlorophyll distribution then follow this trend. Further analyses indicate the crucial role of vertical movement of the water column due to wind in controlling phytoplankton growth. Blooming is triggered when upwelling develops or vertical diffusivity is low. Under these conditions, plankton has a greater chance to stay close to the sea surface, and higher levels of light which is necessary for photosynthesis. Alternatively, if the sea is very rough, the growth will be limited even if nutrients in the water are rich, resulting in a “high nutrients, low chlorophyll” condition. However, increasing nutrients in the water column due to river loads can make plankton blooms intense if other optimal conditions occur coincidently. In order to minimize the severity of red tides due to eutrophic problems, effective

measures need to be applied to control the amount of nutrients released into natural water. On the other hand, the knowledge of seasonal patterns of blooming can be used to construct environmental risk maps which are very useful for planning to mitigate the problems caused by this phenomenon.

REFERENCES

Andersen, J.H., L. Schluter and G. Aertebjerg (2006): Coastal eutrophication: recent development in definitions and implications for monitoring strategies. *Journal of Plankton Research*, 28 (7), 621 – 628.

Antoine, D. and M. Morel (1999): A multiple scattering algorithm for atmospheric correction of remotely sensed ocean color (MERIS instrument): principle and implementation for atmospheres carrying various aerosols including absorbing ones. *International Journal of Remote Sensing*, 20 (9), 1875 – 1916.

Arrigo, K.R. and A.M. Weiss (1998): Physical forcing of phytoplankton dynamics in the southwestern Ross Sea. *Journal of Geophysical Research*, 103, 1007 – 1021.

Arst, H. (2003): *Optical Properties and Remote Sensing of Multicomponental Water Bodies*. Springer-Praxis, Chichester, UK, 231 pp.

Attenborough, D. (1980): *Life on Earth: a Natural History*. Reader's Digest, London, 386 pp.

Bachelet, G., X. Montaudouin, I. Auby and P.J. Labourg (2000): Seasonal changes in macrophyte and macrozoobenthos assemblages in three coastal lagoons under varying degrees of eutrophication. *ICES Journal of Marine Science*, 57, 1495 – 1506.

Barlow, J.P., C.J. Lorenzen and R.T. Myren (1963): Eutrophication of a tidal estuary. *Limnology and Oceanography*, 8 (2), 251 – 262.

Bell, P.R.F. (1991): Status of eutrophication in the Great Barrior Reef lagoon. *Marine Pollution Bulletin*, 23, 89 – 93.

Berner, R.A., A.C. Lasaga and R.M. Garrels (1983): The carbonate-silicate geochemical cycle and its effect on atmospheric carbon dioxide over the past 100 million years. *American Journal of Science*, 283, 641 – 683.

Berner, E.K. and R.A. Berner (1996): *Global Environment: Water, Air, and Geochemical Cycles*. Prentice Hall, New Jersey, 376 pp.

Bleck, R. and L.T. Smith (1990): A wind-driven isopycnic coordinate model of the north and equatorial Atlantic Ocean. 1. Model development and supporting experiments. *Journal of Geophysical Research*, 95, 3273 – 3285.

Blumberg, A.F. and G.L. Mellor (1987): A description of a three-dimensional coastal ocean circulation model. pp. 1–16. In: N. S. Heaps (ed.) *Three-Dimensional Coastal Ocean Models, Coastal and Estuarine Sciences*, *4*. AGU, Washington, D.C.

Booncherm, C. (1999): *The seasonal cycle of residual flows and the tidal currents in the Gulf of Thailand by using the long-term observed data from the SEAWATCH Thailand Program*. M.Sc. thesis, Department of Ocean Science, University of Wales, Bangor.

Bougis, P. (1976): *Marine Plankton Ecology*. North-Holland, Amsterdam, 355 pp.

Brandt, A, C.C. Sarabun, H.H. Seliger and M.A. Tyler (1986): The effect of broad spectrum of physical activity on the biological processes in the Chesapeake Bay. pp. 361 – 384. In: J.C.L. Nihoul (ed.) *Marine Interfaces Ecohydrodynamics*. Elsevier, Amsterdam.

Bricaud, A., A. Morel and L. Prieur (1981): Absorption by dissolved organic matter of the sea (yellow substance) in the UV and Visible domains. *Limnology and Oceanography*, 26 (1), 43 – 53.

Bricaud, A. and D. Stramski (1990): Spatial absorption coefficients of living phytoplankton and nonagal biogenous matter: A comparison between Peru upwelling area and the Sargasso Sea. *Limnology and Oceanography*, 35, 562 – 583.

Bricaud, A., M. Babin, A. Morel and H. Claustre (1995): Variability in the chlorophyll-specific absorption coefficients of natural phytoplankton: Analysis and parameterization. *Journal of Geophysical Research*, 100, 13321 – 13332.

Bryan, K. (1969): A numerical model for the study of circulation of the world oceans. *Journal of Computational Physics*, 4, 347 – 359.

Buckton, D., E. O'Mongain and S. Danaher (1999): The use of Neural Networks for the estimation of oceanic constituents based on the MERIS instrument. *International Journal of Remote Sensing*, 20 (9), 1841 – 1851.

Buesseler K.O. and P.W. Boyd (2003): Will ocean fertilization work? *Science*, 300, 67 – 68.

Bunpapong, M. and T. Piyakarnchana (1987): Some trend in the upper Gulf water quality. *Proceedings of The 4th Seminar on Water Quality and Living Resources in Thai Water*, 270 – 283.

Buranapratheprat, A. and M. Bunpapong (1998): A two dimensional hydrodynamic model for the Gulf of Thailand. *Proceedings of the IOC/WESTPAC Fourth International Scientific Symposium*, 469 – 478.

Buranapratheprat A. and T. Yanagi (2003): Seasonal variations in circulation and average residence time of the Bangpakong estuary, Thailand. *La Mer*, 41, 199 – 213.

Buranapratheprat, A., T. Yanagi and P. Sawangwong (2002a): Seasonal variations in circulation and salinity distribution in the upper Gulf of Thailand: modeling approach. *La Mer*, 40, 147 – 155.

Buranapratheprat, A., T. Yanagi, P. Sojisuporn and C. Booncherm (2006): Influence of local wind field on seasonal circulations in the upper Gulf of Thailand. *Coastal Marine Science*, 30 (1), 19 – 26.

Buranapratheprat, A., T. Yanagi, T. Boonphakdee and P. Sawangwong (2002b): Seasonal variations in inorganic nutrient budgets of the Bangpakong estuary, Thailand. *Journal of Oceanography,* 58, 557-564.

Buttermore, R.E. (1977): Eutrophication of an impounded estuarine lagoon. *Marine Pollution Bulletin*, 8 (1), 13 – 15.

Cameron, W.M. and D.W. Pritchard (1963): Estuaries. pp. 306 – 324. In: M. N. Hill (ed.): *The Sea vol. 2*. John Wiley and Sons, New York.

Chen, X., S.E. Lohrenz and D.A. Wiesenburg (2000): Distribution and controlling mechanisms of primary production on the Lousiana – Texas continental shelf. *Journal of Marine System*, 25, 179 – 207.

Chen, Z., P.J. Curran and J.D. Hanson (1992): Derivative reflectance spectroscopy to estimate suspended sediment concentration. *Remote Sensing of Environment*, 40, 67 – 77.

Cheevaporn, V. and P. Menasveta (2003): Water pollution and habitat degradation in the Gulf of Thailand. *Marine Pollution Bulletin*, 47, 43 – 51.

Chongprasith, P. and V. Srineth (1998): Marine water quality and pollution of the Gulf of Thailand. pp. 137 – 204. In: D.M. Johnston (ed.) *SEAPOL Integrated Studies of the Gulf of Thailand, Vol. 1.* Southeast Asian Programe in Ocean Law, Policy and Management

Clark, D.K. (1997): Algorithm theoretical basis document: Bio-optical algorithms, Case 1 waters, MODIS algorithm theoretical basis document is, version 1.2. Available from http://modis.gsfc.nasa.gov/data/atbd/atbd_mod18.pdf

Cleveland, J.S. (1995): Regional models for phytoplankton absorption as a function of chl-a concentration. *Journal of Geophysical research*, 100, 13333 – 13344.

Cugier, P. and P.L. Hir (2002): Development of a 3D hydrodynamic model for coastal ecosystem modeling: Application to the plume of the Seine River (France). *Estuarine, Coastal and Shelf Science*, 55, 673 – 695.

Darecki, M. and D. Stramski (2004): An evaluation of MODIS and SeaWiFS bio-optical algorithms in the Baltic Sea. *Remote Sensing of Environment*, 89, 326 – 350.

Davis Jr., R.A. (1987): Oceanography: *An Invitation to the Marine Environment*. Wm. C. Brown, Iowa, 431 pp.

Di Toro, D.M., D.J. O'Connor and R.V. Thomann (1971): A dynamic model of the phytoplankton population in the Sacramento-San Joaquin Delta, Non-equilibrium systems in natural water chemistry. *Advances in Chemistry Series*, 106, 131 – 180.

Doerffer, R., K. Sorensen and J. Aiken (1999): MERIS potential for coastal zone applications. *International Journal of Remote Sensing*, 20 (9), 1809 – 1818.

Doxaran, D., J.M. Froidefond, S.P. Lavender and P. Castaing (2002): Spatial signature of highly turbid waters: Application with SPOT data to quantify suspended particle matter concentrations. *Remote Sensing of Environment*, 81, 149 – 161.

Duce, R.A. and N.W. Tindale (1991): Chemistry and biology of iron and other trace metals atmospheric transport of iron and its deposition in the ocean. *Limnology and Oceanography*, 36 (8), 1715 – 1726.

Dustan, P. and J.L. Pinckney, Jr. (1989): Tidally induces estuarine phytoplankton Patchiness. *Limnology and Oceanography*, 34 (2), 410 – 419.

Duxbury A.B. And A.C. Duxbury (1993): *Fundamental of Oceanography*. Wm.C. Brown, Iowa, 291 pp.

Dyer, K.R. (1979): Estuarues and estuarine circulation. pp. 1 – 18. In: K.P. Dyer (ed.) *Estuarine Hydrography and Sedimentation*. Cambridge University Press, Cambridge.

Fasham, M.J.R. (1995): Variations in the seasonal cycle of biological production in subarctic oceans: A model sensitivity analysis. *Deep-Sea Research I*, 42, 1111-1149.

Evan, G.T. and J.S. Parslow (1985): A model of annual plankton cycles. *Biological Oceanography*, 3, 327 – 347.

Falkowski, P.G., R.T. Barter and V. Smectacek (1998): Biogeochemical controls and feedbacks on ocean primary production. *Science*, 281, 200 – 206.

Ferrari, G.M. and M. D. Dowell (1998): CDOM absorption characteristics with relation to fluorescence and salinity in coastal areas of the Southern Baltic Sea. *Estuarine, Coastal and Shelf Science*, 47, 91 – 105.

Field, C.B., M.J. Behrenfield, J.T. Randerson and P. Falkowski (1998): Primary production of the biosphere: integration terrestrial and oceanic components. *Science*, 281, 237 - 240.

Fournier, R.O., M.V. Det, N.B. Hargreaves, J.S. Wilson, T.A. Clair and R. Ernst (1984): Physical factors controlling summer distribution if chlorophyll *a* of southwestern Nova Scotia. *Limnology and Oceanography*, 29 (3), 517 – 526.

Frank, P.J.S, J.S. Wroblewski and G.R. Flierl (1986): Behavior of simple plankton model with food-level acclimation by herbivores. *Marine Biology*, 91, 121 – 129.

Franks, P.J.S. (2002): NPZ models of phytoplankton dynamics: their construction, coupling to physics, and application. *Journal of Oceanography*, 58, 379 – 387.

Frost, B.W. (1993): A modeling study of processes regulating plankton standing stock and production in the open subarctic Pacific Ocean. *Progress in Oceanography*, 32, 17 – 56.

Gacia, E., M.M. Littler and D.S. Littler (1999): An experimental test of the capacity of food web interactions (fish–epiphytes–seagrasses) to offset the negative consequences of eutrophication on seagrass communitie. *Estuarine, Coastal and Shelf Science,* 48, 757–766

Gargett, A.E., D. Stucchi and F. Whitney (2003): Physical processes associates with high primary production in Saanich Inlet, British Columbia. *Estuarine Coastal and Shelf Science*, 56, 1141 – 1156.

Garibotti, I.A., M. Vernet, M.E. Ferrario, R.C. Smith, R.M. Ross and L.B. Quetin (2003): Phytoplankton spatial distribution patterns along the western Antarctic Peninsula (Southern Ocean). *Marine Ecology Progress Series*, 261, 21 – 39.

Glantz, M.H.(2001): *Currents of Change: Impacts of El Nino and La Nina on Climate and Society (2nd ed.)*. Cambridge University Press, NY, 252 pp.

Gordon, H.R. (1997): Atmospheric correction of ocean color imagery in the Earth observing system era. *Journal of Geophysical Research*, 102, 17081 – 17106.

Gordon, H.R., D.K. Clark, J.W. Brown, O.B. Brown, R.H. Evans and W.W. Broenkow (1983): Phytoplankton pigment concentrations in the Middle Atlantic Bright: Comparison of ship determinations and CZCS estimates. *Applied Optics*, 22 (1), 20 – 36.

Greening, H. And A. Jakini (2006): Toward reversal of eutrophic conditions in a subtropical estuary: water quality and seagrass response to nitrogen loading reductions in Tampa Bay, Florida, USA. *Environmental Management*, 38 (2), 163 – 178.

Gross, M.G. (1987): *Oceanography: A View of the Earth (4th ed.)*. Prentice-Hall, New Jersey, 406 pp.

Guo, X. and T. Yanagi (1998): The role of Taiwan Strait in an ecological model in the East China Sea. *Acta Oceanographica Taiwanica*, 37 (2), 139 – 164.

Higdon, R.L. (1999): Implementation of a barotropic–baroclinic time splitting for isopycnic coordinate ocean modeling, *Journal of Computational Physics*. 148 (2), 579 – 604.

Holland, H.D. (1984): *The chemical evolution of the atmosphere and oceans,* Princeton University Press, NJ, 582 pp.

Hu, C., Z. Lee, F.E. Muller-Karger, K.L. Carder and J.J. Walsh (2006): Ocean color reveals phase shift between marine plants and yellow substance. *IEEE Geoscience and Remote Sensing Letters*, 3 (2), 262 – 266.

Hungspreugs, M., W. Utoomprurkporn, S. Dharmvanij and P. Sompongchaiyakul (1989): The present status of the aquatic environment of Thailand. *Marine Pollution Bulletin*, 20 (7), 327 – 332.

IOCCG (1998): Minimum Requirements for an Operational Ocean-colour Sensor for the Open Ocean. In: A. Morel (ed.) *Report of the International Ocean-Colour Co-ordinating Group. No. 1*. IOCCG, Dartmouth, 50 pp.

IOCCG (2000): Remote Sensing of Ocean Colour in Coastal, and Other Optically-Complex, Waters. In: S. Sathyendranath (ed.) *Report of the International Ocean-Colour Co-ordinating Group. No. 3*, IOCCG, Dartmouth, 140 pp.

Jensen, J.R. (2000): *Remote Sensing of the Environment: An Earth Resource Perspective.* Prentice-Hall, New Jersey, 544 pp.

Kang, S.H., J.S. Kang, S. Lee, K.H. Chang, D. Kim and M.G. Park (2001): Antarctic phytoplankton assemblages in the marginal ice zone of the northwestern Weddell Sea. *Journal of Plankton Research*, 23 (4), 333 – 352.

Kantha, L.H. and C.A. Clayson (2000): *Numerical Models of Oceans and Oceanic Processes*. Academic Press, California, 940 pp.

Kasai, H., H. Saito and A. Tsuda (1998): Estimation of standing stock of chlorophyll *a* and primary production from remote-sensed ocean color in the Oyashio region, the western Subarctic Pacific, during the spring bloom in 1997. *Journal of Oceanography*, 54, 527 – 537.

Kauppi, P. and R. Sedjo (2001): Technical and economic potential of options to enhance, maintain, and manage biological carbon reservoirs and geo-engineering. pp. 301 – 343. In: IPCC (ed.) *Climate Change 2001: Mitigation.* Cambridge University Press, New York.

Kawamiya, M. and A. Oschlies (2003): An eddy-permitting, coupled ecosystem-circulation model of the Arabian Sea: comparison with observations. *Journal of Marine Systems,* 38 (3 – 4), 221 – 257.

Kawamiya, M., M.J. Kishi and N. Suginohara (2000): An ecosystem model for the North Pacific embedded in a general circulation model Part I: Model description and characteristics of spatial distributions of biological variables. *Journal of Marine System*, 25, 129 – 157.

Kawamiya, M., M.J. Kishi, Y. Yamanaka and N. Suginohara (1995): An ecological-physical coupled model applied to Station Papa. *J*ournal of *Oceanography*, 51, 635 - 664.

Kershow, S. (2000): *Oceanography: An Earth Science Perspective*. Stanley Thornes, Cheltenham, 276 pp.

Kirk, J.T.O. (1975): A theoretical analysis of the contribution of algal cells to the attenuation of light within waters. II: Spherical cells. *New Phytologist*, 75, 21 – 36.

Kirk, J.T.O. (1994): *Light and Photosynthesis in Aquatic Ecosystems (2nd ed.)*. Cambridge University Press, Cambridge, UK, 509 pp.

Kourafalou, V.H., L.Y. Oey, J.D. Wang and T. N. Lee (1996): The fate of river discharge on the continental shelf 1. Modeling the rive plume and the inner shelf coastal current. *Journal of Geophysical Research*, 101, 3415 – 3434.

Kraufvelin, P., S. Salovius, H. Christie, F.E. Moy, R. Karez and M. F. Pedersen (2006): Eutrophication-induced changes in benthic algae affect the behaviour and fitness of the marine amphipod *Gammarus locusta. Aquatic Botany,* 84, 199 – 209.

Kunte, P.D. (1994): Potential usage of remote sensing data in studying the behavior of shore drift along Kerala coast, India. *Estuarine Coastal and Shelf Science*, 38 (6), 613 – 624.

Kuo Y., L. Leu and I. Kao (1999): Directional spectrum analysis and statistics obtained from ERS-1 SAR wave images. *Ocean Engineering*, 26 (11), 1125 – 1144.

Kutser, T., H. Arst, S. Maekivi and K. Kallaste (1998): Estimation of the water quality of the Baltic Sea and some lakes in Estonia and Finland by passive optical remote sensing measured on board a vessel. *Lake and Reservoirs: Research and Management*, 3, 53 – 66.

Ledbetter, M. (1979): Lagmuir circulations and plankton patchiness. *Ecological Modelling*, 7 (4), 289 – 310.

Leu, L. and H. Chang (2005): Remotely sensing in detecting the water depths and bedload of shallow water and their changes. *Ocean Engineering*, 32 (10), 1174 – 1198.

Li, M., A. Gargett and K. Denman (2000): What determines seasonal and interannual variability of phytoplankton and zooplankton in strongly estuarine system? Application to the semi-enclosed estuary of Georgia and Juan de Fuca Strait. *Estuarine Coastal and Shelf Science*, 50, 467 – 488.

Lillesand, T.M. and R.W. Kiefer (2000): *Remote Sensing and Image Interpretation (4th ed.).* John Wiley & Son, New York, 724 pp.

Lirdwitayaprasit, T., S. Meksumpun, S. Rungsupa and K. Furuya (2006): Seasonal variations in cell abundance of *Noctiluca scintillans* in the coastal waters off Chonburi Province, the upper Gulf of Thailand. *Coastal Marine Science*, 30 (1), 80 – 84.

Lirdwitayaprasit, T., T. Vicharangsan and N. Sawetwong (1994): Occurrences of red tide phenomena in the inner Gulf of Thailand during 1991 – 1994. *Proceedings of the First NRCT – JSPS Joint Seminar on Marine Science.* Chulalongkorn University Printing House, Bangkok, 106 – 110.

Lutjeharms, J.R.E., P. Penven and C. Roy (2003): Modelling the shear edge eddies of the southern Agulhas Current. *Continental Shelf Research*, 23 (11 – 13), 1099 – 1115.

Mann, K.H. and J.R.N. Lazier (1996): *Dynamics of Marine Ecosystems: Biological – Physical Interaction in the Oceans (2nd ed.)*. Blackwell Science, Oxford, 394 pp.

Matsumura, S., A. Siripong and T. Lirdwitayaprasit (2006): Underwater optical environment in the upper Gulf of Thailand. *Coastal Marine Science*, 30 (1), 36 – 43.

McCarthy, J.J. (2000): The evolution of the joint global ocean flux study project. pp. 3 – 15. In: R.B. Hanson, H.W. Ducklow and J.G. Field (eds.) *The Changing Ocean Carbon Cycle*. Cambridge University, Cambridge.

McCormic, J.M. And J.V. Thiruvathukal (1981): *Element of Oceanography (2nd ed.)*. Saunders College, New York, 488 pp.

McGowan, J.A. and J.G. Field (2002): Ocean studies. pp. 9 – 45. In: G.J. Field, G. Hempel and C.P. Summerhayes (eds.) *Ocean 2020*. Island Press, Washington.

Mei, Z.P., L. Legendre, Y. Gratton, J.E. Tremblay, B. LeBlanc, C.J. Mundy, B. Klein, M. Gosselin, P. Larouche, P.N. Papakyriakou, C. Lovejoy and C.H. von Quillfeldt (2002): Physical control of spring–summer phytoplankton dynamics in the North Water, April–July 1998. *Deep Sea Research II*, 49, 4959 – 4982.

Mellor, G.L. (1998): *User's Guide for a Three-Dimensional, Primitive Equation, Numerical Ocean Model*. Program in Atmospheric and Oceanographic Sciences Report, Princeton University, Princeton, N.J., 41 pp.

Menasveta, P. (2000): Marine pollution problems in Thai waters. *Proceedings International Symposium on Protection and Management of Coastal Marine Ecosystem*, 12 – 13 Dec 2000, Bangkok, Thailand, 228 – 229.

Mertes, L.A.K., M.O. Smith and J.B. Adam (1993): Estimating suspended sediment concentration in surface waters of the Amazon river wetlands from Landsat images. *Remote Sensing of Environment*, 43, 281 – 301.

Miller, C.B. (2004): *Biological Oceanography*. Blackwell Science, Oxford, 402 pp.

Mitchell, B.G. and M. Kahru (1998): Algorithms for SeaWiFS developed with the CalCOFI data set. *CalCOFI Report,* 39, 133 – 147.

Mochizuki, M., N. Shiga, M. Saito, K. Imai and Y. Nojiri (2002): Seasonal changes in nutrients, chlorophyll-a and the phytoplankton assemblage of the western subarctic gyre in the Pacific Ocean. *Deep-Sea Research II*, 49, 5421–5439.

Monaldo F.M., D.R. Thompson, N.S. Winstead, W.G. Pichel, P. Clemente-Colón and M.B. Christiansen (2005): Ocean wind field mapping from synthetic aperture radar and its application to research and applied problems. *Johns Hopkins APL Technical Digest*, 26 (2), 102 – 113.

Morel, A. and A. Bricaud (1981): Theoretical results concerning light absorption in a discrete medium, and application to specific absorption of phytoplankton. *Deep Sea Research (Part A)*, 28, 1375 – 1393.

Morel, A. and D. Antoine (2000): *Pigment Index Retrieval in Case 1 waters, MERIS Algorithm Theoretical Basis Document, ATBD2*. Available from http://envisat.esa.int/instruments/meris/pdf/atbd_2_09.pdf

Morel, A. and L. Prieur (1977): Analysis of varirtion in ocean color. *Limnology and Oceanography*, 22, 709 – 722.

Morimoto, A., K. Yoshimoto and T. Yanagi (2000): Characteristics of sea surface circulation and eddy field in the South China Sea revealed by satellite altimetric data. *Journal of Oceanography*, 56, 331 – 344.

Murray, R.J. and C.J.C. Reason (2001): A curvilinear version of the Bryan–Cox–Semtner Ocean Model and its representation of the Arctic Circulation. *Journal of Computational Physics*, 171 (1), 1 – 46.

Murty, V.S.N., G.V.M. Gupta, V.V. Sarma, B.P. Rao, D. Jyothi, P.N.M. Shastri and Y. Supraveena (2000): Effect of vertical stability and circulation on the depth of the chlorophyll maximum in the Bay of Bengal during May – June, 1996. *Deep-Sea Research Part I, 47*, 859 – 873.

Muslin, M. (2004): *Global Warming: A Very Short Introduction*. Oxford University Press, New York, 162 pp.

Nagai, T. and Y. Ogawa (1997): Fisheries production. pp. 61 – 94. In: T. Okaichi and T.Yanagi (eds.) *Sustainable Development in the Seto Inland Sea, Japan—From the Viewpoint of Fisheries.* Terra Scientific Publishing, Tokyo

Nagata, H. (1998): Seasonal changes and vertical distributions of chlorophyll *a* and primary productivity at the Yamato Rise, central Japan Sea. *Plankton Biology and Ecology*, 45, 159 – 170.

NEDECO (1965): *A study on the siltation of the Bangkok Port Channel*. The Hage, Holland.

Neelasri, K. (1981): Analysis of the observed current during the inter-monsoon period. *Proceedings of The 2nd Seminar on Water Quality and Living Resources in Thai Water*, 57 – 63.

Neumann, G. and W.J. Pierson, Jr. (1966): *Principles of Physical Oceanography*. Prentice – Hall, New Jersey, 545 pp.

Nixon, S.W. (1995): Coastal marine eutrophication: a definition, social causes, and future concerns. *Ophelia*, 41, 199 – 219.

North, G.R. and R.A. Duce (2002): Climate change and the ocean. pp 85 – 108. In: G.J. Field, G.Hempel and C.P. Summerhayes (eds.) *Ocean 2020*. Island Press, Washington.

Nurdjaman, S. and T. Yanagi (2002): Ecosystem conditions in wet and dry seasons of Banten Bay, Indonesia. *La Mer*, 40, 1 – 10.

Nybakken, J.W. and M.D. Bertness (2004): *Marine Biology: An Ecological Approach (6th ed.)*. Benjamin Cummings, CA, 592 pp.

O'Connor, D.J., D.M. Di Toto and R.V. Thomann (1975): Phytoplankton models and eutrophication problems. In: C.S. Russell (ed.) *Ecological Modeling in a Resource Management Framework*. Resources for the Future, Washington DC.

Onitsuka, G. and T. Yanagi (2005): Differences in ecosystem dynamics between the northern and southern parts of the Japan Sea: Analyses with two ecosystem models. *Journal of Oceanography*, 61, 415 – 433.

Open University Course Team (1999): *Wave, Tides and Shallow-Water Processes (2nd ed.)*. Butterworth – Heinemann, Oxford, 227 pp.

Open University Course Team (2001): *Ocean Circulation (2nd ed.)*. Butterworth – Heinemann, Oxford, 286 pp.

O'Reilly, J.E., S. Maritorena, B.G. Mitchell, D.A. Siegel, K.L. Carder, S.A. Garver, M. Kahru and C. McClain (1998): Ocean color chlorophyll algorithms for SeaWiFS. *Journal of Geophysical Research*, 103, 24937 – 24953.

Parsons, M.L., Q. Dortch and R.E. Turner (2002): Sedimentological evidence of an increase in *Psudo-nitzchia* (Bacillariophyceae) abundance in response to coastal eutrophication. *Limnology and Oceanography*, 47 (2), 551 – 558.

Parsons, T.R., M. Takahashi and B. Hargrave (1984): *Biological Oceanographic Processes (3rd ed.)*, Pergamon, 330 pp.

Peckol, P. And J.S. Rivers (1995): Physiological responses of the opportunistic macroalgae *Cladophora vagabunda* (L.) van den Hoek and *Gracilaria tikvahiae* (McLachlan) to environmental distubances associate with eutrophication. *Journal of Experimental Marine Biology and Ecology*, 190, 1 – 16.

Peterson, C.H., E.A. Irlandi and R. Black (1994): The crash in suspension-feeding bivalve populations (Katelysia spp.) in Princess Royal Habour: and unexpected consequence of eutrophication. *Journal of Experimental Marine Biological Ecology*, 176, 39 – 52.

Pickard, G.L. and W.J. Emery (1990): *Descriptive Physical Oceanography (5th ed.)*. Butterworth-Heinemann, Oxford, 320 pp.

Piemsomboon, A. (2003): Influential factors on phytoplankton abundance and toxicity. pp. 43 – 54. In: ARRI (ed.) *Red Tide Monitoring in the Gulf of Thailand*. Aquatic Resources Research Institute, Chulalongkorn University and Water Quality Management Section, Pollution Control Department, Bangkok (in Thai).

Pinet, P.R. (1998): *Invitation to Oceanography*, Jones and Bartlett, MA, 508 pp.

Pinkerton, M.H., K.M. Richardson, P.W. Boyd, M.P. Gall, J. Zeldis, M.D. Oliver and R.J. Murphy (2005): Intercomparison of ocean color band-ratio algorithms for chlorophyll concentration on the Subtropical Front east of New Zealand. *Remote Sensing of Environment*, 97, 382 – 402.

Polovina, J.J., G.T. Mitchum and G.T. Evans (1995): Decadal and basin-scale variation in mixed layer depth and the impact on biological production in the Central and North Pacific, 1960–88. *Deep-Sea Research*, 42, 1701 – 1716.

Pope, R.M. and E.S. Fry (1997): Absorption spectrum (380 – 700 nm) of pure water. II. Integrating cavity measurements. *Applied Optics*, 36 (33), 8770 – 8723.

Prentice, I.C., G.D. Farquhar, M.J.R. Fasham, M.L. Goulden, M. Heimann, V.J. Jaramillo, H.S. Kheshgi, C. Le Quéré, R.J. Scholes and D.W.R. Wallace (2001): The carbon cycle and atmospheric carbon dioxide. pp 183 – 237. In: IPCC (ed.) *Climate Change 2001: The Scientific Basis*. Cambridge University Press, New York.

Priddle, J., V. Smetacek and U. Bathmann (1992): Antarctic marine primary production, biogeochemical carbon cycles and climatic change. *Philos. Trans. R. Soc. Lond. B*, 338, 289 – 297.

Ramawamy, V., P.S. Rao, K.H. Rao, S. Thwin, N. S. Rao and V. Raiker (2004): Tidal influence on suspended sediment distribution and dispersal in the nothern Andaman Sea and Gulf of Martaban. *Marine Geology*, 208, 33 - 42.

Redfield, A.C., B.H. Ketchum and F.A. Richards (1963): The influence of organisms on the composition of seawater. pp. 26 – 77. In: M.N. Hill (ed.) *The Sea, Ideas and Observations on Progress in the Study of the Seas, Vol. 2*. Interscience.

Richardson, A.J. And D.S. Schoeman (2004): Climate impact on plankton ecosystems in the Northeast Atlantic. *Science*, 305, 1609 – 1612.

Riding, R. (1992): The algal breath of life. *Nature*, 359, 13 – 14.

Riley, G.A. (1956): Oceanography of Long Island Sound, 1952-1954, II. *Phys. Oceanogr. Bull. Bing. Ocean. Coll.*, 15, 15 - 46.

Riley, J.P. and R. Chester (1971): *Introduction to Marine Chemistry*. Academic Press, London, 465 pp.

Robinson, I.S. (2004): *Measuring the Oceans from Space: the Principle and methods of Satellite Oceanography*. Springer - Praxis, Chichester, UK, 669 pp.

Rundquist, D.C., L. Han, J.F. Schalles and J.S. Peake (1996): Remote measurement of algal chlorophyll in surface waters: the case for the first derivative of reflectance near 690 nm. *Photogrammetric Engineering and Remote Sensing*, 62 (2), 195 – 200.

Rungsupa, S. (1997): Distribution pattern and density of *Noctiluca scintillans* around the upper Gulf of Thailand. *Kasetsart University Seminar: 22th February 1997*. 125 – 137.

Rungsupa, S., C. Throngroop, A. Piemsomboon, N. Paphawasit, A. Panichphon and A. Sophol (2003): Red tide incidences in the Gulf of Thailand. pp. 75 – 106. In ARRI (ed.) *Red Tide Monitoring in the Gulf of Thailand*. Aquatic Resources Research Institute, Chulalongkorn University and Water Quality Management Section, Pollution Control Department, Bangkok (in Thai).

Ryther, J.H. (1969): Photosynthesis and fish production in the sea. *Science*, 166, 72 – 76.

Sarmiento, J.L. and J. C. Orr (1991): Three-dimensional simulations of the impact of southern ocean nutrient depletion on atmospheric CO_2 and ocean chemistry. *Limnology and Oceanography*, 36 (8), 1928-1950.

Sarmiento, J.L. and K. Bryan (1982): An ocean transport model for the North Atlantic. *Journal of Geophysical Research*, 87, 394 – 408.

Sathyendranath, S., G. Cota, V. Stuart, H. Maass and T. Platt (2001): Remote sensing of phytoplankton pigments: a comparison of empirical and theoretical approaches. *International Journal of Remote Sensing*, 22 (2 – 3), 249 – 273.

Sathyendranath, S., R.P. Bukata, R. Arnone, M.D. Dowell, C.O. Davis, M. Babin, J.F. Berthon, O.V. Kopelevich and J.W. Campbell (2000): Colour of case 2 waters. pp 23 – 46. In: S. Sathyendranath (ed.) *ICCG Report No. 1: Remote Sensing of Ocean Colour in Coastal, and Other Optically-Complex, Waters*. MacNab, Dartmouth, UK.

Semtner, A.J. (1995): Modeling ocean circulation. *Science*, 269, 1379 – 1385.

Semtner, A.J., Jr. and R.M. Chervin (1992): Ocean general circulation from a global eddy-resolving model. *Journal of Geophysical Research*, 97, 5493 – 5550.

Shaples, J. (1999): Investigation the seasonal vertical structure of phytoplankton in shelf Seas. *Marine Models*, 1, 3 – 38.

Shiomoto, A., and H. Asami (1999): High-west and low-east distribution patterns of chlorophyll-a, primary productivity and diatoms in the subarctic North Pacific surface waters, midwinter 1996. *Journal of Oceanography*, 55, 493 – 503.

Shiomoto, A., Y. Ishida, M. Tamaki and Y. Yamanaka (1998): Primary production and chlorophyll-a in the northwestern Pacific Ocean in summer. *Journal of Geophysical Research*, 103C, 24651 – 24661.

Siegenthaler, U. and Sarmiento, J.L. (1993): Atmospheric carbon dioxide and the ocean. *Nature*, 365, 119 – 125.

Silpipat, S. (1987): Circulation pattern in the upper Gulf of Thailand. *Proceedings of the Fourth Seminar on the Water Quality and the Quality of Living Resources in Thai Waters*: *7- 9 July 1987.* National Research Council of Thailand, 82 - 93.

Smayda, T.J. (1970): The suspension and sinking of phytoplankton in the sea. *Mar. Biol. Annu. Rev.*, 8, 353 – 414.

Smayda, T.J. (1973): The growth of *Sceletonema costatum* during a winter-spring bloom in Narragansett Bay. *R.I. Norw. J. Bot.*, 20, 219 – 247.

Smectacek, V. (1999): Diatoms and the ocean carbon cycle. *Protist*, 150, 25 – 32.

Smith, R.C. and K.S. Baker (1981): Optical properties of the clearest natural waters (200 – 800 nm). *Applied Optics*, 20 (2), 177 – 184.

Smith, V.H., G.D. Tilman and J.C. Nekola (1999): Eutrophication: impacts of excess nutrients on freshwater, marine, and terrestrial ecosystems. *Environmental Pollution*, 100, 179 – 196.

Snidvongs, A. (1998): The oceanography of the Gulf of Thailand: Research and management policy. pp 1 – 68. In: D. M. Johnston (ed.) *SEAPOL Integrated Studies of the Gulf of Thailand, Vol. 1*. Southeast Asian Programme in Ocean Law, Policy and Management.

Sojisuporn, P. (1994): Density-driven and wind-driven current in the upper Gulf of Thailand. *Proceedings IOC-WESTPAC 3rd International Scientific Symposium*, 374 – 385.

Sojisuporn, P. and P. Putikiatikajorn (1998): Eddy circulation in the upper Gulf of Thailand from 2-D tidal model. *Proceedings of The IOC/WESTPAC Fourth International Scientific Symposium*, 515 – 522.

Strickland, J.D.H. and T.R. Parsons (1972): *A Practical Handbook of Seawater Analysis*. Fishery Research Board of Canada, Ottawa, 310 pp.

Suzuki, K., M. Kishino, K. Sasaoka, S. Saitoh and T. Saino (1998): Chlorophyll-specifuc absorption coefficients and pigments of phytoplankton off Sanriku, Northwestern North Pacific. *Journal of Oceanography*, 54, 517 – 526.

Sverdrup, H.U. (1953): On condition for the vernal blooming of phytoplankton. *Journal Du Conseil International Pour L'Exploration De La Mer*, 18, 287 – 195.

Tamiyavanich, S. (1984): The causes and impacts of the red tide phenomena occurring in the upper Gulf of Thailand. *Proceedings of the Third Seminar on the Water Quality and the Quality of Living Resources in Thai Waters*: *26 - 28 March 1984.* National Research Council of Thailand, 481 – 489 (in Thai with English abstract).

Tang D.L., D.R. Kester, I. Ni, H. Kawamura and H. Hong (2002): Upwelling in the Taiwan Strait during the summer monsoon detected by satellite and shipboard measurements. *Remote Sensing of Environment*, 83 (3), 457 – 471.

Taylor, G.I. (1920): Tidal oscillations in gulfs and rectangular basins. *Proceeding of London Mathematical Society*, 20, 148 – 181.

Thurman, H.V. and A.P. Trujillo (1999): *Essentials of Oceanography (6th ed.)*, Prentice Hall, NJ, 527 pp.

Tomczak, M. (1998): *Shelf and Coastal Oceanography* (Version 1.0): http://gyre.umeoce.maine.edu/physicalocean/Tomczak/ShelfCoast/index.html.

Tomczak, M. and J.S. Godfrey (2005): *Regional Oceanography: An Introduction* (pdf Version 1.1), Elsevier Science, Oxford, 391 pp.

Walsh, J. J., D.A. Dieterle and J. Lenes (2001): A numerical analysis of carbon dynamics of the Southern Ocean phytoplankton community: the roles of light and grazing in effecting both sequestration of atmospheric CO_2 and food availability to larval krill. *Deep-Sea Research Part I*, 48, 1 – 48.

Waluda, C.M., P.G. Rodhouse, P.N. Trathan and G.J. Pierce (2001): Remotely sensed mesoscale oceanography and the distribution of *Illex argentinus* in the South Atlantic. *Fisheries Oceanography*, 10 (2), 207 – 216.

Wang, B. (2006): Cultural eutrophication in the Changjiang (Yangtze River) plume: history and perspective. *Estuarine Coastal and Shelf Science*, 69, 471 – 477.

Ware, D.M. And R.E. Thomson (2005): Bottom-up ecosystem trophic dynamics determine fish production in the northeast Pacific. *Science*, 308, 1280 - 1284.

Watson, A.J. and P.S. Liss (1998): Marine biological controls on climate via the carbon and sulphur geochemical cycles. *Phil. Trans. R. Soc. Lond. B*, 353, 41 – 51.

Webb, K.L. and C.F. D'Elia (1980): Nutrient and oxygen redistribution during a spring neap tidal cycle in a temperate estuary. *Science*, 207, 983 – 985.

Werdell, P.J. and S.W. Bailey (2005): An improved in-situ bio-optical data set for ocean color algorithm development and satellite data product validation. *Remote Sensing of Environment*, 98, 122 – 140.

Wichaimekphat, W., S. Supharatid and T. Tingsanchali (2006): A study of Bang Khun Thien coastal erosion and protection. *Vietnam -Japan Estuary Workshop 2006 August 22nd -24th*. Hanoi, Vietnam, 134 – 139.

Wu, R.S.S. (1999): Eutrophication, water borne pathogens and xenobiotic compounds: environmental risks and challenges. *Marine Pollution Bulletin*, 39, 11 – 22.

Xu, J. and H. R.R. (2006): Modeling biogeochemical cycles in Chesapeake Bay with a coupled physicalebiological model. *Estuarine, Coastal and Shelf Science*, 69, 19 – 46.

Yamada, K., J. Ishizaka, S. Yoo, A. Kim ans S. Chiba (2004): Seasonal and interannual variability of sea surface chlorophyll a concentration in the Japan/East Sea (JES). *Progress in Oceanography*, 61, 193 – 211.

Yamamoto, T. (2003): The Seto Inland Sea – eutrophic or oligotrophic? *Marine Pollution Bulletin*, 47, 37 – 42.

Yanagi, T. (1999): *Coastal Oceanography*. Terra Scientific Publishing Company, Tokyo, 162 pp.

Yanagi T., G. Onisuka, N. Hirose and J.H. Yoon (2001a): A numerical simulation on the mesoscale dynamics of the spring bloom in the Sea of Japan. *Journal of Oceanography*, 57, 617 – 630.

Yanagi, T., K. Inoue, S. Montani and M. Yamada (1997): Ecological modeling as a tool for coastal zone management in Dokai Bay, Japan. *Journal of Marine System*, 13, 123 – 136.

Yanagi, T, S.I. Sachoemar, T. Takao and S. Fujiwara (2001b): Seasonal variation of stratification in the Gulf of Thailand. *Journal of Oceanography*, 57, 461 – 470.

Yanagi, T. and T. Takao (1998): Clockwise phase propagation of semi-diurnal tides in the Guf of Thailand. *Journal of Oceanography*, 54, 143 – 150.

Yates, M.G., A.R. Jones, S. McGrorty and J.D. Gross-Custard (1993): The use of satellite Imagery to determine the distribution of intertidal surface sediments of the Wash, England. *Estuarine Coastal and Shelf Science*, 36, 333 – 344.

Yin, K., J. Zhang, P.Y. Qian, W. Jian, L. Huang, J. Chen and M.C.S. Wu (2004): Effect of wind events on phytoplankton blooms in the Pearl River estuary during summer. *Continental Shelf Research*, 24, 1909 – 1923.

APPENDIX A

MERIS LEVEL 2 PRODUCT SPECIFICATIONS

Reference Level 2 full resolution

PRODUCT ID	**MER_FR__2P**
NAME	**Reference Level 2 full resolution**
DESCRIPTION	**Meris product generated on request from MERIS L1B Water leaving radiance (reflectance) and geophysical products Floating scene concept for distribution**
COVERAGE	**575 km x 575km**
THROUGHPUT	**6 PDHS-E 3 PDHS-K**
GEOMETRICAL SAMPLING	**300 x 300 meters resampled in a "pseudo satellite" projection along track**
SCENE SIZE	**187 Mbytes per scene**
RADIOMETRIC RESOLUTION	**NEDR=5.7 X 10^{-4} at sea level @ 442.5nm**
PRODUCT ACCURACY	**Surface reflectance (ocean) <2 x 10 -4 Surface reflectance (Land) < 5% Chlorophyll retrieval < 15 % Yellow substance < 30 % Suspended matter < 15 % Water vapour < 20% Cloud albedo < 2 % Cloud optical thickness ~ 10% Cloud top pressure ~ 40 hPa MERIS Vegetation Index:-N/A**
AUXILIARY DATA	**Surface identification flags included in the level 1b product Orbit state vector, Time correlation parameters, Latitude, Longitude, altitude and topographic corrections Sun azimuth, Sun elevation, view azimuth, view elevation Resampled ECMWF data: Mean Sea Level pressure, Total column ozone, Total column water vapour, Wind speed,**
NOTES	**On demand dissemination of multiple of scene size (575km x 575km)**

Source: http://envisat.esa.int/instruments/meris/data-app/prodspread.html

APPENDIX B

BASIC EQUATIONS OF THE PRINCETON OCEAN MODEL (POM)

Mathematical details of POM, presented here, are adapted from Mellor (1998). Since POM is a sigma coordinate model in that the vertical coordinate is scaled on the water column depth, the vertical terms of the Navier-Stokes equations of fluid dynamics with the gravitational buoyancy force and Coriolis force will be converted to such a coordinate (Figure B-1) based on the transformation,

$$\sigma = \frac{z - \eta}{H + \eta}. \tag{B-1}$$

Here H (x, y) is the bottom topography; η (x, y, t) is the surface elevation; D is the instantaneous depth which is defined as $D \equiv H + \eta$; x, y, z are the conventional Cartesian coordinates.

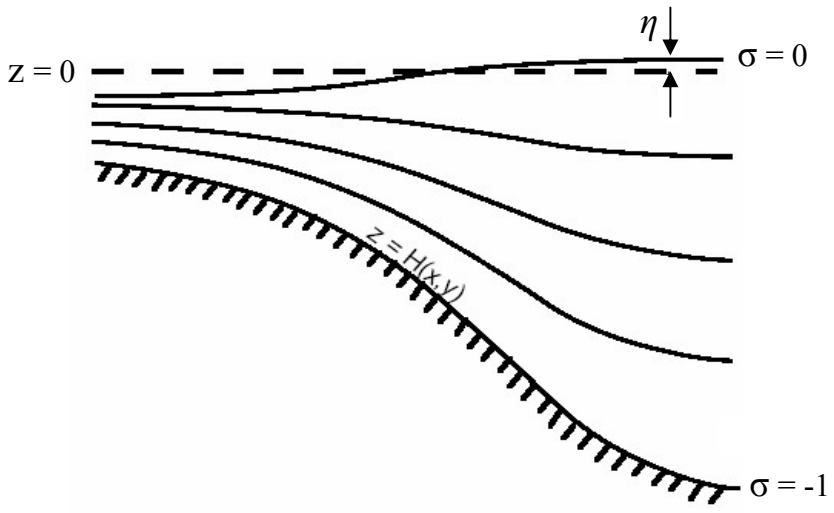

Figure B-1 The sigma coordinate system

σ ranges from $\sigma = 0$ at $z = \eta$ to $\sigma = -1$ at $z = -H$ as clearly shown in Figure B-1. The governing equations of POM in the internal mode for three-dimensional circulation are composed of the continuity equation, and the conservations of masses, salinity, temperature and turbulence kinetic energy. The equations after converted to sigma coordinate are shown as the follows.

$$\frac{\partial DU}{\partial x}+\frac{\partial DV}{\partial y}+\frac{\partial \omega}{\partial \sigma}+\frac{\partial \sigma}{\partial t}=0\,, \tag{B-2}$$

$$\frac{\partial UD}{\partial t}+\frac{\partial U^2D}{\partial x}+\frac{\partial UVD}{\partial y}+\frac{\partial U\omega}{\partial \sigma}-fVD+gD\frac{\partial \eta}{\partial x}$$

$$+\frac{gD^2}{\rho_0}\int_\sigma^0\left[\frac{\partial \rho'}{\partial x}-\frac{\sigma'}{D}\frac{\partial D}{\partial x}\frac{\partial \rho'}{\partial \sigma'}\right]d\sigma'=\frac{\partial}{\partial \sigma}\left[\frac{K_M}{D}\frac{\partial U}{\partial \sigma}\right]+F_x\,, \tag{B-3}$$

$$\frac{\partial VD}{\partial t}+\frac{\partial UVD}{\partial x}+\frac{\partial V^2D}{\partial y}+\frac{\partial V\omega}{\partial \sigma}+fUD+gD\frac{\partial \eta}{\partial y}$$

$$+\frac{gD^2}{\rho_0}\int_\sigma^0\left[\frac{\partial \rho'}{\partial y}-\frac{\sigma'}{D}\frac{\partial D}{\partial y}\frac{\partial \rho'}{\partial \sigma'}\right]d\sigma'=\frac{\partial}{\partial \sigma}\left[\frac{K_M}{D}\frac{\partial V}{\partial \sigma}\right]+F_y\,, \tag{B-4}$$

$$\frac{\partial TD}{\partial t}+\frac{\partial TUD}{\partial x}+\frac{\partial TVD}{\partial y}+\frac{\partial T\omega}{\partial \sigma}=\frac{\partial}{\partial \sigma}\left[\frac{K_H}{D}\frac{\partial T}{\partial \sigma}\right]+F_T-\frac{\partial R}{\partial z}\,, \tag{B-5}$$

$$\frac{\partial SD}{\partial t}+\frac{\partial SUD}{\partial x}+\frac{\partial SVD}{\partial y}+\frac{\partial S\omega}{\partial \sigma}=\frac{\partial}{\partial \sigma}\left[\frac{K_H}{D}\frac{\partial S}{\partial \sigma}\right]+F_S\,, \tag{B-6}$$

$$\frac{\partial q^2 D}{\partial t}+\frac{\partial q^2 UD}{\partial x}+\frac{\partial q^2 VD}{\partial y}+\frac{\partial q^2 \omega}{\partial \sigma}=\frac{\partial}{\partial \sigma}\left[\frac{K_q}{D}\frac{\partial q^2}{\partial \sigma}\right]$$

$$+\frac{2K_M}{D}\left[\left(\frac{\partial U}{\partial \sigma}\right)^2+\left(\frac{\partial V}{\partial \sigma}\right)^2\right]+\frac{2g}{\rho_0}K_H\frac{\partial \tilde{\rho}}{\partial \sigma}-\frac{2Dq^3}{B_1 l}+F_q, \qquad \text{(B-7)}$$

$$\frac{\partial q^2 lD}{\partial t}+\frac{\partial q^2 lUD}{\partial x}+\frac{\partial q^2 lVD}{\partial y}+\frac{\partial q^2 l\omega}{\partial \sigma}=\frac{\partial}{\partial \sigma}\left[\frac{K_q}{D}\frac{\partial q^2 l}{\partial \sigma}\right]$$

$$+E_1 l\left(\frac{K_M}{D}\left[\left(\frac{\partial U}{\partial \sigma}\right)^2+\left(\frac{\partial V}{\partial \sigma}\right)^2\right]+E_3\frac{g}{\rho_0}K_H\frac{\partial \tilde{\rho}}{\partial \sigma}\right)-\frac{Dq^3}{B_1}\tilde{W}+F_l, \qquad \text{(B-8)}$$

It should be noted here first that ω is the transformed vertical velocity which is the velocity component normal to sigma surfaces. The relation between the Cartesian vertical velocity (W) and ω is shown in the following equation.

$$W=\omega+U\left(\sigma\frac{\partial D}{\partial x}+\frac{\partial \eta}{\partial x}\right)+V\left(\sigma\frac{\partial D}{\partial y}+\frac{\partial \eta}{\partial y}\right)+\sigma\frac{\partial D}{\partial t}+\frac{\partial \eta}{\partial t}, \qquad \text{(B-9)}$$

Here U and V are horizontal velocities (m s^{-1}) along x and y, respectively; T is potential temperature (K) while S is salinity (psu); t is time (s); g is the gravitational acceleration (9.8 m s^{-2}), f is the Coriolis parameter which is defined as $f = 2\Omega \sin\varphi$; Ω is angular acceleration of the Earth rotation (7.29×10^{-5} rad s^{-1}); φ is latitude (rad);

q^2 is twice the turbulence kinetic energy ($m^2\ s^{-2}$); l is turbulence length scale (m); ρ_0 is the reference density of seawater (1,025 kg m^{-3}); ρ' is the water density difference by subtraction the instantaneous density with the mean density (ρ_{mean}), however ρ_{mean} is generally the initial density in the model operation; $\tilde{\rho} = \rho_{mean} + \rho'$; σ' is defined as an intermediate layer lined at the middle between two σ layers; R is short wave radiation flux (m s^{-1} K); K_M, K_H and K_q are vertical kinematic viscosity ($m^2\ s^{-1}$), vertical diffusivity ($m^2\ s^{-1}$) and vertical diffusivity of turbulence kinetic energy ($m^2\ s^{-1}$), respectively; B_1 is a turbulence closure constant (16.6); E_1 and E_3 are constants which are 1.8 and 1.0, respectively. $\tilde{W}$ is called the wall proximity function which is prescribed as:

$$\tilde{W} = 1 + E_2 (l / \kappa L), \tag{B-10}$$

where $L^{-1} = (\eta - z)^{-1} + (H - z)^{-1}$; E_2 is a constant (1.33); κ is the Von Kerman's constant (0.4). Also $\partial\tilde{\rho} / \partial\sigma \equiv \partial\rho / \partial\sigma - c_s^2 \partial p / \partial\sigma$ where c_s is the speed of sound (m s^{-1}) and p is water pressure (kg $m^{-1}\ s^{-2}$).

The horizontal viscosity and diffusion terms in Eq. (B-3) and (B-4) are defined according to:

$$F_x \equiv \frac{\partial}{\partial x}(H\tau_{xx}) + \frac{\partial}{\partial y}(H\tau_{xy}), \tag{B-11}$$

$$F_y \equiv \frac{\partial}{\partial x}(H\tau_{xy}) + \frac{\partial}{\partial y}(H\tau_{yy}), \tag{B-12}$$

where

$$\tau_{xx} = 2A_M \frac{\partial U}{\partial x}, \tag{B-13}$$

$$\tau_{xy} = \tau_{yx} = A_M \left(\frac{\partial U}{\partial y} + \frac{\partial V}{\partial x} \right), \tag{B-14}$$

$$\tau_{yy} = 2 A_M \frac{\partial V}{\partial y}. \tag{B-15}$$

Also those in Eq. (B-5) to Eq. (B-8) are defined as:

$$F_\phi \equiv \frac{\partial}{\partial x}(H q_x) + \frac{\partial}{\partial y}(H q_y), \tag{B-16}$$

where

$$q_x = A_H \frac{\partial \phi}{\partial x}, \tag{B-17}$$

$$q_y = A_H \frac{\partial \phi}{\partial y}. \tag{B-18}$$

Here ϕ represents T, S, q^2 or $q^2 l$. A_M and A_H are horizontal kinematic viscosity ($m^2\ s^{-1}$) and horizontal diffusivity ($m^2\ s^{-1}$), respectively. A_M is calculated at first and then A_H is computed with the relation of $A_H/A_M \equiv$ Tprni, where Tprni is the horizontal diffusivity/viscosity inverse Prandtl number (1.0).

The Smagorinsky diffusivity is applied for the horizontal kinematic viscosity (A_M) which the formula is:

$$A_M = C\,\Delta x\,\Delta y \left[\left(\frac{\partial U}{\partial x} \right)^2 + \frac{1}{2} \left(\frac{\partial V}{\partial x} + \frac{\partial U}{\partial y} \right)^2 + \left(\frac{\partial V}{\partial y} \right)^2 \right], \tag{B-19}$$

where C is called the Horcon parameter which is in the range of 0.10 to 0.20. If the horizontal grid spacing is very small, C can be nil. C is set as 0.20 in the model code.

POM is a turbulence closure model that the vertical diffusion terms (K_M, K_H and K_q) are calculated in sub-models. The equations are defined according to:

$$K_M = ql\,S_M\,, \tag{B-20}$$

$$K_H = ql\,S_H\,, \tag{B-21}$$

$$K_q = 0.41\,ql\,S_H\,. \tag{B-22}$$

The coefficient, S_H and S_M, are the stability functions given by:

$$S_H\left[1-\left(3\,A_2B_2+18\,A_1A_2\right)G_H\right] = A_2\left[1-6\frac{A_1}{B_1}\right], \tag{B-23}$$

$$S_M\left[1-9\,A_1A_2\,G_H\right]-S_H\left[\left(18\,A_1^2+9\,A_1A_2\right)G_H\right] = A_1\left[1-3C_1-6\frac{A_1}{B_1}\right], \tag{B-24}$$

where the Richardson number (G_H) could be presented as the following formula:

$$G_H = -\frac{l^2}{q^2}\frac{g}{\rho_0}\left[\frac{\partial\rho}{\partial z}-\frac{1}{c_s^2}\frac{\partial p}{\partial z}\right]. \tag{B-25}$$

Here the constants A_1, B_1, A_2, B_2 and C_1 are 0.92, 16.6, 0.74, 10.1 and 0.08, respectively. It should be noted here that the stability functions will be infinity if G_H approaches the value of 0.0288 which is unexpected to find in nature.

Vertical Boundary Conditions

The transform vertical velocity (ω) at the sea surface (σ = 0) and the sea bottom (σ = -1) are set to be zero for the continuity equation (Eq.(B-2)) which is:

$$\omega(0) = \omega(-1) = 0\,, \tag{B-26}$$

Surface boundary conditions for the momentum equations, Eq.(B-3) and Eq.(B-4), are:

$$\frac{K_M}{D}\left(\frac{\partial U}{\partial \sigma},\frac{\partial V}{\partial \sigma}\right) = -\frac{\rho_a C_d |W|\left(W_x, W_y\right)}{\rho_0},\ \sigma \to 0. \tag{B-27}$$

Here W_x and W_y are wind speeds (m/s) in x and y components, respectively. $|W|$ is wind magnitude which is calculated from $\left(W_x^2 + W_y^2\right)^{\frac{1}{2}}$; ρ_a is air density (1.2 kg m^{-3}); and C_d is drag coefficient at the sea surface (0.0013).

Bottom boundary conditions for the momentum equations are as the follow:

$$\frac{K_M}{D}\left(\frac{\partial U}{\partial \sigma},\frac{\partial V}{\partial \sigma}\right) = C_Z\left[U^2 + V^2\right]^{\frac{1}{2}}(U,V),\ \sigma \to -1, \tag{B-28}$$

where the bottom drag coefficient (C_z) is:

$$C_Z = MAX\left[\frac{\kappa^2}{\left[\frac{\ln\left(1+\sigma_{kb-1}\right)H}{z_0}\right]^2}, 0.0025\right]. \tag{B-29}$$

Here σ_{kb-1} is the σ layer just above the last layer at the sea bottom; and z_0 is the roughness parameter (0.01 m).

The boundary conditions for the conservations of salinity and temperature, Eq.(B-5) and Eq.(B-6), respectively, allow exchanging fluxes at the sea surface but not at the sea bottom which are:

$$\frac{K_H}{D}\left(\frac{\partial T}{\partial \sigma},\frac{\partial S}{\partial \sigma}\right) = \left(Q_T, Q_S\right),\ \sigma \to 0, \tag{B-30}$$

$$\frac{K_H}{D}\left(\frac{\partial T}{\partial \sigma},\frac{\partial S}{\partial \sigma}\right) = (0,\ 0),\ \sigma \to -1, \tag{B-31}$$

where Q_T and Q_S are the surface fluxes of heat (ms^{-1} K) and salinity (ms^{-1} psu), respectively. The boundary conditions for the conservation of turbulence kinetic energy, Eq.(B-7) and (B-8), are as follows:

$$\left(q^2(0),\ q^2 l(0)\right) = \left(B_1^{\frac{2}{3}}\, u_\tau^2(0),\ 0\right), \tag{B-32}$$

$$\left(q^2(-1),\ q^2 l(-1)\right) = \left(B_1^{\frac{2}{3}}\, u_\tau^2(-1),\ 0\right), \tag{B-33}$$

where B_1 is one of the turbulence closure constants (16.6); and u_τ is the friction velocity (m s^{-1}) at the surface or the bottom.

The Vertically Integrated Equations

It should be addressed here that the governing equations of POM contain fast moving external gravity wave (the external mode) and slow moving internal gravity wave (the internal mode) which is solved separately in the computer program with a technique called mode splitting in order to reduce computational time. With this technique, the free surface elevation and the velocity transport are solved separately from the three-dimensional circulation of the velocity and the thermodynamic properties.

The external mode of POM or the two-dimensional circulation part is obtained by integrating the internal mode equations over the depth. Therefore, by integrating Eq.(B-2) to Eq.(B-5) and using the boundary condition according to Eq.(B-26) - Eq.(B-29), the governing equations for the external mode can be written as:

$$\frac{\partial \eta}{\partial t} + \frac{\partial \overline{U} D}{\partial x} + \frac{\partial \overline{V} D}{\partial y} = 0, \tag{B-34}$$

$$\frac{\partial \overline{U} D}{\partial t} + \frac{\partial \overline{U}^2 D}{\partial x} + \frac{\partial \overline{U}\overline{V} D}{\partial y} - \widetilde{F}_x - f\overline{V} D + gD\frac{\partial \eta}{\partial x} = -\frac{\rho_a C_d |W| W_x}{\rho_0}$$

$$+ C_Z \left[U_b^2 + V_b^2\right]^{\frac{1}{2}} U_b + G_x - \frac{gD}{\rho_0}\int_{-1}^{0}\int_{\sigma}^{0}\left[D\frac{\partial \rho'}{\partial x} - \frac{\partial D}{\partial x}\sigma'\frac{\partial \rho'}{\partial \sigma'}\right] d\sigma' d\sigma, \tag{B-35}$$

$$\frac{\partial \overline{V} D}{\partial t} + \frac{\partial \overline{U}\overline{V} D}{\partial x} + \frac{\partial \overline{V}^2 D}{\partial y} - \widetilde{F}_y + f\overline{U} D + gD\frac{\partial \eta}{\partial y} = -\frac{\rho_a C_d |W| W_y}{\rho_0}$$

$$+ C_Z \left[U_b^2 + V_b^2\right]^{\frac{1}{2}} V_b + G_y - \frac{gD}{\rho_0}\int_{-1}^{0}\int_{\sigma}^{0}\left[D\frac{\partial \rho'}{\partial y} - \frac{\partial D}{\partial y}\sigma'\frac{\partial \rho'}{\partial \sigma'}\right] d\sigma' d\sigma, \tag{B-36}$$

where U_b and V_b are the current velocity just above the sea bottom from the internal mode in x and y direction, respectively. The over bars denote the vertical integration of vectors or any parameters (θ) defined as:

$$\overline{\theta} = \int_{-1}^{0} \theta \, d\sigma. \tag{B-37}$$

The definitions of $\widetilde{F}_x$, $\widetilde{F}_y$, G_x and G_y are shown below:

$$\widetilde{F}_x = \frac{\partial}{\partial x}\left[H 2\overline{A}_M \frac{\partial \overline{U}}{\partial x}\right] + \frac{\partial}{\partial y}\left[H\overline{A}_M\left(\frac{\partial \overline{U}}{\partial y} + \frac{\partial \overline{V}}{\partial x}\right)\right], \tag{B-38}$$

$$\widetilde{F}_y = \frac{\partial}{\partial y}\left[H 2\overline{A}_M \frac{\partial \overline{V}}{\partial y}\right] + \frac{\partial}{\partial x}\left[H\overline{A}_M\left(\frac{\partial \overline{U}}{\partial y} + \frac{\partial \overline{V}}{\partial x}\right)\right], \tag{B-39}$$

$$G_x = -\frac{\partial \overline{U^2 D}}{\partial x} - \frac{\partial \overline{UVD}}{\partial y} + \overline{F}_x, \tag{B-40}$$

$$G_y = -\frac{\partial \overline{UVD}}{\partial x} - \frac{\partial \overline{V^2 D}}{\partial y} + \overline{F}_y. \tag{B-41}$$

The details of lateral boundary conditions and model operations are shown in the circulation model section of Chapter 6.

APPENDIX C

NUTRIENTS AND OCEANOGRAPHIC PARAMETERS

Cruise CU-1 (9-11 October 2003)

Station	depth (m)	ammonia µM	nitrite µM	nitrate µM	phosphate µM	silicate µM	temperature (°C)	salinity (psu)	DO (ml/l)	pH
1	0	11.39	0.41	0.09	0.59	15.61	29.46	29.99	5.33	8.16
	5	10.00	0.49	0.08	0.57	17.19	29.53	30.35	4.25	8.14
	10	11.59	0.69	0.16	0.55	17.54	29.44	32.03	3.32	8.06
2	0	11.19	0.08	0.06	0.74	15.61	29.49	27.85	6.03	8.19
	5	11.99	0.06	1.93	2.63	12.63	29.53	29.65	4.39	8.07
	10	10.99	1.87	0.40	0.47	14.91	29.49	31.70	2.26	8.00
	14	10.40	2.89	0.59	0.45	15.26	29.39	32.07	3.31	8.10
3	0	9.60	0.08	0.00	0.60	12.45	30.42	27.45	6.86	8.40
	5	10.20	0.08	0.03	0.55	13.50	29.81	27.73	7.20	8.41
	9	14.39	0.06	0.00	1.64	23.67	29.66	29.65	1.56	7.92
4	0	9.20	0.04	0.17	1.37	10.87	31.20	22.19	7.50	8.59
	5	8.60	0.06	0.00	0.60	9.82	29.93	27.86	4.70	8.23
	8	10.20	0.08	0.00	1.01	18.41	29.68	30.95	2.18	7.93
5	0	7.00	0.06	0.00	1.35	18.06	31.28	20.15	9.96	8.65
	5	9.00	0.04	0.00	0.20	13.15	29.75	31.09	7.89	8.39
	10	8.80	2.85	0.63	0.92	17.71	29.67	31.95	2.21	7.96
	15	9.00	3.38	0.81	0.86	19.47	29.67	32.03	0.41	7.86
6	0	7.60	0.06	0.00	0.88	18.59	31.00	22.92	5.35	8.47
	5	9.20	0.06	0.00	0.39	15.61	30.04	30.51	4.57	8.37
	10	10.20	2.16	0.47	0.66	18.41	29.67	31.77	2.82	8.15
	17	8.80	0.69	0.09	0.39	13.68	29.66	32.35	0.74	7.94
7	0	6.80	0.04	0.00	0.64	16.83	30.05	24.01	4.70	8.57
	5	10.60	0.06	0.01	0.20	12.63	29.85	31.58	4.68	8.40
	10	11.59	0.33	1.24	0.25	12.98	29.67	32.47	3.54	8.25
	19	9.80	1.55	0.01	0.45	18.06	29.64	32.71	2.14	8.10
8	0	10.40	0.08	0.00	0.49	13.15	29.53	28.06	4.26	8.46
	5	7.60	0.04	0.00	0.43	11.57	29.35	31.20	3.55	8.38
	10	9.60	0.04	0.00	0.18	7.37	29.56	32.06	3.40	8.30
	20	10.60	0.20	0.22	0.25	15.08	29.76	32.69	2.45	8.23
9	0	10.40	0.04	0.03	0.20	6.14	29.65	29.11	1.45	8.41
	5	10.20	0.04	0.03	0.16	5.26	29.75	31.77	1.83	8.32
	10	9.40	0.04	0.00	0.14	5.09	29.73	31.91	1.97	8.31
	22	10.40	0.04	0.00	0.18	7.89	29.60	32.42	2.30	8.30
10	0	8.00	0.04	0.03	0.12	4.56	30.50	31.55	4.39	8.29
	5	7.60	0.04	0.00	0.12	4.56	30.33	31.57	4.92	8.30
	10	11.99	0.06	0.00	0.21	10.00	29.84	31.64	4.54	8.30
	27	8.20	0.04	0.00	0.10	6.31	29.47	32.23	4.37	8.29
11	0	9.60	0.04	0.00	0.21	9.29	29.54	30.17	3.11	8.37
	5	9.80	0.04	0.00	0.18	7.37	29.60	31.29	3.16	8.33
	10	9.60	0.06	0.00	0.21	6.14	29.71	32.49	3.21	8.29
	26	10.40	0.53	0.25	0.25	15.43	29.82	33.01	2.74	8.19
12	0	10.00	0.04	0.00	0.16	4.91	30.28	32.26	2.66	8.30
	5	10.00	0.06	0.00	0.18	5.09	29.79	32.44	2.85	8.30
	10	10.00	0.04	0.03	0.20	5.61	29.70	32.50	3.13	8.29
	23	9.80	0.04	0.00	0.18	7.72	29.47	32.71	2.83	8.28
13	0	8.00	0.04	0.00	0.12	4.38	30.41	31.34	2.52	8.30
	5	8.00	0.04	0.00	0.14	4.91	29.91	31.53	2.58	8.30
	10	8.40	0.04	0.03	0.16	5.09	29.67	31.89	2.67	8.30
	36	8.60	0.04	0.00	0.14	5.61	29.25	33.09	2.59	8.26

14	0	9.60	0.06	0.08	0.41	15.43	29.95	28.36	1.17	8.38
	5	9.20	0.04	0.00	0.25	11.57	29.66	31.51	1.26	8.30
	10	9.40	0.04	0.00	0.12	5.61	29.51	31.67	1.51	8.30
	18	10.99	0.04	0.03	0.18	10.52	29.44	32.70	2.37	8.28
15	0	11.79	0.06	0.15	0.14	7.54	30.14	31.24	1.39	8.31
	5	10.99	0.04	0.00	0.12	5.61	29.74	31.57	1.32	8.31
	10	10.60	0.04	0.00	0.12	6.66	29.76	31.90	1.56	8.30
	15	11.19	0.04	0.00	0.14	8.94	29.99	32.08	1.81	8.29
16	0	9.00	0.04	0.03	0.29	13.85	30.75	28.95	0.41	8.25
	5	10.00	0.04	0.00	0.27	14.73	30.31	31.20	2.82	8.27
	10	nd	nd	nd	nd	nd	29.75	31.03	3.39	8.34
	19	8.20	0.08	0.20	0.21	10.17	29.47	32.08	5.81	8.27
17	0	8.00	0.04	0.00	0.16	9.12	30.14	28.15	5.32	8.27
	5	8.80	0.04	0.00	0.20	9.12	30.10	30.29	3.46	8.30
	10	8.40	0.04	0.00	0.18	8.94	29.80	30.47	4.68	8.31
	26	9.80	0.16	0.05	0.23	12.10	29.41	31.05	3.29	8.15

nd = no data

Cruise CU-2 (4-6 December 2003)

Station	depth (m)	ammonia µM	nitrite µM	nitrate µM	phosphate µM	silicate µM	temperature (°C)	salinity (psu)	DO (ml/l)	pH
1	0	9.00	0.04	0.17	0.20	5.61	27.55	31.34	8.12	8.37
	5	8.40	0.06	0.05	0.20	6.31	27.58	31.36	8.04	8.40
	10	9.80	0.08	0.00	0.20	6.31	27.59	31.36	8.05	8.41
2	0	10.60	0.08	0.06	0.20	7.19	27.87	31.30	8.37	8.40
	5	10.00	0.06	0.01	0.18	6.14	27.90	31.30	8.24	8.41
	10	11.79	0.06	0.15	0.18	6.84	27.90	31.30	8.25	8.41
	15	9.40	0.04	0.07	0.18	5.44	27.89	31.30	8.24	8.41
3	0	9.20	0.04	0.00	0.18	7.37	27.71	31.36	4.10	8.39
	5	11.59	0.04	0.07	0.20	6.49	27.72	31.36	4.50	8.41
	10	9.20	0.04	0.00	0.18	6.49	27.68	31.36	1.48	8.42
4	0	10.00	0.04	0.17	0.20	9.47	27.60	30.61	10.58	8.45
	5	10.00	0.04	0.00	0.20	8.24	27.22	30.65	11.29	8.48
	9	10.40	0.04	0.00	0.18	7.37	27.20	30.70	10.15	8.45
5	0	9.00	0.06	0.00	0.39	15.61	27.99	30.00	9.62	8.45
	5	10.40	0.04	0.00	0.35	13.85	27.69	30.69	10.45	8.47
	10	10.79	0.06	0.00	0.25	11.75	27.79	31.06	9.21	8.42
	15	10.40	0.04	0.03	0.27	11.92	27.76	31.19	8.67	8.41
6	0	9.20	0.04	0.00	0.64	20.69	28.04	29.05	9.60	8.42
	5	12.99	0.08	0.20	0.43	14.55	27.94	30.65	9.27	8.41
	10	10.79	0.08	0.06	0.31	11.22	27.92	30.93	8.30	8.38
	15	11.39	0.08	0.06	0.35	13.85	28.01	31.11	7.56	8.36
7	0	9.60	0.04	0.07	0.21	11.40	27.86	31.17	8.32	8.40
	5	9.20	0.04	0.00	0.23	11.92	27.87	31.17	8.33	8.42
	10	8.60	0.04	0.00	0.20	10.87	27.87	31.17	8.35	8.42
	18	11.99	0.04	0.03	0.23	11.75	27.88	31.17	8.36	8.43
8	0	10.60	0.08	0.03	0.20	5.09	28.01	31.30	8.57	8.43
	5	8.40	0.04	0.00	0.16	4.73	28.00	31.30	5.59	8.44
	10	11.59	0.08	0.00	0.21	4.73	28.01	31.30	5.59	8.44
	23	10.40	0.06	0.01	0.20	4.56	27.93	31.30	8.48	8.44
9	0	9.00	0.04	0.00	0.16	7.19	28.22	31.24	8.09	8.29
	5	9.20	0.04	0.00	0.12	6.66	28.23	31.24	8.09	8.37
	10	10.20	0.04	0.07	0.14	7.54	28.23	31.25	8.10	8.39
	20	10.60	0.04	0.03	0.20	8.77	28.20	31.34	8.04	8.40
10	0	10.00	0.04	0.00	0.16	7.89	28.65	31.26	8.23	8.40
	5	7.20	0.04	0.00	0.16	7.19	28.65	31.27	8.20	8.41
	10	9.20	0.08	0.00	0.12	7.01	28.64	31.27	8.21	8.41
	25	9.00	0.04	0.10	0.14	6.66	28.52	31.26	8.14	8.41

11	0	10.99	0.02	0.00	0.14	7.72	28.41	31.25	8.34	8.41
	5	10.40	0.02	0.05	0.18	7.37	28.41	31.25	8.30	8.42
	10	15.19	0.08	0.10	0.21	10.00	28.35	31.25	8.30	8.42
	26	10.20	0.04	0.00	0.20	7.72	28.27	31.25	8.27	8.42
12	0	9.80	0.04	0.00	0.16	7.72	28.41	31.25	8.34	8.41
	5	10.20	0.04	0.07	0.16	8.77	28.41	31.25	8.30	8.42
	10	10.99	0.04	0.07	0.14	8.42	28.35	31.25	8.30	8.42
	24	10.40	0.04	0.00	0.16	7.37	28.27	31.25	8.27	8.42
13	0	9.00	0.04	0.00	0.16	7.72	28.76	31.19	8.30	8.41
	5	8.60	0.04	0.00	0.16	6.66	28.75	31.19	8.25	8.42
	10	9.20	0.04	0.00	0.16	6.84	28.63	31.18	8.27	8.42
	35	8.80	0.02	0.00	0.12	6.49	28.59	31.18	8.19	8.42
14	0	7.40	0.02	0.02	0.12	6.84	27.98	31.37	8.39	8.40
	5	10.99	0.04	0.03	0.25	8.59	27.98	31.37	8.37	8.41
	10	13.79	0.04	0.03	0.21	8.94	27.98	31.37	8.33	8.41
	19	10.60	0.04	0.00	0.14	7.37	27.97	31.37	8.30	8.41
15	0	10.40	0.04	0.00	0.18	9.12	28.26	31.28	8.38	8.37
	5	10.00	0.02	0.02	0.14	8.24	28.26	31.27	8.29	8.40
	10	11.19	0.04	0.03	0.16	9.29	28.53	31.28	8.27	8.41
	15	10.99	0.04	0.00	0.18	8.94	28.21	31.29	8.22	8.41
16	0	9.00	0.04	0.03	0.16	8.59	28.12	31.41	8.56	8.40
	5	10.20	0.04	0.03	0.20	8.94	28.09	31.41	8.50	8.40
	10	9.40	0.04	0.03	0.16	7.89	28.01	31.41	8.50	8.41
	19	9.40	0.04	0.00	0.20	8.07	27.92	31.42	8.40	8.41
17	0	10.00	0.04	0.00	0.20	7.19	28.22	31.41	8.56	8.38
	5	11.19	0.04	0.07	0.20	6.66	28.22	31.42	8.54	8.39
	10	9.40	0.02	0.00	0.16	6.66	28.16	31.42	8.54	8.39

nd = no data

Cruise CU-3 (13-15 January 2004)

Station	Depth (m)	ammonia µM	nitrite µM	nitrate µM	phosphate µM	silicate µM	temperature (°C)	salinity (psu)	DO (ml/l)	pH
1	0	9.40	0.04	0.07	0.23	4.91	26.38	31.70	8.60	8.41
	5	9.80	0.04	0.03	0.21	4.73	26.41	31.72	8.42	8.46
	10	9.40	0.04	0.10	0.21	4.73	26.41	31.72	8.40	8.47
2	0	10.00	0.06	0.01	0.18	8.59	26.62	31.79	8.49	8.39
	5	10.00	0.08	0.00	0.20	8.59	26.57	31.80	8.39	8.42
	10	7.40	0.04	0.07	0.14	6.84	26.55	31.79	8.38	8.43
	15	10.79	0.06	0.01	0.20	8.42	26.55	31.80	8.31	8.43
3	0	9.00	0.41	0.37	0.29	9.47	26.56	31.24	2.19	8.40
	5	9.80	0.08	0.06	0.27	9.29	26.50	31.52	3.66	8.42
	10	10.99	0.08	0.06	0.25	10.52	26.52	31.61	6.54	8.43
4	0	10.60	0.08	0.17	0.35	12.28	26.88	30.80	7.12	8.26
	5	12.99	0.10	0.11	0.45	12.80	26.36	30.86	7.01	8.30
	8	12.59	0.12	0.06	0.41	11.75	26.31	30.92	6.70	8.30
5	0	7.00	0.12	0.00	0.29	8.77	26.51	30.24	9.06	8.48
	5	7.20	0.06	0.00	0.27	8.77	26.14	30.28	9.12	8.48
	10	8.80	0.06	0.00	0.27	7.89	26.05	30.33	9.04	8.49
	15	9.80	0.08	0.06	0.29	13.68	26.13	31.22	7.13	8.39
6	0	12.79	0.16	1.12	0.68	22.97	26.47	30.16	8.72	8.40
	5	9.60	0.49	0.22	0.39	17.36	26.32	30.64	8.71	8.46
	10	9.20	0.29	0.00	0.25	11.05	26.14	30.87	8.58	8.47
	15	11.79	0.04	0.39	0.39	17.54	26.20	31.32	7.40	8.42
7	0	8.00	0.16	0.00	0.20	11.05	26.25	31.16	8.75	8.47
	5	5.40	0.04	0.00	0.18	8.94	26.27	31.18	8.75	8.48
	10	8.80	0.04	0.07	0.20	10.00	26.34	31.40	8.56	8.47
	18	11.19	0.06	0.05	0.25	14.03	26.35	31.55	8.04	8.45
8	0	8.00	0.08	0.00	0.16	7.37	26.83	32.01	8.76	8.46

	5	7.80	0.04	0.03	0.14	8.42	26.82	32.01	8.61	8.48
	10	8.00	0.04	0.03	0.16	7.72	26.82	32.01	8.57	8.48
	24	8.00	0.04	0.03	0.16	7.01	26.83	32.01	8.54	8.48
9	0	10.99	0.04	0.10	0.20	6.84	27.08	32.26	8.50	8.42
	5	7.60	0.08	0.06	0.16	6.31	27.08	32.26	8.45	8.44
	10	10.99	0.04	0.03	0.20	7.01	27.09	32.27	8.43	8.44
	20	8.80	0.04	0.03	0.16	5.79	27.10	32.26	8.40	8.44
10	0	10.00	0.04	0.03	0.16	6.66	27.40	32.17	8.53	8.45
	5	9.40	0.04	0.03	0.16	6.49	27.28	32.23	8.54	8.46
	10	9.60	0.04	0.00	0.14	6.31	27.18	32.24	8.53	8.47
	26	8.80	0.04	0.03	0.14	5.61	27.12	32.26	8.38	8.46
11	0	9.80	0.04	0.07	0.16	7.37	27.03	32.14	8.68	8.44
	5	12.99	0.08	0.03	0.20	9.29	27.04	32.13	8.54	8.46
	10	9.40	0.08	0.00	0.16	6.49	27.03	32.14	8.52	8.46
	28	9.40	0.08	0.00	0.12	6.31	27.01	32.14	8.44	8.46
12	0	8.20	0.06	0.00	0.18	6.31	27.19	32.31	8.53	8.46
	5	9.80	0.08	0.00	0.21	5.96	27.14	32.32	8.52	8.46
	10	8.60	0.08	0.00	0.18	5.79	27.09	32.31	8.51	8.46
	24	7.00	0.08	0.06	0.16	5.96	27.07	32.31	8.39	8.47
13	0	9.20	0.08	0.06	0.14	5.44	27.68	32.21	8.57	8.47
	5	8.20	0.08	0.03	0.14	4.73	27.22	32.28	8.62	8.47
	10	9.40	0.08	0.03	0.16	5.44	27.30	32.39	8.53	8.47
	36	10.60	0.08	0.13	0.16	6.14	27.23	32.42	8.33	8.46
14	0	7.20	0.08	0.06	0.16	8.42	26.80	31.92	8.71	8.44
	5	11.19	0.06	0.08	0.20	11.22	26.76	31.90	8.68	8.45
	10	10.00	0.08	0.06	0.20	9.47	26.75	31.90	8.66	8.45
	19	9.20	0.04	0.07	0.16	10.52	26.75	31.91	8.61	8.45
15	0	10.00	0.08	0.00	0.16	8.59	27.47	32.17	8.48	8.43
	5	8.00	0.06	0.05	0.12	6.84	27.16	32.16	8.50	8.44
	10	9.00	0.04	0.10	0.14	7.01	27.07	32.15	8.50	8.44
	15	8.20	0.04	0.07	0.12	6.84	27.05	32.15	8.43	8.45
16	0	8.00	0.04	0.10	0.12	8.59	27.23	31.96	8.60	8.42
	5	8.00	0.04	0.17	0.12	8.59	26.81	31.95	8.63	8.44
	10	8.40	0.04	0.17	0.12	8.59	26.78	31.95	8.61	8.44
	20	8.00	0.04	0.17	0.12	8.42	26.76	31.95	8.51	8.44
17	0	9.20	0.04	0.10	0.16	5.79	27.48	31.90	8.59	8.41
	5	10.40	0.04	0.03	0.21	5.79	26.73	31.88	8.69	8.44
	10	8.60	0.04	0.03	0.18	5.44	26.64	31.88	8.62	8.44

nd = no data

Cruise CU-4 (12-15 May 2004)

Station	Depth (m)	ammonia µM	nitrite µM	nitrate µM	phosphate µM	silicate µM	temperature (°C)	salinity (psu)	DO (ml/l)	pH
1	0	10.60	3.91	1.91	1.11	19.29	30.80	31.01	6.52	8.14
	5	10.99	3.59	1.81	1.01	19.64	30.76	31.00	6.32	8.42
	10	11.99	2.57	1.41	0.84	17.89	30.57	31.04	6.03	8.41
2	0	7.40	0.00	0.14	0.23	21.92	30.79	30.60	6.59	8.64
	5	10.00	0.06	0.29	0.31	23.15	30.79	30.60	6.50	8.64
	10	12.99	0.08	0.63	0.39	14.55	30.70	31.58	6.04	8.59
	15	11.19	0.08	0.56	0.43	15.08	30.70	32.12	4.09	8.45
3	0	5.60	0.04	0.14	0.29	25.43	30.66	30.01	6.64	8.60
	5	7.40	0.04	0.17	0.35	25.60	30.65	30.01	6.65	8.62
	10	9.40	0.24	0.54	0.41	17.36	30.79	31.19	5.25	8.51
4	0	8.00	0.04	0.10	0.18	22.45	30.74	30.39	6.88	8.57
	5	6.00	0.02	0.12	0.18	16.13	30.55	30.36	6.84	8.56
	8	9.60	0.12	0.34	0.43	19.82	30.76	31.57	5.93	8.48
5	0	8.80	0.06	0.15	0.18	14.03	30.73	32.25	6.41	8.53
	5	9.00	0.04	0.24	0.21	14.55	30.73	32.26	6.43	8.54

	10	8.40	0.02	0.19	0.23	9.64	30.68	32.32	6.34	8.54
	14	9.40	0.08	0.98	0.33	13.85	30.85	32.68	5.53	8.50
6	0	8.60	0.04	0.24	0.18	12.98	30.72	32.56	6.21	8.55
	5	9.00	0.08	0.13	0.21	15.08	30.73	32.57	6.33	8.57
	10	5.60	0.04	0.17	0.18	7.89	30.76	32.67	6.22	8.56
	15	9.80	0.12	0.30	0.23	12.28	30.81	32.86	5.50	8.53
7	0	6.20	0.04	0.17	0.16	4.21	30.45	32.97	6.04	8.56
	5	8.00	0.04	0.17	0.16	7.19	30.46	32.98	5.97	8.57
	10	8.80	0.04	0.39	0.21	6.14	30.46	32.98	5.95	8.57
	16	8.80	0.04	0.31	0.18	6.31	30.46	32.98	5.92	8.57
8	0	9.00	0.06	0.44	0.18	10.17	30.35	32.91	6.10	8.52
	5	5.40	0.04	0.17	0.12	6.84	30.36	32.91	6.03	8.55
	10	7.00	0.04	0.31	0.16	9.47	30.36	32.91	6.01	8.55
	23	8.40	0.04	0.17	0.18	10.87	30.35	32.91	5.97	8.55
9	0	8.20	0.04	0.17	0.20	8.24	30.26	32.77	6.25	8.55
	5	10.00	0.04	0.31	0.20	8.94	30.27	32.78	6.23	8.56
	10	7.60	0.04	0.17	0.14	6.66	30.28	32.78	6.22	8.56
	20	8.00	0.04	0.17	0.16	8.24	30.28	32.78	6.18	8.56
10	0	nd	nd	nd	nd	nd	30.35	32.67	6.09	8.53
	5	nd	nd	nd	nd	nd	30.37	32.68	6.02	8.54
	10	nd	nd	nd	nd	nd	30.38	32.68	6.01	8.54
	28	nd	nd	nd	nd	nd	30.38	32.68	5.96	8.54
11	0	7.80	0.04	0.24	0.16	10.52	30.25	32.73	6.59	8.53
	5	7.80	0.04	0.24	0.16	9.12	30.23	32.74	6.49	8.54
	10	10.00	0.04	0.39	0.23	11.92	30.21	32.74	6.43	8.54
	27	9.40	0.04	0.24	0.18	12.45	30.19	32.75	6.29	8.53
12	0	6.60	0.04	0.24	0.16	12.63	30.58	32.63	6.68	8.53
	5	7.00	0.04	0.14	0.16	12.45	30.41	32.62	6.59	8.53
	10	9.60	0.04	0.17	0.16	12.28	30.32	32.63	6.56	8.53
	23	8.20	0.04	0.10	0.16	13.50	30.29	32.64	6.44	8.53
13	0	7.40	0.04	0.17	0.16	8.42	30.74	32.74	6.52	8.53
	5	7.00	0.04	0.17	0.16	9.47	30.71	32.74	6.53	8.53
	10	8.80	0.04	0.24	0.21	10.00	30.47	32.74	6.54	8.54
	35	11.59	0.04	0.46	0.35	10.17	30.42	32.75	6.33	8.53
14	0	8.60	0.04	0.31	0.18	10.17	30.33	32.42	6.46	8.54
	5	8.40	0.04	0.31	0.20	10.17	30.43	32.42	6.35	8.56
	10	7.20	0.02	0.33	0.16	9.29	30.30	32.42	6.29	8.55
	19	5.60	0.04	0.17	0.14	8.77	30.30	32.42	6.21	8.55
15	nd	nd	nd	nd	nd	nd	nd	nd	nd	nd
	nd	nd	nd	nd	nd	nd	nd	nd	nd	nd
	nd	nd	nd	nd	nd	nd	nd	nd	nd	nd
	nd	nd	nd	nd	nd	nd	nd	nd	nd	nd
16	0	7.40	0.04	0.31	0.20	14.20	30.58	31.80	6.29	8.54
	5	7.40	0.04	0.24	0.20	13.50	30.49	31.80	6.39	8.55
	10	8.80	0.04	0.46	0.23	13.50	30.43	31.96	6.34	8.53
	18	6.80	0.04	0.31	0.14	10.52	30.65	32.55	6.14	8.51
17	0	6.80	0.04	0.39	0.29	13.15	30.86	30.80	7.38	8.60
	5	8.00	0.04	0.46	0.39	13.33	30.62	30.80	7.91	8.63
	10	6.80	0.06	0.44	0.23	14.55	30.72	31.37	7.22	8.57

nd = no data

Cruise CU-5 (7-10 October 2004)

Station	Depth (m)	ammonia µM	nitrite µM	nitrate µM	phosphate µM	silicate µM	temperature (°C)	salinity (psu)	DO (ml/l)	pH
1	0	10.32	0.48	0.36	0.53	11.94	29.54	32.19	4.86	8.42
	5	9.74	0.48	0.36	0.40	11.94	29.38	32.21	4.78	8.49
	10	12.04	3.85	0.63	0.60	15.92	29.41	32.45	4.49	8.50
	13	12.04	9.51	1.71	0.93	29.00	29.44	32.58	3.32	8.47

2a	0	13.76	2.05	6.93	1.59	43.21	29.19	24.65	5.39	8.62
	5	13.18	1.81	6.05	1.39	37.52	29.48	32.27	5.21	8.60
	10	9.17	0.18	0.10	0.40	6.82	29.48	32.38	5.20	8.64
	15	11.46	0.96	2.40	0.66	18.76	29.48	32.50	4.74	8.63
2b	0	6.31	0.24	0.04	0.27	5.69	29.52	32.35	5.60	8.58
	5	7.45	0.24	0.32	0.33	6.82	29.49	32.40	5.57	8.60
	10	8.02	0.24	0.18	0.33	9.67	29.54	32.49	5.52	8.62
	15	7.45	0.12	0.16	0.33	6.25	29.51	32.53	5.34	8.63
3	0	11.46	1.08	3.12	1.06	21.04	29.86	24.33	6.32	8.63
	5	5.73	1.93	1.16	0.53	10.23	29.53	30.96	4.68	8.60
	11	9.17	0.84	2.80	0.93	18.19	29.39	31.74	3.40	8.50
4	0	8.02	0.18	0.10	0.53	4.55	30.95	23.67	8.09	8.87
	5	9.74	0.12	0.02	0.50	4.55	29.49	30.49	6.54	8.78
	9	9.74	0.12	0.02	0.53	5.69	29.59	31.07	3.96	8.60
5	0	8.60	0.12	0.30	1.19	1.14	30.99	23.75	7.87	8.97
	5	9.17	0.18	0.00	0.93	1.71	29.70	30.15	2.44	8.66
	10	13.18	1.32	3.72	1.09	34.11	29.75	32.23	0.84	8.41
	16	13.18	1.57	2.64	0.99	34.11	29.68	32.44	0.39	8.32
6	0	10.32	0.36	0.76	1.06	3.41	31.70	22.84	7.90	8.86
	5	14.33	0.36	1.04	1.46	2.84	29.74	29.54	4.86	8.77
	10	10.32	1.32	4.29	0.93	35.25	29.65	32.61	1.68	8.46
	16	10.32	0.72	2.08	1.09	14.78	29.60	32.88	1.07	8.35
7	0	6.88	0.12	0.02	0.60	1.14	29.47	24.51	6.59	8.90
	5	8.60	0.30	0.00	0.60	18.19	29.89	30.41	3.48	8.63
	10	6.88	0.36	0.20	0.53	25.58	29.60	33.00	2.17	8.51
	17	10.32	6.62	2.07	0.93	37.52	29.58	33.23	1.48	8.40
8	0	10.89	0.18	0.66	0.60	6.25	29.57	29.56	5.75	8.86
	5	12.61	0.24	0.32	0.60	7.39	29.37	32.33	5.60	8.65
	10	9.17	0.12	0.00	0.27	6.25	29.26	32.50	5.57	8.65
	23	11.46	1.20	0.20	0.53	3.41	29.51	33.38	4.63	8.59
9	0	9.74	0.12	0.16	0.20	5.12	29.41	32.32	5.29	8.66
	5	10.32	0.12	0.30	0.33	4.55	29.46	32.33	5.32	8.68
	10	10.32	0.12	0.30	0.27	5.69	29.63	32.81	5.28	8.68
	21	8.60	0.18	0.10	0.30	5.69	29.59	33.04	5.07	8.65
10	0	8.02	0.12	0.02	0.27	6.25	30.74	32.21	5.69	8.63
	5	6.88	0.12	0.02	0.20	5.69	29.94	32.25	5.78	8.66
	10	8.02	0.12	0.02	0.20	5.69	29.80	32.29	5.76	8.67
	26	7.45	0.18	0.10	0.27	6.82	29.59	32.73	5.52	8.65
11	0	6.88	0.12	0.02	0.20	5.12	29.56	32.67	5.63	8.61
	5	7.45	0.12	0.16	0.20	5.12	29.45	32.68	5.66	8.65
	10	7.45	0.12	0.16	0.23	3.41	29.32	32.82	5.65	8.66
	26	7.45	0.12	0.16	0.27	1.14	29.53	33.56	4.97	8.60
12	0	8.02	0.12	0.16	0.27	6.82	30.93	32.75	5.59	8.61
	5	8.60	0.18	0.10	0.27	6.82	29.70	32.85	5.66	8.66
	10	6.88	0.24	0.04	0.33	5.12	29.72	33.04	5.59	8.66
	24	6.88	0.18	0.10	0.27	3.98	29.69	33.11	5.46	8.65
13	0	7.45	0.12	0.16	0.23	7.39	30.86	31.84	5.66	8.63
	5	8.02	0.12	0.30	0.27	6.82	29.78	32.00	5.73	8.66
	10	9.17	0.12	0.30	0.27	8.53	29.74	32.42	5.67	8.66
	35	7.45	0.12	0.30	0.27	7.39	29.63	33.09	5.16	8.62
14	0	8.60	0.12	0.30	0.33	6.82	29.70	32.55	5.52	8.64
	5	8.60	0.18	0.24	0.33	6.82	29.67	32.56	5.53	8.65
	10	8.60	0.18	0.10	0.33	6.25	29.72	32.79	5.47	8.65
	17	8.60	0.12	0.02	0.27	6.82	29.73	32.98	5.17	8.63
15	0	8.60	0.24	0.04	0.33	4.55	29.81	32.20	5.65	8.56
	5	8.60	0.18	0.10	0.27	5.12	29.54	32.25	5.71	8.60
	10	8.60	0.18	0.10	0.27	6.25	29.51	32.30	5.71	8.61
	15	8.02	0.18	0.10	0.33	9.67	29.59	32.67	5.46	8.60
16	0	8.60	0.18	0.10	0.33	10.80	30.09	32.68	5.13	8.53
	5	6.88	0.18	0.00	0.33	10.23	29.86	32.68	5.12	8.57
	10	9.74	0.24	0.04	0.33	15.35	29.48	32.65	5.07	8.58
	20	8.60	0.72	0.00	0.33	13.64	29.43	32.67	4.90	8.58

17	0	7.45	0.24	0.00	0.30	10.80	29.65	32.43	5.70	8.54
	5	6.31	0.24	0.00	0.27	9.67	29.62	32.46	5.74	8.60
	10	5.73	0.24	0.04	0.33	10.23	29.46	32.48	5.62	8.62
	28	7.45	0.24	0.04	0.33	11.94	29.38	32.51	5.60	8.58

nd = no data

Cruise CU-6 (26-29 July 2005)

Station	Depth	ammonia	nitrite	nitrate	phosphate	silicate	temperature	salinity	DO	pH
	(m)	µM	µM	µM	µM	µM	(°C)	(psu)	(ml/l)	
1	0	11.63	0.00	0.08	1.53	2.55	28.99	28.77	8.36	7.91
	5	15.36	0.13	0.30	1.46	5.28	29.00	28.76	7.72	7.87
	10	17.44	0.08	2.09	1.42	17.31	29.22	31.76	6.76	7.82
2	0	10.79	0.19	0.06	1.42	10.57	29.35	30.62	8.59	7.82
	5	14.53	0.00	0.06	1.57	14.58	29.32	30.65	6.96	7.78
	10	14.53	0.10	0.39	1.34	12.75	29.39	32.17	6.86	7.76
	26	14.12	0.78	3.80	0.55	22.23	nd	nd	nd	nd
3	0	16.61	0.00	0.14	0.31	7.29	29.29	31.24	7.05	7.71
	5	14.53	0.00	0.17	0.49	9.47	29.25	31.22	6.64	7.68
	10	16.61	0.48	3.14	0.59	14.94	29.32	32.84	6.55	7.67
4	0	19.10	0.29	0.55	0.47	20.59	29.67	31.57	6.81	7.49
	5	15.78	0.45	0.28	0.43	16.76	29.35	31.61	5.38	7.44
	10	15.78	0.32	0.52	0.38	19.86	29.20	31.41	5.53	7.47
5	0	20.34	0.32	0.17	0.31	9.47	29.77	33.05	7.31	7.23
	5	28.65	0.92	0.17	0.35	8.38	29.49	33.00	6.59	7.16
	10	24.50	0.29	0.17	0.28	8.56	29.33	33.03	6.63	7.15
6	0	19.10	0.13	0.11	0.28	10.57	29.54	33.28	8.51	7.78
	5	22.42	0.71	0.14	0.31	19.50	29.54	33.27	6.44	7.75
	10	17.85	0.21	0.22	0.28	19.86	29.42	33.28	6.43	7.74
	14	18.27	0.34	0.14	0.24	21.50	29.36	33.29	6.21	7.73
7	0	16.61	0.27	0.17	0.35	25.14	29.48	33.25	6.01	7.70
	5	15.78	0.00	0.11	0.20	20.77	29.39	33.46	6.10	7.70
	10	16.61	0.00	0.11	0.31	23.87	29.33	33.51	6.06	7.70
	15	12.04	0.00	0.08	0.20	18.58	29.30	33.52	5.95	7.69
8	0	15.36	0.00	0.11	0.24	20.41	29.04	33.54	6.09	7.67
	5	14.53	0.00	0.11	0.20	20.77	29.04	33.54	6.09	7.67
	10	16.61	0.00	0.11	0.24	21.32	29.06	33.56	6.09	7.68
	20	16.19	0.00	0.11	0.20	14.58	29.20	33.81	6.05	7.68
9	0	14.12	0.00	0.11	0.16	6.56	28.84	33.90	6.10	7.66
	5	12.46	0.00	0.06	0.16	7.83	29.15	33.87	6.28	7.68
	10	14.12	0.00	0.08	0.22	6.74	28.96	33.87	6.31	7.69
	20	12.46	0.00	0.08	0.22	6.74	28.85	33.88	6.15	7.68
10	0	14.95	0.00	0.11	0.28	6.74	28.80	33.79	6.43	7.73
	5	14.12	0.00	0.11	0.28	5.47	28.80	33.79	6.04	7.71
	10	15.36	0.00	0.11	0.28	6.01	28.80	33.79	6.01	7.71
	20	10.79	0.00	0.11	0.16	5.83	28.80	33.80	5.99	7.71
11	0	14.53	0.00	0.11	0.24	10.75	28.88	33.97	8.04	7.77
	5	8.72	0.26	1.71	0.16	4.37	28.88	33.97	6.34	7.74
	10	15.78	0.09	0.11	0.24	7.65	28.88	33.97	6.28	7.74
	20	15.78	0.16	0.08	0.28	8.56	28.88	33.97	6.25	7.73
12	0	12.46	0.00	0.11	0.24	6.92	28.72	33.98	7.62	7.77
	5	13.70	0.00	0.08	0.24	4.19	28.72	33.97	6.32	7.73
	10	15.78	0.00	0.11	0.28	6.56	28.71	33.98	6.20	7.72
	20	12.46	0.00	0.08	0.20	4.01	28.70	33.97	6.20	7.73
13	0	15.36	0.00	0.11	0.31	6.56	28.76	33.86	6.30	7.65
	5	14.12	0.00	0.11	0.31	2.73	28.75	33.85	6.31	7.66
	10	14.53	0.00	0.11	0.28	3.46	28.72	33.86	6.23	7.67
	20	14.53	0.00	0.13	0.28	7.47	28.71	33.84	6.20	7.66
14	0	14.12	0.00	0.11	0.31	14.94	29.18	32.76	6.20	7.69

	5	15.36	0.00	0.10	0.31	15.49	29.13	32.76	6.17	7.70
	10	12.46	0.00	0.06	0.20	10.02	29.05	32.89	6.18	7.70
	18	9.96	0.00	0.04	0.14	7.29	29.05	33.76	6.09	7.68
15	0	11.63	0.00	0.06	0.16	9.47	29.08	33.69	6.09	7.66
	5	9.55	0.00	0.06	0.08	8.38	29.12	32.80	6.21	7.69
	10	11.42	0.00	0.06	0.12	7.65	29.08	33.68	6.13	7.68
	15	9.55	0.00	0.00	0.08	10.39	29.07	33.63	6.16	7.68
16	0	13.49	0.00	0.06	0.16	5.10	28.99	31.37	8.19	7.86
	5	11.00	0.00	0.06	0.16	5.10	29.01	31.37	6.47	7.83
	10	10.38	0.00	0.06	0.12	9.47	29.07	32.42	6.41	7.82
	18	11.63	0.31	0.06	0.16	10.93	29.32	33.30	5.91	7.72
17	0	12.25	0.04	0.08	0.30	4.55	28.95	30.90	14.24	7.54
	5	10.38	0.64	0.08	0.30	4.55	28.95	31.05	10.25	7.59
	10	11.63	1.52	0.17	0.39	12.75	29.26	32.67	9.49	7.57

nd = no data